Distinct roles of LARP1 and 4EBP1/2 in regulating translation and stability of 5′TOP mRNAs

Inauguraldissertation

zur Erlangung der Würde eines Doktors der Philosophie

vorgelegt der

Philosophisch-Naturwissenschaftlichen Fakultät

der Universität Basel

von

Tobias Hochstöger

Basel, 2024

Genehmigt von der Philosophisch-Naturwissenschaftlichen Fakultät

auf Antrag von

Erstbetreuer: Dr. Jeffrey A. Chao

Zweitbetreuer: Prof. Helge Grosshans

Externer Experte: Dr. Marvin Tanenbaum

Basel, den 27. Februar 2024

Prof. Marcel Mayor

The Dean of Faculty

Acknowledgments

I would like to thank all of the people that accompanied me during my PhD and without whom this project would not have been possible.

First and foremost, I would like to thank Jeff for giving me the opportunity to pursue my PhD in his lab. He has always been a very supportive mentor who gave me the freedom to explore, learn and grow as a scientist. Furthermore, I would like to express my gratitude and appreciation to the members of my thesis committee, Helge Grosshans and Marvin Tanenbaum, for your input and constructive feedback.

Next, I would like to thank all present and former members of the Chao lab, that I had the pleasure to meet and work with: Jessica Desogus, Pratik Dave, Aileen-Diane Bamford, Esther Griesbach, Daniel Mateju, Varun Bhaskar, Julia Nörpel, Bastian Eichenberger, Caroline Artus-Revel, Melissa Moula, Jessica Mitchell, Yuhui Dou, Agata Misiaszek, Tobias Williams, and Simon Waldner. A big thanks goes to Ewa Piskadlo for her help with this project. I want to especially thank Franka Voigt, who introduced me to single-molecule techniques in the lab and who I had the pleasure to work with on several projects over the years. I very much enjoyed our conversations, whether they were about science or politics.

A big thanks goes to members of the excellent FMI facilities. I want to thank all members of the Facility For Advanced Imaging And Microscopy, especially, Laurent Gelman, Laure Plantard, Sabine Reither, and Tim-Oliver Buchholz. I would also like to highlight the support of the Functional Genomics facility, especially Sebastien Smallwood and the support from Hubertus Köhler for cell sorting. Last but not least, a big thanks goes to Panagiotis Papasaikas and Hans-Rudolf Hotz from the Computational Biology facility.

I would like to express my gratitude towards my friends, especially Maxim, Pia, Jessica, Sandra and Pedro. Our weekly gaming nights were a highlight of my time in Basel. Most of all, I would like to thank my partner Claudia, who has supported me throughout this journey. Her patience, understanding, and encouragement during moments of frustration have been invaluable. Finally, I am eternally grateful to my entire family, especially my parents, Elisabeth and Peter. They shaped me into the person I am today.

Table of Contents

List of Abbreviations

4EBP1 eIF4E-binding protein 1.
4EBP1/2 eIF4E-binding proteins 1 and 2.
4EBP2 eIF4E-binding protein 2.
5′TOP 5′ terminal oligopyrimidine.

Cas9 CRISPR associated protein 9.
CBC cap binding complex.
cDNA complementary DNA.
CLIP crosslinking and immunoprecipitation.
CRISPR clustered regularly interspaced short palindromic repeats.

DMEM dulbecco's modified eagle medium.
DNA deoxyribonucleic acid.

eIF4A eukaryotic translation initiation factor 4A.
eIF4E eukaryotic translation initiation factor 4E.
eIF4F eukaryotic translation initiation factor 4F.
eIF4G eukaryotic translation initiation factor 4G.
EMSA electrophoretic mobility shift assay.

FBS fetal bovine serum.

Halo haloalkane dehalogenase tag.
HEK293T human embryonic kidney 293T cells.
HeLa Henrietta Lacks cells.

KD knockdown.
KO knockout.

LARP1 La-related protein 1.
LARP1/1B La-related proteins 1 and 1B.
LARP1B La-related protein 1B.
LARPs La-related proteins.

MCP MS2 coat protein.

MEF mouse embryonic fibroblast.
MNK1/2 MAP kinase interacting serine/threonine kinase 1/2.
mRNA messenger RNA.
mTOR mechanistic target of rapamycin.
mTORC1 mechanistic target of rapamycin complex 1.

PABPC1 poly(A)-binding protein cytoplasmic 1.
PAGE polyacrylamide gel electrophoresis.
PAR-CLIP photoactivatable ribonucleoside-enhanced crosslinking and immunoprecipitation.
PBS phosphate-buffered saline.
PCR polymerase chain reaction.
PP242 mTOR inhibitor PP242 (Torkinib).
PRTE pyrimidine rich translation element.

RBP RNA-binding protein.
RNA ribonucleic acid.
RNAseq RNA sequencing.
ROI region-of-interest.
RPL11 60S Ribosomal Protein L11.
RPL32 60S ribosomal protein L32.
RPL5 60S ribosomal protein L5.
RPS6 40S ribosomal protein S6.
RPTOR regulatory associated protein of mTORC1.
rtTA2-M2 reverse tetracycline-controlled transactivator.

S4U 4-thiouridine.
S6K1 ribosomal protein S6 kinase 1.
S6K1/2 ribosomal protein S6 kinases 1 and 2.
SDS sodium dodecyl sulfate.
sgRNA single guide RNA.
shRNA small hairpin RNA.
SLAMseq (SH)-linked alkylation for the metabolic sequencing of RNA.
smFISH single-molecule fluorescence *in situ* hybridization.
SSB/LA Small RNA binding exonuclease protection factor La.
SunTag supernova tag.

TAK228 mTOR inhibitor TAK228 (Sapanisertib, MLN0128/INK128).
TBS tris-buffered saline.
TCT polypyrimidine initiator.
TIA1 TIA1 cytotoxic granule associated RNA binding protein.
TIAL1/TIAR TIA1 cytotoxic granule associated RNA binding protein like 1.
TISU translation initiator of short 5′UTR.

TRIBE targets of RNA binding proteins identified by editing.
TSS transcription start site.

UTR untranslated region.

WT wild-type.

List of Figures

List of Tables

Abstract

Vertebrate cells have evolved a simple, yet elegant, mechanism for coordinated regulation of ribosome biogenesis mediated by the 5′ terminal oligopyrimidine (5′TOP) motif. This motif allows cells to rapidly adapt to changes in the environment by specifically modulating the translation of messenger RNAs (mRNAs) encoding the translation machinery. The core signaling pathway which links nutrient availability with the production of ribosomes is the mechanistic target of rapamycin complex 1 (mTORC1), which integrates a variety of nutrient cues to modulate the translation of 5′TOP mRNAs. While the role of mTORC1 in regulating the translation of 5′TOP mRNA has been well established, the identity of the key factor which binds to the 5′TOP motif to regulate translation has been challenging to elucidate.

Recently, La-related protein 1 (LARP1) was proposed to be the specific regulator of 5′TOP mRNA translation downstream of mTORC1, while eIF4E-binding proteins 1 and 2 (4EBP1/2) were suggested to have a general role in translational repression of all transcripts. To address these questions, we employed single-molecule translation site imaging of 5′TOP and canonical mRNAs to study the translation of single mRNAs in living cells. We reveal that 4EBP1/2 play a dominant role in the translational repression of both 5′TOP and canonical mRNAs during pharmacological inhibition of mTOR. In contrast, we find that LARP1 selectively protects 5′TOP mRNAs from degradation in a transcriptome-wide analysis of mRNA half-lives. Our results clarify the roles of 4EBP1/2 and LARP1 in regulating 5′TOP mRNAs and provide a framework to further study how these factors control cell growth during development and disease.

Outline

This thesis describes both published work and work "in press", which are listed below with co-authorships attributed. It consists of three chapters:

Chapter 1 is an introduction to the topic of translational regulation of ribosomal protein mRNAs. Sections and the figures have been reproduced or adapted from the following publication:

> Towards a molecular understanding of the 5′TOP motif in regulating translation of ribosomal mRNAs
> **Hochstoeger, T.,** & Chao, J. A.
> *Seminars in Cell & Developmental Biology.*, 154:99-104. (2024)
> https://doi.org/10.1016/j.semcdb.2023.06.001

Chapter 2 summarizes the results of this dissertation, describing the distinct roles of 4EBP1/2 and LARP1 in regulating 5′TOP mRNAs. The contents of this chapter are reproduced or adapted from the following publication:

> Distinct roles of LARP1 and 4EBP1/2 in regulating translation and stability of 5′TOP mRNAs
> **Hochstoeger, T.**, Papasaikas, P., Piskadlo E., & Chao, J. A.
> *Science Advances*., 10(7), eadi7830. (2024)
> https://doi.org/10.1126/sciadv.adi7830

Chapter 3 is a discussion of the results described in **Chapters 2** placing the results in the context of the current understanding in the field.

The references for all chapters are summarized in a final **References** chapter. The **Supplementary Information** contain all further data related to **Chapter 2**. The above-mentioned manuscripts can be found in the **Appendix**.

Chapter 1

Introduction

Tobias Hochstoeger[1,2], Jeffrey A. Chao[1]*

[1] Friedrich Miescher Institute for Biomedical Research, 4058 Basel, Switzerland
[2] University of Basel, 4003 Basel, Switzerland
* Corresponding author

Contribution

The contents of this chapter have been published in *Seminars in Cell & Developmental Biology* on the 15th February 2024 (Hochstoeger & Chao, 2024). My contribution included the writing of this review article in collaboration with Jeffrey A. Chao.

1.1 Regulation of ribosome biogenesis

In order for cells to grow and proliferate they must orchestrate the biogenesis of thousands of ribosomes, the cellular machines that carry out protein synthesis, every minute (Lewis & Tollervey, 2000; Warner, 1999). This endeavor is particularly challenging due to both the size of the macromolecular complex and the number of components that must be appropriately put together to generate functional ribosomes. In prokaryotes, this requires coordinating the production and assembly of three ribosomal RNAs (16S, 23S and 5S rRNAs) and ∼52 ribosomal proteins into two subunits (30S small subunit, 50S large subunit) that join to form the active 70S ribosome (Kaczanowska & Rydén-Aulin, 2007). This process becomes even more complex in eukaryotes, not only because of the partitioning of the cell into the nucleus and cytoplasm by the nuclear membrane, but the ribosome itself has increased in size and contains four ribosomal RNAs (18S, 28S, 5S and 5.8S rRNAs) as well as ∼79 ribosomal proteins that must be assembled into the 40S small subunit, 60S large subunit and 80S ribosome (Thomson *et al.*, 2013). Importantly, synthesizing ribosomes at this scale utilizes considerable cellular resources necessitating that this process be tightly regulated.

The production of stoichiometric levels of rRNAs and ribosomal proteins is controlled at multiple levels. In prokaryotes, regulation of the synthesis of rRNAs is achieved, in part, by the processing of a single pre-rRNA transcript into three distinct rRNAs (Espejo & Plaza, 2018). While the prokaryotic ribosomal protein genes are located throughout the genome, many are arranged in operons which co-regulate their expression levels: one of the ribosomal proteins encoded in the operon can bind to a sequence within its own mRNA to repress the translation of all ribosomal proteins encoded in the operon (Draper, 1990; Mikhaylina *et al.*, 2021). In eukaryotes, three of the rRNAs (18S, 28S and 5.8S rRNAs) are generated from the processing of a precursor transcript, however, the 5S rRNA is encoded by a separate gene that is transcribed by RNA polymerase III instead of RNA polymerase I (Ciganda & Williams, 2011; Henras *et al.*, 2015). While co-regulation of eukaryotic ribosomal proteins does not occur through the arrangement of genes within operons, their coordinated expression has been shown to be regulated by specific transcriptional and post-transcriptional pathways that are controlled by the mechanistic target of rapamycin (mTOR) kinase in species ranging from plants, yeast to vertebrates (Meyuhas, 2000; Powers & Walter, 1999; Scarpin *et al.*, 2020).

The mTOR kinase is a central controller of cell growth, integrating nutrient cues and adjusting cell growth accordingly (Fig. 1.1, Schmelzle and Hall, 2000). In both yeast and vertebrate cells, mTOR controls ribosome biogenesis through at least two main mechanisms: rRNA synthesis and ribosomal protein production (Mayer & Grummt, 2006). While rRNA synthesis is transcriptionally regulated in both cases, control of ribosomal protein production is achieved in unique ways. In yeast, production of the ribosomal proteins is regulated mostly at the transcriptional level (Shore *et al.*, 2021), with quick adaptation mediated by short mRNA half-lives (average half-life of ribosomal protein mRNAs: 16 min, Chan *et al.*, 2018). In vertebrates, production of ribosomal proteins is regulated mostly at the translational level by modulating translation of long-lived ribosomal protein mRNAs (average half-life of ribosomal protein mRNAs in humans: >9 hours, Schofield *et al.*, 2018).

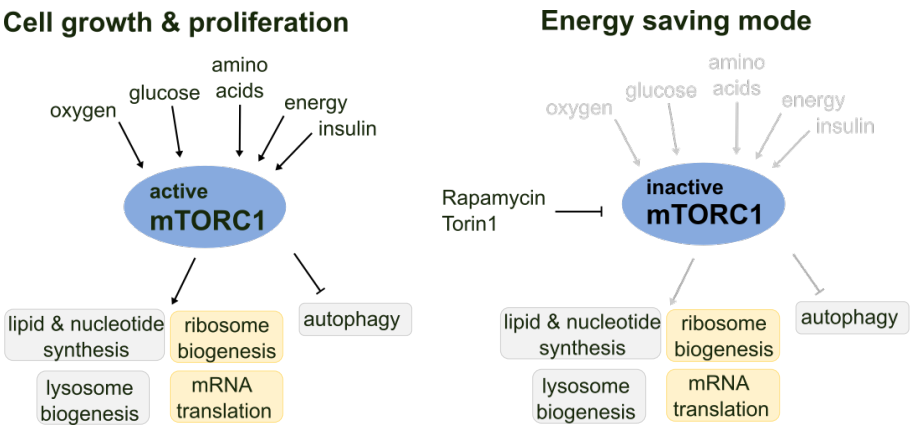

Figure 1.1: The mTORC1 signaling pathway. Schematic of mTORC1, showing the upstream signals sensed by mTORC1, which integrates them to regulate downstream biosynthetic processes. When nutrients are not available or when mTORC1 is pharmacologically inhibited, mTORC1 becomes inactive and its downstream regulatory effects are relieved. Fig. adapted from Sabatini, 2017.

mTOR control of ribosomal protein translation becomes activated when vertebrate cells are exposed to unfavorable growth conditions (e.g., deprivation of amino acids, serum, oxygen or insulin) that leads to inhibition of the mTOR kinase, resulting in a rapid translational downregulation of ribosomal protein mRNAs, thereby reducing the biogenesis of new ribosomes (Meyuhas, 2000). Conversely, providing nutrients to starved cells results in a rapid re-activation of ribosomal protein mRNA translation (Meyuhas, 2000). This has led to the hypothesis of a molecular switch that toggles vertebrate ribosomal protein mRNA translation by specific regulators that recognize unique features within these transcripts and are controlled by mTOR (Meyuhas & Kahan, 2015; Schneider *et al.*, 2022).

1.2 The 5′TOP motif

In the 1980s, characterization of the sequences of ribosomal protein mRNAs from a variety of vertebrates led to the observation that this class of transcripts contained a conserved sequence motif at the 5′ end of the transcript that is directly adjacent to the 7-methylguanosine cap (Chen & Roufa, 1988; Dudov & Perry, 1984; Huxley & Fried, 1990; Mariottini *et al.*, 1988; Rhoads *et al.*, 1986; Wagner & Perry, 1985; Wiedemann & Perry, 1984). Since this motif contained a conserved cytidine in the +1 position followed by an uninterrupted stretch of 4-15 pyrimidine nucleotides it became known as the 5′ terminal oligopyrimidine (5′TOP) motif (Fig. 1.2, Avni *et al.*, 1994). Initial studies of the 5′TOP motif determined that it was both essential and sufficient to mediate translational control because mutation of the first invariable nucleotide converts a 5′TOP mRNA into a non-5′TOP mRNA that is not rapidly repressed under stress (Avni *et al.*, 1994), while mutating the 5′ end of a non-5′TOP mRNA enables it to be repressed like an endogenous 5′TOP mRNA during stress (Biberman & Meyuhas, 1997). Additional sequence analysis of mRNAs that encode translation factors and other proteins involved in translation indicated that the 5′TOP motif is more broadly utilized to regulate additional aspects of translation beyond only ribosomal proteins (Meyuhas, 2000; Thoreen *et al.*, 2012).

This coordinated regulation of translation, however, requires a well-defined transcription start site (TSS). In vertebrates, ribosomal protein mRNAs have core promoters that contain a unique consensus motif found at the TSS of these genes termed the polypyrimidine initiator (TCT) (Parry *et al.*, 2010; van den Elzen *et al.*, 2022). The TCT motif comprises nucleotides in the -2 to +6 positions with respect to the TSS and is distinct from other core promoter motifs (e.g., TATA box). While the mechanism by which the TCT motif functions in transcription initiation is not fully understood, it ensures that the 5′UTR of ribosomal protein transcripts begins with an invariable cytosine followed by a short stretch of pyrimidine nucleotides (Parry *et al.*, 2010). Interestingly, the positioning of the 5′TOP motif at the 5′ end of mRNAs allows for the expression of both 5′TOP and non-5′TOP mRNAs for the same genes utilizing alternative TSSs, and recent evidence suggests that many genes indeed are expressed as both variants, with some cases of tissue-specific expression of the 5′TOP or non-5′TOP isoform of the transcript (Nepal *et al.*, 2020; Philippe *et al.*, 2020). Nevertheless, the core set of 5′TOP mRNAs involved in translation were found to be constitutively expressed as 5′TOP mRNAs across 16 human tissues in a recent analysis of genome-wide transcription initiation events (Philippe *et al.*, 2020).

While the function of the 5′TOP motif in conferring mTOR-dependent translational regulation has been well established, the role of sequence elements located in the 5′UTR of these transcripts is unclear. Pyrimidine rich translation elements (PRTEs) are found downstream of the 5′ cap in the 5′UTR of many mTOR regulated mRNAs, with a large overlap of mRNAs that contain both a 5′TOP and PRTE (Hsieh *et al.*, 2012). Using ribosome profiling, 144 mRNAs were found to be sensitive to mTOR inhibition. Of those, 37 possessed only a 5′TOP element, 30 possessed only a PRTE within their 5′ UTR, and 61 mRNAs possessed both a 5′TOP and PRTE (Hsieh *et al.*, 2012). The PRTE consensus motif consists of an invariant uridine at position 6 of a 9 nt long pyrimidine stretch. As the core 5′TOP motif has been shown to be essential and sufficient for mTOR-dependent translational regulation, research has focused on studying the 5′TOP motif, and the function of the PRTE in contributing to this regulation remains to be determined.

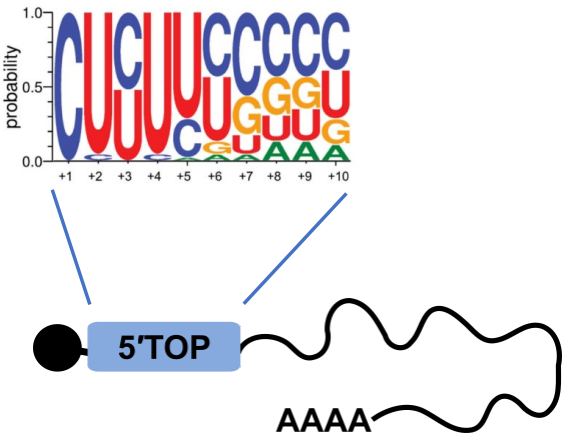

Figure 1.2: The 5′TOP motif. Schematic of a 5′TOP mRNA, showing the sequence logo of the first 10 nucleotides of human 5′TOP mRNAs encoding ribosomal proteins. Note the conserved +1 cytosine, followed by a minimum of four pyrimidines. Fig. adapted from Berman *et al.*, 2020.

1.3 The identification of *trans*-acting factors that regulate translation of 5′TOP mRNAs

While the conservation of the consensus sequence within the 5′TOP motif suggested that it could be specifically recognized by a *trans*-acting factor, it has proven difficult to identify its interaction partner. Since the 5′TOP motif is located at the 5′ end of mRNAs that are bound by the eukaryotic translation initiation factor 4F (eIF4F) complex (eIF4E, eIF4G and eIF4A) during translation initiation, the *trans*-acting factor could either be part of the canonical translation initiation machinery that also has partial specificity for the 5′TOP motif, or a specialized protein that selectively recognizes the 5′TOP motif. In both cases, the molecule mediating 5′TOP translational regulation needs to fulfill several criteria (Meyuhas & Kahan, 2015). First, it is essential for selective 5′TOP translational regulation to occur, and loss or mutation of the factor results in 5′TOP mRNAs and non-5′TOP mRNAs behaving similarly during stress. Second, it specifically interacts with the 5′TOP motif in order to provide a molecular link between the 5′TOP sequence and translational regulation. Third, its role in translational regulation can be altered in response to mTOR activity.

mTOR can globally regulate translation through phosphorylation of eIF4E binding proteins (4EBP1 and 4EBP2) and ribosomal protein S6 kinases 1 and 2 (S6K1/2) (Fig. 1.3A, Fonseca *et al.*, 2014). Since both physiological and pharmacological inhibition of mTOR results in rapid translational repression of 5′TOP mRNAs and dephosphorylation of S6K1/2 and 4EBP1/2, they have both been proposed to be the 5′TOP motif specificity factor. S6K1/2 activity, however, could be uncoupled from 5′TOP regulation in S6K1/2 knockout (KO) mice without abolishing rapamycin-sensitive 5′TOP regulation indicating that it was unlikely to be the main regulator (Pende *et al.*, 2004; Ruvinsky *et al.*, 2005). Additionally, selective ribosome profiling also indicated that 40S ribosomal protein S6 (RPS6), which is one of the substrates of S6K1/2 and could potentially mediate an interaction with 5′TOP transcripts during translation initiation, does not promote their translation (Bohlen *et al.*, 2021). When mTOR is inactivated under unfavorable growth conditions, 4EBP1/2 become dephosphorylated which enables their binding to eIF4E, blocking the eIF4E-eIF4G interaction and preventing the assembly of the eIF4F complex, thus inhibiting translation initiation. While eIF4E specifically recognizes the 5′ cap structure, its affinity for a capped oligo has also been shown to depend on the nucleotide in the +1 position with a preference for adenine or guanine over cytosine (Tamarkin-Ben-Harush *et al.*, 2017). While a more detailed analysis of eIF4E 's sequence specificity has not been performed, this suggests that while eIF4E is a canonical translation factor, it may allow for selective reduction in 5′TOP mRNA translation when mTORC1 is inhibited and the pool of active eIF4E is reduced. Interestingly, while 5′TOP mRNAs are translated when mTOR is active, they have been found to be less efficiently translated than other housekeeping transcripts even in growing cells, as estimated by polysome analysis (Meyuhas, 2000). This suggests that their initiation is partially impaired which could result from reduced eIF4E affinity, however, it is also possible that mTOR is inactive in a subpopulation of cells even under nutrient rich conditions, which cannot be resolved by bulk methods such as polysome analysis. Consistent with a specific role of eIF4E, 4EBP1/2 KO mouse embryonic fibroblasts

(MEFs) demonstrated an involvement of 4EBP1/2 in regulating 5′TOP mRNA translation, as loss of 4EBP1/2 resulted in a rescue of 5′TOP translational repression upon Torin1 treatment (Thoreen *et al.*, 2012). A follow-up study, however, demonstrated that under long-term oxygen deprivation or serum starvation, 4EBP1/2 KO MEFs retain strong 5′TOP translational regulation indicating that an additional factor must be involved (Miloslavski *et al.*, 2014). Miloslavski and colleagues were, however, able to replicate the initial finding by Thoreen *et al.*, 2012 that loss of 4EBP1/2 is sufficient to rescue short-term pharmacological inhibition of 5′TOP translation indicating that different 5′TOP binding partners might function sequentially or with differing kinetics in order to repress translation.

Since the 5′TOP motif contains a stretch of sequential pyrimidines, this sequence could be bound by a number of RNA-binding proteins that share this RNA-binding specificity. Among them, TIA1 cytotoxic granule associated RNA binding protein (TIA1) and TIA1 cytotoxic granule associated RNA binding protein like 1 (TIAL1/TIAR) were reported to mediate translational repression of 5′TOP mRNAs under amino acid starvation (Damgaard & Lykke-Andersen, 2011), but not hypoxia (Miloslavski *et al.*, 2014). Knockdown (KD) of TIA1 and TIAL1/TIAR also failed to rescue 5′TOP translational repression upon Torin1 treatment indicating that it may not be a general translational repressor of 5′TOP mRNA translation but could play a more specialized role (Thoreen *et al.*, 2012).

More recently, LARP1 has emerged as the putative key specificity factor that regulates translation of 5′TOP mRNAs. LARP1 was first implicated in 5′TOP translational regulation in a proteomic screen for 5′ cap binding proteins whose binding is regulated by mTOR (Tcherkezian *et al.*, 2014). Early studies found that LARP1 also associates with poly(A)-binding protein cytoplasmic 1 (PABPC1) and has a stimulatory effect on mRNA translation (Aoki *et al.*, 2013; Burrows *et al.*, 2010). More recently, it has become clear that LARP1 also plays a key role specifically in 5′TOP translational repression (Fonseca *et al.*, 2015; Philippe *et al.*, 2018). Importantly, a crystal structure revealed the specific binding of the LARP1 DM15 domain to the 5′ cap and the first five nucleotides of the 5′TOP motif (Lahr *et al.*, 2017). This structure suggested that the LARP1 DM15 domain directly binds the 5′ cap and 5′TOP motif and thereby competes with eIF4E and blocks translation initiation. The 5′TOP-binding activity of LARP1 is also regulated by mTORC1 via direct binding of LARP1 to regulatory associated protein of mTORC1 (RPTOR) and phosphorylation of LARP1 by the mTOR kinase on residues adjacent to the DM15 domain has been suggested to induce a conformational rearrangement of LARP1 and inhibit its binding to the 5′TOP motif (Fig. 1.3B, Jia *et al.*, 2021). A pull-down of endogenously tagged eIF4E cross-linked to mRNA 5′ ends (cap-crosslinking and immunoprecipitation (CLIP)) also showed that 5′TOP mRNA reads are specifically depleted upon mTOR inhibition, consistent with a model in which LARP1 specifically competes with eIF4E for binding to these mRNAs (Jensen *et al.*, 2021).

Although LARP1 KO leads to a reduction in the translational repression of 5′TOP mRNAs, experiments by several research groups have consistently found that there is only a partial rescue of 5′TOP mRNAs translation during mTORC1 inhibition (Jia *et al.*, 2021; Philippe *et al.*, 2020). LARP1 was deleted by CRISPR-Cas9 by two research groups in HEK293T cells independently, which made it possible to study 5′TOP translational repression in the absence of any LARP1 protein (Jia *et al.*, 2021; Philippe *et al.*, 2020). Both research groups found that loss of LARP1 is not sufficient for a full rescue of

translational repression, suggesting the existence of one or more additional specificity mediating factors which are regulated downstream of mTORC1, but can function independent of LARP1 binding to the 5′TOP motif. It is possible that KO of LARP1 leads to the upregulation of compensatory proteins that can mediate some 5′TOP translational repression in its stead. In order to identify a potential compensatory role of the LARP1 homologue LARP1B (also called LARP2) , LARP1/LARP1B KO human embryonic kidney 293T cells (HEK293T) were generated (Philippe *et al.*, 2020). LARP1B, however, was not found to contribute to 5′TOP translational repression and therefore cannot explain the persistent sensitivity of 5′TOP mRNAs to mTORC1 inhibition. While there are other LARP family members, they do not contain the DM15 domain that recognizes the 5′TOP motif (Maraia *et al.*, 2017). Consequently, the possible role of an additional factor that contributes to 5′TOP-specific regulation during mTORC1 inhibition has not been fully resolved.

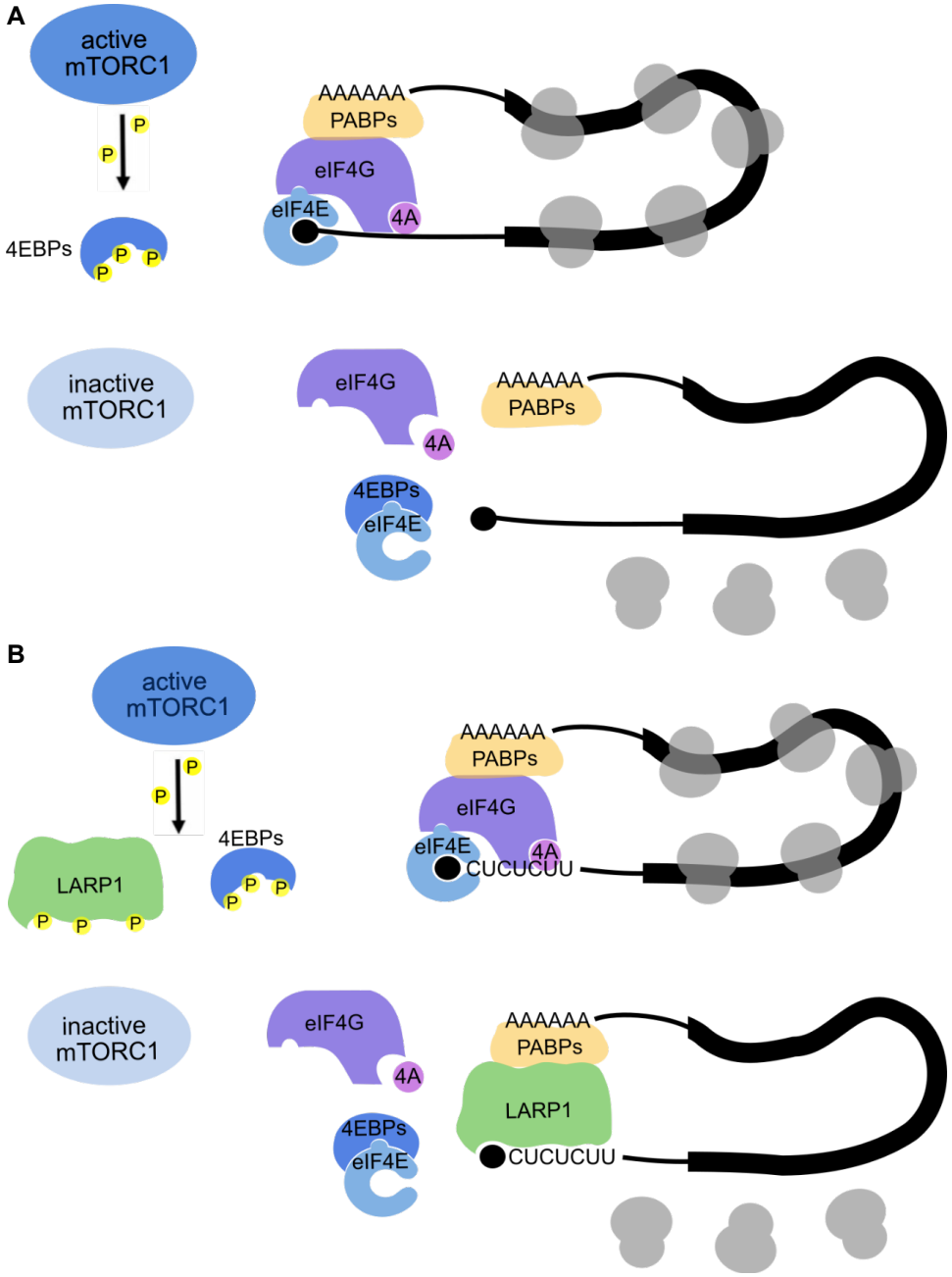

Figure 1.3: Regulation of mRNA translation by mTORC1. (**A**) Canonical mRNA translational control mediated by 4EBPs. When mTORC1 is active, 4EBPs are phosphorylated, preventing their binding to eIF4E. Upon mTORC1 inactivation, 4EBPs are dephosphorylated and sequester eIF4E, thereby inhibiting cap-dependent mRNA translation globally. (**B**) 5′TOP mRNA selective translational control mediated by LARP1 and/or 4EBP proteins. LARP1 has been proposed to be similarly regulated in its activity as 4EBPs, becoming dephosphorylated and active upon mTORC1 inactivation. LARP1 has been shown to directly bind the cap and first five nucleotides of a 5′TOP oligo (Lahr *et al.*, 2017).

1.4 Mechanism of LARP1's interaction with 5′TOP transcripts

LARP1 is a large multidomain protein (1,096 amino acids) that contains a La-module and the DM15 domain, however, most of the protein is predicted to be disordered (Schwenzer *et al.*, 2021). While the DM15 domain's interaction with the 5′TOP motif has been extensively biochemically and structurally characterized, how the rest of the protein may contribute to regulation of 5′TOP transcripts is less well understood (Cassidy *et al.*, 2019; Lahr *et al.*, 2017).

In vitro RNA-binding studies of the LARP1 La-motif have identified a sequence preference for both poly(A) RNAs as well as pyrimidine-rich sequences that are similar to the 5′TOP motif, but lack the 5′ cap (Al-Ashtal *et al.*, 2019). Interestingly, it was found that the La-motif may interact with poly(A) RNA and the pyrimidine sequence simultaneously suggesting that this domain has at least two distinct RNA-binding surfaces. The La-module, consisting of a La-motif followed by an RNA recognition motif (RRM), is the common characteristic of the family of Small RNA binding exonuclease protection factor La (SSB/LA) and La-related proteins (LARPs), and combines two distinct RNA-binding activities. While it was assumed that LARP1 shares this domain architecture, recent experiments demonstrate that LARP1 only contains the La-motif, and the downstream region thought to be an RRM is unfolded (Kozlov *et al.*, 2022). The in vivo RNA-binding specificity of full-length LARP1 has also been determined using photoactivatable ribonucleoside-enhanced crosslinking and immunoprecipitation (PAR-CLIP), which determined that LARP1 binds to pyrimidine-rich sequences in the 5′UTR of transcripts and this interaction is enhanced upon mTOR inhibition (Hong *et al.*, 2017). The exact 5′TOP sequence, however, was not specifically identified by PAR-CLIP and the pyrimidine nucleotides were located distally from the cap in the 5′UTR though this discrepancy might arise for technical reasons associated with library preparation or biases caused by T1 RNase digestion. Interestingly, LARP1 was also found to bind to the 3′UTR of transcripts, albeit with limited sequence specificity. Additionally, LARP1 also contains a PABP-interacting motif-2 (PAM2) downstream of the La-motif that enables it to interact with the mademoiselle domain of PABPC1 (Mattijssen *et al.*, 2021). This interaction with PABPC1 and, potentially, the polyA tail has been found to protect poly(A) tail length and stabilize the mRNA (Aoki *et al.*, 2013; Mattijssen *et al.*, 2021; Ogami *et al.*, 2022).

It remains unclear if the La-module and DM15 domain are able to simultaneously interact with the 5′TOP motif, PRTE, 3′UTR, poly(A) tail and PABC1 of the same transcripts or if any of these interactions are mutually exclusive and how the combination of the interactions affects 5′TOP regulation. While the La-motif and DM15 domain are separated by ∼400 amino acids that do not contain any known globular domains, AlphaFold predicts that this region may not be entirely disordered and could bring the La-motif and DM15 domain in close physical proximity (Figure 1.4) (Jumper *et al.*, 2021). Though this conformation requires experimental validation, nonetheless, it suggests that the function of the individual domains may be more tightly coupled than previously appreciated and provides a framework for further characterization. It should be noted, however, that the individual isolated La-motif and DM15 domains have been shown to retain functionality indicating that they can function autonomously to some extent (Jia *et al.*, 2021; Philippe *et al.*, 2018).

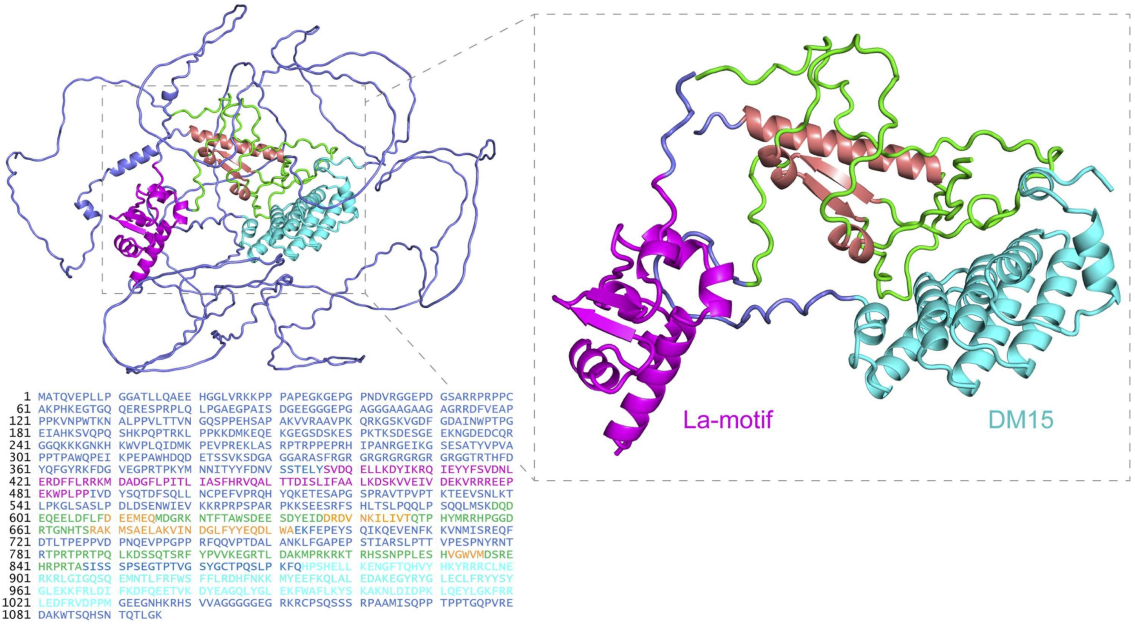

Figure 1.4: AlphaFold prediction of full-length human LARP1 structure. The known structured domains of the La-motif and DM15 are shown in magenta and cyan, respectively. Note the extensive disordered regions shown in blue. Additional predicted structural elements are marked in orange (with connecting loops in green) and could bring the La-motif and DM15 domain in close proximity. Shown here is the 1096 aa isoform, which is the main isoform expressed in human cells (Schwenzer *et al.*, 2021).

Though the regulation of 5′TOP translation and LARP1 has been well described, loss of LARP1 has also been found to result in a specific decrease in the mRNA stability of 5′TOP mRNAs (Aoki *et al.*, 2013; Gentilella *et al.*, 2017). As 5′TOP mRNAs are some of the most stable mRNAs in mammalian cells, it is tempting to speculate that LARP1 functions to protect this class of mRNAs from degradation and directly contributes to their high stability. This raises the question of how LARP1 is specifically recruited to these mRNAs to mediate stability under nutrient-rich conditions, when the DM15 domain is phosphorylated and unable to bind the 5′TOP motif (Jia *et al.*, 2021). Consequently, it has been suggested that LARP1 binds to 5′TOP mRNAs via its La-motif to either the 5′TOP or PRTE (in a cap-independent manner that does not block eIF4E) and the poly(A) tail and PABPC1, potentially circularizing mRNAs to allow translation while protecting them from decay (see Figure 1.5). While evidence exists for the close-loop model in promoting translation and stability in yeast, current single-molecule RNA imaging in human cells has indicated that translating mRNAs are less compact than translationally-inhibited ones (Adivarahan *et al.*, 2018; Amrani *et al.*, 2008). Therefore, LARP1 may specifically promote a closed-loop confirmation for only 5′TOP mRNAs to selectively promote their stability.

While the closed-loop model of 5′TOP mRNPs provides an explanation for their enhanced stability, it is not entirely clear where the specificity for 5′TOP transcripts comes from when mTORC1 is active and eIF4E is presumably bound to the 5′ cap. Additionally, it is not known if eIF4E and LARP1 can simultaneously interact on the same 5′UTR and how this might influence translation initiation. Recent structural studies of the human 48S preinitiation complex have suggested that initiation occurs

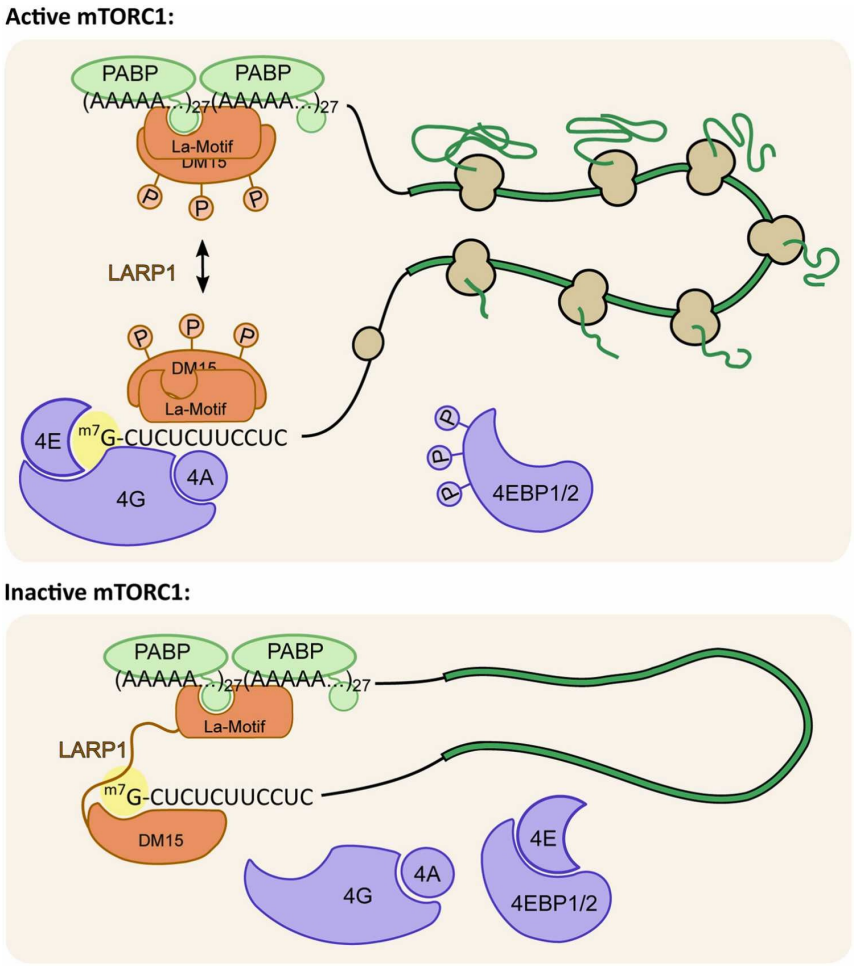

Figure 1.5: Interaction of LARP1 with a 5′TOP mRNA. Under nutrient-rich conditions (top), mTORC1 is active and phosphorylates both 4EBP1/2 and LARP1. The eIF4F complex (composed of eIF4E, eIF4G, and eIF4A) can bind the m7G cap and recruit the 43S preinitiation complex. Under these conditions, LARP1's La-motif can bind to either the 5′TOP motif or the poly(A)-tail and LARP1's PAM2 motif can bind the mademoiselle domain of PABPC1. Under nutrient starvation (bottom), mTORC1 is inactive and 4EBP1/2 and LARP1 are dephosphorylated. 4EBP1/2 sequesters eIF4E, thereby blocking translation initiation, while LARP1 can bind the m7G cap with its DM15 domain and its La-motif and PAM2 could bind to the poly(A)-tail and PABPC1, respectively. Simultaneous binding of a single LARP1 molecule to both mRNA ends is possible under both active and inactive mTORC1 and could serve to protect the mRNAs from degradation. Further research will be needed to verify the existence of such LARP1-mediated 5′TOP mRNA closed loops and their functional implication.

via a cap-tethered mechanism that results in a "blind spot" of ∼30 nucleotides adjacent to the 5′ cap, which could enable translation initiation to be compatible with LARP1 binding (Brito Querido *et al.*, 2020). A recent study showed that LARP1 has a protective effect on 5′TOP mRNA levels under prolonged mTOR inhibition, which is thought to preserve these mRNAs for reactivation of translation in a closed-loop conformation via DM15 binding to the 5′TOP and La-motif binding to the poly(A)tail/PABPC1 (Fuentes *et al.*, 2021). It is possible that the closed-loop conformation only becomes relevant under mTOR inhibition, when LARP1 can circularize 5′TOP mRNAs without interference from translation initiation, thereby protecting them from the decay machinery.

1.5 Summary

While the biological importance of the regulation of translation and stability of 5′TOP mRNAs during normal cell growth and disease has long been appreciated, the molecular mechanisms that enable this specific control have been challenging to elucidate. Any inhibition of a core cellular process that impacts ribosome biogenesis can be expected to have global pleiotropic effects making it difficult to isolate specific pathways, particularly when studying prolonged deprivation of amino acids or growth factors. While acute pharmacological inhibition of mTOR mitigates some of these experimental complications, the inhibition of translation or changes in mRNA stability are usually determined using ensemble techniques that measure the average change of all the 5′TOP mRNAs in thousands or even millions of cells. Consequently, cellular heterogeneity can mask differences between models for 5′TOP regulation and has prevented a detailed kinetic analysis of the effect of mTOR inhibition.

The recent development of single-molecule methods for directly imaging mRNAs and their translation and degradation provides an opportunity to further characterize the regulation of 5′TOP mRNAs (Horvathova *et al.*, 2017; Tanenbaum *et al.*, 2014). Using these approaches, it will be possible to directly measure both the fraction of individual mRNAs undergoing active translation as well as their ribosome occupancy in living cells (Tanenbaum *et al.*, 2014). Previously, we have characterized the localization and translation of 5′TOP reporter mRNAs in cells treated with sodium arsenite, which activates the integrated stress response, but does not inhibit mTOR (Mateju *et al.*, 2020; Wilbertz *et al.*, 2019). These experiments showed that stable association of a 5′TOP reporter mRNA to stress granules and processing bodies required both LARP1 and the 5′TOP motif indicating the potential of this system to characterize LARP1- and 5′TOP-dependent regulation. We anticipate that single-molecule imaging will enable quantification of the magnitude and timing of 5′TOP regulation during mTOR inhibition, and clarify how the *trans*-acting factors LARP1 and 4EBP1/2 exert their effects. Using these tools, it will be possible to precisely compare and contrast the efficiency of translational repression of a 5′TOP reporter in cells depleted of either LARP1 or 4EBP1/2 and long-term imaging of mRNA reporters will also enable researchers to precisely quantify translation parameters of 5′TOP mRNAs (e.g., initiation rates and bursting kinetics) (Livingston *et al.*, 2022). Finally, further advances in imaging technologies may soon make it possible to directly observe binding of individual *trans*-acting factors to the 5′TOP motif in order to measure their impact on the translation status of individual mRNAs.

In parallel, advances in pull-down assays such as cap-CLIP will shed further light onto the regulators involved in displacing eIF4E from 5′TOP mRNAs upon mTOR inhibition. It will be interesting to see whether the specific displacement of eIF4E can still occur in absence of either LARP1 or 4EBP1/2, which will allow functional separation of the role of the cap-binding regulators of 5′TOP translation, and clarify whether their action is coupled or independent from each other.

1.6 Aim of this thesis

The identity of the key regulatory factor which directly binds to and controls 5′TOP mRNA translation has been challenging to elucidate, with recent evidence converging on LARP1 and 4EBP1/2. The goal of this thesis is a detailed analysis of the dynamics of 5′TOP mRNA translation in mTORC1 active and inactive cells, addressing the following main questions:

- What are the dynamics of 5′TOP mRNA translation under mTORC1 inhibition?
- How do the dynamics of 5′TOP mRNA translation change upon loss of the proposed key regulatory factors LARP1 and 4EBP1/2?
- What is the role of LARP1 in regulating the abundance of endogenous 5′TOP mRNA transcripts?

To address these questions, I employed a single-molecule imaging approach to directly visualize and quantify the translation of 5′TOP reporter mRNAs in living cells uncoupled from confounding effects of transcription and mRNA stability. This revealed a dominant role of 4EBP1/2 in mediating 5′TOP mRNA translational repression. Furthermore, I measured the changes in global mRNA half-lives in the absence of LARP1, finding a highly selective role of LARP1 in stabilizing 5′TOP mRNAs in mTOR active cells. The results of this work are described in chapter 2, and its implications are discussed in chapter 3.

Chapter 2

Regulation of 5′TOP mRNA translation and stability

Tobias Hochstoeger[1,2], Panagiotis Papasaikas[1], Ewa Piskadlo[1], Jeffrey A. Chao[1]*

[1] Friedrich Miescher Institute for Biomedical Research, 4058 Basel, Switzerland
[2] University of Basel, 4003 Basel, Switzerland
* Corresponding author

Contribution

The contents of this chapter have been published in *Science Advances* on the 16th February 2024 (Hochstoeger *et al.*, 2024). This project was a collaboration with the other authors listed in the manuscript. My contributions included the conception of this study and the writing of the manuscript together with Jeffrey A. Chao as well as carrying out the experiments and their interpretation. Namely, I carried out the live-cell imaging experiments and prepared samples for transcriptomic analyses. Panagiotis Papasaikas and Ewa Piskadlo performed the bioinformatic analysis of global mRNA half-lives.

2.1 Abstract

A central mechanism of mTORC1 signaling is the coordinated translation of ribosomal protein and translation factor mRNAs mediated by the 5′TOP. Recently, LARP1 was proposed to be the specific regulator of 5′TOP mRNA translation downstream of mTORC1, while 4EBP1/2 were suggested to have a general role in translational repression of all transcripts. Here, we employ single-molecule translation site imaging of 5′TOP and canonical mRNAs to study the translation of single mRNAs in living cells. Our data reveals that 4EBP1/2 has a dominant role in repression of translation of both 5′TOP and canonical mRNAs during pharmacological inhibition of mTOR. In contrast, we find that LARP1 selectively protects 5′TOP mRNAs from degradation in a transcriptome-wide analysis of mRNA half-lives. Our results clarify the roles of 4EBP1/2 and LARP1 in regulating 5′TOP mRNAs and provide a framework to further study how these factors control cell growth during development and disease.

2.2 Introduction

For cellular homeostasis, ribosome biogenesis needs to be tightly coupled to nutrient availability. In eukaryotic cells, mTORC1 is the central signaling hub that integrates nutrient cues to match cell growth by stimulating or inhibiting ribosome biogenesis (Battaglioni *et al.*, 2022; Liu & Sabatini, 2020). When nutrients are available, active mTORC1 promotes translation by the phosphorylation of key substrates such as S6K1/2 and 4EBP1/2 that stimulate eIF4F assembly and translation. When nutrients are limited, mTORC1 substrates are dephosphorylated, allowing 4EBP1/2 to bind and sequester the cap-binding eIF4E, thereby inhibiting mRNA translation initiation. In addition, LARP1 has recently been described as a direct mTORC1 substrate and translational regulator (Fonseca *et al.*, 2015; Hong *et al.*, 2017; Jia *et al.*, 2021; Philippe *et al.*, 2018; Tcherkezian *et al.*, 2014). While mTORC1-dependent translation regulation acts on all mRNAs via multiple routes, it exerts a much more rapid and pronounced effect on ribosomal protein and translation factor mRNAs (∼100 mRNAs) that carry a 5′TOP motif (4-15 pyrimidines) directly adjacent to the 5′ cap (Meyuhas & Kahan, 2015). While it has been well established that the 5′TOP motif is both essential and sufficient for rapid mTORC1-mediated translational regulation (Avni *et al.*, 1994; Biberman & Meyuhas, 1997), the underlying molecular mechanism has been challenging to resolve (Berman *et al.*, 2020). Both 4EBP1/2 and LARP1 have been found to contribute to 5′TOP translational inhibition, as loss of either factor partially relieved 5′TOP translational repression in cells acutely treated with the mTOR inhibitor Torin1 (Fonseca *et al.*, 2015; Hsieh *et al.*, 2012; Miloslavski *et al.*, 2014; Philippe *et al.*, 2018; Thoreen *et al.*, 2012). Though binding of 4EBP1/2 to eIF4E reduces cap-dependent translation of all transcripts, eIF4E may have lower affinity for 5′TOP mRNAs, which could make them more sensitive to mTORC1 inhibition (Lindqvist *et al.*, 2008; Tamarkin-Ben-Harush *et al.*, 2017). Recently, co-crystal structures of LARP1 bound to both the 5′ cap and the first five nucleotides of a 5′TOP oligo suggested that LARP1 could specifically repress 5′TOP mRNAs upon mTORC1 inhibition, leading to a model in which dephosphorylated

LARP1 specifically binds the 5′ end of 5′TOP mRNAs to prevent assembly of the eIF4F complex (Lahr *et al.*, 2017).

An additional layer of ribosome biogenesis control is the pool of 5′TOP mRNAs available for translation, which are among the most highly expressed and stable transcripts in eukaryotic cells (Herzog *et al.*, 2017; Schofield *et al.*, 2018). LARP1 has been found to associate with PABPC1 and inhibit deadenylation of mRNA transcripts (Kozlov *et al.*, 2022; Mattijssen *et al.*, 2021; Ogami *et al.*, 2022). It is currently unclear how LARP1 is recruited to the mRNAs it stabilizes, the importance of the 5′TOP motif for target selection, and the relevance of mTORC1 activity in this process. Crosslinking studies have found LARP1 associates with thousands of mRNAs including 5′TOP mRNAs and a subset of these transcripts have increased binding upon mTORC1 inhibition (Hong *et al.*, 2017; Mura *et al.*, 2015; Smith *et al.*, 2020). In contrast, polyA tail sequencing in mTORC1 active cells have found LARP1 to inhibit mRNA deadenylation globally, but that 5′TOP transcripts were among the most strongly affected transcripts upon LARP1 depletion (Park *et al.*, 2023).

In this study, we sought to clarify the roles of LARP1 and 4EBP1/2 in regulating the translation and stability of 5′TOP mRNAs. Direct measurements of translation of 5′TOP and non-5′TOP (canonical) mRNAs using single-molecule SunTag imaging revealed a dominant role of 4EBP1/2 in mediating 5′TOP translational repression. In contrast, we find a highly selective role of LARP1 in protecting 5′TOP mRNAs from degradation by measuring transcriptome-wide changes in mRNA half-lives using (SH)-linked alkylation for the metabolic sequencing of RNA (SLAMseq). Our study provides insights into the distinct roles of LARP1 and 4EBP1/2 in mediating 5′TOP regulation, and a framework for further investigations into the mechanisms by which these factors regulate cell growth under normal physiological conditions and disease.

2.3 Results

2.3.1 Single-molecule imaging of translation during mTOR inhibition

To study the regulation of translation during mTOR inhibition, we engineered Henrietta Lacks cells (HeLa) that express fluorescent proteins for single-molecule imaging of mRNA (MS2 coat protein (MCP)-Halo) and translation (scFV-GFP), together with the reverse tetracycline-controlled transactivator to enable induction of reporter mRNAs (Wilbertz *et al.*, 2019). Into this cell line, we integrated two different constructs into a single genomic locus under the control of a doxycycline-inducible promoter. The reporter mRNAs were identical except for their 5′ untranslated region (UTR), where one contains the full-length 60S ribosomal protein L32 (RPL32) 5′UTR that begins with a 5′TOP motif, and the other has a canonical 5′UTR that does not contain a 5′TOP sequence. The coding sequence encodes 24 GCN4 epitope tags for translation site imaging (SunTag, Tanenbaum *et al.*, 2014) followed by Renilla luciferase for bulk measurements of translation and the FKBP12-derived destabilization domain to reduce the accumulation of mature proteins (Banaszynski *et al.*, 2006). In

addition, the 3′UTR contains 24 MS2 stem-loops for mRNA imaging (Fig. 2.1A). The 5′ end of both reporter mRNAs was sequenced to determine the transcription start sites. All 5′TOP transcripts contained a 5′TOP motif and the canonical transcripts initiated with AGA, which is similar to the most common transcription start site (Fig. 2.2) (Carninci *et al.*, 2006). To inhibit mTOR, we used the ATP-competitive inhibitor Torin1, which has been widely used to study the translation of 5′TOP mRNAs. For both the 5′TOP and canonical mRNA reporter cell lines, Torin1 treatment for 1 hour resulted in inhibition of mTORC1 as seen by 4EBP1 dephosphorylation, consistent with previous results (Fig. 2.3) (Smith *et al.*, 2020; Thoreen *et al.*, 2009).

To observe the effect of mTORC1 inhibition on translation, we induced expression of the reporter mRNAs in both cell lines and imaged them in either the presence or absence of Torin1. Treatment with Torin1 was found to strongly repress translation of most 5′TOP transcripts as seen by the disappearance of scFv-GFP spots that co-localized with mRNA spots, whereas the canonical mRNAs were largely unaffected (Fig. 2.1B). For quantification of single mRNAs and their translation, we employed a high-throughput image analysis pipeline that tracks individual mRNAs and measures the corresponding SunTag intensities. mRNA trajectories were determined using single-particle tracking of MCP-Halo spots, and scFv-GFP intensities at those same coordinates were quantified for each mRNA as background corrected mean spot intensity (SunTag intensity). Using this analysis pipeline, we quantified the translation of >1000 mRNAs for both the 5′TOP and canonical mRNA cell lines (Fig. 2.1C), which revealed a broad distribution of SunTag intensities for both types of transcripts indicating a heterogeneity of ribosomes engaged in translation of individual transcripts (Tanenbaum *et al.*, 2014; Wilbertz *et al.*, 2019). The average SunTag intensity for the 5′TOP mRNAs was slightly lower compared to the canonical mRNAs indicating fewer ribosomes engaged in translation when mTOR is active (Fig. 2.1C). The mean SunTag intensity for the 5′TOP mRNAs decreased markedly upon Torin1 treatment, whereas the mean SunTag intensity of the canonical mRNAs decreased only slightly.

While changes in SunTag intensity indicate differences in ribosome number, translation site imaging can also be used to quantify the fraction of transcripts actively translating within a cell. Puromycin treatment, which inhibits translation due to premature termination, was used to measure SunTag spot intensities in the absence of translation to calibrate a threshold for identifying translating mRNAs (>1.5-fold over background, Fig. 2.4). Quantifying translation as the fraction of translating mRNAs per cell revealed slightly fewer translating 5′TOP mRNAs (mean: 74%) compared to the canonical mRNAs (mean: 86%) when mTOR is active (Fig. 2.1D). Upon 1 hour Torin1 treatment, the fraction of translating 5′TOP mRNAs per cell decreased drastically (mean: 16%), though many cells retained a minor fraction of translating 5′TOP mRNAs. In contrast, the fraction of translating canonical mRNAs decreased only slightly upon Torin1 treatment (mean: 77%). To determine whether the remaining fraction of translating 5′TOP mRNAs after 1 hour Torin1 treatment represented stalled ribosomes, Torin1 treated cells were co-treated with harringtonine, which stalls ribosome at the start codon and allows elongating ribosomes to run-off. Addition of harringtonine abolished the remaining translation

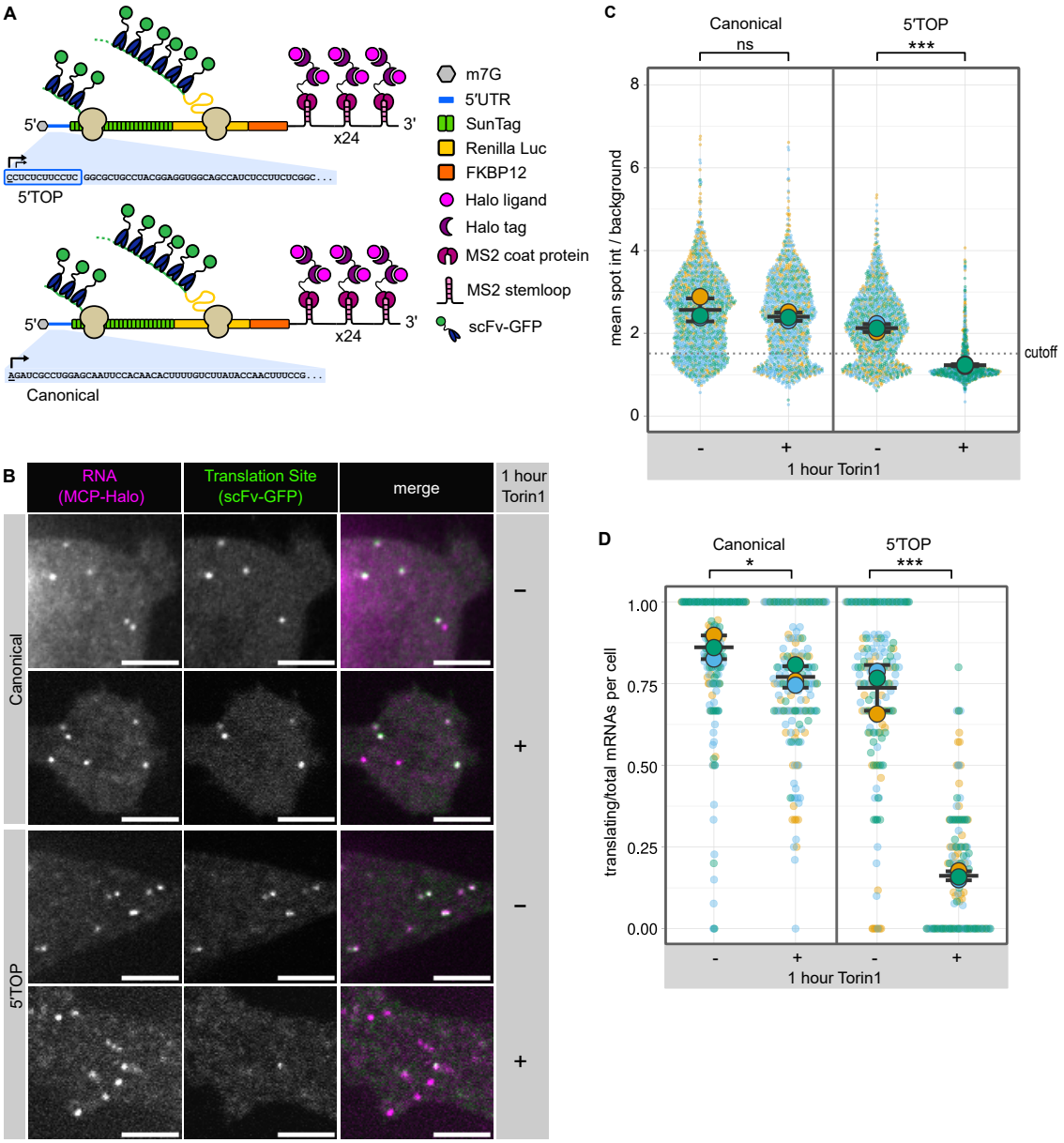

Figure 2.1: Single-molecule imaging recapitulates 5′TOP translational repression. (**A**) Schematic representation of reporter mRNAs for single molecule imaging of translation. The 5′TOP reporter contains the full-length RPL32 5′UTR, whereas the canonical reporter has a control 5′UTR of similar length. Black arrows indicate transcription start sites. (**B**) Representative images of canonical and 5′TOP reporter mRNAs (MCP-Halo foci, magenta) undergoing translation (scFv-GFP foci, green) in absence or presence of mTOR inhibitor Torin1 (250 nM, 1 hour). Scale bars = 5 μm. (**C**) Translation site intensities of canonical and 5′TOP reporter mRNAs quantified in absence and presence of Torin1 (250 nM, 1 hour). SunTag intensities are plotted for all mRNAs (colored circles) overlaid with the mean ± SD (≥1089 mRNAs per condition, n=3). (**D**) Fraction of mRNAs undergoing translation quantified per cell for canonical and 5′TOP reporter in absence or presence of Torin1 (250 nM, 1 hour). Values are plotted for each cell (colored circles) overlaid with the mean ± SD (≥162 cells per condition, n=3). For statistics, unpaired t tests were performed, with statistical significance claimed when $p < 0.05$ (ns = not significant, * = $p < 0.05$, *** = $p < 0.001$).

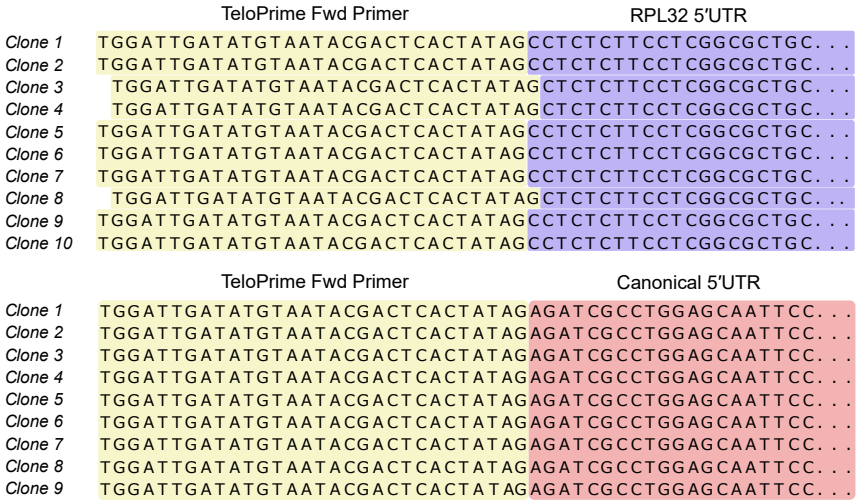

Figure 2.2: Validation of TSS selection. Mapping of canonical and 5′TOP reporter TSS using cap-specific adaptor ligation. Sequencing results for single clones of each reporter are shown with the TeloPrime adaptor sequence joined to the start of the reporter 5′UTR. For the 5′TOP reporter, there is some variability in the precise cytosine in the +1 position, however, all sequenced clones initiate with a cytosine and contain a 5′TOP motif.

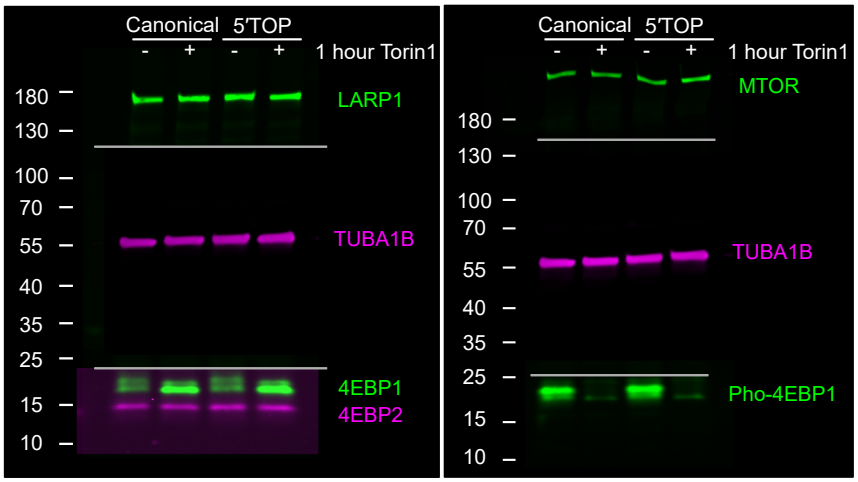

Figure 2.3: mTORC1 signaling in canonical and 5′TOP mRNA cell lines treated with Torin1. Western blot analysis of mTORC1 signaling using a phosphorylation-specific antibody against 4EBP1. Upon Torin1 addition (250 nM, 1 hour), 4EBP1 is dephosphorylated, as seen by the lower migration size of 4EBP1 (left), and the disappearance of Pho-4EBP1^{Ser65} (right). Lines indicate cut membrane pieces probed with different mouse (magenta) and rabbit (green) antibodies, and imaged together using two-color fluorescent imaging. Brightness and contrast were individually adjusted for each antibody shown.

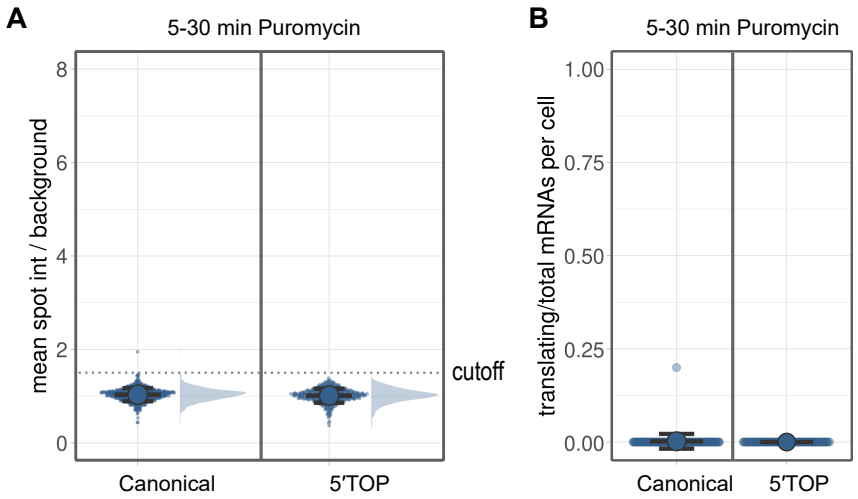

Figure 2.4: Translation site intensities following global translation inhibition. (**A**) Quantification of translation site intensities after puromycin treatment (100 µg/ml, 5-30 min). SunTag intensities are plotted for >400 mRNAs per condition overlaid with the mean ± SD. A cutoff of 1.5 (dotted line) was determined to distinguish translating from non-translating mRNAs. (**B**) Fraction of mRNAs undergoing translation after puromycin treatment. Values are plotted for each cell overlaid with the mean ± SD (≥87 cells per condition).

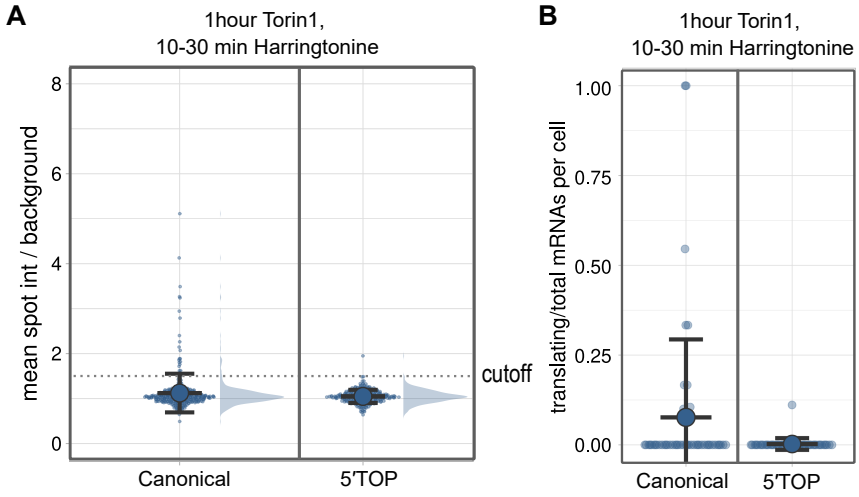

Figure 2.5: Translation site intensities following ribosome run-off. (**A**) Quantification of translation site intensities after mTOR inhibition (250 nM Torin1, 1 hour) followed by translation inhibition (3 µg/ml Harringtonine, 10-30 min). SunTag intensities are plotted for >250 mRNAs per condition overlaid with the mean ± SD. (**B**) Fraction of mRNAs undergoing translation after mTOR inhibition (250 nM Torin1, 1 hour) followed by translation inhibition (Harringtonine 3 µg/ml, 10-30 min). Values are plotted for each cell overlaid with the mean ± SD (≥46 cells per condition).

sites in the Torin1-treated 5′TOP cell line within 10 minutes (Fig. 2.5), demonstrating that the low number of 5′TOP mRNAs that co-localize with SunTag signal are still actively translating.

To verify our findings with other mTOR inhibitors, we repeated the imaging of canonical and 5′TOP mRNAs with the allosteric mTOR inhibitor Rapamycin (Wullschleger *et al.*, 2006) and the ATP-competitive mTOR inhibitors PP242 and TAK228 (Apsel *et al.*, 2008; Jessen *et al.*, 2009). While PP242 and TAK228 treatment closely mirror the response seen for Torin1 treatment, Rapamycin treatment did not significantly alter the translation of either canonical or 5′TOP mRNAs (Fig. 2.6). Rapamycin insensitivity has been described for a number of cell lines including HeLa (Hassan *et al.*, 2014), and, in agreement with previous studies (Huo *et al.*, 2012; Thoreen *et al.*, 2009), we find that Rapamycin selectively inhibits S6K1 phosphorylation, while levels of phosphorylated 4EBP1 remain high (Fig. 2.7). Taken together, our data captures both inter- and intracellular variability in the translation of canonical and 5′TOP mRNAs in the presence and absence of mTOR inhibitors, providing direct translation measurements independent of effects arising from transcriptional regulation or mRNA stability.

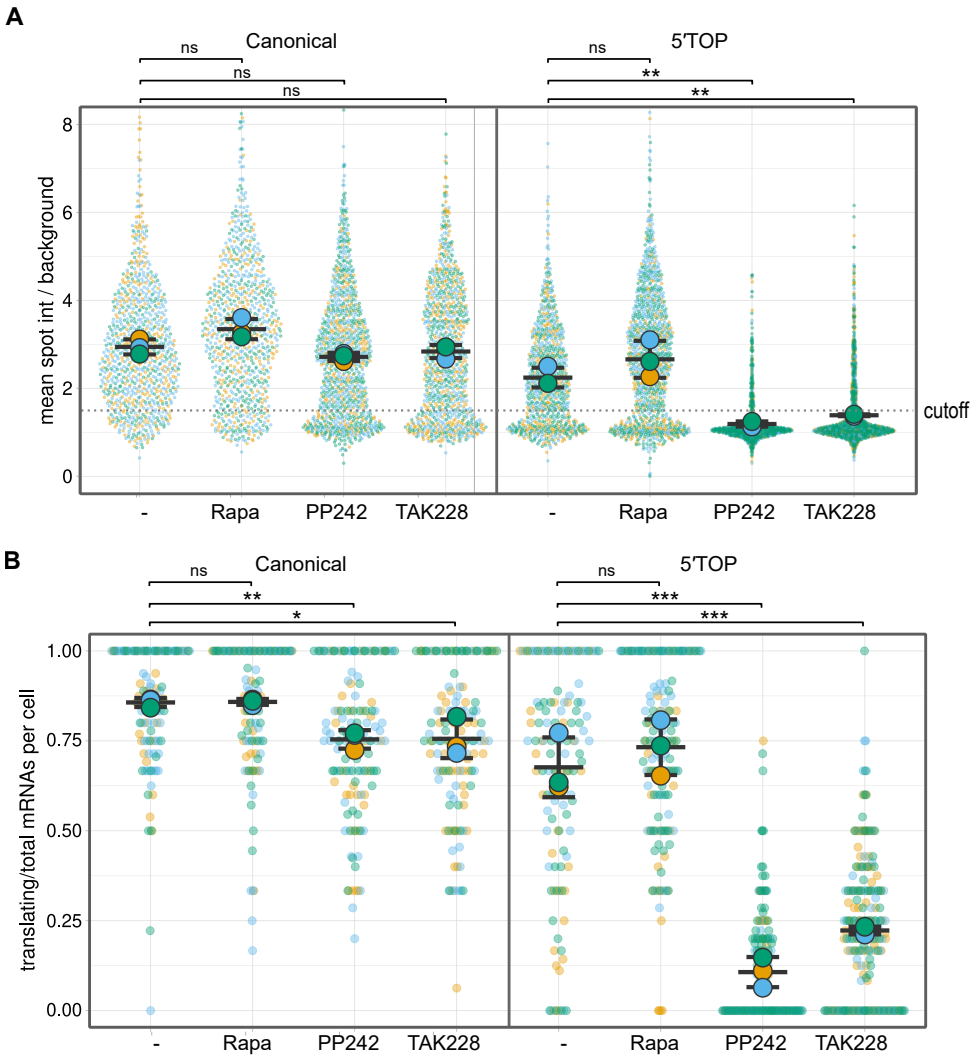

Figure 2.6: Single-molecule imaging of 5′TOP translational repression using additional mTOR inhibitors. (**A**) Quantification of translation site intensities of canonical and 5′TOP mRNAs in absence or presence of mTOR inhibitors Rapamycin (100 nM, 1 hour), PP242 (2.5 μM, 1 hour), or TAK228 (250 nM, 1 hour). SunTag intensities are plotted for all mRNAs overlaid with the mean ± SD (≥821 mRNAs per condition, n=3). (**B**) Fraction of mRNAs undergoing translation quantified per cell for canonical and 5′TOP reporter cell lines in absence or presence of Rapamycin (100 nM, 1 hour), PP242 (2.5 μM, 1 hour), or TAK228 (250 nM, 1 hour). Values are plotted for each cell overlaid with the mean ± SD (≥112 cells per condition, n=3). For statistics, unpaired t tests were performed, with statistical significance claimed when $p < 0.05$ (ns = not significant, * = $p < 0.05$, ** = $p < 0.01$, *** = $p < 0.001$).

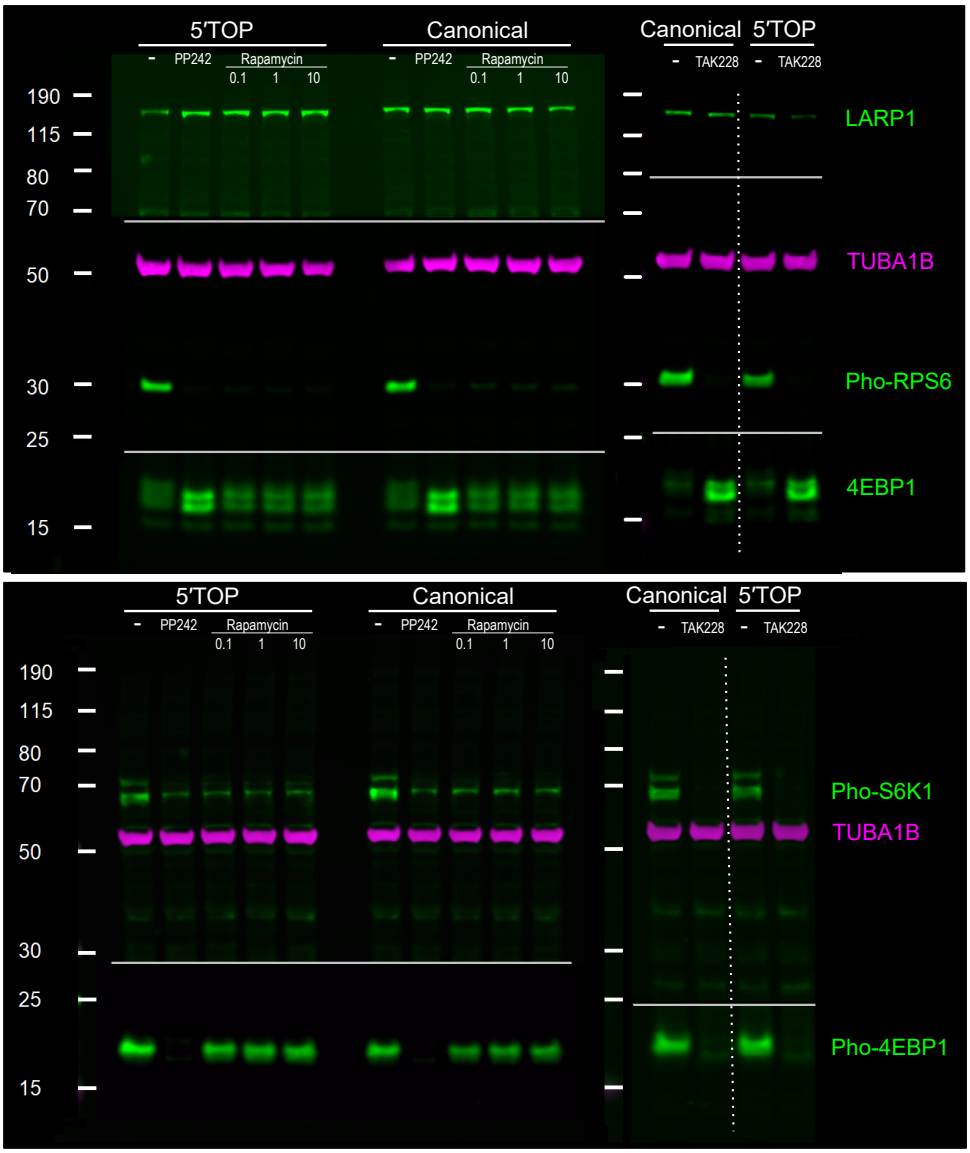

Figure 2.7: Western blot analysis of mTORC1 activity in cells treated with additional mTOR inhibitors. To inhibit mTOR, cells were treated for 1 hour with Rapamycin (0.1 µM, 1 µM, 10 µM), PP242 (2.5 µM), or TAK228 (250 nM), and mTORC1 activity was measured using phosphorylation-specific antibodies against Pho-RPS6, Pho-S6K1, Pho-4EBP1^{Ser65}, and the shift in migration size of 4EBP1. In agreement with previous studies (Huo *et al.*, 2012; Thoreen *et al.*, 2009), Rapamycin causes substrate-selective inhibition of mTORC1 in HeLa cells, inhibiting Pho-RPS6 and Pho-S6K1, but not Pho-4EBP1 independent of drug concentration.

2.3.2 LARP1 KO partially rescues translation of 5′TOP mRNAs during Torin1 treatment

Recently, LARP1 has been found to specifically bind the 5′TOP motif in an mTOR-dependent manner to regulate translation (Jia *et al.*, 2021; Lahr *et al.*, 2017; Smith *et al.*, 2020). To further investigate the role of LARP1 in translational repression of 5′TOP mRNAs during mTOR inhibition, we generated LARP1 CRISPR-Cas9 KOs in the 5′TOP and canonical mRNA cell lines. Genomic DNA sequencing confirmed frameshift mutations in all alleles of LARP1 exon 4 that are upstream of any domain of known function (aa205-aa240) (Fig. 2.8A and B). Loss of LARP1 protein in the KO cell lines was confirmed by western blot analysis using two LARP1 antibodies targeting either the N- or C-terminal regions, which did not detect alternative LARP1 isoforms (Fig. 2.8C). Importantly, loss of LARP1 did not disrupt the regulation of other mTORC1 targets, as seen by dephosphorylation of 4EBP1, S6K1, and RPS6 upon 1 hour Torin1 treatment (Fig. 2.8D). Consistent with earlier reports in HEK cells, deletion of LARP1 in HeLa cells resulted in decreased cell proliferation (Fonseca *et al.*, 2015; Philippe *et al.*, 2018).

Following the validation of the LARP1 KO cell lines, we quantified the translation of 5′TOP and canonical mRNAs (>600 mRNAs per condition) in the absence of LARP1 (Fig. 2.9). Analysis of SunTag intensities of the canonical and 5′TOP mRNAs revealed similar translation levels in the LARP1 KO compared to wild-type (WT), indicating that LARP1 does not regulate 5′TOP mRNA translation in cells when mTOR is active. Upon 1 hour Torin1 treatment, canonical mRNAs decreased slightly in mean SunTag intensity, whereas the 5′TOP mRNAs decreased more strongly (Fig. 2.10A). Calculating the fraction of translating mRNAs per cell revealed that the canonical mRNAs show a mild response to Torin1 in the absence of LARP1 (mean untreated: 87%, mean 1 hour Torin1: 75%, Fig. 2.10B), mirroring the response observed for the canonical mRNAs in LARP1 WT cells. Interestingly, the 5′TOP mRNAs in LARP1 KO cells displayed a partial rescue of translation upon Torin1 treatment (mean untreated: 79%, mean 1 hour Torin1: 41%) compared to LARP1 WT cells (mean 1 hour Torin1: 16%). The incomplete rescue of 5′TOP mRNA translation in the absence of LARP1 suggested the existence of additional trans-acting factors in mediating 5′TOP translational repression.

One possible *trans*-acting factor that could repress 5′TOP mRNAs in the absence of LARP1 is the homolog LARP1B (also called LARP2), which shares the DM15 domain that binds the 5′TOP motif, though it is lowly expressed in HeLa cells. To test this possibility, we used CRISPR-Cas9 to generate KOs of LARP1B in the LARP1 KO background (Fig. 2.11A). Genomic DNA sequencing of the edited alleles identified frameshift mutations in all alleles of LARP1B exon 4, and PCR confirmed loss of WT LARP1B mRNA (Fig. 2.11B and C). Western blot analysis confirmed unperturbed mTORC1 signaling in the LARP1/1B KO cells, as seen by dephosphorylation of 4EBP1, S6K1, and RPS6 upon 1 hour Torin1 treatment (Fig. 2.11D).

Figure 2.8: Validation of LARP1 knockout cell lines. (**A**) CRISPR-Cas9 editing strategy for deletion of LARP1 protein expression in canonical and 5′TOP mRNA cell lines. Two sgRNAs targeting exon 4 upstream of any domains of known function were used to ensure high editing efficiency in polyploidal HeLa genome (sgRNA 1 taken from Philippe *et al.*, 2018). (**B**) Genotyping of canonical and 5′TOP KO single clonal cell lines used for single-molecule imaging (Fig. 2A, 2B, 2E), showing 100 bp truncations of LARP1 exon 4 resulting in frameshifting and premature termination codons. (**C**) Western Blot analysis of LARP1 protein expression in WT and LARP1 KO single clonal cell lines. Clones B5 and E6 were used for single-molecule imaging of the canonical and 5′TOP mRNAs respectively.

Figure 2.8: *continued from previous page:* Note the presence of a weak shorter band of LARP1 (highlighted with *) for some clones, indicating the presence of an in-frame truncated allele of LARP1 in these clones (KD). (**D**) Western blot analysis of mTORC1 signaling in canonical and 5′TOP LARP1 KO cell lines used for single-molecule imaging. Upon 1 hour Torin1 (250 nM), mTORC1 targets are dephosphorylated, as shown with phosphorylation-specific antibodies for Pho-4EBP1^{Ser65}, Pho-S6K1 and Pho-RPS6. 4EBP1 dephosphorylation is also seen by the lower migration size of dephosphorylated 4EBP1. Lines indicate cut membrane pieces probed with different mouse (magenta) and rabbit (green) antibodies, and imaged together using two-color fluorescent imaging. Brightness and contrast were individually adjusted for each antibody shown.

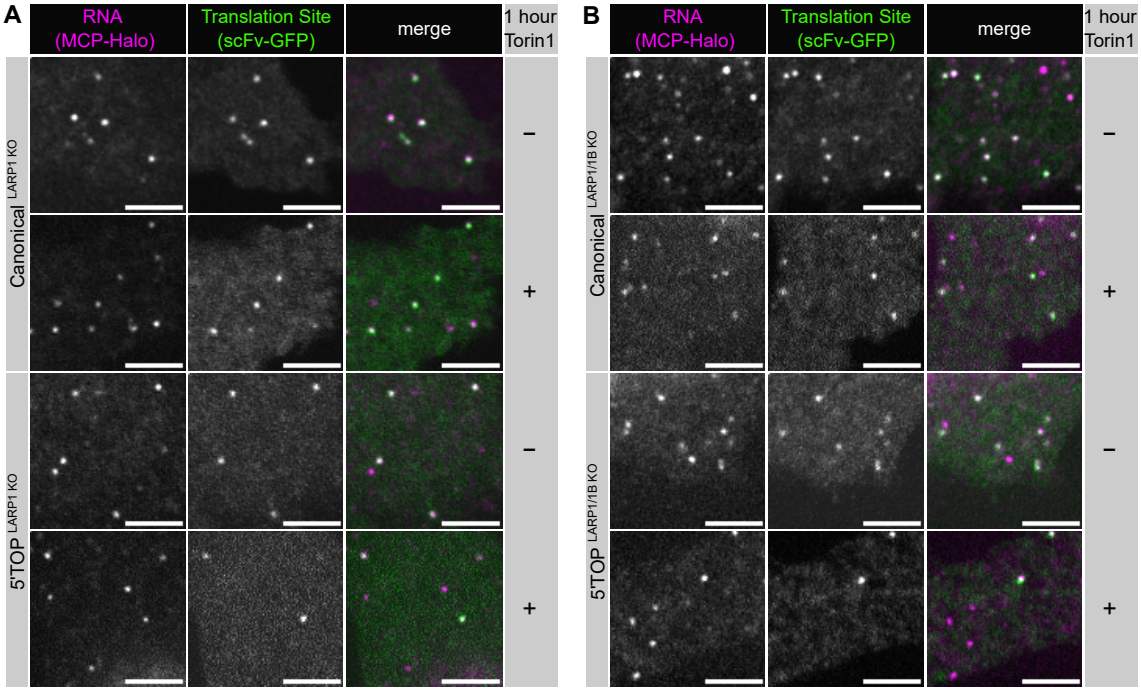

Figure 2.9: Single-molecule imaging of translation in LARP1 KO and LARP1/1B KO cell lines. (**A**) Representative images of LARP1 KO cell lines expressing canonical and 5′TOP mRNAs (MCP-Halo foci, magenta) undergoing translation (scFv-GFP foci, green) in the absence or presence of mTOR inhibitor Torin1 (250 nM, 1 hour). (**B**) Representative images of LARP1/1B KO cell lines expressing canonical and 5′TOP mRNAs (MCP-Halo foci, magenta) undergoing translation (scFv-GFP foci, green) in absence or presence of mTOR inhibitor Torin1 (250 nM, 1 hour). Scale bars = 5 μm.

Following the validation of the LARP1/1B KO cell lines, we quantified the translation of 5′TOP and canonical mRNAs (>200 mRNAs per condition) in the absence of LARP1/1B (Fig. 2.9B). Both the distribution of SunTag intensities (Fig. 2.10C) and the fraction of translating canonical and 5′TOP mRNAs per cell (Fig. 2.10D) responded similarly to Torin1 treatment (1 hour) as obtained for LARP1 KO cells, suggesting that LARP1B does not affect 5′TOP translational regulation. These results are consistent with an earlier study in HEK cells, which also found that translational repression of endogenous 5′TOP transcripts could not be rescued further by combinatory deletion of LARP1/1B (Philippe *et al.*, 2020), arguing against functional redundancy of LARP1 and LARP1B.

While we did not observe a rescue of 5′TOP translation when cells were treated with Torin1 for 1 hour, we could not exclude the possibility that the effect of loss of LARP1/1B might be more pronounced at other time points. To characterize the kinetics of Torin1-mediated translational inhibition, we

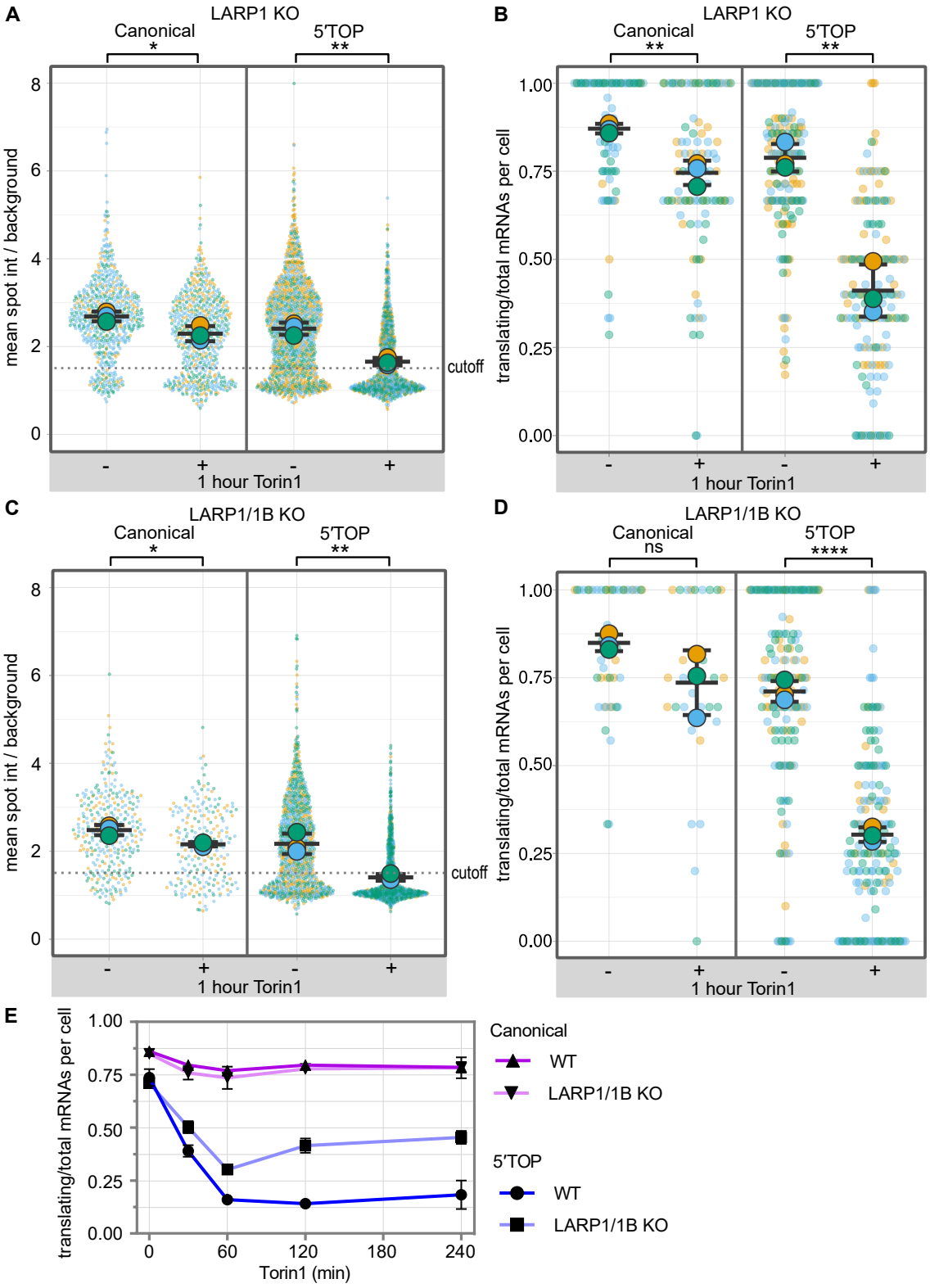

Figure 2.10: Loss of LARP1 partially alleviates 5′TOP translational repression during Torin1 treatment. (**A**) Quantification of translation site intensities in LARP1 KO cells ± Torin1 (250 nM, 1 hour). SunTag intensities are plotted for all mRNAs overlaid with the mean ± SD (≥652 mRNAs per condition, n=3). (**B**) Fraction of mRNAs undergoing translation quantified per cell in LARP1 KO cells ± Torin1 (250 nM, 1 hour). Values are plotted for each cell (colored circles) overlaid with the mean ± SD (≥91 cells per condition, n=3).

Figure 2.10: *continued from previous page:* (**C**) Quantification of translation site intensities in LARP1/1B KO cells ± Torin1 (250 nM, 1 hour). SunTag intensities are plotted for all mRNAs (colored circles) overlaid with the mean ± SD ($\geq$218 mRNAs per condition, n=3). (**D**) Fraction of mRNAs undergoing translation quantified per cell in LARP1/1B KO cells ± Torin1 (250 nM, 1 hour). Values are plotted for each cell (colored circles) overlaid with the mean ± SD ($\geq$30 cells per condition, n=3). For statistics, unpaired t tests were performed, with statistical significance claimed when $p < 0.05$ (ns = not significant, * = $p < 0.05$, ** = $p < 0.01$, **** = $p < 0.0001$. (**E**) Time course of fraction of translating mRNAs per cell for canonical and 5′TOP reporter cell lines in the presence (WT) or absence of LARP1/1B (KO). Cells were treated with 0, 30, 60, 120, and 240 min Torin1. Values are plotted as the mean ± SEM ($\geq$30 cells per condition, n=3).

performed SunTag imaging of the canonical and 5′TOP cell lines at additional time points (30 minutes, 2 hours, and 4 hours, Fig. 2.10E). For both WT and LARP1/1B KO cells, the canonical mRNAs showed a gradual decrease in translation during the first hour of Torin1 treatment that remained low at later time points. To test whether prolonged mTOR inhibition is required to repress canonical mRNA translation, we quantified translation of canonical mRNAs in WT cells treated with Torin1 for 24 hours. Interestingly, the majority of canonical mRNAs remained translating at this longer timepoint (Fig. 2.12). 5′TOP mRNAs in WT cells decreased in translation within 1 hour of Torin1 to a minor fraction of translating mRNAs (30min Torin1: 39%, 1 hour Torin1: 16%) and remained at this level at the 2 hours (14%) and 4 hours (19%) timepoints (Fig. 2.10E). In LARP1/1B KO cells, translation of 5′TOP mRNAs also decreased with no change in the timing of repression, but a decrease in its extent (30min Torin1: 50%, 1 hour Torin1: 30%), however at the 2 hours (42%) and 4 hours (46%) timepoints, we observed a slight increase in translation. These results suggested that while LARP1 may contribute to translation repression of 5′TOP mRNAs, it is not the dominant regulatory factor during mTOR inhibition.

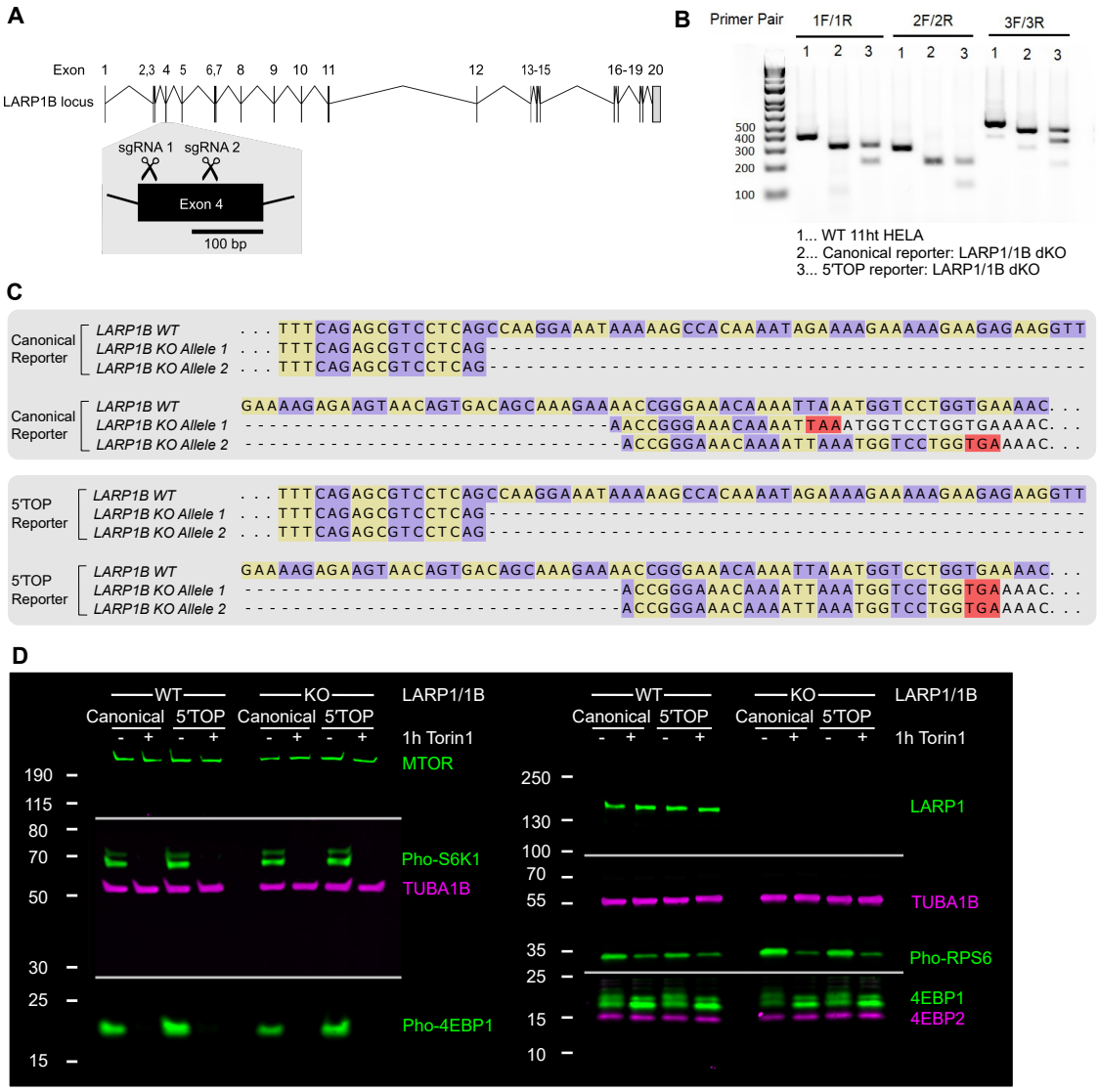

Figure 2.11: Validation of LARP1/1B KO cell lines. (**A**) CRISPR-Cas9 editing strategy for LARP1B gene locus, using two sgRNAs targeting exon 4 of LARP1B upstream of any domain of known function (sgRNA 1 taken from Philippe *et al.*, 2020). (**B**) Validation of 100bp truncations of LARP1B, using cDNA generated from total RNA extracted from LARP1/1B KO canonical and 5′TOP mRNA cell lines used for single-molecule imaging. (**C**) Genotyping of canonical and 5′TOP LARP1/1B KO clones used for single-molecule imaging (Fig. 2C-E), showing 100 bp truncations of LARP1B exon 4 resulting in frameshifting and premature termination codons. (**D**) Western blot analysis of mTORC1 signaling in canonical and 5′TOP LARP1/1B KO cell lines used for single-molecule imaging. Upon 1 hour Torin1 (250 nM), mTORC1 targets are dephosphorylated, as shown with phosphorylation-specific antibodies for Pho-4EBP1Ser65, Pho-S6K1 and Pho-RPS6, and the shift of 4EBP1 migration size. Lines indicate cut membrane pieces probed with different mouse (magenta) and rabbit (green) antibodies, and imaged together using two-color fluorescent imaging. Brightness and contrast were individually adjusted for each antibody shown.

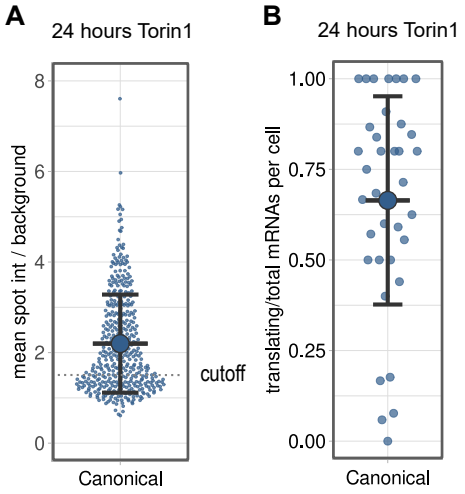

Figure 2.12: Translation of canonical mRNAs under long-term Torin1 treatment. (**A**) Quantification of SunTag translation site intensities for canonical mRNAs in WT cells after 24 hours Torin1 treatment (250 nM). SunTag intensities are plotted for 420 mRNAs overlaid with the mean ± SD. (**B**) Fraction of mRNAs undergoing translation quantified per cell after 24 hours Torin1 treatment (250 nM). Individual values are plotted overlaid with the mean ± SD of 37 cells.

2.3.3 4EBP1/2 KD rescues translation of 5′TOP mRNAs during Torin1 treatment

4EBP1/2 are thought to generally repress translation during mTORC1 inhibition but have also been previously implicated in specifically affecting 5′TOP mRNAs (Thoreen *et al.*, 2012). Using lentiviral infection, stable small hairpin RNA (shRNA)-mediated KD cell lines were generated in the WT and LARP1/1B KD background for both 5′TOP and canonical mRNA cell lines. Western blot analysis confirmed the depletion of 4EBP1/2 levels in all four cell lines (Fig. 2.13A and B). Furthermore, the dephosphorylation of RPS6 and residual 4EBP1 upon 1 hour Torin1 indicated that mTORC1 signaling was unperturbed in the 4EBP1/2 KD cell lines (Fig. 2.13C and D).

Having validated the 4EBP1/2 KD cell lines, we measured the translation of canonical and 5′TOP mRNAs in the absence of 4EBP1/2 (Fig. 2.14). In untreated cells, the reduction of 4EBP1/2 resulted in increased SunTag intensities for both canonical and 5′TOP mRNAs in cell lines with WT LARP1 (Fig. 2.15A, >1000 mRNAs per condition) and LARP1/1B KO (Fig. 2.15C, >700 mRNAs per condition) compared to cells with WT levels of 4EBP1/2 (Fig. 2.1C). This suggested that when mTOR is active, 4EBP1/2 can still weakly repress translation initiation presumably through fluctuations in mTOR signaling during cell growth. Surprisingly, the SunTag intensities of both canonical and 5′TOP mRNAs were not reduced upon 1 hour Torin1 treatment in 4EBP1/2 KD cell lines with WT LARP1 (Fig. 2.15A) or LARP1/1B KO (Fig. 2.15C). Analyzing the fraction of translating canonical mRNAs revealed no change in translation upon Torin1 treatment for cells with WT LARP1 (Fig. 2.15B) and LARP1/1B KO (Fig. 2.15D), in contrast to the previously observed mild decrease in translation of canonical mRNAs upon 1 hour Torin1 (Fig. 2.1D). Importantly, the fraction of translating 5′TOP mRNAs was not significantly reduced by Torin1 treatment in 4EBP1/2 KD cell lines with WT LARP1 (Fig. 2.15B, untreated: 77%, treated: 70%) or LARP1/1B KO (Fig. 2.15D, untreated: 79%, treated: 77%), indicating a full rescue of translation compared to the previous partial rescue observed in LARP1 KO cells. To exclude the possibility that translational repression is delayed in the absence of 4EBP1/2, we investigated the kinetics of mTOR inhibition in the 4EBP1/2 KD cell lines (Fig. 2.15E), which revealed that canonical and 5′TOP mRNAs remain similarly insensitive to Torin1 treatment at prolonged Torin1 treatment (2 hours, 4 hours). These experiments indicate that despite the difference

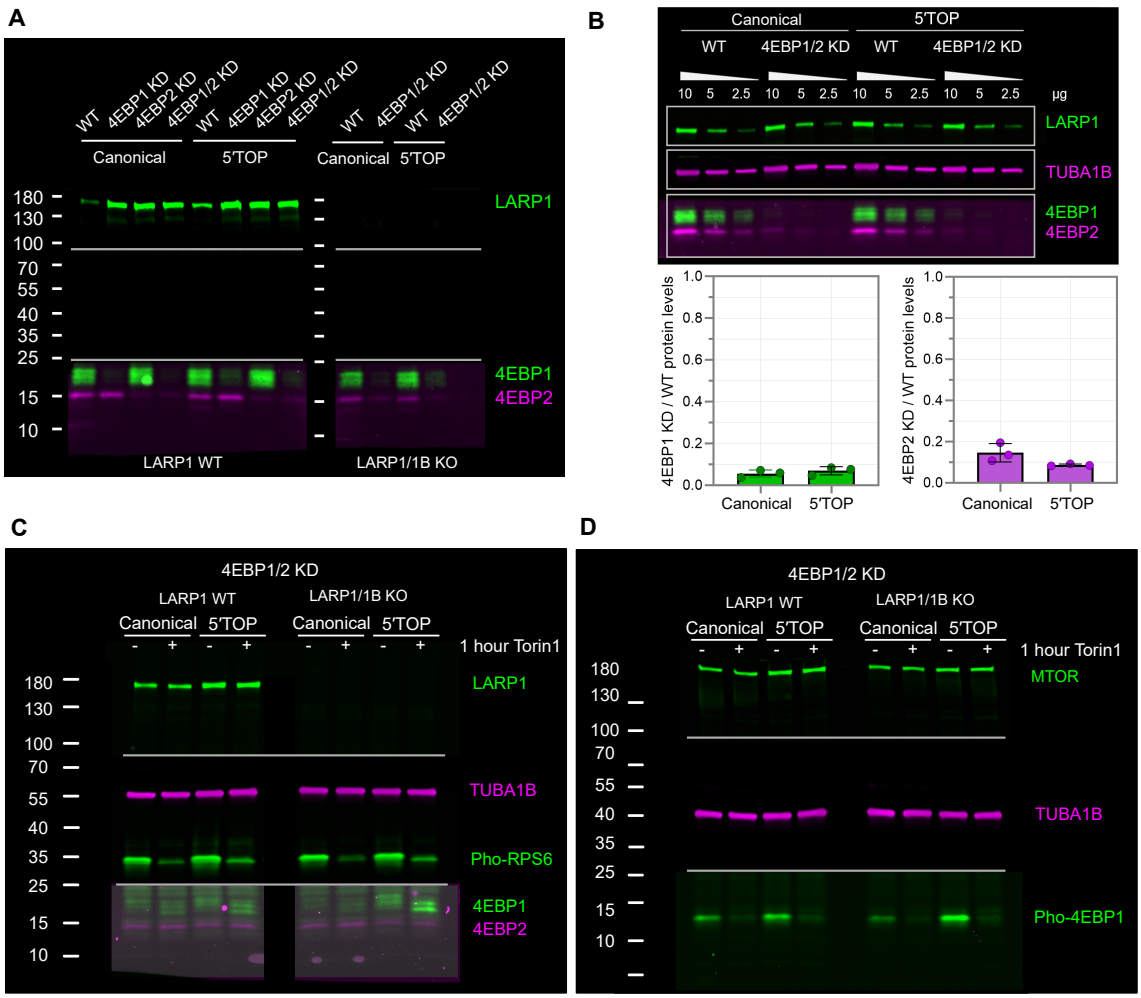

Figure 2.13: Validation of shRNA-mediated KD of 4EBP1/2 proteins. (**A**) Western blot analysis of stable KD of 4EBP1/2 proteins in canonical and 5′TOP mRNA cell lines with WT LARP1 (left) or LARP1/1B KO (right). Depletion of 4EBP1 and 4EBP2 proteins was analyzed in mTOR active cells with 4EBP1 and 4EBP2 antibodies. (**B**) Quantification of KD efficiency in canonical and 5′TOP mRNA cell lines with WT LARP1. Total lysate was loaded in amounts of 10, 5, and 2.5 μg to test antibody linearity, and semi-quantitative estimates of KD efficiency were calculated (4EBP1/2 KD/WT) for both cell lines. (**C**) Western blot analysis of mTORC1 signaling in 4EBP1/2 KD cell lines with WT LARP1 (left) or LARP1/1B KO (right). Upon 1 hour Torin1, RPS6 became dephosphorylated as seen by the decreased signal for Pho-RPS6. 4EBP1 and 4EBP2 are detected at low levels. (**D**) Western blot analysis of mTORC1 signaling in 4EBP1/2 KD reporter cell lines with WT LARP1 (left) or LARP1/1B KO (right). Upon 1 hour Torin1 (250 nM), residual 4EBP1 becomes dephosphorylated as seen by the disappearance of Pho-4EBP1^{Ser65}. Lines indicate cut membrane pieces probed with different mouse (magenta) and rabbit (green) antibodies, and imaged together using two-color fluorescent imaging. Brightness and contrast were individually adjusted for each antibody shown.

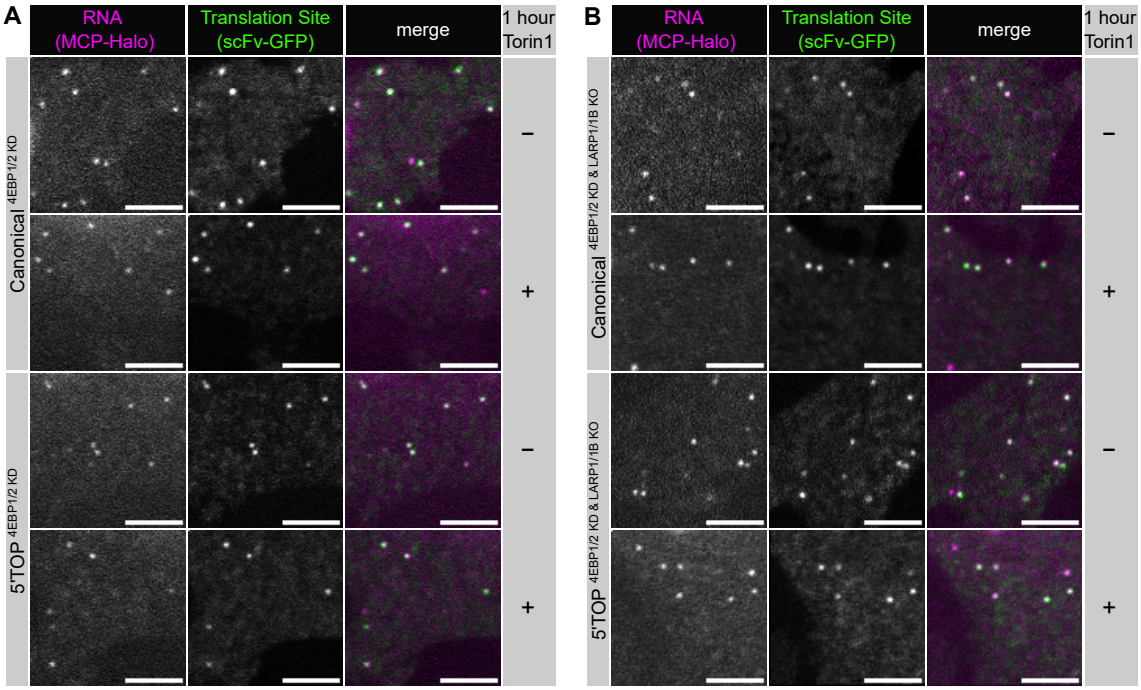

Figure 2.14: Single-molecule imaging of translation in 4EBP1/2 KD, 4EBP1/2 KD_LARP1/1B KO cell lines. (**A**) Representative images of canonical and 5′TOP reporter mRNAs in 4EBP1/2 KD cells (MCP-Halo foci, magenta) undergoing translation (scFv-GFP foci, green) in absence or presence of mTOR inhibitor Torin1 (250 nM, 1 hour). (**B**) Representative images of canonical and 5′TOP mRNAs in 4EBP1/2 KD_LARP1/1B KO cells (MCP-Halo foci, magenta) undergoing translation (scFv-GFP foci, green) in absence or presence of mTOR inhibitor Torin1 (250 nM, 1 hour). Scale bars = 5 μm.

in magnitude of translation repression during Torin1 treatment, 4EBP1/2 is responsible for the weak inhibition of canonical mRNAs and the stronger inhibition of 5′TOP mRNAs. Our data supports a model where 5′TOP mRNAs are intrinsically more sensitive to 4EBP1/2-mediated translational regulation, which results in a minor difference in translation when mTOR is active, and a pronounced difference in translation when mTOR is inhibited.

Alternatively, our data could potentially be explained by the presence of additional cis-acting sequence elements within the RPL32 5′UTR of our 5′TOP mRNA reporter that were absent in the 5′UTR of the canonical mRNAs. The RPL32 5′UTR is 50 nucleotides in length and contains the 5′TOP motif (positions +1 to +11) as well as a PRTE at positions +38 to +47 (Fig. 2.16A). A PRTE is found in the 5′UTRs of the majority of 5′TOP mRNAs and has been proposed to also be an alternative binding site for LARP1, though its contribution to translational regulation during mTOR inhibition remains largely unknown (Hong *et al.*, 2017). To further dissect the contribution of the 5′TOP and PRTE motifs, we generated two additional live-cell imaging cell lines carrying a single-copy genomic integration of modified RPL32 5′UTR reporters, one where only the 5′TOP motif was mutated (Δ5′TOP) and one where the 5′TOP and the PRTE motifs were mutated (Δ5′TOP/PRTE, Fig. 2.16A). We confirmed the sequence of the 5′UTRs in the Δ5′TOP and Δ5′TOP/PRTE mRNAs by 5′ end sequencing, and imaged their translation in the absence or presence of Torin1. Importantly, we find that both the Δ5′TOP and Δ5′TOP/PRTE mRNAs respond only weakly to Torin1 treatment, with a similar decrease in

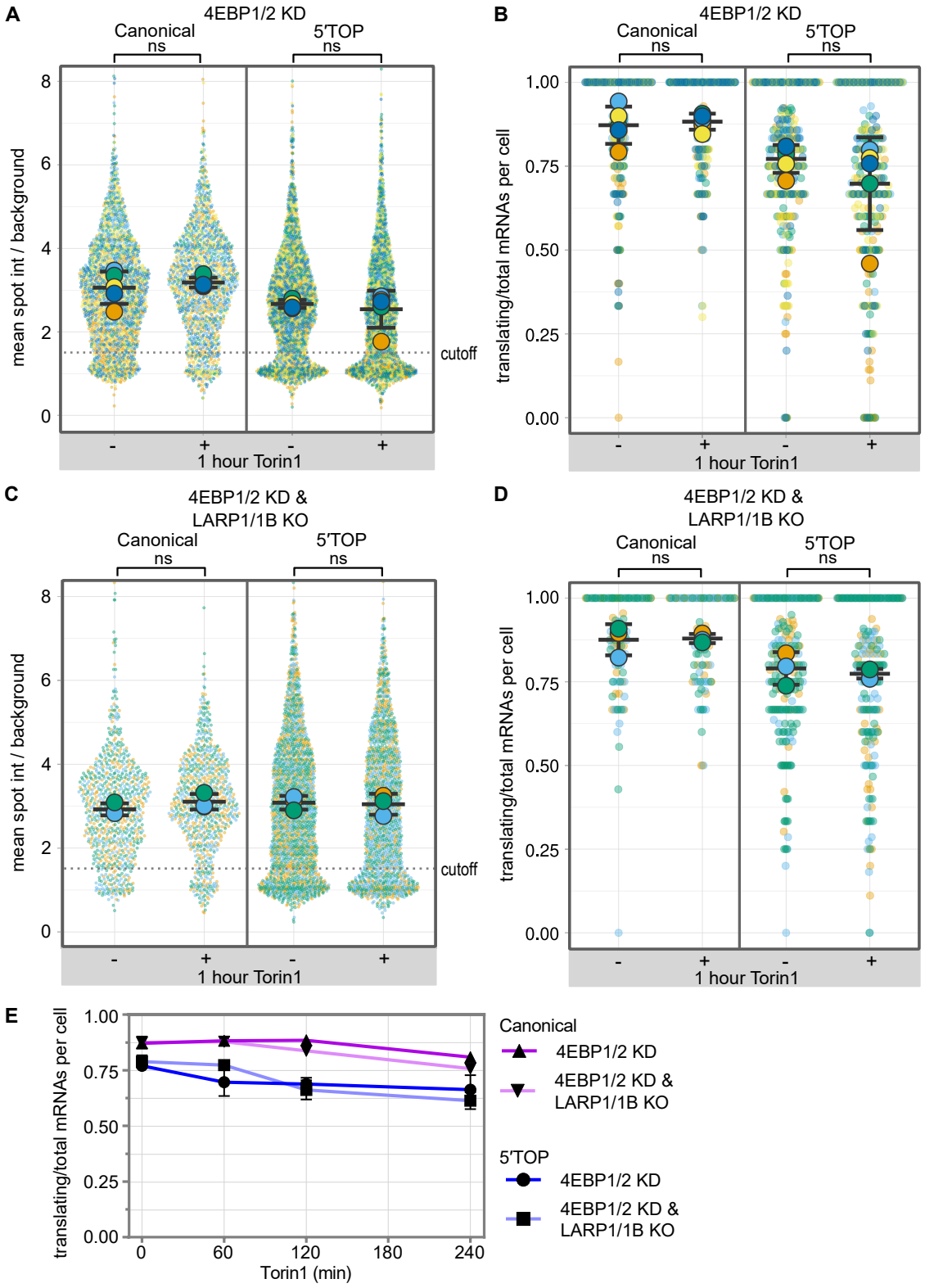

Figure 2.15: Loss of 4EBP1/2 is sufficient to alleviate 5′TOP translational repression during Torin1 treatment. (**A**) Quantification of translation site intensities of reporter mRNAs in 4EBP1/2 KD cells ± Torin1 (250 nM, 1 hour). SunTag intensites are plotted for all mRNAs (colored circles) overlaid with the mean ± SD (≥1344 mRNAs per condition, n=5). (**B**) Fraction of mRNAs undergoing translation quantified per cell for reporter mRNAs in 4EBP1/2 KD cells ± Torin1 (250 nM, 1 hour).

Figure 2.15: *continued from previous page:* Values are plotted for each cell (colored circles) overlaid with the mean ± SD (≥204 cells per condition, n=5). (**C**) Quantification of translation site intensities of reporter mRNAs in 4EBP1/2 KD_LARP1/1B KO cells ± 1 hour Torin1 (250 nM). SunTag intensities are plotted for all mRNAs overlaid with the mean ± SD (≥783 mRNAs per condition, n=3). (**D**) Fraction of mRNAs undergoing translation quantified per cell of reporter mRNAs in 4EBP1/2 KD_LARP1/1B KO cells ± Torin1 (250 nM, 1 hour). Values are plotted for each cell (colored circles) overlaid with the mean ± SD (≥97 cells per condition, n=3). For statistics, unpaired t tests were performed, with statistical significance claimed when $p < 0.05$ (ns = not significant). (**E**) Time course of fraction of translating mRNAs per cell for canonical and 5′TOP reporters in 4EBP1/2 KD cells with WT LARP1 or with LARP1/1B KO. Cells were treated with 0, 30, 60, 120, and 240 min Torin1. Values are plotted as the mean ± SEM (≥97 cells per condition, n=3-5).

the fraction of translating mRNAs per cell as observed for the canonical mRNAs (Fig. 2.16B, C, H), which is consistent with previous reports that the 5′TOP motif is both necessary and sufficient for the selective translational repression upon mTOR inhibition (Avni *et al.*, 1997; Biberman & Meyuhas, 1997).

Next, we generated both CRISPR-Cas9 LARP1 KO and shRNA-mediated 4EBP1/2 KD cell lines carrying the Δ5′TOP mRNAs, and validated the loss of the respective protein and unperturbed mTORC1 signaling by western blot (Fig. 2.17A, B). Similar to our previous experiments with canonical mRNAs (Fig. 2.10B, 2.15B), we found that loss of LARP1 did not alleviate the mild translational repression of Δ5′TOP mRNAs upon Torin1 treatment (Fig. 2.16D, E), and that depletion of 4EBP1/2 fully alleviated Torin1-mediated translational repression (Fig. 2.16F, G, H).

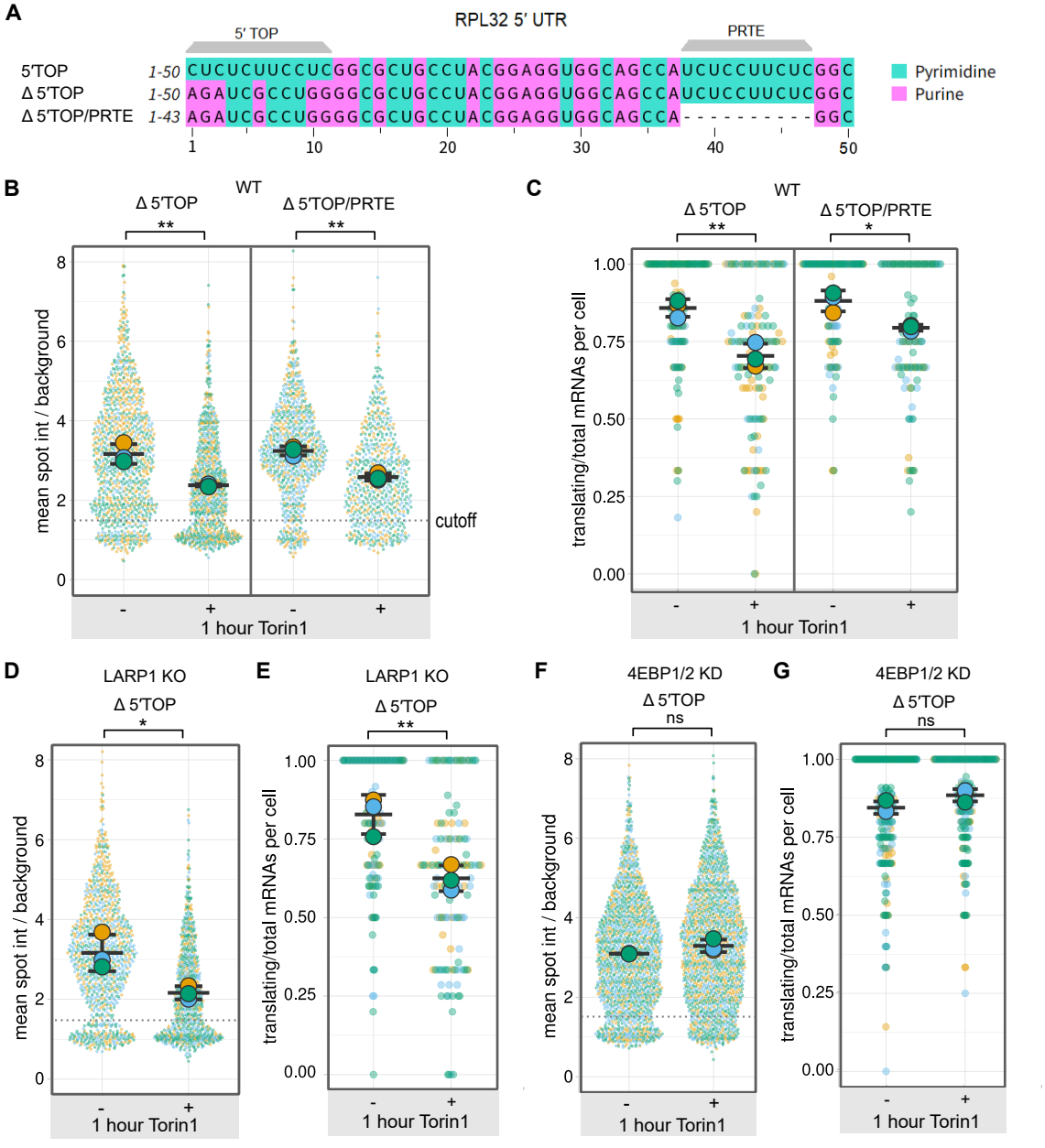

H

mean / sd

Genotype	Canonical		5′TOP		Δ 5′TOP		Δ 5′TOP/PRTE	
1 hour Torin1	-	+	-	+	-	+	-	+
WT	0.86 / 0.04	0.77 / 0.03	0.74 / 0.07	0.16 / 0.01	0.86 / 0.03	0.70 / 0.04	0.88 / 0.03	0.79 / 0.01
LARP1 KO	0.87 / 0.01	0.75 / 0.03	0.79 / 0.04	0.41 / 0.07	0.83 / 0.06	0.62 / 0.04		
4EBP1/2 KD	0.87 / 0.06	0.88 / 0.02	0.77 / 0.04	0.70 / 0.14	0.84 / 0.02	0.88 / 0.02		

Figure 2.16: Mutation of 5′TOP motif is sufficient to relieve 5′TOP translational repression of RPL32 5′TOP mRNAs. Single-molecule imaging of 5′TOP reporter mRNAs with the 5′TOP motif mutated (Δ5′TOP), or the 5′TOP motif and downstream pyrimidine-rich translational element mutated (Δ5′TOP/PRTE). (**A**) Full-length RPL32 5′UTR contained in the 5′TOP reporter mRNA aligned against the mutated RPL32 5′UTRs contained in the Δ5′TOP and Δ5′TOP/PRTE reporter mRNAs. The mutated 5′TOP motif sequence matches the cap-adjacent sequence of the canonical reporter mRNA (+1 - +11).

Figure 2.16: *continued from previous page:* (**B**) Quantification of translation site intensities of Δ5′TOP and Δ5′TOP/PRTE mRNAs in absence or presence of Torin1 (250 nM, 1 hour). SunTag intensities are plotted for all mRNAs overlaid with the mean ± SD (≥628 mRNAs per condition, n=3). (**C**) Fraction of mRNAs undergoing translation quantified per cell for Δ5′TOP and Δ5′TOP/PRTE mRNAs in absence or presence of Torin1 (250 nM, 1 hour). Values are plotted for each cell overlaid with the mean ± SD (≥110 cells per condition, n=3). (**D**) Quantification of translation site intensities of Δ5′TOP mRNAs in LARP1 KO cells ± Torin1 (250 nM, 1 hour). SunTag intensities are plotted for all mRNAs overlaid with the mean ± SD (≥730 mRNAs per condition, n=3). (**E**) Fraction of translating mRNAs per cell for Δ5′TOP mRNAs in LARP1 KO cells ± Torin1 (250 nM, 1 hour). Values are plotted for each cell overlaid with the mean ± SD (≥127 cells per condition, n=3). (**F**) Quantification of translation site intensities of Δ5′TOP mRNAs in 4EBP1/2 KD cells ± Torin1 (250 nM, 1 hour). SunTag intensities are plotted for all mRNAs overlaid with the mean ± SD (≥1598 mRNAs per condition, n=3). (**G**) Fraction of translating mRNAs per cell for Δ5′TOP mRNAs in 4EBP1/2 KD cells ± Torin1 (250 nM, 1 hour). Values are plotted for each cell overlaid with the mean ± SD (≥235 cells per condition, n=3). For statistics, unpaired t tests were performed, with statistical significance claimed when $p < 0.05$ (ns = not significant, * = $p < 0.05$, ** = $p < 0.01$). (**H**) Overview of the mean fraction of translating mRNAs per cell for canonical, 5′TOP, Δ5′TOP, and Δ5′TOP/PRTE mRNAs in absence or presence of 1 hour Torin1, listed for WT cells, LARP1 KO cells, and 4EBP1/2 KD cells.

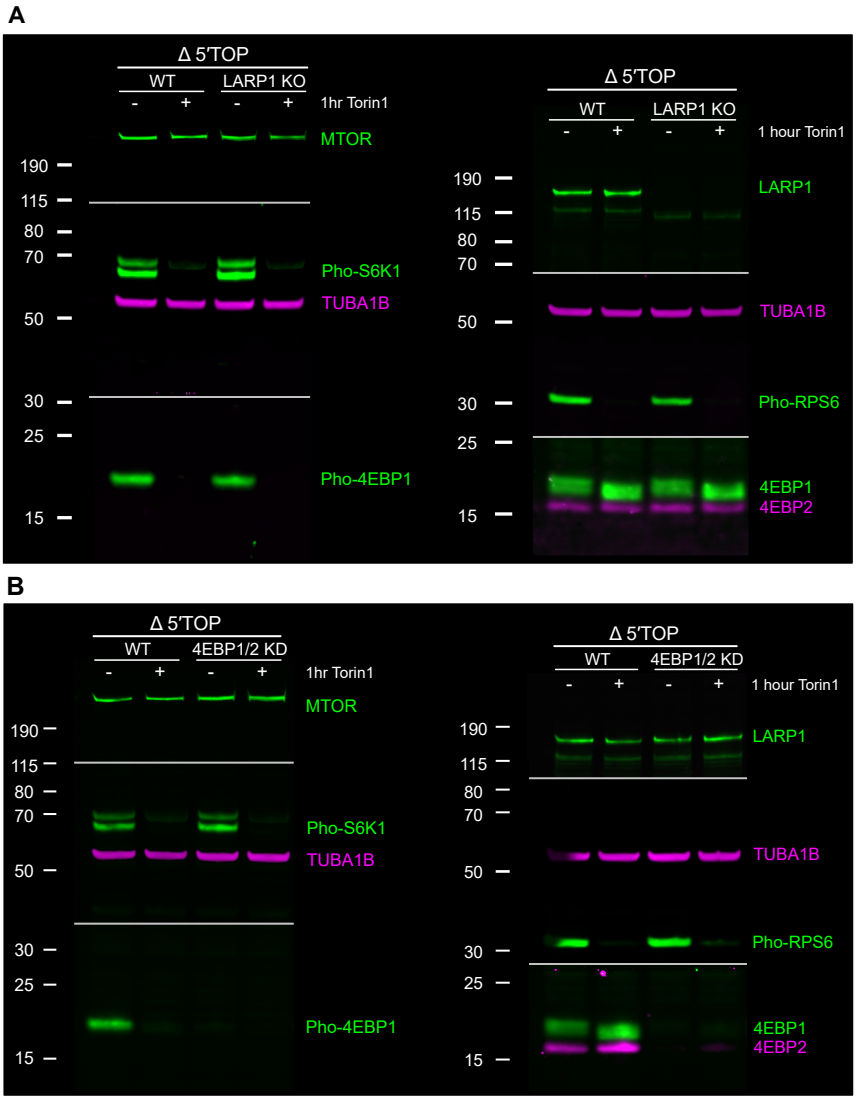

Figure 2.17: Western blot validation of LARP1 KO and 4EBP1/2 KD for Δ5′TOP and Δ5′TOP/PRTE cell lines. (**A**) Western blot analysis of LARP1 protein expression in WT and LARP1 CRISPR-Cas9 edited single clonal cell lines, confirming full loss of LARP1 protein expression. mTORC1 signaling is unperturbed in the LARP1 KO cells, as shown with phosphorylation-specific antibodies for Pho-4EBP1^{Ser65}, Pho-S6K1 and Pho-RPS6. (**B**) Western blot analysis of 4EBP1/2 protein levels in WT and stable shRNA-mediated KD cells, confirming high KD efficiency. mTORC1 signaling of S6K1 and RPS6 phosphorylation is unperturbed in the 4EBP1/2 KD cells, as shown with phosphorylation-specific antibodies for Pho-S6K1 and Pho-RPS6. Lines indicate cut membrane pieces probed with different mouse (magenta) and rabbit (green) antibodies, and imaged together using two-color fluorescent imaging. Brightness and contrast were individually adjusted for each antibody shown.

2.3.4 LARP1 KO results in global decreased mRNA stability of 5′TOP mRNAs

In addition to its role in 5′TOP translational repression, LARP1 has been reported to protect mRNAs from degradation (Al-Ashtal *et al.*, 2019; Aoki *et al.*, 2013; Kozlov *et al.*, 2022; Mattijssen *et al.*, 2021; Park *et al.*, 2023). It is currently unclear whether this protective role of LARP1 is restricted to 5′TOP mRNAs, TOP-like mRNAs, or affects all mRNAs (Philippe *et al.*, 2020). To study the effect of LARP1 and 4EBP1/2 loss on global gene expression in growing cells when mTOR is active, we extracted total RNA from our cell lines and performed RNAseq. The canonical and 5′TOP mRNA cell lines of the same genotype were sequenced together as biological replicates since expression of different reporter mRNAs should not have a global effect on gene expression and combining the independently generated cell lines reduces potential off-target effects caused by either CRISPR KO or shRNA KD.

To determine the effect of LARP1 loss on gene expression, we compared the transcriptome of LARP1 KO and WT cells (12,403 transcripts, CPM>1, pseudogenes excluded). As expected, LARP1 transcript levels were downregulated in the KO cell lines to 30% of WT levels. Volcano-plot analysis of the transcriptome changes of KO vs WT cell lines (biological replicates: n=2 for LARP1 WT, n=8 for LARP1 KO) revealed that the most significantly affected mRNAs are endogenous 5′TOP mRNAs, which are almost all downregulated in the LARP1 KO cells (Fig. 2.18A, blue circles). Analyzing all known 5′TOP mRNAs, 70 out of 94 5′TOPs are found to be significantly downregulated (log2 FC $\leq$ -0.5, -log10 p-value $\geq$ 5), as well as 85 significantly downregulated non-5′TOP RNAs and 40 significantly upregulated non-5′TOP RNAs (orange circles). In contrast, previously identified TOP-like mRNAs, which were predicted to be translationally regulated by LARP1 based on sequence similarity (Philippe *et al.*, 2020), were mostly unaffected in their expression.

In order to determine if depletion of 4EBP1/2 also affected the levels of 5′TOP transcripts, we compared the transcriptome of 4EBP1/2 KD cells to WT cells (13,832 transcripts, CPM>1, pseudogenes excluded). Consistent with shRNA KD of 4EBP1/2, we found the levels of these two transcripts to be reduced by 91% (4EBP1) and 71% (4EBP2), and that LARP1 expression was unaltered in both cell lines. A small number of transcripts showed significantly altered expression, however, these do not include known 5′TOP mRNAs (65 transcripts, Fig. 2.18B, orange circles, abs log2 FC $\geq$ 0.5, -log 10 p-value $\geq$ 5). Additionally, the altered mRNAs did not match mRNAs described to be sensitive to eIF4E levels in mice (Truitt *et al.*, 2015). In contrast to the dominant role of 4EBP1/2 in regulating translation during mTOR inhibition, these results indicate that LARP1 regulates levels of 5′TOP transcripts when mTOR is active (Fig. 2.18C). To validate our RNAseq results with an orthogonal approach, we performed single-molecule fluorescence *in situ* hybridization (smFISH) on three endogenous 5′TOP transcripts (RPL5, RPL11, RPL32) and a non-5′TOP control (MYC), which confirmed the selective decrease of 5′TOP mRNAs in the LARP1 KO cell lines, with no change of 5′TOP mRNAs in the 4EBP1/2 KD cell lines (Fig. 2.19).

The selective downregulation of endogenous 5′TOP mRNAs we observed in the absence of LARP1 suggested that LARP1 specifically stabilizes 5′TOP mRNAs. To confirm that the changes in steady-state expression were caused by mRNA destabilization and were not due to changes in transcription, we

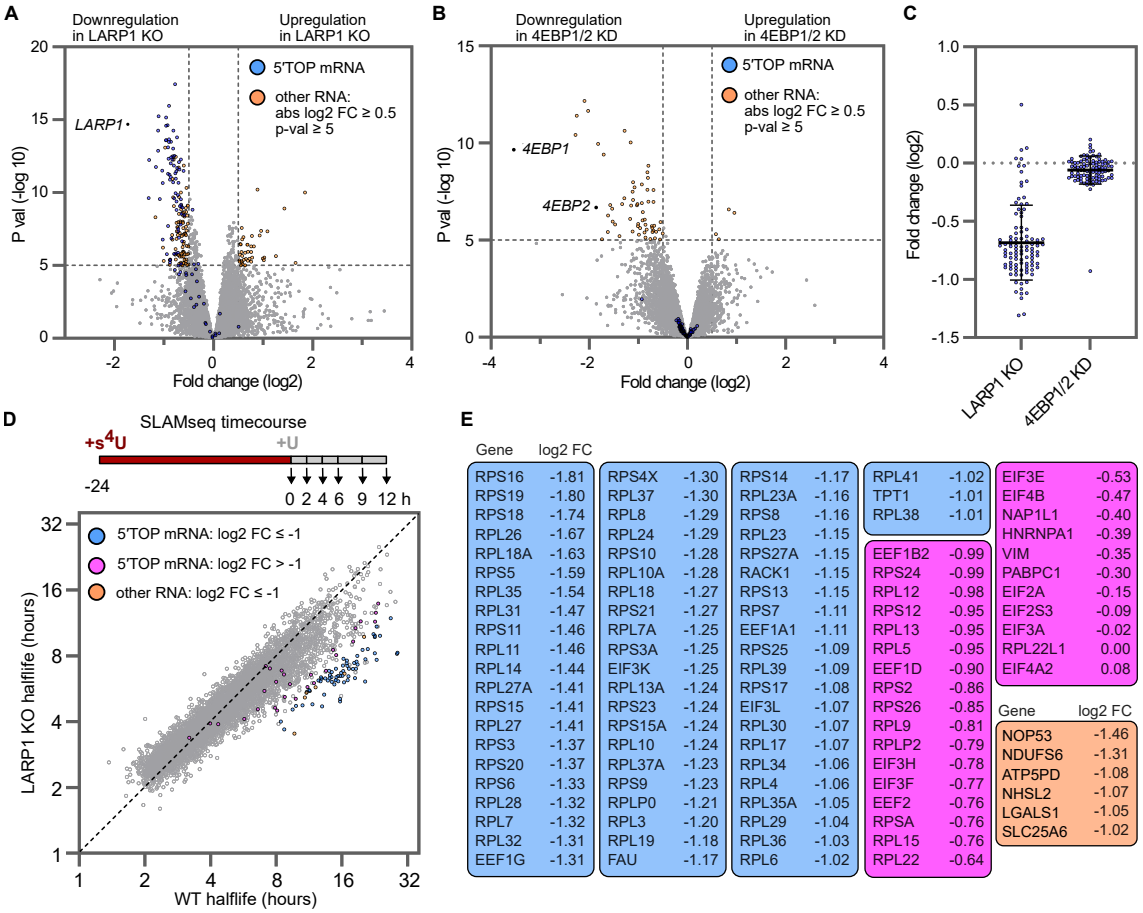

Figure 2.18: Loss of LARP1 results in selective destabilization of 5′TOP mRNAs. (**A**) Differential gene expression analysis of LARP1 KO cells compared to WT cell lines. Significantly down- and upregulated mRNAs are highlighted (-log10 p-value $\geq$ 5, and abs log2 FC $\geq$ 0.5) indicating all classical 5′TOP mRNAs (blue circles) as well as all significant non-5′TOP mRNAs (orange circles). For WT, data is the average of n=2 biological replicates (canonical and 5′TOP reporter cell lines, averaged). For LARP1 KO, data is the average of n=8 biological replicates (4 KO clones of each reporter cell line). (**B**) Differential gene expression analysis of 4EBP1/2 KD reporter cell lines compared to WT reporter cell lines. Significantly down- and upregulated mRNAs are highlighted (orange circles, -log10 p-value $\geq$ 5, and abs log2 FC $\geq$ 0.5). 5′TOP mRNAs (blue) are unaffected by 4EBP1/2 KD. Data shown for n=2 biological replicates (canonical and 5′TOP reporter cell lines, averaged). (**C**) Fold change of 5′TOP mRNAs shown in (A) and (B). Mean fold change (log2) in LARP1 KO cells = -0.68, in 4EBP1/2 KD cells = -0.06. (**D**) Correlation plot of mRNA half-lives in LARP1 KO compared to WT reporter cells. Experimental setup of global mRNA stability analysis using 4-thiouridine (S4U) labelling (SLAMseq) shown on top, with 24 hours S4U labelling, wash-out, and timepoint collection. RNAs with significantly decreased stability (log2 FC $\leq$ -1) are highlighted for 5′TOP mRNAs (blue circles) and non-5′TOP mRNAs (orange circles), as well as non-significantly downregulated 5′TOP mRNAs (magenta circles). (**E**) List of all RNAs highlighted in (D), ranked by log2 FC for 5′TOP mRNAs and non-5′TOP mRNAs separately.

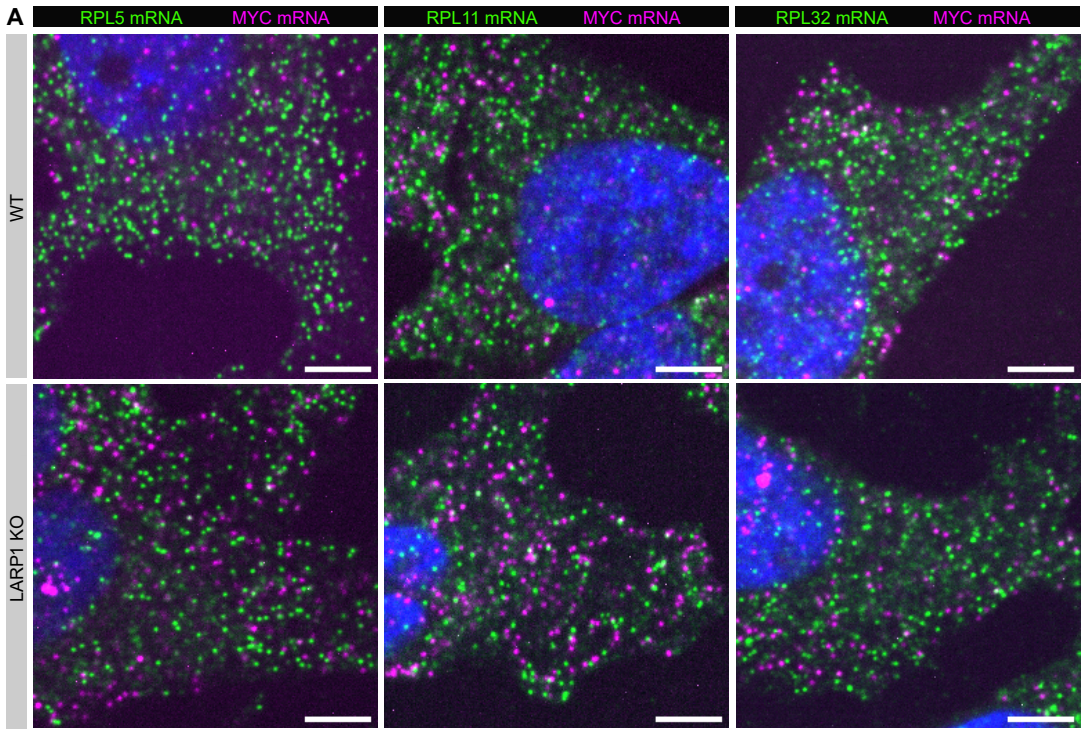

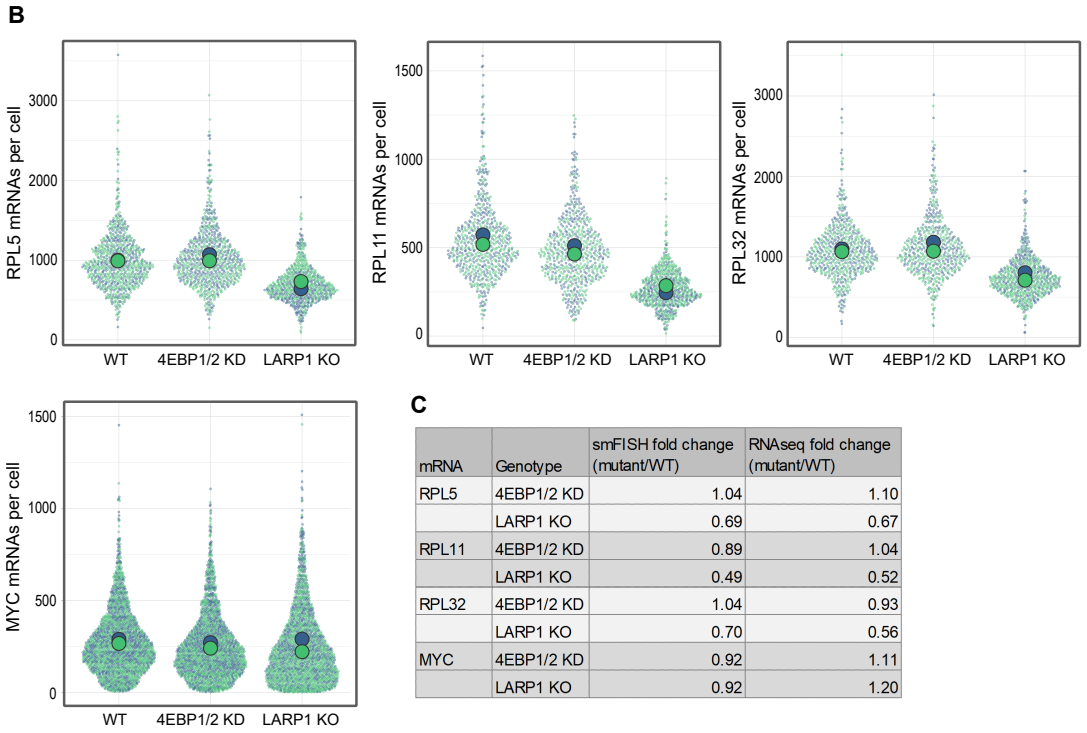

C

mRNA	Genotype	smFISH fold change (mutant/WT)	RNAseq fold change (mutant/WT)
RPL5	4EBP1/2 KD	1.04	1.10
	LARP1 KO	0.69	0.67
RPL11	4EBP1/2 KD	0.89	1.04
	LARP1 KO	0.49	0.52
RPL32	4EBP1/2 KD	1.04	0.93
	LARP1 KO	0.70	0.56
MYC	4EBP1/2 KD	0.92	1.11
	LARP1 KO	0.92	1.20

Figure 2.19: Validation of RNAseq results for select 5′TOP mRNAs by smFISH. (**A**) Representative smFISH images of WT and LARP1 KO cells, showing smFISH spots for endogenous 5′TOP (RPL5, RPL11, RPL32: green, quasar-570 dye) and non-5′TOP control mRNAs (MYC: magenta, atto-633 dye). (**B**) Quantification of 5′TOP (RPL5, RPL11, RPL32), and non-5′TOP (MYC) mRNA spots per cell for WT, 4EBP1/2 KD, and LARP1 KO cell lines used in Fig. 2.18A-C. The mean of canonical and 5′TOP reporter cell lines are shown as biological replicates (n=2). (**C**) Mean fold changes of RPL5, RPL11, RPL32, and MYC mRNA levels (mutant/WT) as determined by smFISH or RNAseq (Fig. 2.18). For all 5′TOP mRNAs tested, smFISH recapitulates the selective decrease of 5′TOP mRNA levels measured for LARP1 KO cells.

performed global mRNA half-life measurements using SLAMseq (Herzog *et al.*, 2017)). WT and LARP1 KO cells of both canonical and 5′TOP cell lines were incubated with S4U for 24 hours, followed by wash-out and harvesting of cells over a 12 hour time course. Half-lives of mRNAs were calculated using a single-exponential decay fit for 9,837 transcripts (R2 $\geq$ 0.75, pseudogenes excluded). In agreement with previous measurements of mammalian mRNA half-lives, the global median half-life for both WT and LARP1 KO HeLa cell lines was $\sim$4 hours (Fig. 2.20A), indicating that loss of LARP1 does not globally destabilize all mRNAs. Correlation analyses showed a high correlation in mRNA half-lives among the four cell lines (r=0.90-0.94), allowing us to compare the mRNA half-lives in WT vs LARP1 KO cell lines (Fig. 2.18D, n=2). In agreement with our RNAseq results, nearly all 94 5′TOP mRNAs detected in the SLAMseq experiment have decreased mRNA stability, with 66 5′TOP mRNAs changing by > 2-fold (Fig. 2.18D). A few 5′TOP mRNAs seem largely unaffected by LARP1 loss (including PABPC1), suggesting the potential involvement of additional stabilizing factors for these transcripts. Furthermore, the length of the 5′TOP motif or presence of a PRTE motif within the 5′UTR does not correlate with the change in mRNA half-lives (Fig. 2.20B). Only six non-5′TOP mRNAs were found to be destabilized > 2-fold and three of these transcripts (NOP53, LGALS1, SLC25A6) have annotated transcription start sites that contain 5′ TOP motifs suggesting that they could be similarly regulated in HeLa cells. Taken as a whole, our results support a model of LARP1-mediated stabilization that is highly selective for 5′TOP mRNAs.

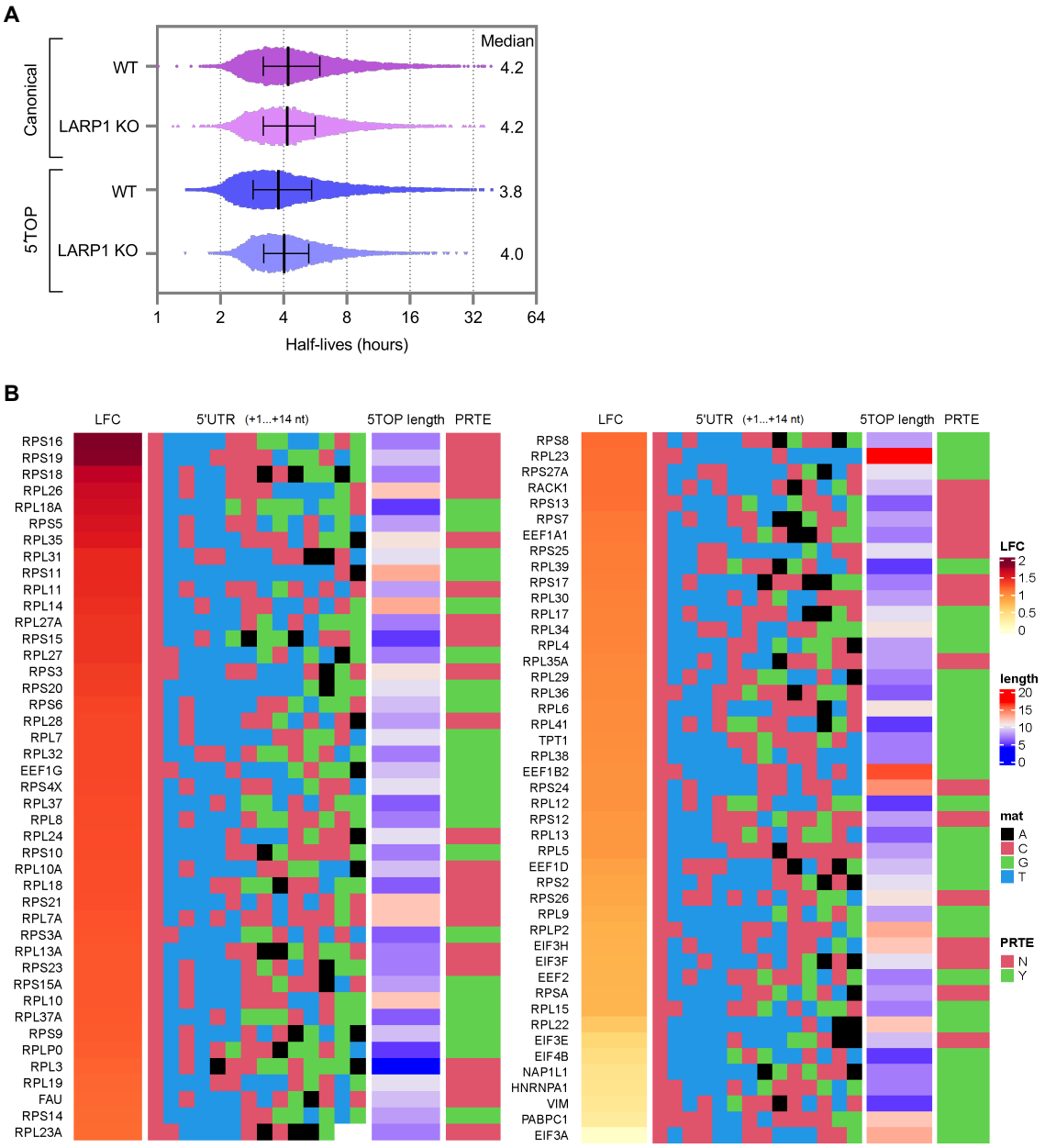

Figure 2.20: Global analysis of mRNA half-lives determined by SLAMseq.(**A**) Distribution of RNA half-lives estimated from SLAMseq data for WT and LARP1 KO cell lines. Values are plotted with the median and interquartile range. (**B**) List of 5′TOP mRNAs from SLAMseq data, ranked by log2 fold change (LFC). The sequence of the first 14 nt of the 5′UTR containing the 5′TOP motif (RPL23A 5′UTR: 12 nt), the length of the 5′TOP motif, and presence or absence of a PRTE within the 5′UTR is shown.

2.4 Discussion

In this study, we employed single-molecule imaging to study the regulation of translation of 5′TOP mRNAs upon mTOR inhibition that allowed us to directly quantify the effect of LARP1 and 4EBP1/2. By imaging and quantifying the translation status of individual mRNAs, we find that 4EBP1/2 plays a dominant role compared to LARP1 in mediating 5′TOP translational repression during short-term (30 minutes - 4 hours) pharmacological inhibition of mTOR in HeLa cells. Previously, studies that used genome-wide ribosome or polysome profiling determined that LARP1 and 4EBP1/2 regulate 5′TOP translation during mTOR inhibition (Fonseca *et al.*, 2015; Gandin *et al.*, 2016; Jia *et al.*, 2021; Miloslavski *et al.*, 2014; Philippe *et al.*, 2020; Thoreen, 2017; Thoreen *et al.*, 2012), however, the magnitude of their respective contributions was difficult to measure due to the inherent limitations of these approaches. We believe this highlights the power of single-molecule imaging methods for quantifying translation in living cells in order to determine the specific effects of translation factors.

While our results indicate that 4EBP1/2 is the critical factor in mediating 5′TOP translational repression, the underlying molecular mechanism is not entirely clear. Although we cannot exclude the possibility of a still unknown factor acting downstream of 4EBP1/2, we favor a model where the translation of 5′TOP mRNAs is more sensitive to active eIF4E levels. In vitro experiments have determined that eIF4E binds with ∼3-fold weaker affinity to m7GTP-capped oligonucleotides with a +1 cytosine than either purine, which is consistent with translation of 5′TOP mRNAs being slightly lower than a non-5′TOP mRNA when mTOR is active and then preferentially repressed when available eIF4E levels become extremely limited during mTOR inhibition (Meyuhas, 2000; Tamarkin-Ben-Harush *et al.*, 2017; van den Elzen *et al.*, 2022). This model is also in line with previous work that found inducible overexpression of eIF4E to specifically upregulate the translation of 5′TOP mRNAs (Mamane *et al.*, 2007), as well as recent work that showed that 5′TOP mRNAs are less sensitive to mTOR inhibition in acutely PABPC1-depleted cells where global mRNA levels are reduced (Kajjo *et al.*, 2024).

Interestingly, in the X-ray structure of human eIF4E in complex with m7pppA, the C-terminal tail of eIF4E adopts a conformation that enables Thr205 to form a hydrogen bond with the exocyclic amine of the adenine base (Tomoo *et al.*, 2002). While the position of the eIF4E C-terminal tail has not been determined when bound to longer RNA sequences, phosphorylation of Ser209 is known to enhance translation indicating that additional residues in this region may have functional roles (Furic *et al.*, 2010). Alternatively, other canonical translation factors (e.g. eIF4G or 4EBP1/2) may also contribute to 5′TOP specificity through additional interactions (Jin *et al.*, 2020; Zinshteyn *et al.*, 2017).

While LARP1 may not be the key repressor in 5′TOP translational regulation, our data supports a major role of LARP1 in mediating 5′TOP mRNA stability when mTOR is active. Previous work established a link between LARP1 and mRNA stability, with LARP1 binding both PABPC1 and the polyA tail and inhibiting deadenylation (Al-Ashtal *et al.*, 2019; Aoki *et al.*, 2013; Fuentes *et al.*, 2021; Gentilella *et al.*, 2017; Kozlov *et al.*, 2022; Mattijssen *et al.*, 2021; Ogami *et al.*, 2022; Smith *et al.*, 2020). It has been unclear whether this protective role is restricted to 5′TOP mRNAs as binding to PABPC1/polyA is

anticipated to not be selective, and crosslinking studies have found LARP1 complexed with thousands of mRNAs (Hong *et al.*, 2017; Mura *et al.*, 2015; Smith *et al.*, 2020). Our results show a highly selective destabilization of nearly all 5′TOP mRNAs upon loss of LARP1, with virtually all other mRNAs being largely unaffected. Similarly, a recent study found that loss of LARP1 resulted in rapid deadenylation of short polyA tails of all mRNAs, with 5′TOP mRNAs being more affected than other types of mRNAs (Park *et al.*, 2023). It is possible that differences in LARP1 depletion or measurement of mRNA stability versus polyA-tail length may account for the differences in specificity for 5′TOP mRNAs between the studies.

Previous studies have focused on the role of LARP1 in protecting 5′TOP mRNAs in mTOR inhibited cells, as LARP1 has been shown to be recruited to 5′TOP mRNAs upon mTOR inhibition (Fuentes *et al.*, 2021; Smith *et al.*, 2020). Our findings raise the intriguing question of how LARP1 can be specifically recruited to 5′TOP mRNAs when mTOR is active. While it has been proposed that LARP1 can interact with its La-motif with both the 5′TOP motif and PABPC1 (Al-Ashtal *et al.*, 2019), it is not clear that this interaction is compatible with eIF4F binding and translation initiation. Recent structural work of the human 48S preinitiation complex suggests that there could be a "blind spot" of ∼30 nucleotides adjacent to the cap that might allow LARP1 to bind the 5′TOP sequence without blocking initiation though this model requires biochemical and structural characterization (Brito Querido *et al.*, 2020). Importantly, we do not observe any correlation between change in mRNA half-lives with either length of 5′TOP motif or presence of PRTE in the 5′UTR suggesting that the position of the pyrimidines directly adjacent to the cap is necessary for this effect on mRNA stability. Interestingly, LARP1 was shown to promote the localization of ribosomal mRNAs in a PRTE-dependent manner but did not require the more strict 5′TOP motif suggesting that LARP1's interaction with ribosomal mRNAs and its functional consequence could be context-dependent (Goering *et al.*, 2023).

While our translation site imaging experiments are limited to the characterization of four reporter mRNAs (canonical, 5′TOP, Δ5′TOP, Δ5′TOP/PRTE), we have shown that the results are consistent with previous studies that characterized endogenous ribosomal protein mRNAs, however, single-molecule experiments in living cells allow more accurate quantification of the effect of loss of LARP1 and 4EBP1/2. We anticipate that similar results would be obtained with 5′TOP sequences derived from ribosomal protein mRNAs other than RPL32, though the magnitude of the difference in translation repression could be different if compared to another non-5′TOP transcript. Additionally, the continued development of methodologies for imaging translation of single mRNAs for extended time periods and the interplay of translation with mRNA decay will enable the dynamics of mTOR regulation to be quantified in greater detail (Dave *et al.*, 2023; Livingston *et al.*, 2022).

2.5 Materials and Methods

Materials

All antibodies used in this study are listed in Table 2.1. All chemicals, plasmids, viruses, cell lines, sgRNA, and shRNA used in this study are listed in Supplementary Table S1.

Primary Antibodies	**Provider**	**Cat. #**
LARP1	Bethyl Labs	A302-087A
LARP1	Cell Signaling Technology	70180
TUBA1B	Cell Signaling Technology	3873
MTOR	Cell Signaling Technology	2983
Pho-RPS6 (Ser235/236)	Cell Signaling Technology	2211
Pho-RPS6 (Ser235/236)	Cell Signaling Technology	4856
Pho-4EBP1 (Ser65)	Cell Signaling Technology	9451
4EBP1	Cell Signaling Technology	9452
4EBP2	Sigma-Aldrich	MABS1865
Pho-S6K1 (Thr389)	Cell Signaling Technology	9234
Secondary Antibodies		
IRDye® 680RD Goat anti-Mouse IgG	LI-COR	926-68070
IRDye® 800CW Goat anti-Rabbit IgG	LI-COR	926-32211

Table 2.1: Antibodies.

Cell culture

The HeLa-11ht cell lines expressing either RPL32 5′TOP SunTag or non-5′TOP canonical SunTag mRNAs used in this study were previously generated in the Chao lab (Wilbertz *et al.*, 2019), and the corresponding plasmids are available from Addgene (#119946, #119945). The reporter cell lines were grown in 10% fetal bovine serum (FBS)-dulbecco's modified eagle medium (DMEM) containing 4.5 g/L glucose, 100 μg/ml penicillin and streptomycin, 4 mM L-glutamine, and 10% FBS at 37°C and 5% CO_2. To maintain the reverse tetracycline-controlled transactivator (rtTA2-M2) for inducible expression, the medium was supplemented with 0.2 mg/ml G418.

HEK293T used for lentivirus production were grown in 10% FBS-DMEM medium containing 4.5 g/L glucose, 100 μg/ml penicillin and streptomycin, 4mM L-glutamine, and 10% FBS at 37°C and 5% CO_2.

Validation of transcription start sites for 5′TOP and canonical SunTag transcripts

For mapping of transcription start sites, total RNA was converted into full-length adapter-ligated double-stranded cDNA using the TeloPrime Full-Length cDNA Amplification Kit V2 (Lexogen), which employs a cap-specific adapter selective for intact mRNAs. cDNA 5′-terminal sequences were amplified by PCR using a gene-specific primer and TeloPrime forward primer, cloned into the pCR-Blunt vector (Thermo Fisher Scientific), and sequenced.

CRISPR KO cell line generation

To generate LARP1 CRISPR KO clones, parental HeLa-11ht cell lines expressing the reporter mRNAs were transiently co-transfected with two Cas9 plasmids, each containing Cas9 and a sgRNA targeting a sequence within exon 4 of LARP1, enhancing efficiency of KO cell line generation (Chu *et al.*, 2015; Cong *et al.*, 2013). Transient transfections were performed following the manufacturer's instructions using Lipofectamine 2000 (Invitrogen) and Opti-MEM (Thermo Fisher Scientific). Two days after transient transfections, highly transfected cells were single-cell sorted into 96-well plates for monoclonal selection (10% highest mCherry positive cells, using Cas9-T2A-mCherry). Single clonal cell populations were screened for loss of LARP1 by immunostaining (Bethyl Labs #A302-087A) in 96-well plates. For both 5′TOP and canonical SunTag cell lines, four KO clones each were verified by western blot for loss of LARP1 protein expression. To generate LARP1B CRISPR KO clones, the LARP1 KO reporter cell lines were similarly co-transfected with two Cas9 plasmids carrying two different sgRNAs targeting sequences within exon 4 of LARP1B. Following the same steps as described for generating LARP1 KO cell lines, clonal cell populations were screened by PCR for presence of truncated LARP1B alleles, and subsequently verified by genomic DNA sequencing and cDNA amplification.

shRNA stable KD cell lines

To generate 4EBP1/2 KD cells, two lentiviruses expressing different resistance genes were used that contained shRNA sequences from the RNAi Consortium public library (https://www.broadinstitute.org/rnai-consortium/rnai-consortium-shrna-library) that were previously described (Thoreen *et al.*, 2012). The 4EBP1 shRNA lentivirus carrying puromycin resistance was purchased as lentiviral particles (Sigma-Aldrich). The 4EBP2 shRNA was cloned into the pLKO.1_BlastR lentiviral backbone (Bryant *et al.*, 2010). To produce 4EBP2 shRNA lentivirus, HEK293T cells were co-transfected with the 4EBP2 shRNA, the psPax2 envelope and the vsv-G packaging plasmids using Fugene6 (Promega) according to the manufacturer's instructions. Supernatant containing viral particles was harvested daily for the next four days, centrifuged at 500 g for 10 minutes, and filtered through a 0.45 μm filter to remove cell debris. The viral particles were concentrated by precipitation using the Lenti-X concentrator (Clontech) and resuspended in cell culture medium.

For infection of HeLa cells expressing the reporter mRNAs, 10,000 cells were seeded in 12-well dishes and co-infected the next day with 4EBP1 and 4EBP2 shRNA viruses in medium supplemented with 4 μg/ml polybrene (Merck). Cells were grown until confluency and re-seeded into 6-well dishes prior to addition of 1 μg/ml puromycin (InvivoGen) and 5 μg/ml blasticidin (InvivoGen). Uninfected HeLa-11ht cells were used to determine the minimal antibiotic concentrations that resulted in lethality within 2-5 days. Double resistant cell lines with dual integration of 4EBP1/2 shRNAs were validated by western blot for efficient stable KD of the targeted proteins.

Genomic DNA extraction

For genotyping of CRISPR edited cell lines, cells were harvested by trypsinization, and the genomic DNA was extracted using the DNeasy kit (Qiagen) according to the manufacturer's instructions.

Primers specific to the target genes were designed using the Primer-Blast tool (https://www.ncbi.nlm.nih.gov/tools/primer-blast/). Genomic DNA was amplified using Phusion High-Fidelity polymerase (NEB), PCR products were cleaned using a PCR purification kit (Qiagen), and purified PCR products were cloned into the pCR-Blunt vector (Thermo Fisher Scientific). For each cell line, a minimum of 10 clones were isolated and analyzed by Sanger sequencing to identify all edited alleles.

SDS-PAGE and Western Blotting

For protein extraction, cells were harvested by trypsinization and lysed in RIPA buffer (150 mM NaCl, 50 mM Tris, 0.1% SDS, 0.5% sodium deoxycholate, 1% Triton X-100) supplemented with 1x protease inhibitor (Bimake.com) and SuperNuclease (Sino Biological). Cell lysate was centrifuged at 12,000 rpm for 10 minutes to remove cell debris, and the supernatant was loaded on a 4-15% gradient gel using loading buffer supplemented with 100 mM dithiothreitol. Following SDS-PAGE, proteins were transferred onto nitrocellulose or polyvinylidenfluorid membranes by semi-dry transfer (Trans-Blot Turbo) and blocked in 5% BSA-TBST buffer (TBS supplemented with 0.1% Tween-20) for 1 hour at room temperature. Primary antibodies were incubated overnight at 4°C in TBST or Intercept® blocking buffer (LI-COR) supplemented with 0.1% Tween-20. The next day, the membrane was washed 3-5 times in TBST, and incubated for 1 hour at room temperature with the fluorescent secondary antibodies diluted 1:10,000 in Intercept® blocking buffer with 0.1% Tween-20 (supplemented with 0.01% SDS for polyvinylidenfluorid membranes). Following 3-5 washes in TBST, membranes were transferred to PBS and antibody fluorescence was detected at 700 and 800 nm using an Odyssey infrared imaging system (LI-COR).

Total RNA extraction and cDNA synthesis

For total RNA extraction, cells were harvested by trypsinization and lysed in RNA lysis buffer following the RNA Miniprep kit (Agilent). Genomic DNA contamination was reduced by on-column DNase digestion as described in the manual, and purified RNA was stored at -80°C. For validation of LARP1B CRISPR KO, total RNA was reverse transcribed to cDNA, which was used as the template for cDNA amplification of edited LARP1B transcripts. LARP1B transcripts were amplified as described above for genomic DNA validation.

Live-cell imaging

For live-cell imaging, cells were seeded at low density (20,000-30,000) in 35 mm glass-bottom μ-dishes (Ibidi) and grown for 2-3 days. On the day of imaging, the cells were incubated with JF549 or JF646 dyes (HHMI Janelia Research Campus, Grimm *et al.*, 2015) to label the MCP-Halo coat protein for 30 minutes, unbound dye was removed (3 washes, PBS), and cells were kept in culture medium until imaging. For induction of reporter mRNAs, 1 μg/ml doxycycline (Sigma-Aldrich) was added to each dish at appropriate time points before each imaging session (30 minutes) to ensure the same duration of doxycycline induction at the start of imaging for all dishes of an experiment.

At the start of imaging of each dish, culture medium was replaced with FluoroBrite imaging DMEM (Thermo Fisher Scientific) supplemented with 10% FBS , 2 mM glutamine, and 1 μg/ml doxycycline.

To inhibit mTOR, cells were treated with 250 nM Torin1, 100 nM Rapamycin, 2.5 μM PP242, or 250 nM TAK228 for the specified duration, and the inhibitor was maintained throughout the imaging session. To inhibit translation, cells were treated with 100 μg/ml puromycin 5 minutes prior to the start of imaging, which was maintained throughout imaging. To allow elongating ribosomes to run-off, cells were treated with 3 μg/ml harringtonine 10 minutes prior to the start of imaging, which was maintained throughout imaging. For all experiments, the start of the 30 minutes imaging window was recorded as the timepoint shown in the figures (e.g. imaging 60-90 minutes after Torin1 addition = 60 minutes timepoint).

Cells were kept at 37°C and 5% CO_2 throughout image acquisition. All dual-color live-cell imaging was performed on an inverted Ti2-E Eclipse (Nikon) microscope equipped with a CSU-W1 scan head (Yokogawa), two back-illuminated EMCCD cameras iXon-Ultra-888 (Andor) with chroma ET525/50 m and ET575lp emission filters, and an MS-2000 motorized stage (Applied Scientific Instrumentation). Cells were illuminated with 561 Cobolt Jive (Cobolt), 488 iBeam Smart, 639 iBeam Smart (Toptica Photonics) lasers, and a VS-Homogenizer (Visitron Systems GmbH). Using a CFI Plan Apochromat Lambda 100x oil/NA1.45 objective (Nikon), images were obtained with a pixel size of 0.134 μm. To allow for simultaneous tracking of mRNA and translation sites, both channels were simultaneously acquired by both cameras at 20 Hz for 100 frames in a single Z-plane (5 sec movies).

Live-cell data analysis

For image analysis, the first 5-14 frames of each movie (500 ms) were selected for single particle tracking. First, images were corrected for any offset between the two cameras using TetraSpeck fluorescent beads acquired on each imaging day. Using the FIJI (Rueden *et al.*, 2017; Schindelin *et al.*, 2012) descriptor-based registration plugin (Preibisch *et al.*, 2010) in affine transformation mode, a transformation model was obtained to correct the bead offset, and applied to all images of an imaging day using a custom macro (Mateju *et al.*, 2020). Subsequently, fine correction of remaining offsets between images were corrected for each dish individually using the FIJI translate function run in a custom macro, correcting for offsets occurring progressively throughout an imaging session.

Single-particle tracking and translation site quantification was performed as described previously (Mateju *et al.*, 2020). In short, using the KNIME analytics platform and a custom-build data processing workflow, regions-of-interest (ROIs) were manually annotated in the mRNA channel, selecting cytosolic regions with multiple bright spots. Importantly, annotation solely in the mRNA channel excludes any bias in selection attributable to the translational state of the cell. Next, spots in the ROIs corresponding to single mRNAs were tracked using TrackMate (Tinevez *et al.*, 2017) integrated in KNIME, using the "Laplacian of Gaussian" detector with an estimated spot radius of 200 nm and sub-pixel localization. Detection thresholds were adjusted based on the SNR of images and varied between 1.25-2. For particle-linking, the parameters linking max distance (600 nm), gap closing max distance (1200 nm), and gap closing max frame gap (2) were optimized for single-particle tracking of mRNAs. To assay whether an mRNA is translating, the mean intensity of the SunTag channel was measured at the coordinates of each mRNA spot, and quantified as fold-change / ROI background

intensity. A cut-off of <1.5 fold/background was determined to classify an mRNA as non-translating based on calibration data using the translation inhibitor harringtonine. Excluding cells with <3 mRNAs, the fraction of translating mRNAs per cell was calculated (translating/all mRNAs per ROI).

For data visualization, the fraction of translating mRNAs per cell and translation site intensities were plotted using SuperPlots (https://huygens.science.uva.nl/SuperPlotsOfData/), showing all data points together with the mean (± SD) of each biological replicate (Lord *et al.*, 2020).

RNAseq

For RNAseq, total RNA samples extracted using the RNA Miniprep kit (Agilent) were assessed for RNA integrity using the Agilent Tapestation, and library preparation was performed using the Illumina TruSeq Stranded mRNA reagents according to the manufacturer's protocol. Libraries were sequenced on the Illumina HiSeq2500 (GEO submission GSE233183: single reads, 50 cycles) or NovaSeq6000 platforms (GEO submission GSE233182: paired-end reads, 100 cycles).

For our analysis, we used a reference list of experimentally validated 5′TOP mRNAs (Philippe *et al.*, 2020), expanded with additional experimentally verified 5′TOP mRNAs (RACK1, EIF3K) as well as computationally predicted 5′TOP mRNAs with known roles in translation (EIF2A, EIF2S3, EIF3L, EIF4A2, and RPL22L1) (Philippe *et al.*, 2020). The presence or absence of a PRTE in the 5′UTR was taken from Hsieh *et al.*, 2012, and expanded by manual annotation for the subset of 5′TOP mRNAs not listed (Supplementary Table S2).

Sequenced reads were aligned against the human genome (GENCODE GRCh38 primary assembly, https://www.gencodegenes.org/human/release_38.html) using R version 4.1.1 with Bioconductor version 3.13 to execute the qAlign tool (QuasR package, version 1.32.0, Gaidatzis *et al.*, 2014), with default parameters except for aligner = "Rhisat2", splicedAlignment = "TRUE", allowing only uniquely mapping reads. Raw gene counts were obtained using the qCount tool (QuasR) with a TxDb generated from gencode.v38.primary_assembly.annotation.gtf as query, with default parameters counting only alignments on the opposite strand as the query region. The count table was filtered to only keep genes which had at least 1 cpm in at least 3 samples.

smFISH

For smFISH, HeLa-11ht cell lines were seeded on high precision glass coverslips placed in 12-well tissue culture plates, grown for two days to reach ∼50% confluency, and fixed using 4% paraformaldehyde (10 minutes, room temperature). To detect endogenous mRNAs, atto633 conjugated smFISH probes targeting human MYC mRNA were generated by enzymatic oligonucleotide labeling (Gaspar *et al.*, 2018), using Amino-11-ddUTP and Atto633-NHS. Quasar570 conjugated smFISH probes targeting RPL5, RPL11, and RPL32 were purchased ready-to-use (Biosearch Technologies). Probe sequences are listed in Supplementary Table S3. smFISH was performed as described previously (Mateju *et al.*, 2020). In brief, fixed cells were washed twice in PBS (5 minutes), permeabilized overnight in 70% ethanol, washed thrice in smFISH wash buffer (2x saline-sodium citrate, 10% formamide, 5min), and hybridized with smFISH probes (2x saline-sodium citrate, 10% formamide, 10% dextran sulfate, 125

nM Quasar570/atto633 smFISH probe) at 37°C for 4 hours. Coverslips were washed twice with smFISH wash buffer (30 minutes), and mounted on glass slides using Prolong Gold mounting medium containing DAPI. Cells were imaged using an upright spinning-disk confocal microscope equipped with a CSU-W1 scan head (Yokogawa) and sCMOS detectors. Using a Plan Apochromat 63x oil/NA1.4 objective, Z-stacks were obtained with a pixel size of 103 nm and Z-stack spacing of 200 nm using single-camera sequential acquisition.

Analysis of smFISH data was performed using custom-build python scripts. Nuclei were segmented in 3D using the triangle threshold method, merged nuclei were split by applying a seeded watershed on the Euclidian distance transformed segmentation mask, and segmentation nuclei with an area < 200 or a solidity < 0.5 were removed. The cytoplasm was segmented on a maximum intensity projection by using the median as a threshold to obtain a semantic segmentation, and then splitting this segmentation into cell instance with a seeded watershed applied to the Euclidian distance transform of the semantic segmentation. The maximum projection of the 3D nuclei labeling were taken as seeds for cell segmentation. mRNA spots were detected using a Laplacian of Gaussian filter to detect diffraction limited spots, and refined by applying a h-maxima detector to remove detections below a transcript-specific threshold.

SLAMseq

For SLAMseq, HeLa-11ht cell lines were incubated with a dilution series of S4U for 24 hours, exchanging S4U-containing media every 3 hours according to the manufacturer's instructions. S4U cytotoxicity was assessed using a luminescent cell viability assay, and the half-maximal inhibitory concentration (IC50) was calculated at 209 μM (n=2). Based on the IC50, a trial RNAseq was conducted with 24 hours S4U labelling using a dilution series (0, 3, 6, 12, 24 and 48 μM) of S4U and exchanging media every 3 hours. The 12 μM S4U concentration was selected as the optimal experimental S4U concentration with minimal effects on gene expression for all cell lines.

For assessing global RNA half-lives, HeLa-11ht cell lines were labelled with 12 μM S4U for 24 hours (exchanging media every 3 hours), labeling was stopped using 100x excess uridine (1.2 mM), and cells were harvested at timepoints 0, 2, 4, 6, 9, and 12 hours after the uridine quench. For isolation of total RNA, RNA was extracted using an RNA miniprep kit (Agilent) with on-column DNase digestion, followed by iodoacetamide treatment and ethanol precipitation of modified total RNA. For RNAseq, total RNA was assessed for RNA integrity using the Agilent Tapestation, and library preparation was performed using the Illumina TruSeq Stranded Total RNA Library Prep Gold kit according to the manufacturer's protocol. Libraries were sequenced on the Illumina NextSeq500 (GEO submission GSE233186: single reads, 75cycles). Samples were submitted as three independent technical replicates (cells harvested on separate days), with the exception of one sample with only two replicates (E6_0h).

In total ∼3.7 billion SLAMseq reads were produced corresponding to ∼52M reads per replicate. S4U incorporation events were analyzed using the SlamDunk software (v0.3.4) for SLAMseq analysis (Neumann *et al.*, 2019). SLAMseq reads were first reverse complemented to match the hard-coded assumed SlamDunk orientation using fastx_reverse_complement from the FASTX-toolkit (http://hannonlab.cshl.edu/fastx_toolkit) with default settings. The resulting fastq files were mapped to

the reference genome (GENCODE GRCh38 primary assembly) with slamdunk map and parameters -5 0 -ss q. The mapped reads were subsequently filtered to only retain intragenic mappings according to the reference transcriptome (GRCh38, GENCODE v33) with a high identity using slamdunk filter and parameters -mi 0.9. SNP variants in the samples were called with slamdunk snp with parameters -c 1 -f 0.2. The SNP variants from all samples were combined in a single master vcf file by indexing the individual vcf file using tabix of the htslib package (https://github.com/samtools/htslib) and merging using vcf-merge from the VCFtools package (Danecek *et al.*, 2011). S4U incorporation and conversion rates were calculated separately for exonic gene segments of the reference transcriptome using slamdunk count with default parameters and the master SNP vcf file for SNP filtering. The exonic segments counts were then aggregated to obtain gene level total mapping reads, multimapping reads and converted reads counts. During aggregation, total and converted counts from exonic segment with multimappers were downweighted by the fraction of multimappers over the total mapped reads of the exonic segment (fm). Finally, gene conversion rates were calculated as the number of gene-level aggregated converted reads over the gene-level aggregated total read counts. Gene conversion rates in each context were fitted to an exponential time decay model to obtain gene half-life estimates. Fitting was performed by non-linear least squares using the R stats::nls function. Example fit command:

$$fit <- nls(rates \sim exp(a + k * timepoints), control = list(minFactor = 10^{-7}, tol = 10^{-5}, maxiter = 256)$$

where rates are the conversion rates for the gene (including all replicates) and timepoints are the corresponding times in hours. The half-life (in minutes) was obtained from the fitted coefficient:

$$t1/2 = -1/k * ln(2) * 60$$

Half-life estimates and the fitting R2 values are listed in Suppl. Table 4 for all transcripts with $R^2 \geq 0.75$ in all conditions.

Statistical Analysis

For live-cell imaging, biological replicates (n) were defined as independent days of imaging. Statistical analyses were performed using GraphPad Prism, with n numbers and statistical tests described in the figure legends. Technical replicates within biological replicates were pooled before statistical tests.

For RNAseq analysis of LARP1 WT cells, biological replicates (n) were defined as independent clonal cell lines (canonical and 5′TOP mRNA cell lines, n=2). For RNAseq of LARP1 KO clones, four single-cell derived clones were sequenced for both canonical and 5′TOP cell lines and treated as independent biological replicates (n=8 total). For each n, three independent replicates (cells harvested on separate days) were submitted for RNAseq and averaged before statistical tests. Differential gene expression was calculated with the Bioconductor package edgeR (version 3.34.0, Lun *et al.*, 2016) using the quasi-likelihood F-test after applying the calcNormFactors function, obtaining the dispersion estimates and fitting the negative binomial generalized linear models.

For SLAMseq analysis, biological replicates (n) were defined as independent clonal cell lines for both LARP1 WT and LARP1 KO cells (canonical and 5′TOP mRNA cell lines, n=2). For analysis of changes

in mRNA stability, the estimated half-lives were averaged for n1 and n2, and changes in mRNA stability were calculated between genotypes (log2 FC). Significant differences in mRNA stability were classified with abs log2 FC $\geq$ 1, excluding spurious transcripts overlapping in sequence with known 5′TOP mRNAs (read-through transcripts AC135178.3, AP002990.1, AC245033.1, lncRNA AL022311.1, MIR4426, MIR3654).

Data and materials availability

All data needed to evaluate the conclusions in the paper are present in the paper and/or the Supplementary Materials. Sequencing data for this study has been deposited in the GEO repository (GSE233187). All reagents generated in this study are available from the lead contact, Dr. Jeffrey A. Chao (jeffrey.chao@fmi.ch) with a completed material transfer agreement. All original code (KNIME workflows and ImageJ macros) and image analysis output files have been deposited at Zenodo and are publicly available (https://doi.org/10.5281/zenodo.10057405).

Chapter 3

Discussion

While the role of the 5′TOP motif in translational regulation of ribosome biogenesis has been known for decades, the identity of the crucial regulatory factor that controls this mechanism has been much less clear. In this thesis, I investigated the role of the regulatory factors LARP1 and 4EBP1/2 in mediating 5′TOP translational regulation utilizing single-molecule imaging in living cells. In chapter 2, I presented evidence that 4EBP1/2 play a dominant role in 5′TOP translational repression, and that LARP1 plays a crucial role in stabilizing 5′TOP mRNAs from degradation in mTOR active cells.

In this chapter, I will place these findings in the context of the current research in the field, describing their implications, discussing open questions, and outlining possible strategies for future research.

3.1 Implications of the 5′ terminal location of the 5′TOP motif

A key question regarding the selective translational regulation of 5′TOP mRNAs is the identity of the proteins that interact with the 5′TOP motif, which at its core consists of the 5′ cap, +1 cytosine and adjacent four pyrimidines. The structure of LARP1's DM15 domain bound to these residues of a 5′TOP oligonucleotide provided strong evidence for LARP1 as the key specificity factor (Lahr *et al.*, 2017). However, our data show that even in the absence of LARP1, 5′TOP mRNAs are still selectively regulated in their translation (Fig. 2.10). What is the identity of the additional specificity mediating factor(s)?

First, it is possible that an unknown *trans*-acting factor is recruited to 5′TOP mRNAs downstream of 4EBP1/2. This factor may not be able to bind 5′TOP mRNAs when they are actively translating with eIF4F bound to the 5′ cap blocking accessibility to the 5′TOP motif, and may only be recruited to 5′TOP mRNAs upon 4EBP1/2 activation when eIF4F is released from the 5′ cap. It appears unlikely that such a factor has been missed in previous pull-down studies of RNA-binding protein (RBP) recruited to the 5′ cap and 5′TOP mRNAs (Smith *et al.*, 2020; Tcherkezian *et al.*, 2014), while previously identified pyrimidine binding proteins (TIA1 and TIAL1/TIAR) appear to be dispensable

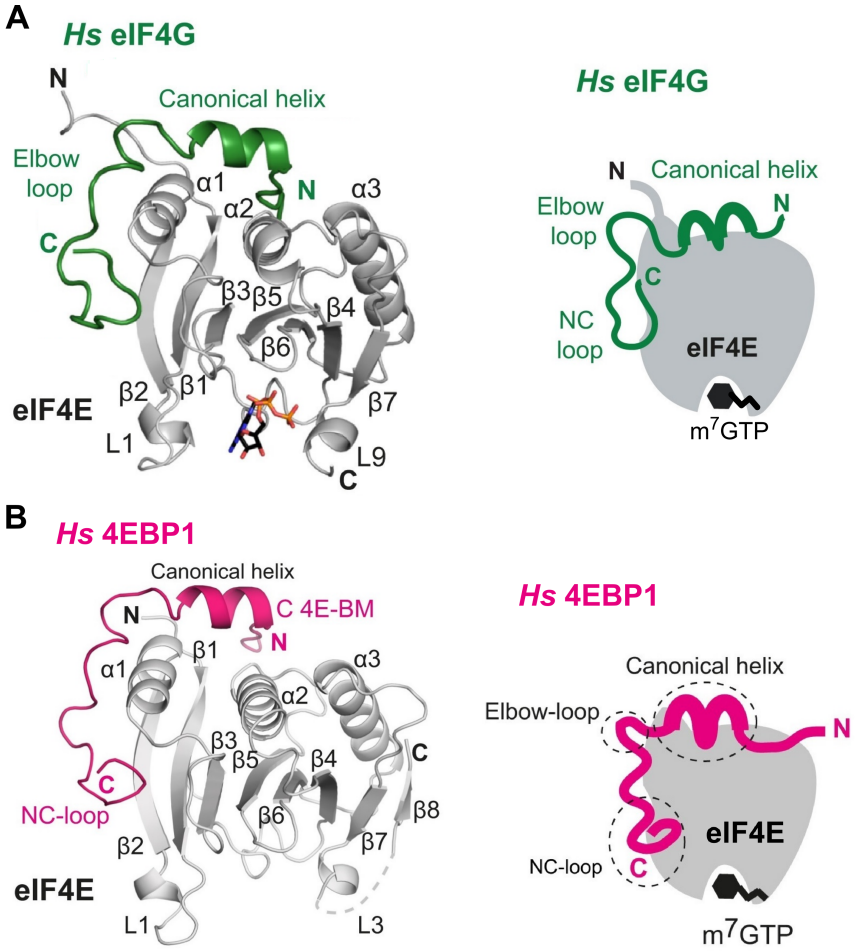

Figure 3.1: Molecular architecture of eIF4E-eIF4G and eIF4E-4EBP1 complexes. (**A**) Structure of eIF4E bound to the eIF4E binding regions of eIF4G (aa608–642), including the bound m^7GTP cap. Adapted from Grüner *et al.*, 2016. (**B**) Structure of eIF4E bound to the eIF4E binding regions of 4EBP1 (aa49–83). Adapted from Peter *et al.*, 2015. For both eIF4G and 4EBP1, 4E-binding motifs (4E-BM) consist of a canonical helix and non-canonical (NC) loop connected by a flexible elbow loop.

for mTORC1-dependent translational regulation of 5′TOP mRNAs (Damgaard & Lykke-Andersen, 2011; Thoreen *et al.*, 2012). Second, 4EBP1/2 may directly recognize the 5′TOP element, thereby acting not only as a general inhibitor of cap-dependent translation, but also as a 5′TOP RBP. Third, eIF4E may have inherent sequence preference for cap-adjacent nucleotides, binding more weakly to 5′TOP mRNAs, thereby being selectively depleted from 5′TOP mRNAs upon mTOR inhibition. The location of the 5′TOP motif at the 5′ end of mRNAs strongly suggests that translation initiation factors are able to contact the 5′TOP motif. To evaluate the plausibility of the second and third model, it is useful to consider the structural architecture of eIF4E, 4EBP1/2, and eIF4G bound to 5′TOP mRNAs (Fig. 3.1).

Co-crystal structures of the central region of eIF4E bound to the 5′ cap have provided insight into how eIF4E engages the 5′ cap, with the ventral surface of eIF4E wrapping around the 5′ cap (Fig. 3.1). How the cap-adjacent nucleotides interact with eIF4E is not understood at a structural level, but *in vitro* experiments have reported striking differences in eIF4E affinity to RNA ligands depending on the

nucleotide context. In one study, while the cap m^7GpppG had a relatively weak affinity for eIF4E (561 nM), the affinity increased ∼4x for a capped 10 nts oligonucleotide carrying a 5 nts 5′TOP motif (149 nM), and increased further when the +1 cytosine was replaced for a +1 adenine (72 nM) or guanosine (39 nM), suggesting that 5′TOP mRNAs are more weakly bound to eIF4E (Tamarkin-Ben-Harush *et al.*, 2017). As these experiments were limited to short oligos, the role of additional, longer sequence contexts is still unexplored. Importantly, it remains to be shown that these differences in eIF4E affinity are sufficient to significantly affect mRNA translation rates, but these measurements are consistent with our data showing a slightly decreased translation rate for 5′TOP mRNAs in mTOR active cells (see Fig. 2.16H).

As structural and biochemical studies of eIF4E binding have mostly focused on the affinity of eIF4E to the cap in isolation, it is largely unclear how well these measurements translate to *in vivo* mRNP complexes. Importantly, eIF4G, 4EBP1/2, and PABPC1 are known to enhance eIF4E affinity to the 5′ cap through allosteric stabilization of the eIF4E-5′ cap interaction (Gross *et al.*, 2003; Kahvejian *et al.*, 2005; O'Leary *et al.*, 2013). Crystal structures of eIF4E-eIF4G and eIF4E-4EBP1 complexes obtained from eIF4E (excluding the N-terminal unstructured region) co-crystallized with the conserved eIF4E-binding regions of eIF4G and 4EBP1 have revealed a highly similar mode of binding (Fig. 3.1). While different architectures of the eIF4E-eIF4G complex have been suggested (Peter *et al.*, 2015), recent results suggest that eIF4G and 4EBP1 share a conserved mode of binding eIF4E, engaging both dorsal and lateral surfaces of eIF4E with canonical and non-canonical (NC) motifs respectively (Grüner *et al.*, 2016). eIF4G also possesses RNA binding activity and seems poised to contact cap-adjacent nucleotides (Yanagiya *et al.*, 2009), while 4EBP1/2 could engage cap-adjacent nucleotides with either its N- or C-terminal unstructured regions (Fig. 3.2). Structures of eIF4G-eIF4E or 4EBP1/2-eIF4E complexes with capped oligonucleotides have not been solved, and it remains uncertain to what extend cap-adjacent nucleotides can modulate the binding of these translationally relevant complexes. As 5′TOP mRNAs were found to be selectively repressed upon eIF4G depletion, it was postulated that 5′TOP mRNAs uniquely require eIF4G to anchor eIF4E to the 5′ cap (Thoreen *et al.*, 2012), though it seems plausible that eIF4G depletion mirrors the effects of pharmacological mTOR inhibition as both result in low levels of translationally active eIF4E-eIF4G complexes.

In addition to protein interactions, eIF4E affinity could be further modulated by post-translational modifications. Phosphorylation of eIF4E occurs on a single site on Serine 209, which is located in a flexible loop close to the 5′ cap binding pocket (highlighted in Fig. 3.2A). eIF4E Ser209 phosphorylation has been suggested to alter 5′ cap affinity and enhance the translation of a subset of mRNAs, though its relevance for mRNA translation remains poorly understood (Furic *et al.*, 2010; Proud, 2015). Interestingly, while Ser209 is phosphorylated by MAP kinase interacting serine/threonine kinase 1/2 (MNK1/2) independent of mTOR signaling, Ser209 becomes rapidly dephosphorylated upon mTOR inhibition. As MNK1/2 are recruited to eIF4E by binding eIF4G on translationally active mRNAs, mTOR inhibition is thought to trigger eIF4E dephosphorylation by displacement of the MNK1/2-eIF4G complex (Proud, 2015). Therefore, mTOR inhibition is temporally coupled with eIF4E dephosphorylation, raising the possibility that eIF4E dephosphorylation may contribute to

5′TOP translational repression.

Evidence for direct mRNA binding by 4EBP1/2 is currently inconclusive, with findings from recent studies arguing both in support and against this hypothesis. Support for this model comes from two studies, one utilizing RBP-RNA proximity labeling (Jin *et al.*, 2020), the other utilizing RBP-RNA crosslinking (Wolin *et al.*, 2023). The first study utilized targets of RNA binding proteins identified by editing (TRIBE) to map the interactions of tagged 4EBP1 with mRNAs, finding an enrichment of RNA editing events in a subset of transcripts which carry a PRTE. The second study utilized multiplexed CLIP, finding a strong selective increase of 5′TOP mRNAs crosslinked with 4EBP1 upon mTOR inhibition. Together, these findings suggest that 4EBP1/2 may be able to directly bind and repress the translation of 5′TOP and PRTE-containing mRNAs upon mTOR inhibition. A limitation of these studies is the uncertainty whether the interactions measured correspond to direct 4EBP1/2-mRNA interactions, or are instead indirect interactions bridged by other factors such as eIF4E or LARP1. Findings arguing against a role of 4EBP1/2 in directly interacting with the 5′TOP motif come from studies utilizing eIF4E-RNA crosslinking (Jensen *et al.*, 2021) and live-cell imaging of single eIF4E and 4EBP1/2 molecules (Gandin *et al.*, 2022), which described the dissociation of eIF4E-4EBP1/2 complexes from mRNAs upon mTOR inhibition. Biochemically, both 4EBP1/2 and eIF4G peptides enhance the affinity of eIF4E to the 5′ cap (Siddiqui *et al.*, 2012), which appears counterintuitive for eIF4E dissociation, but the removal of eIF4G and concurrent loss of stabilizing mRNA and protein interactions (notably PABPC1) may be sufficient to dissociate 4EBP1/2-eIF4E from mRNAs in the context of physiological mRNP complexes involving additional factors such as RNA helicases.

Given the current lack of clear evidence of direct mRNA binding by 4EBP1/2, it appears premature to classify 4EBP1/2 as a RBP, and further biochemical studies are needed to interrogate 4EBP1/2-mRNA associations. Overall, current evidence leans towards 4EBP1/2 being recruited to 5′TOP mRNAs by directly binding eIF4E, and our results support a model in which differences in 4EBP1/2 recruitment and/or 4EBP1/2-eIF4E dissociation kinetics are sufficient to drive differential translational regulation of 5′TOP and canonical mRNAs.

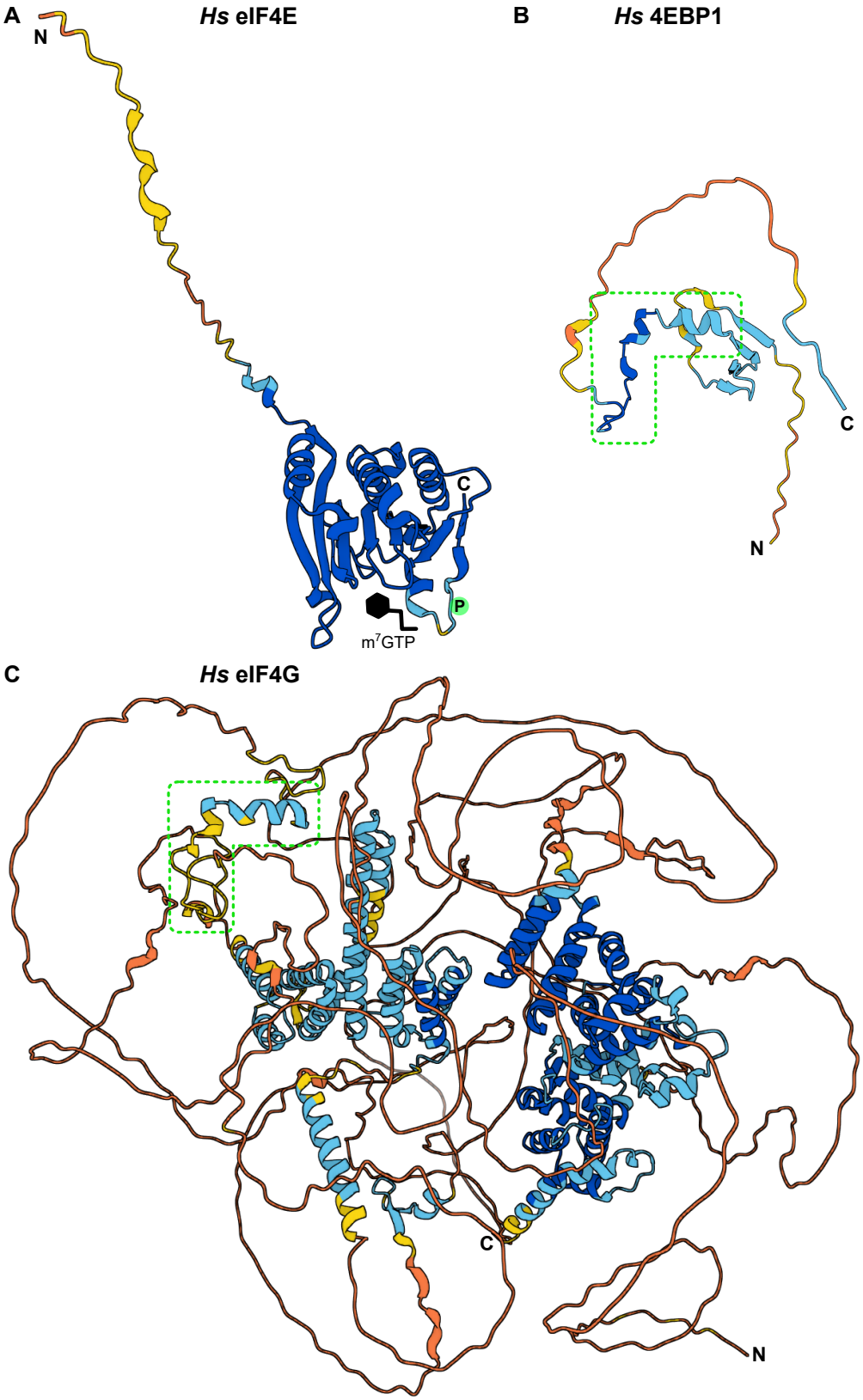

Figure 3.2: Structure Predictions of translation factors with potential cap-adjacent nucleotide contacts. The AlphaFold structure predictions for the ENSEMBL canonical isoforms of full-length human (**A**) eIF4E, (**B**) 4EBP1, and (**C**) eIF4G are shown. For (A), the phosphorylated Ser209 of eIF4E is highlighted, and the mRNA cap is added in accordance with co-crystal structures. For (B, C), the eIF4E binding sites are highlighted (green box). Residue color represents model confidence (dark blue = very high, light blue = high, yellow = low, orange = very low).

3.2 LARP1 binding and stabilization of actively translating 5′TOP mRNAs

4EBP1/2 and LARP1 are often described as analogous proteins, which both become dephosphorylated, undergo conformational switching, and are recruited to mRNAs upon mTOR inhibition. In contrast to 4EBP1/2, LARP1 possesses multiple RNA binding domains and can in principle associate with mRNAs in an mTOR-independent manner due to its interactions with PABPC1 and the polyA tail, which has been linked to stabilizing mRNAs by inhibiting deadenylation (Park *et al.*, 2023). While the recruitment of LARP1 to mRNA 3′ ends is still poorly understood, more is known about the induced recruitment to 5′TOP mRNAs upon mTOR inhibition. LARP1 is a highly phosphorylated protein, and electrophoretic mobility shift assays (EMSAs) with phosphomimetic mutants have indicated a cluster of dephosphorylated residues that could enable LARP1's DM15 domain to bind the 5′TOP motif upon mTOR inhibition (Jia *et al.*, 2021). As we find a highly selective stabilization of 5′TOP mRNAs by LARP1 in mTOR active cells, it appears likely that LARP1 is also selectively recruited to 5′TOP mRNAs in its phosphorylated state, and dephosphorylation may further enhance LARP1's affinity for 5′TOP mRNAs (Smith *et al.*, 2020). Alternatively, a minor pool of dephosphorylated LARP1 may persist in mTOR active cells, though this seems insufficient to stabilize all 5′TOP mRNAs, which are estimated to constitute up to 20% of all cellular mRNAs (Meyuhas & Kahan, 2015).

How can LARP1 be recruited to actively translating 5′TOP mRNAs, in a situation where the 5′ ends are constitutively bound by eIF4F? First, LARP1 may bind prior to binding of eIF4F to the 5′ cap, with binding taking place in the nucleus soon after transcription (Fig. 3.3A). In this model, the 5′ cap of 5′TOP mRNAs would be bound by the cap binding complex (CBC), leaving the adjacent 5′TOP motif accessible for LARP1 recruitment. Following mRNA export and the start of translation, LARP1 would remain associated with the 5′TOP mRNA at its 3′ end due to its interactions with PABPC1 and the polyA tail. Arguing against this model is the exceptionally long half-lives of 5′TOP mRNAs as LARP1 would not be able to rebind 5′TOP mRNAs in the cytoplasm, necessitating a very low dissociation rate from 5′TOP mRNAs.

Second, LARP1 may bind 5′TOP mRNAs in the cytoplasm in brief pauses of translation (Fig. 3.3B). In our experiments, we observed a minor fraction of non-translating mRNAs in mTOR active cells for both canonical and 5′TOP mRNAs, which likely represent temporarily inactive mRNAs. In support of this, a recently published *in vivo* SunTag study of immobilized mRNAs imaged over long timecourses revealed the presence of translational bursts intersected with brief pauses in translation, with the inactive state suggested to represent eIF4E dissociation events (Livingston *et al.*, 2022). Such events would provide windows of opportunity for LARP1 binding to occur, allowing LARP1 to be continuously recruited to 5′TOP mRNAs while mTOR is active, resulting in a steady-state enrichment of LARP1 bound to 5′TOP mRNA 3′ ends and polyA tail stabilization. In addition, certain models of translation initiation create additional opportune moments for LARP1 binding to occur. In the threading model of 43S recruitment, eIF4E has to dissociate from the 5′ cap to allow the mRNA to be threaded into the 40S ribosomal subunit, creating free 5′ ends during each round of translation

initiation (Brito Querido *et al.*, 2023). Additionally, in the cap-severed model of translation initiation, the 48S initiation complex dissociates eIF4F from the 5′ cap as it moves along the 5′UTR, thereby creating free 5′ ends (Archer *et al.*, 2016). Of note, current evidence favors other models of translation initiation in which eIF4F remains associated with the 5′ cap throughout each round of translation (i.e. the slotting model of 43S recruitment, and the 48S cap-tethered scanning model (Bohlen *et al.*, 2020; Brito Querido *et al.*, 2023).

Third, LARP1 binding may be compatible with eIF4F binding (Fig. 3.3C). While the previous section highlighted the proximity of eIF4E and eIF4G to cap-adjacent nucleotides, it remains possible that LARP1 can recognize the 5′TOP motif while the 5′ cap is bound by eIF4E. The 5′TOP motif could be rotated away from eIF4E and eIF4G to engage with LARP1, while the extensive unstructured regions of LARP1 could provide sufficient flexibility to place the 5′TOP binding domain into position without sterically clashing with translation initiation factors. Recruitment of LARP1 to the 5TOP motif could be aided by interactions with initiation factors (eIF4E, eIF4G), providing selectivity for binding 5′TOP mRNAs over other mRNAs containing 5′TOP-like pyrimidine stretches in their 5′UTR (i.e. mRNAs containing only a PRTE motif).

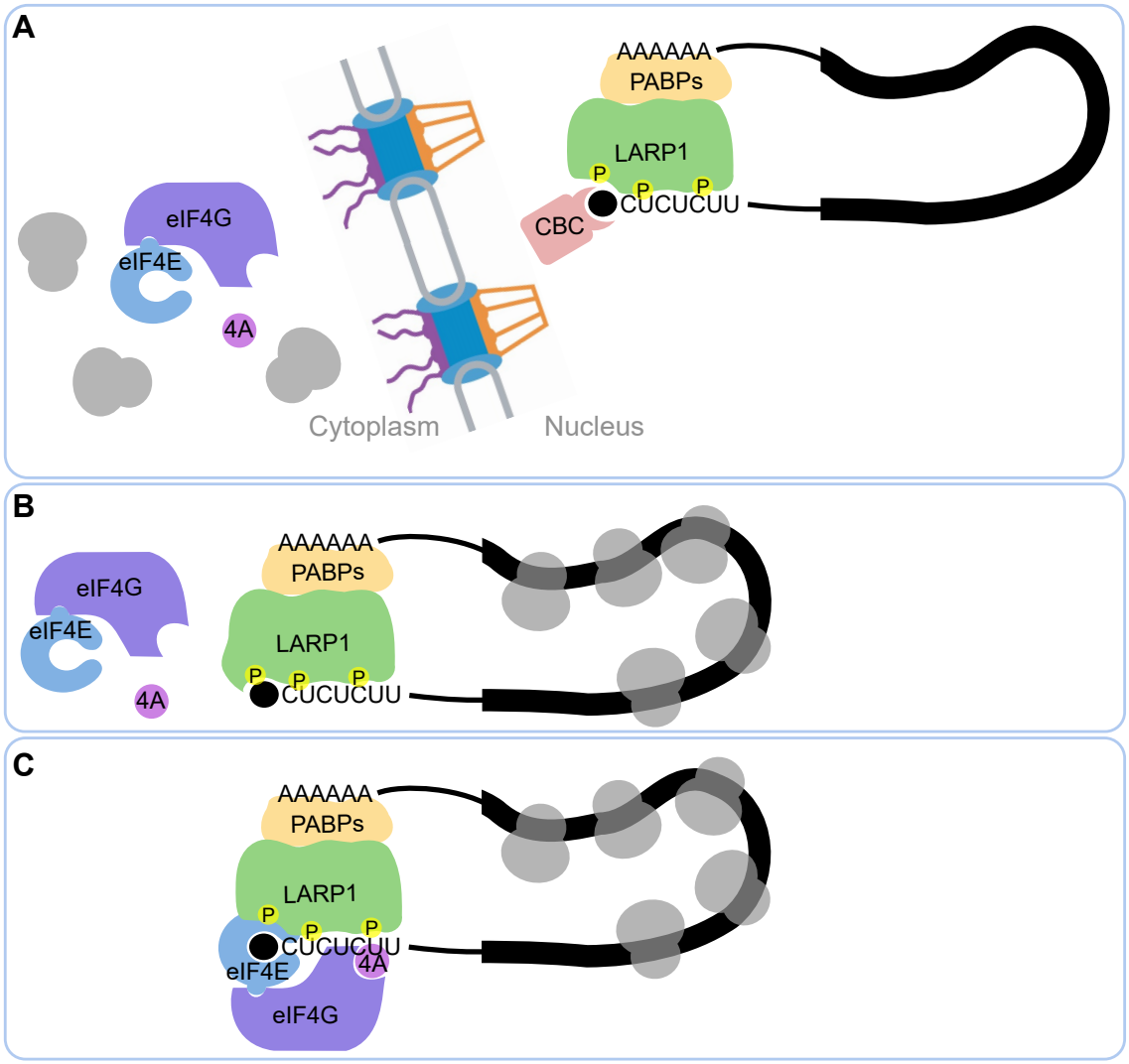

Figure 3.3: Models of LARP1 recruitment to 5′TOP mRNAs in mTORC1 active cells. (**A**) Binding of LARP1 to a newly synthesized 5′TOP mRNA in the nucleus. The 5′ cap is bound by the CBC, while LARP1 is bound to the 5′TOP motif. LARP1 would be exported as part of the 5′TOP mRNP, and stay associated with the 5′TOP mRNA in the cytoplasm. (**B**) Binding of LARP1 during inactive states of 5′TOP mRNA translation caused by eIF4F dissociation, with LARP1 able to bind both the 5′ cap and 5′TOP motif. (**C**) Simultaneous binding of LARP1 and eIF4F to 5′TOP mRNAs, with eIF4E bound to the 5′ cap and LARP1 bound to the 5′TOP motif.

3.3 The role of the PRTE in the regulation of 5′TOP mRNAs

While early studies of 5′TOP mRNA reporters characterized the 5′TOP motif as both sufficient and essential for rapid translational repression upon mTOR inhibition, it is unclear whether the remainder of 5′TOP 5′UTRs are functionally important. Of note, 5′TOP mRNAs contain shorter than usual 5′UTRs, with an average length of only 45 nts (Davuluri *et al.*, 2000). The shortest 5′UTR is found on RPL23A, which possesses a minimal 5′UTR of only 12 nts and a conserved translation initiator of short 5′UTR (TISU) start codon context. The exact mechanism of translation initiation of TISU mRNAs is not known, but due to their short 5′UTRs, ribosome assembly at the start codon likely requires eIF4F dissociation as the 5′ cap and 5′UTR are expected to be located within the ribosome exit channel (Sinvani *et al.*, 2015). The majority of 5′TOP 5′UTRs contain a PRTE, including our RPL32 reporter, which allowed us to test whether 5′TOP translational repression is fully abolished upon mutation of the 5′TOP motif. While mutation of the 5′TOP motif (Δ5′TOP) is sufficient to abolish most of the 5′TOP selective translational repression, the Δ5′TOP mRNAs are slightly but significantly more repressed than mRNAs with both the 5′TOP and PRTE motifs mutated (Δ5′TOP/PRTE), suggesting a minor repressive role of the downstream PRTE element on its own. This difference persists in the absence of LARP1, arguing against LARP1 binding the PRTE element to weakly repress 5′TOP mRNAs. The minor PRTE-specific translational repression we find may not be a significant contributor to 5′TOP translational repression *in vivo*, as the presence or absence of a PRTE element did not affect the extent of 5′TOP translational repression in a global analysis of endogenous 5′TOP mRNAs (Philippe *et al.*, 2020). Alternatively, PRTE-mediated effects on translational repression may be too weak to be picked up by less sensitive methods.

Aside from regulating translation, a recent study described a role of the PRTE in 5′TOP mRNA localization, which is abolished upon loss of LARP1 (Goering *et al.*, 2023). It is possible that LARP1 can bind to either the 5′TOP or PRTE in the 5′UTR in a manner which does not inhibit translation initiation, allowing these elements to be utilized for intracellular mRNA targeting. Of note, ribosomal protein mRNAs in intestinal epithelium show a distinct localization pattern, with an enrichment in either the apical or basal side of the polarized cell in fed and starved organoids respectively (Moor *et al.*, 2017). It remains to be seen whether LARP1 is required for the localization of 5′TOP mRNAs observed in intestinal cells.

3.4 Future strategies

In sections 3.1 - 3.3, I described a number of models for the regulation of 5′TOP mRNA translation by 4EBP1/2 and LARP1. A shared limitation of these models is the lack of knowledge regarding the dynamics of translation initiation factor binding to mRNAs: where, when, for how long, and in what order do eIF4F, 4EBP1/2 and LARP1 bind to 5′TOP mRNAs? For 4EBP1/2, it remains unclear whether binding and eIF4G dissociation occurs predominantly at eIF4E-eIF4G complexes bound to

mRNAs or apo eIF4E-eIF4G complexes. For eIF4F, it remains unclear how stably the eIF4E-eIF4G complex is bound to mRNAs. For mTORC1-mediated translational repression, it remains unclear whether 4EBP1/2 and LARP1 are sequentially or simultaneously recruited to 5′TOP mRNAs.

To resolve these and further questions, future strategies will focus on structural isolation of 5′TOP mRNP complexes in either mTORC1 active or inactive cells, and imaging of single labeled molecules of translation initiation factors bound to 5′TOP mRNAs. To facilitate long-term tracking of single molecules, 5′TOP mRNAs can be immobilizing with stemloop-mediated membrane anchoring, enabling the imaging of translation bursts and pauses (Livingston *et al.*, 2022). Visualizing single molecules of translation factors is highly technically challenging, but can be performed *in vivo* by utilizing sparse-labeling of a subset of protein molecules and motion-blurring of free proteins. Combining such an approach with SunTag translation site imaging will enable the visualization and quantification of translation factor binding together with direct read-outs of downstream effects on translation. As a sparse-labeling approach is not suitable for the simultaneous imaging of two translation factors, studying combinatory effects of translation factor binding (such as recruitment of 4EBP1/2 and LARP1 to a 5′TOP mRNA) will require both experimental (e.g. improved fluorescent tagging strategies) and computational advances (e.g. deep-learning based image restoration).

3.5 Conclusion

This study provides a characterization of the translational regulation of 5′TOP mRNAs mediated by key regulatory factors. This work utilized single-molecule imaging and genome engineering as powerful tools to directly compare and contrast the contribution of these factors to 5′TOP mRNA regulation, advancing our understanding of how cells respond to the availability of nutrients by regulating the biosynthesis of ribosomes. The strength of the methodology allowed for direct measurements of translation uncoupled from effects of transcription or mRNA stability, showing that 4EBP1/2 play a dominant role in 5′TOP mRNA translational regulation, while LARP1 facilitates the stabilization of 5′TOP mRNAs. These unexpected findings recontextualize results from earlier studies, and are in good agreement with a current complementary study (Kajjo *et al.*, 2024). Finally, this work provides the basis for further investigations aimed at unraveling the intricate mechanisms of translational regulation for 5′TOP and other cellular mRNAs.

References

Adivarahan, S., Livingston, N., Nicholson, B., Rahman, S., Wu, B., Rissland, O. S., & Zenklusen, D. (2018). Spatial Organization of Single mRNPs at Different Stages of the Gene Expression Pathway. *Molecular Cell*, *72*(4), 727–738.e5. https://doi.org/10.1016/j.molcel.2018.10.010

Al-Ashtal, H. A., Rubottom, C. M., Leeper, T. C., & Berman, A. J. (2019). The LARP1 La-Module recognizes both ends of TOP mRNAs. *RNA Biology*, 1–11. https://doi.org/10.1080/15476286.2019.1669404

Amrani, N., Ghosh, S., Mangus, D. A., & Jacobson, A. (2008). Translation factors promote the formation of two states of the closed-loop mRNP. *Nature*, *453*(7199), 1276–1280. https://doi.org/10.1038/nature06974

Aoki, K., Adachi, S., Homoto, M., Kusano, H., Koike, K., & Natsume, T. (2013). LARP1 specifically recognizes the 3′ terminus of poly(A) mRNA. *FEBS Letters*, *587*(14), 2173–2178. https://doi.org/10.1016/j.febslet.2013.05.035

Apsel, B., Blair, J. A., Gonzalez, B., Nazif, T. M., Feldman, M. E., Aizenstein, B., Hoffman, R., Williams, R. L., Shokat, K. M., & Knight, Z. A. (2008). Targeted polypharmacology: Discovery of dual inhibitors of tyrosine and phosphoinositide kinases. *Nature chemical biology*, *4*(11), 691. https://doi.org/10.1038/nchembio.117

Archer, S. K., Shirokikh, N. E., Beilharz, T. H., & Preiss, T. (2016). Dynamics of ribosome scanning and recycling revealed by translation complex profiling. *Nature*, *535*(7613), 570–574. https://doi.org/https://doi.org/10.1038/nature18647

Avni, D., Shama, S., Loreni, F., & Meyuhas, O. (1994). Vertebrate mRNAs with a 5'-terminal pyrimidine tract are candidates for translational repression in quiescent cells: Characterization of the translational cis-regulatory element. *Molecular and Cellular Biology*, *14*(6), 3822–3833. https://doi.org/10.1128/mcb.14.6.3822-3833.1994

Avni, D., Biberman, Y., & Meyuhas, O. (1997). The 5′ Terminal Oligopyrimidine Tract Confers Translational Control on Top Mrnas in a Cell Type-and Sequence Context-Dependent Manner. *Nucleic Acids Research*, *25*(5), 995–1001. https://doi.org/10.1093/nar/25.5.995

Banaszynski, L. A., Chen, L.-c., Maynard-Smith, L. A., Ooi, A. G. L., & Wandless, T. J. (2006). A Rapid, Reversible, and Tunable Method to Regulate Protein Function in Living Cells Using Synthetic Small Molecules. *Cell*, *126*(5), 995–1004. https://doi.org/10.1016/j.cell.2006.07.025

Battaglioni, S., Benjamin, D., Wälchli, M., Maier, T., & Hall, M. N. (2022). mTOR substrate phosphorylation in growth control. *Cell*, *185*(11), 1814–1836. https://doi.org/10.1016/j.cell.2022.04.013

Berman, A. J., Thoreen, C. C., Dedeic, Z., Chettle, J., Roux, P. P., & Blagden, S. P. (2020). Controversies around the function of LARP1. *RNA Biology*, 1–11. https://doi.org/10.1080/15476286.2020.1733787

Biberman, Y., & Meyuhas, O. (1997). Substitution of just five nucleotides at and around the transcription start site of rat β-actin promoter is sufficient to render the resulting transcript a subject for translational control. *FEBS Letters*, *405*(3), 333–336. https://doi.org/10.1016/S0014-5793(97)00234-2

Bohlen, J., Fenzl, K., Kramer, G., Bukau, B., & Teleman, A. A. (2020). Selective 40S Footprinting Reveals Cap-Tethered Ribosome Scanning in Human Cells. *Molecular Cell*, *79*(4), 561–574.e5. https://doi.org/10.1

016/j.molcel.2020.06.005

Bohlen, J., Roiuk, M., & Teleman, A. A. (2021). Phosphorylation of ribosomal protein S6 differentially affects mRNA translation based on ORF length. *Nucleic Acids Research*, *49*(22), 13062–13074. https://doi.org/10.1093/nar/gkab1157

Brito Querido, J., Díaz-López, I., & Ramakrishnan, V. (2023). The molecular basis of translation initiation and its regulation in eukaryotes. *Nature Reviews Molecular Cell Biology*, 1–19. https://doi.org/https://doi.org/10.1038/s41580-023-00624-9

Brito Querido, J., Sokabe, M., Kraatz, S., Gordiyenko, Y., Skehel, J. M., Fraser, C. S., & Ramakrishnan, V. (2020). Structure of a human 48S translational initiation complex. *Science (New York, N.Y.)*, *369*(6508), 1220–1227. https://doi.org/10.1126/science.aba4904

Bryant, D. M., Datta, A., Rodríguez-Fraticelli, A. E., Peränen, J., Martín-Belmonte, F., & Mostov, K. E. (2010). A molecular network for de novo generation of the apical surface and lumen [Edition: 2010/10/05]. *Nat Cell Biol*, *12*(11), 1035–45. https://doi.org/10.1038/ncb2106

Burrows, C., Abd Latip, N., Lam, S. J., Carpenter, L., Sawicka, K., Tzolovsky, G., Gabra, H., Bushell, M., Glover, D. M., Willis, A. E., & Blagden, S. P. (2010). The RNA binding protein Larp1 regulates cell division, apoptosis and cell migration [Edition: 2010/05/01]. *Nucleic Acids Res*, *38*(16), 5542–53. https://doi.org/10.1093/nar/gkq294

Carninci, P., Sandelin, A., Lenhard, B., Katayama, S., Shimokawa, K., Ponjavic, J., Semple, C. A., Taylor, M. S., Engström, P. G., Frith, M. C., Forrest, A. R., Alkema, W. B., Tan, S. L., Plessy, C., Kodzius, R., Ravasi, T., Kasukawa, T., Fukuda, S., Kanamori-Katayama, M., … Hayashizaki, Y. (2006). Genome-wide analysis of mammalian promoter architecture and evolution [Edition: 2006/04/29]. *Nat Genet*, *38*(6), 626–35. https://doi.org/10.1038/ng1789

Cassidy, K. C., Lahr, R. M., Kaminsky, J. C., Mack, S., Fonseca, B. D., Das, S. R., Berman, A. J., & Durrant, J. D. (2019). Capturing the Mechanism Underlying TOP mRNA Binding to LARP1. *Structure*. https://doi.org/10.1016/j.str.2019.10.006

Chan, L. Y., Mugler, C. F., Heinrich, S., Vallotton, P., & Weis, K. (2018). Non-invasive measurement of mRNA decay reveals translation initiation as the major determinant of mRNA stability. *eLife*, *7*, e32536. https://doi.org/10.7554/eLife.32536

Chen, I. T., & Roufa, D. J. (1988). The transcriptionally active human ribosomal protein S17 gene [Edition: 1988/10/15]. *Gene*, *70*(1), 107–16. https://doi.org/10.1016/0378-1119(88)90109-6

Chu, V. T., Weber, T., Wefers, B., Wurst, W., Sander, S., Rajewsky, K., & Kühn, R. (2015). Increasing the efficiency of homology-directed repair for CRISPR-Cas9-induced precise gene editing in mammalian cells [Edition: 2015/03/25]. *Nat Biotechnol*, *33*(5), 543–8. https://doi.org/10.1038/nbt.3198

Ciganda, M., & Williams, N. (2011). Eukaryotic 5S rRNA biogenesis [Edition: 2011/10/01]. *Wiley Interdiscip Rev RNA*, *2*(4), 523–33. https://doi.org/10.1002/wrna.74

Cong, L., Ran, F. A., Cox, D., Lin, S., Barretto, R., Habib, N., Hsu, P. D., Wu, X., Jiang, W., Marraffini, L. A., & Zhang, F. (2013). Multiplex genome engineering using CRISPR/Cas systems [Edition: 2013/01/05]. *Science*, *339*(6121), 819–23. https://doi.org/10.1126/science.1231143

Damgaard, C. K., & Lykke-Andersen, J. (2011). Translational coregulation of 5'TOP mRNAs by TIA-1 and TIAR [Edition: 2011/10/08]. *Genes Dev*, *25*(19), 2057–68. https://doi.org/10.1101/gad.17355911

Danecek, P., Auton, A., Abecasis, G., Albers, C. A., Banks, E., DePristo, M. A., Handsaker, R. E., Lunter, G., Marth, G. T., Sherry, S. T., McVean, G., & Durbin, R. (2011). The variant call format and VCFtools [Edition: 2011/06/10]. *Bioinformatics*, *27*(15), 2156–8. https://doi.org/10.1093/bioinformatics/btr330

Dave, P., Roth, G., Griesbach, E., Mateju, D., Hochstoeger, T., & Chao, J. A. (2023). Single-molecule imaging reveals translation-dependent destabilization of mRNAs. *Molecular Cell*, *83*(4), 589–606.e6. https://doi.org/10.1016/j.molcel.2023.01.013

Davuluri, R. V., Suzuki, Y., Sugano, S., & Zhang, M. Q. (2000). Cart classification of human 5′ utr sequences. *Genome research*, *10*(11), 1807–1816. https://doi.org/https://doi.org/10.1101/gr.gr-1460r

Draper, D. E. (1990). Mechanisms of ribosomal protein translational autoregulation. In *Post-transcriptional control of gene expression* (pp. 299–308). Springer. https://doi.org/10.1007/978-3-642-75139-4_28

Dudov, K. P., & Perry, R. P. (1984). The gene family encoding the mouse ribosomal protein L32 contains a uniquely expressed intron-containing gene and an unmutated processed gene. *Cell*, *37*(2), 457–468. https://doi.org/10.1016/0092-8674(84)90376-3

Espejo, R. T., & Plaza, N. (2018). Multiple Ribosomal RNA Operons in Bacteria; Their Concerted Evolution and Potential Consequences on the Rate of Evolution of Their 16S rRNA. *Frontiers in Microbiology*, *9*. https://doi.org/10.3389/fmicb.2018.01232

Fonseca, B. D., Smith, E. M., Yelle, N., Alain, T., Bushell, M., & Pause, A. (2014). The ever-evolving role of mTOR in translation [Edition: 2014/09/30]. *Semin Cell Dev Biol*, *36*, 102–12. https://doi.org/10.1016/j.semcdb.2014.09.014

Fonseca, B. D., Zakaria, C., Jia, J. J., Graber, T. E., Svitkin, Y., Tahmasebi, S., Healy, D., Hoang, H. D., Jensen, J. M., Diao, I. T., Lussier, A., Dajadian, C., Padmanabhan, N., Wang, W., Matta-Camacho, E., Hearnden, J., Smith, E. M., Tsukumo, Y., Yanagiya, A., … Damgaard, C. K. (2015). La-related Protein 1 (LARP1) Represses Terminal Oligopyrimidine (TOP) mRNA Translation Downstream of mTOR Complex 1 (mTORC1) [Edition: 2015/05/06]. *J Biol Chem*, *290*(26), 15996–6020. https://doi.org/10.1074/jbc.M114.621730

Fuentes, P., Pelletier, J., Martinez-Herráez, C., Diez-Obrero, V., Iannizzotto, F., Rubio, T., Garcia-Cajide, M., Menoyo, S., Moreno, V., Salazar, R., Tauler, A., & Gentilella, A. (2021). The 40S-LARP1 complex reprograms the cellular translatome upon mTOR inhibition to preserve the protein synthetic capacity [Edition: 2021/11/25]. *Sci Adv*, *7*(48), eabg9275. https://doi.org/10.1126/sciadv.abg9275

Furic, L., Rong, L., Larsson, O., Koumakpayi, I. H., Yoshida, K., Brueschke, A., Petroulakis, E., Robichaud, N., Pollak, M., Gaboury, L. A., Pandolfi, P. P., Saad, F., & Sonenberg, N. (2010). eIF4E phosphorylation promotes tumorigenesis and is associated with prostate cancer progression [Edition: 2010/08/04]. *Proc Natl Acad Sci U S A*, *107*(32), 14134–9. https://doi.org/10.1073/pnas.1005320107

Gaidatzis, D., Lerch, A., Hahne, F., & Stadler, M. B. (2014). QuasR: Quantification and annotation of short reads in R. *Bioinformatics*, *31*(7), 1130–1132. https://doi.org/10.1093/bioinformatics/btu781

Gandin, V., Masvidal, L., Hulea, L., Gravel, S. P., Cargnello, M., McLaughlan, S., Cai, Y., Balanathan, P., Morita, M., Rajakumar, A., Furic, L., Pollak, M., Porco, J. A., Jr., St-Pierre, J., Pelletier, J., Larsson, O., & Topisirovic, I. (2016). nanoCAGE reveals 5' UTR features that define specific modes of translation of functionally related MTOR-sensitive mRNAs [Edition: 2016/03/18]. *Genome Res*, *26*(5), 636–48. https://doi.org/10.1101/gr.197566.115

Gandin, V., English, B. P., Freeman, M., Leroux, L.-P., Preibisch, S., Walpita, D., Jaramillo, M., & Singer, R. H. (2022). Cap-dependent translation initiation monitored in living cells. *Nature communications*, *13*(1), 6558. https://doi.org/10.1038/s41467-022-34052-8

Gaspar, I., Wippich, F., & Ephrussi, A. (2018). Terminal deoxynucleotidyl transferase mediated production of labeled probes for single-molecule FISH or RNA capture. *Bio-protocol*, *8*(5), e2750–e2750. https://doi.org/10.21769/BioProtoc.2750

Gentilella, A., Moron-Duran, F. D., Fuentes, P., Zweig-Rocha, G., Riano-Canalias, F., Pelletier, J., Ruiz, M., Turon, G., Castano, J., Tauler, A., Bueno, C., Menendez, P., Kozma, S. C., & Thomas, G. (2017). Autogenous Control of 5'TOP mRNA Stability by 40S Ribosomes [Edition: 2017/07/05]. *Mol Cell*, *67*(1), 55–70 e4. https://doi.org/10.1016/j.molcel.2017.06.005

Goering, R., Arora, A., Pockalny, M. C., & Taliaferro, J. M. (2023). RNA localization mechanisms transcend cell morphology. *eLife*, *12*, e80040. https://doi.org/10.7554/eLife.80040

References

Grimm, J. B., English, B. P., Chen, J., Slaughter, J. P., Zhang, Z., Revyakin, A., Patel, R., Macklin, J. J., Normanno, D., Singer, R. H., Lionnet, T., & Lavis, L. D. (2015). A general method to improve fluorophores for live-cell and single-molecule microscopy. *Nature Methods*, *12*(3), 244–250. https://doi.org/10.1038/nmeth.3256

Gross, J. D., Moerke, N. J., von der Haar, T., Lugovskoy, A. A., Sachs, A. B., McCarthy, J. E., & Wagner, G. (2003). Ribosome loading onto the mrna cap is driven by conformational coupling between eif4g and eif4e. *Cell*, *115*(6), 739–750. https://doi.org/https://doi.org/10.1016/S0092-8674(03)00975-9

Grüner, S., Peter, D., Weber, R., Wohlbold, L., Chung, M.-Y., Weichenrieder, O., Valkov, E., Igreja, C., & Izaurralde, E. (2016). The structures of eif4e-eif4g complexes reveal an extended interface to regulate translation initiation. *Molecular Cell*, *64*(3), 467–479. https://doi.org/https://doi.org/10.1016/j.molcel.2016.09.020

Hassan, B., Akcakanat, A., Sangai, T., Evans, K. W., Adkins, F., Eterovic, A. K., Zhao, H., Chen, K., Chen, H., Do, K. A., Xie, S. M., Holder, A. M., Naing, A., Mills, G. B., & Meric-Bernstam, F. (2014). Catalytic mTOR inhibitors can overcome intrinsic and acquired resistance to allosteric mTOR inhibitors [Edition: 2014/09/28]. *Oncotarget*, *5*(18), 8544–57. https://doi.org/10.18632/oncotarget.2337

Henras, A. K., Plisson-Chastang, C., O'Donohue, M.-F., Chakraborty, A., & Gleizes, P.-E. (2015). An overview of pre-ribosomal RNA processing in eukaryotes. *Wiley Interdisciplinary Reviews: RNA*, *6*(2), 225–242. https://doi.org/10.1002/wrna.1269

Herzog, V. A., Reichholf, B., Neumann, T., Rescheneder, P., Bhat, P., Burkard, T. R., Wlotzka, W., von Haeseler, A., Zuber, J., & Ameres, S. L. (2017). Thiol-linked alkylation of RNA to assess expression dynamics. *Nature Methods*, *14*(12), 1198–1204. https://doi.org/10.1038/nmeth.4435

Hochstoeger, T., & Chao, J. A. (2024). Towards a molecular understanding of the 5′TOP motif in regulating translation of ribosomal mRNAs. *Seminars in Cell & Developmental Biology*, *154*, 99–104. https://doi.org/10.1016/j.semcdb.2023.06.001

Hochstoeger, T., Papasaikas, P., Piskadlo, E., & Chao, J. A. (2024). Distinct roles of LARP1 and 4EBP1/2 in regulating translation and stability of 5′TOP mRNAs. *Science Advances*, *10*(7), eadi7830. https://doi.org/10.1126/sciadv.adi7830

Hong, S., Freeberg, M. A., Han, T., Kamath, A., Yao, Y., Fukuda, T., Suzuki, T., Kim, J. K., & Inoki, K. (2017). LARP1 functions as a molecular switch for mTORC1-mediated translation of an essential class of mRNAs [Edition: 2017/06/27]. *Elife*, *6*. https://doi.org/10.7554/eLife.25237

Horvathova, I., Voigt, F., Kotrys, A. V., Zhan, Y., Artus-Revel, C. G., Eglinger, J., Stadler, M. B., Giorgetti, L., & Chao, J. A. (2017). The Dynamics of mRNA Turnover Revealed by Single-Molecule Imaging in Single Cells [Edition: 2017/10/24]. *Mol Cell*, *68*(3), 615–625.e9. https://doi.org/10.1016/j.molcel.2017.09.030

Hsieh, A. C., Liu, Y., Edlind, M. P., Ingolia, N. T., Janes, M. R., Sher, A., Shi, E. Y., Stumpf, C. R., Christensen, C., Bonham, M. J., Wang, S., Ren, P., Martin, M., Jessen, K., Feldman, M. E., Weissman, J. S., Shokat, K. M., Rommel, C., & Ruggero, D. (2012). The translational landscape of mTOR signalling steers cancer initiation and metastasis. *Nature*, *485*(7396), 55–61. https://doi.org/10.1038/nature10912

Huo, Y., Iadevaia, V., Yao, Z., Kelly, I., Cosulich, S., Guichard, S., Foster, L. J., & Proud, C. G. (2012). Stable isotope-labelling analysis of the impact of inhibition of the mammalian target of rapamycin on protein synthesis. *Biochemical Journal*, *444*(1), 141–151. https://doi.org/10.1042/bj20112107

Huxley, C., & Fried, M. (1990). The mouse rpL7a gene is typical of other ribosomal protein genes in it's 5' region but differs in being located in a tight cluster of CpG-rich islands. *Nucleic Acids Research*, *18*(18), 5353–5357. https://doi.org/10.1093/nar/18.18.5353

Jensen, K. B., Dredge, B. K., Toubia, J., Jin, X., Iadevaia, V., Goodall, G. J., & Proud, C. G. (2021). capCLIP: A new tool to probe translational control in human cells through capture and identification of the eIF4E–mRNA interactome. *Nucleic Acids Research*, *49*(18), e105–e105. https://doi.org/10.1093/nar/

gkab604

Jessen, K., Wang, S., Kessler, L., Guo, X., Kucharski, J., Staunton, J., Lan, L., Elia, M., Stewart, J., Brown, J., Li, L., Chan, K., Martin, M., Ren, P., Rommel, C., & Liu, Y. (2009). Abstract B148: INK128 is a potent and selective TORC1/2 inhibitor with broad oral antitumor activity. *Molecular Cancer Therapeutics*, *8*(12_Supplement), B148–B148. https://doi.org/10.1158/1535-7163.Targ-09-b148

Jia, J.-J., Lahr, R. M., Solgaard, M. T., Moraes, B. J., Pointet, R., Yang, A.-D., Celucci, G., Graber, T. E., Hoang, H.-D., Niklaus, M. R., Pena, I. A., Hollensen, A. K., Smith, E. M., Chaker-Margot, M., Anton, L., Dajadian, C., Livingstone, M., Hearnden, J., Wang, X.-D., … Fonseca, B. D. (2021). mTORC1 promotes TOP mRNA translation through site-specific phosphorylation of LARP1. *Nucleic Acids Research*. https://doi.org/10.1093/nar/gkaa1239

Jin, H., Xu, W., Rahman, R., Na, D., Fieldsend, A., Song, W., Liu, S., Li, C., & Rosbash, M. (2020). TRIBE editing reveals specific mRNA targets of eIF4E-BP in Drosophila and in mammals. *Science Advances*, *6*(33), eabb8771. https://doi.org/10.1126/sciadv.abb8771

Jumper, J., Evans, R., Pritzel, A., Green, T., Figurnov, M., Ronneberger, O., Tunyasuvunakool, K., Bates, R., Žídek, A., Potapenko, A., Bridgland, A., Meyer, C., Kohl, S. A. A., Ballard, A. J., Cowie, A., Romera-Paredes, B., Nikolov, S., Jain, R., Adler, J., … Hassabis, D. (2021). Highly accurate protein structure prediction with AlphaFold. *Nature*, *596*(7873), 583–589. https://doi.org/10.1038/s41586-021-03819-2

Kaczanowska, M., & Rydén-Aulin, M. (2007). Ribosome Biogenesis and the Translation Process in Escherichia coli. *Microbiology and Molecular Biology Reviews*, *71*(3), 477–494. https://doi.org/10.1128/MMBR.00013-07

Kahvejian, A., Svitkin, Y. V., Sukarieh, R., M'Boutchou, M.-N., & Sonenberg, N. (2005). Mammalian poly (a)-binding protein is a eukaryotic translation initiation factor, which acts via multiple mechanisms. *Genes & development*, *19*(1), 104–113. https://doi.org/https://doi.org/10.1101/gad.1262905

Kajjo, S., Sharma, S., Brothers, R. W., Delisle, V., & Fabian, R. M. (2024). PABPC plays a critical role in establishing mTORC-mediated translational control. *Under Preparation.*

Kozlov, G., Mattijssen, S., Jiang, J., Nyandwi, S., Sprules, T., Iben, J. R., Coon, S. L., Gaidamakov, S., Noronha, A. M., Wilds, C. J., Maraia, R. J., & Gehring, K. (2022). Structural basis of 3'-end poly(A) RNA recognition by LARP1. *Nucleic Acids Research*, *50*(16), 9534–9547. https://doi.org/10.1093/nar/gkac696

Lahr, R. M., Fonseca, B. D., Ciotti, G. E., Al-Ashtal, H. A., Jia, J. J., Niklaus, M. R., Blagden, S. P., Alain, T., & Berman, A. J. (2017). La-related protein 1 (LARP1) binds the mRNA cap, blocking eIF4F assembly on TOP mRNAs [Edition: 2017/04/06]. *Elife*, *6*. https://doi.org/10.7554/eLife.24146

Lewis, J. D., & Tollervey, D. (2000). Like Attracts Like: Getting RNA Processing Together in the Nucleus. *Science*, *288*(5470), 1385–1389. https://doi.org/10.1126/science.288.5470.1385

Lindqvist, L., Imataka, H., & Pelletier, J. (2008). Cap-dependent eukaryotic initiation factor-mRNA interactions probed by cross-linking [Edition: 2008/03/28]. *Rna*, *14*(5), 960–9. https://doi.org/10.1261/rna.971208

Liu, G. Y., & Sabatini, D. M. (2020). mTOR at the nexus of nutrition, growth, ageing and disease. *Nature Reviews Molecular Cell Biology*, *21*(4), 183–203. https://doi.org/10.1038/s41580-019-0199-y

Livingston, N. M., Kwon, J., Valera, O., Saba, J. A., Sinha, N. K., Reddy, P., Nelson, B., Wolfe, C., Ha, T., Green, R., Liu, J., & Wu, B. (2022). Bursting Translation on Single mRNAs in Live Cells. *bioRxiv*, 2022.11.07.515520. https://doi.org/10.1101/2022.11.07.515520

Lord, S. J., Velle, K. B., Mullins, R. D., & Fritz-Laylin, L. K. (2020). SuperPlots: Communicating reproducibility and variability in cell biology. *Journal of Cell Biology*, *219*(6). https://doi.org/10.1083/jcb.202001064

Lun, A. T., Chen, Y., & Smyth, G. K. (2016). It's DE-licious: A Recipe for Differential Expression Analyses of RNA-seq Experiments Using Quasi-Likelihood Methods in edgeR [Edition: 2016/03/24]. *Methods Mol Biol*, *1418*, 391–416. https://doi.org/10.1007/978-1-4939-3578-9_19

References

Mamane, Y., Petroulakis, E., Martineau, Y., Sato, T. A., Larsson, O., Rajasekhar, V. K., & Sonenberg, N. (2007). Epigenetic activation of a subset of mRNAs by eIF4E explains its effects on cell proliferation [Edition: 2007/02/22]. *PLoS One*, *2*(2), e242. https://doi.org/10.1371/journal.pone.0000242

Maraia, R. J., Mattijssen, S., Cruz-Gallardo, I., & Conte, M. R. (2017). The La and related RNA-binding proteins (LARPs): Structures, functions, and evolving perspectives. *WIREs RNA*, *8*(6), e1430. https://doi.org/10.1002/wrna.1430

Mariottini, P., Bagni, C., Annesi, F., & Amaldi, F. (1988). Isolation and nucleotide sequences of cDNAs for Xenopus laevis ribosomal protein S8: Similarities in the 5' and 3' untranslated regions of mRNAs for various r-proteins [Edition: 1988/07/15]. *Gene*, *67*(1), 69–74. https://doi.org/10.1016/0378-1119(88)90009-1

Mateju, D., Eichenberger, B., Voigt, F., Eglinger, J., Roth, G., & Chao, J. A. (2020). Single-Molecule Imaging Reveals Translation of mRNAs Localized to Stress Granules. *Cell*, *183*(7), 1801–1812.e13. https://doi.org/10.1016/j.cell.2020.11.010

Mattijssen, S., Kozlov, G., Gaidamakov, S., Ranjan, A., Fonseca, B. D., Gehring, K., & Maraia, R. J. (2021). The isolated La-module of LARP1 mediates 3' poly(A) protection and mRNA stabilization, dependent on its intrinsic PAM2 binding to PABPC1. *RNA Biology*, *18*(2), 275–289. https://doi.org/10.1080/15476286.2020.1860376

Mayer, C., & Grummt, I. (2006). Ribosome biogenesis and cell growth: mTOR coordinates transcription by all three classes of nuclear RNA polymerases [Edition: 2006/10/17]. *Oncogene*, *25*(48), 6384–91. https://doi.org/10.1038/sj.onc.1209883

Meyuhas, O. (2000). Synthesis of the translational apparatus is regulated at the translational level [Edition: 2000/10/13]. *Eur J Biochem*, *267*(21), 6321–30. https://doi.org/10.1046/j.1432-1327.2000.01719.x

Meyuhas, O., & Kahan, T. (2015). The race to decipher the top secrets of TOP mRNAs. *Biochimica et Biophysica Acta (BBA) - Gene Regulatory Mechanisms*, *1849*(7), 801–811. https://doi.org/10.1016/j.bbagrm.2014.08.015

Mikhaylina, A., Nikonova, E., Kostareva, O., & Tishchenko, S. (2021). Regulation of Ribosomal Protein Synthesis in Prokaryotes. *Molecular Biology*, *55*(1), 16–36. https://doi.org/10.31857/S0026898421010110

Miloslavski, R., Cohen, E., Avraham, A., Iluz, Y., Hayouka, Z., Kasir, J., Mudhasani, R., Jones, S. N., Cybulski, N., Rüegg, M. A., Larsson, O., Gandin, V., Rajakumar, A., Topisirovic, I., & Meyuhas, O. (2014). Oxygen sufficiency controls TOP mRNA translation via the TSC-Rheb-mTOR pathway in a 4E-BP-independent manner. *Journal of Molecular Cell Biology*, *6*(3), 255–266. https://doi.org/10.1093/jmcb/mju008

Moor, A. E., Golan, M., Massasa, E. E., Lemze, D., Weizman, T., Shenhav, R., Baydatch, S., Mizrahi, O., Winkler, R., Golani, O., *et al.* (2017). Global mrna polarization regulates translation efficiency in the intestinal epithelium. *Science*, *357*(6357), 1299–1303. https://doi.org/https://doi.org/10.1126/science.aan2399

Mura, M., Hopkins, T. G., Michael, T., Abd-Latip, N., Weir, J., Aboagye, E., Mauri, F., Jameson, C., Sturge, J., Gabra, H., Bushell, M., Willis, A. E., Curry, E., & Blagden, S. P. (2015). LARP1 post-transcriptionally regulates mTOR and contributes to cancer progression. *Oncogene*, *34*(39), 5025–5036. https://doi.org/10.1038/onc.2014.428

Nepal, C., Hadzhiev, Y., Balwierz, P., Tarifeño-Saldivia, E., Cardenas, R., Wragg, J. W., Suzuki, A.-M., Carninci, P., Peers, B., Lenhard, B., Andersen, J. B., & Müller, F. (2020). Dual-initiation promoters with intertwined canonical and TCT/TOP transcription start sites diversify transcript processing. *Nature Communications*, *11*(1), 168. https://doi.org/10.1038/s41467-019-13687-0

Neumann, T., Herzog, V. A., Muhar, M., von Haeseler, A., Zuber, J., Ameres, S. L., & Rescheneder, P. (2019). Quantification of experimentally induced nucleotide conversions in high-throughput sequencing datasets. *BMC Bioinformatics*, *20*(1), 258. https://doi.org/10.1186/s12859-019-2849-7

Ogami, K., Oishi, Y., Sakamoto, K., Okumura, M., Yamagishi, R., Inoue, T., Hibino, M., Nogimori, T., Yamaguchi, N., Furutachi, K., Hosoda, N., Inagaki, H., & Hoshino, S. I. (2022). mTOR- and LARP1-dependent regulation of TOP mRNA poly(A) tail and ribosome loading [Edition: 2022/10/27]. *Cell Rep*, *41*(4), 111548. https://doi.org/10.1016/j.celrep.2022.111548

O'Leary, S. E., Petrov, A., Chen, J., & Puglisi, J. D. (2013). Dynamic recognition of the mrna cap by saccharomyces cerevisiae eif4e. *Structure*, *21*(12), 2197–2207. https://doi.org/https://doi.org/10.1016/j.str.2013.09.016

Park, J., Kim, M., Yi, H., Baeg, K., Choi, Y., Lee, Y.-s., Lim, J., & Kim, V. N. (2023). Short poly(A) tails are protected from deadenylation by the LARP1–PABP complex. *Nature Structural & Molecular Biology*, *30*(3), 330–338. https://doi.org/10.1038/s41594-023-00930-y

Parry, T. J., Theisen, J. W. M., Hsu, J.-Y., Wang, Y.-L., Corcoran, D. L., Eustice, M., Ohler, U., & Kadonaga, J. T. (2010). The TCT motif, a key component of an RNA polymerase II transcription system for the translational machinery [Edition: 2010/08/27]. *Genes & development*, *24*(18), 2013–2018. https://doi.org/10.1101/gad.1951110

Pende, M., Um, S. H., Mieulet, V., Sticker, M., Goss, V. L., Mestan, J., Mueller, M., Fumagalli, S., Kozma, S. C., & Thomas, G. (2004). S6K1(-/-)/S6K2(-/-) mice exhibit perinatal lethality and rapamycin-sensitive 5'-terminal oligopyrimidine mRNA translation and reveal a mitogen-activated protein kinase-dependent S6 kinase pathway [Edition: 2004/04/03]. *Mol Cell Biol*, *24*(8), 3112–24. https://doi.org/10.1128/mcb.24.8.3112-3124.2004

Peter, D., Igreja, C., Weber, R., Wohlbold, L., Weiler, C., Ebertsch, L., Weichenrieder, O., & Izaurralde, E. (2015). Molecular architecture of 4e-bp translational inhibitors bound to eif4e. *Molecular Cell*, *57*(6), 1074–1087. https://doi.org/https://doi.org/10.1016/j.molcel.2015.01.017

Philippe, L., Vasseur, J. J., Debart, F., & Thoreen, C. C. (2018). La-related protein 1 (LARP1) repression of TOP mRNA translation is mediated through its cap-binding domain and controlled by an adjacent regulatory region [Edition: 2017/12/16]. *Nucleic Acids Res*, *46*(3), 1457–1469. https://doi.org/10.1093/nar/gkx1237

Philippe, L., van den Elzen, A. M., Watson, M. J., & Thoreen, C. C. (2020). Global analysis of LARP1 translation targets reveals tunable and dynamic features of 5′ TOP motifs. *Proceedings of the National Academy of Sciences*, *117*(10), 5319–5328. https://doi.org/10.1073/pnas.1912864117

Powers, T., & Walter, P. (1999). Regulation of Ribosome Biogenesis by the Rapamycin-sensitive TOR-signaling Pathway in Saccharomyces cerevisiae. *Molecular Biology of the Cell*, *10*(4), 987–1000. https://doi.org/10.1091/mbc.10.4.987

Preibisch, S., Saalfeld, S., Schindelin, J., & Tomancak, P. (2010). Software for bead-based registration of selective plane illumination microscopy data. *Nature methods*, *7*(6), 418–419. https://doi.org/10.1038/nmeth0610-418

Proud, C. G. (2015). Mnks, eif4e phosphorylation and cancer [Translation and Cancer]. *Biochimica et Biophysica Acta (BBA) - Gene Regulatory Mechanisms*, *1849*(7), 766–773. https://doi.org/https://doi.org/10.1016/j.bbagrm.2014.10.003

Rhoads, D. D., Dixit, A., & Roufa, D. J. (1986). Primary structure of human ribosomal protein S14 and the gene that encodes it. *Molecular and Cellular Biology*, *6*(8), 2774–2783. https://doi.org/10.1128/mcb.6.8.2774-2783.1986

Rueden, C. T., Schindelin, J., Hiner, M. C., DeZonia, B. E., Walter, A. E., Arena, E. T., & Eliceiri, K. W. (2017). ImageJ2: ImageJ for the next generation of scientific image data. *BMC bioinformatics*, *18*(1), 1–26. https://doi.org/10.1186/s12859-017-1934-z

Ruvinsky, I., Sharon, N., Lerer, T., Cohen, H., Stolovich-Rain, M., Nir, T., Dor, Y., Zisman, P., & Meyuhas, O. (2005). Ribosomal protein S6 phosphorylation is a determinant of cell size and glucose homeostasis

[Edition: 2005/09/17]. *Genes Dev*, *19*(18), 2199–211. https://doi.org/10.1101/gad.351605

Sabatini, D. M. (2017). Twenty-five years of mtor: Uncovering the link from nutrients to growth. *Proceedings of the National Academy of Sciences*, *114*(45), 11818–11825. https://doi.org/10.1073/pnas.1716173114

Scarpin, M. R., Leiboff, S., & Brunkard, J. O. (2020). Parallel global profiling of plant TOR dynamics reveals a conserved role for LARP1 in translation. *eLife*, *9*, e58795. https://doi.org/10.7554/eLife.58795

Schindelin, J., Arganda-Carreras, I., Frise, E., Kaynig, V., Longair, M., Pietzsch, T., Preibisch, S., Rueden, C., Saalfeld, S., & Schmid, B. (2012). Fiji: An open-source platform for biological-image analysis. *Nature methods*, *9*(7), 676–682. https://doi.org/10.1038/nmeth.2019

Schmelzle, T., & Hall, M. N. (2000). TOR, a central controller of cell growth [Edition: 2000/11/01]. *Cell*, *103*(2), 253–62. https://doi.org/10.1016/s0092-8674(00)00117-3

Schneider, C., Erhard, F., Binotti, B., Buchberger, A., Vogel, J., & Fischer, U. (2022). An unusual mode of baseline translation adjusts cellular protein synthesis capacity to metabolic needs [Edition: 2022/10/13]. *Cell Rep*, *41*(2), 111467. https://doi.org/10.1016/j.celrep.2022.111467

Schofield, J. A., Duffy, E. E., Kiefer, L., Sullivan, M. C., & Simon, M. D. (2018). TimeLapse-seq: Adding a temporal dimension to RNA sequencing through nucleoside recoding. *Nature Methods*, *15*(3), 221–225. https://doi.org/10.1038/nmeth.4582

Schwenzer, H., Abdel Mouti, M., Neubert, P., Morris, J., Stockton, J., Bonham, S., Fellermeyer, M., Chettle, J., Fischer, R., Beggs, A. D., & Blagden, S. P. (2021). LARP1 isoform expression in human cancer cell lines [Edition: 2020/04/14]. *RNA biology*, *18*(2), 237–247. https://doi.org/10.1080/15476286.2020.1744320

Shore, D., Zencir, S., & Albert, B. (2021). Transcriptional control of ribosome biogenesis in yeast: Links to growth and stress signals. *Biochemical Society transactions*, *49*(4), 1589–1599. https://doi.org/10.1042/BST20201136

Siddiqui, N., Tempel, W., Nedyalkova, L., Volpon, L., Wernimont, A. K., Osborne, M. J., Park, H.-W., & Borden, K. L. (2012). Structural insights into the allosteric effects of 4ebp1 on the eukaryotic translation initiation factor eif4e. *Journal of molecular biology*, *415*(5), 781–792. https://doi.org/https://doi.org/10.1016/j.jmb.2011.12.002

Sinvani, H., Haimov, O., Svitkin, Y., Sonenberg, N., Tamarkin-Ben-Harush, A., Viollet, B., & Dikstein, R. (2015). Translational tolerance of mitochondrial genes to metabolic energy stress involves tisu and eif1-eif4gi cooperation in start codon selection. *Cell metabolism*, *21*(3), 479–492. https://doi.org/https://doi.org/10.1016/j.cmet.2015.02.010

Smith, E. M., Benbahouche, N. E. H., Morris, K., Wilczynska, A., Gillen, S., Schmidt, T., Meijer, H. A., Jukes-Jones, R., Cain, K., Jones, C., Stoneley, M., Waldron, J. A., Bell, C., Fonseca, B. D., Blagden, S., Willis, A. E., & Bushell, M. (2020). The mTOR regulated RNA-binding protein LARP1 requires PABPC1 for guided mRNA interaction. *Nucleic Acids Research*, *49*(1), 458–478. https://doi.org/10.1093/nar/gkaa1189

Tamarkin-Ben-Harush, A., Vasseur, J. J., Debart, F., Ulitsky, I., & Dikstein, R. (2017). Cap-proximal nucleotides via differential eIF4E binding and alternative promoter usage mediate translational response to energy stress [Edition: 2017/02/09]. *Elife*, *6*. https://doi.org/10.7554/eLife.21907

Tanenbaum, M. E., Gilbert, L. A., Qi, L. S., Weissman, J. S., & Vale, R. D. (2014). A protein-tagging system for signal amplification in gene expression and fluorescence imaging [Edition: 2014/10/14]. *Cell*, *159*(3), 635–46. https://doi.org/10.1016/j.cell.2014.09.039

Tcherkezian, J., Cargnello, M., Romeo, Y., Huttlin, E. L., Lavoie, G., Gygi, S. P., & Roux, P. P. (2014). Proteomic analysis of cap-dependent translation identifies LARP1 as a key regulator of 5'TOP mRNA translation [Edition: 2014/02/18]. *Genes Dev*, *28*(4), 357–71. https://doi.org/10.1101/gad.231407.113

Thomson, E., Ferreira-Cerca, S., & Hurt, E. (2013). Eukaryotic ribosome biogenesis at a glance. *Journal of Cell Science*, *126*(21), 4815–4821. https://doi.org/10.1242/jcs.111948

Thoreen, C. C. (2017). The molecular basis of mTORC1-regulated translation. *Biochemical Society Transactions*, *45*(1), 213–221. https://doi.org/10.1042/bst20160072

Thoreen, C. C., Chantranupong, L., Keys, H. R., Wang, T., Gray, N. S., & Sabatini, D. M. (2012). A unifying model for mTORC1-mediated regulation of mRNA translation. *Nature*, *485*(7396), 109–113. https://doi.org/10.1038/nature11083

Thoreen, C. C., Kang, S. A., Chang, J. W., Liu, Q., Zhang, J., Gao, Y., Reichling, L. J., Sim, T., Sabatini, D. M., & Gray, N. S. (2009). An ATP-competitive Mammalian Target of Rapamycin Inhibitor Reveals Rapamycin-resistant Functions of mTORC1*. *Journal of Biological Chemistry*, *284*(12), 8023–8032. https://doi.org/10.1074/jbc.M900301200

Tinevez, J.-Y., Perry, N., Schindelin, J., Hoopes, G. M., Reynolds, G. D., Laplantine, E., Bednarek, S. Y., Shorte, S. L., & Eliceiri, K. W. (2017). TrackMate: An open and extensible platform for single-particle tracking. *Methods*, *115*, 80–90. https://doi.org/10.1016/j.ymeth.2016.09.016

Tomoo, K., Shen, X., Okabe, K., Nozoe, Y., Fukuhara, S., Morino, S., Ishida, T., Taniguchi, T., Hasegawa, H., Terashima, A., Sasaki, M., Katsuya, Y., Kitamura, K., Miyoshi, H., Ishikawa, M., & Miura, K. (2002). Crystal structures of 7-methylguanosine 5'-triphosphate (m(7)GTP)- and P(1)-7-methylguanosine-P(3)-adenosine-5',5'-triphosphate (m(7)GpppA)-bound human full-length eukaryotic initiation factor 4E: Biological importance of the C-terminal flexible region [Edition: 2002/03/07]. *Biochem J*, *362*(Pt 3), 539–44. https://doi.org/10.1042/0264-6021:3620539

Truitt, M. L., Conn, C. S., Shi, Z., Pang, X., Tokuyasu, T., Coady, A. M., Seo, Y., Barna, M., & Ruggero, D. (2015). Differential Requirements for eIF4E Dose in Normal Development and Cancer [Edition: 2015/06/23]. *Cell*, *162*(1), 59–71. https://doi.org/10.1016/j.cell.2015.05.049

van den Elzen, A. M. G., Watson, M. J., & Thoreen, C. C. (2022). mRNA 5' terminal sequences drive 200-fold differences in expression through effects on synthesis, translation and decay [Edition: 2022/11/29]. *PLoS Genet*, *18*(11), e1010532. https://doi.org/10.1371/journal.pgen.1010532

Wagner, M., & Perry, R. P. (1985). Characterization of the multigene family encoding the mouse S16 ribosomal protein: Strategy for distinguishing an expressed gene from its processed pseudogene counterparts by an analysis of total genomic DNA. *Molecular and cellular biology*, *5*(12), 3560–3576. https://doi.org/10.1128/mcb.5.12.3560-3576.1985

Warner, J. R. (1999). The economics of ribosome biosynthesis in yeast [Edition: 1999/11/05]. *Trends Biochem Sci*, *24*(11), 437–40. https://doi.org/10.1016/s0968-0004(99)01460-7

Wiedemann, L. M., & Perry, R. P. (1984). Characterization of the expressed gene and several processed pseudogenes for the mouse ribosomal protein L30 gene family. *Molecular and Cellular Biology*, *4*(11), 2518–2528. https://doi.org/10.1128/mcb.4.11.2518-2528.1984

Wilbertz, J. H., Voigt, F., Horvathova, I., Roth, G., Zhan, Y., & Chao, J. A. (2019). Single-Molecule Imaging of mRNA Localization and Regulation during the Integrated Stress Response. *Molecular Cell*, *73*(5), 946–958.e7. https://doi.org/10.1016/j.molcel.2018.12.006

Wolin, E., Guo, J. K., Blanco, M. R., Perez, A. A., Goronzy, I. N., Abdou, A. A., Gorhe, D., Guttman, M., & Jovanovic, M. (2023). Spidr: A highly multiplexed method for mapping rna-protein interactions uncovers a potential mechanism for selective translational suppression upon cellular stress. *bioRxiv*, 2023–06. https://doi.org/10.1101/2023.06.05.543769

Wullschleger, S., Loewith, R., & Hall, M. N. (2006). TOR Signaling in Growth and Metabolism. *Cell*, *124*(3), 471–484. https://doi.org/10.1016/j.cell.2006.01.016

Yanagiya, A., Svitkin, Y. V., Shibata, S., Mikami, S., Imataka, H., & Sonenberg, N. (2009). Requirement of rna binding of mammalian eukaryotic translation initiation factor 4gi (eif4gi) for efficient interaction of eif4e with the mrna cap. *Molecular and cellular biology*, *29*(6), 1661–1669. https://doi.org/https://doi.org/10.1128/MCB.01187-08

References

Zinshteyn, B., Rojas-Duran, M. F., & Gilbert, W. V. (2017). Translation initiation factor eIF4G1 preferentially binds yeast transcript leaders containing conserved oligo-uridine motifs [Edition: 2017/05/27]. *Rna*, *23*(9), 1365–1375. https://doi.org/10.1261/rna.062059.117

Supplementary Information

Supplementary Tables

Supplementary Table S1: Reagent list

Chemicals		Catalogue number
JF549/646 HaloTag ligand	Grimm et al., 2015	N/A
Torin1	Selleckchem	S2827
PP242	Sigma-Aldrich	475988-5MG
TAK228 (INK 128/MLN0128/Sapanisertib)	Selleckchem	S2811-10MM/1ML
Rapamycin (Sirolimus)	Lubioscience	HY-10219-1ML
Lipofectamine 2000	Invitrogen	11668027
Opti-MEM I Reduced Serum Medium	Thermo Fisher Scientific	31985062
FluoroBrite DMEM	Thermo Fisher Scientific	A1896701
Harringtonine	MedChemExpress	HY-N0862
Puromycin	InvivoGen	ant-pr-1
Doxycycline	Sigma-Aldrich	D9891-1G
Antibiotic G418 Sulfate	Promega	V8091
Polybrene	Merck	TR-1003-G
Blasticidin	InvivoGen	ant-bl-1
Protease Inhibitor Cocktail	Bimake.com	B14001
SuperNuclease	Sino Biological	SINOSSNP01
4x Laemmli Sample Buffer	BioRad	1610747
4x LDS Sample Buffer	Thermo Fisher Scientific	NP0007
Bolt 4-12% Bis-Tris Plus Gel, 17 Well	Thermo Fisher Scientific	NW04127BOX
NuPAGE MES SDS Running Buffer	Thermo Fisher Scientific	NP0002
DTT	VWR	A2948.0025
4-15% TGX Pre-cast gel	BioRad	4561086
Trans-Blot Turbo Nitrocellulose Transfer Pack	Bio-Rad	1704158
Trans-Blot Turbo PVDF Transfer Pack	Bio-Rad	1704156
BSA	Sigma	A2153
Tween-20	Mp Biomedicals Inc	ICNA04806576
Intercept® (TBS) Protein-Free Blocking Buffer	LI COR (VWR)	927-60003
DNeasy Blood & Tissue Kit	QIAGEN	69504
Phusion High-Fidelity Polymerase	NEB	M0530L
Zero Blunt PCR cloning kit	Thermo Fisher Scientific	K275040
QIAquick PCR Purification Kit	QIAGEN	28106

QIAprep Spin Miniprep Kit	QIAGEN	27106
Absolutely RNA RT-PCR Miniprep Kit	Agilent	400800
QuantiTect Reverse Transcription Kit	Qiagen	205311
SLAMseq Catabolic Kinetics Kit	Lexogen	062.24
CellTiter-Glo Luminescent Cell Viability Assay	Promega	G7570
TeloPrime Full-Length cDNA Amplification Kit V2	Lexogen	013.08
Fugene 6	Promega	E2691
Lenti-X concentrator	Clontech	631231
u-dish 35mm, high NA, glass bottom	Ibidi	81158-IBI
Precision Cover Glasses, No 1.5H, 18 mm	Marienfeld	0117580
Amino-11-ddUTP	Lumiprobe	15040
Atto 633-NHS	ATTO-tec	AD 633-31
Paraformaldehyde (EM grade)	Electron Microscopy Sciences	15713-S
SSC (20X, Ultrapure)	Life technologies	15557036
Formamide (deionized)	MP Biomedicals VWR	11FORMD002
Dextran Sulfate (50% Solution)	Millipore	S4030
ProLong™ Gold Antifade Mountant with DAPI	ThermoFisher Scientific	P36935
Plasmids		
Cas9 (pX330)	Addgene	42230
Cas9-T2A-mCherry (modified from pX330)	Addgene	64324
Cas9_LARP1 sgRNA1	this study	N/A
Cas9-T2A-mCherry_LARP1 sgRNA2	this study	N/A
Cas9-T2A-mCherry_LARP1B sgRNA1	this study	N/A
Cas9-T2A-mCherry_LARP1B sgRNA2	this study	N/A
pLKO.1_BlastR	Addgene	26655
pLKO.1_BlastR_4EBP2 shRNA	this study, shRNA sequence from TRCN0000117814	N/A
psPAX2	Addgene	12260
vsv-G	Addgene	12259
Viruses		
Lentivirus EIF4EBP1 shRNA (PuroR)	TRCN0000040203	Sigma-Aldrich
Lentivirus EIF4EBP2 shRNA (BlastR)	this study	N/A
Cell Lines (human)		
HeLa-11ht + NLS-stdMCP-stdHalo + scAB-GFP + Canonical SunTag-Renilla	Wilbertz et al., 2019	N/A
HeLa-11ht + NLS-stdMCP-stdHalo + scAB-GFP + 5′TOP-SunTag-Renilla	Wilbertz et al., 2019	N/A
LARP1 KO HeLa-11ht + NLS-stdMCP-stdHalo + scAB-GFP + Canonical SunTag-Renilla	this study	N/A
LARP1 KO HeLa-11ht + NLS-stdMCP-stdHalo + scAB-GFP + 5′TOP-SunTag-Renilla	this study	N/A
LARP1/1B KO HeLa-11ht + NLS-stdMCP-stdHalo + scAB-GFP + Canonical SunTag-Renilla	this study	N/A
LARP1/1B KO HeLa-11ht + NLS-stdMCP-stdHalo + scAB-GFP + 5′TOP-SunTag-Renilla	this study	N/A
4EBP1/2 KD HeLa-11ht + NLS-stdMCP-stdHalo + scAB-GFP + Canonical SunTag-Renilla	this study	N/A
4EBP1/2 KD LARP1 KO HeLa-11ht + NLS-stdMCP-stdHalo + scAB-GFP + 5′TOP-SunTag-Renilla	this study	N/A

4EBP1/2 KD & LARP1/1B KO HeLa-11ht + NLS-stdMCP-stdHalo + scAB-GFP + Canonical SunTag-Renilla	this study	N/A
4EBP1/2 KD & LARP1/1B KO HeLa-11ht + NLS-stdMCP-stdHalo + scAB-GFP + 5′TOP-SunTag-Renilla	this study	N/A
HeLa-11ht + NLS-stdMCP-stdHalo + scAB-GFP + Δ5′TOP-SunTag-Renilla	this study	N/A
HeLa-11ht + NLS-stdMCP-stdHalo + scAB-GFP + Δ5′TOP/PRTE-SunTag-Renilla	this study	N/A
LARP1 KO HeLa-11ht + NLS-stdMCP-stdHalo + scAB-GFP + Δ5′TOP-SunTag-Renilla	this study	N/A
4EBP1/2 KD HeLa-11ht + NLS-stdMCP-stdHalo + scAB-GFP + Δ5′TOP-SunTag-Renilla	this study	N/A
CRISPR Guides		
LARP1 sgRNA1	GATGAGGATTGCCAGCGAGG	
LARP1 sgRNA2	GCCACCCAAGAAGGACATGA	
LARP1B sgRNA1	TTTCAGAGCGTCCTCAGCCA	
LARP1B sgRNA2	CAGTGACAGCAAAGAAAACC	
shRNA		
4EBP1	GCCAGGCCTTATGAAAGTGAT	
4EBP2	CGCAGCTACCTCATGACTATT	

Table S1: Reagent list.

Supplementary Table S2: Reference list of 5′TOP mRNAs

Absence (0) or presence (1) of a putative pyrimidine-rich translational element is listed.

gene name	PRTE
EEF1A1	0
EEF1B2	1
EEF1D	1
EEF1G	1
EEF2	1
EIF2A	0
EIF2S3	0
EIF3A	1
EIF3E	0
EIF3F	0
EIF3H	0
EIF3K	0
EIF3L	0
EIF4A2	0
EIF4B	1
FAU	0
GNB2L1	1
HNRNPA1	1
NAP1L1	1
PABPC1	1
RACK1	0
RPL10	1
RPL10A	0
RPL11	0
RPL12	1
RPL13	1

gene name	PRTE
RPL13A	0
RPL14	1
RPL15	1
RPL17	1
RPL18	0
RPL18A	1
RPL19	0
RPL21	0
RPL22	1
RPL22L1	0
RPL23	1
RPL23A	0
RPL24	0
RPL26	0
RPL27	1
RPL27A	0
RPL28	0
RPL29	1
RPL3	0
RPL30	0
RPL31	1
RPL32	1
RPL34	1
RPL35	0
RPL35A	0
RPL36	1

gene name	PRTE
RPL36A	1
RPL37	1
RPL37A	1
RPL38	1
RPL39	1
RPL3L	0
RPL4	1
RPL41	1
RPL5	1
RPL6	1
RPL7	1
RPL7A	0
RPL8	1
RPL9	1
RPLP0	1
RPLP1	0
RPLP2	1
RPS10	1
RPS11	1
RPS12	0
RPS13	0
RPS14	1
RPS15	0
RPS15A	1
RPS16	0
RPS17	0

gene name	PRTE
RPS18	0
RPS19	0
RPS2	1
RPS20	1
RPS21	0
RPS23	0
RPS24	0
RPS25	0
RPS26	0
RPS27	0
RPS27A	1
RPS28	0
RPS29	0
RPS3	0
RPS3A	1
RPS4X	1
RPS4Y1	0
RPS4Y2	0
RPS5	1
RPS6	1
RPS7	0
RPS8	1
RPS9	1
RPSA	0
TPT1	1
VIM	1

Supplementary Table S3: smFISH probe sequences

Target	Sequence (5′ to 3′)	Species	Dye
MYC_1	atgggcaaagtttcgtggat	human	atto633
MYC_2	tgttgtaagttccagtgcaa	human	atto633
MYC_3	caaatgggcagaatagcctc	human	atto633
MYC_4	tttcagagaagcgggtcctg	human	atto633
MYC_5	ctaagcagctgcaaggagag	human	atto633
MYC_6	gttttccactacccgaaaaa	human	atto633
MYC_7	ggtgaagctaacgttgaggg	human	atto633
MYC_8	tcgtagtcgaggtcatagtt	human	atto633
MYC_9	agtagaaatacggctgcacc	human	atto633
MYC_10	aacgtaggagggcgagcaga	human	atto633
MYC_11	cgaagggagaagggtgtgac	human	atto633
MYC_12	aaactctggttcaccatgtc	human	atto633
MYC_13	agaagccgctccacatacag	human	atto633
MYC_14	cttctctgagacgagcttgg	human	atto633
MYC_15	ttgagagggtaggggaagac	human	atto633
MYC_16	agagaaggcgctggagtctt	human	atto633
MYC_17	cgtcgaggagagcagagaat	human	atto633
MYC_18	tttccttacttttccttacg	human	atto633
MYC_19	gcatttgatcatgcatttga	human	atto633
MYC_20	gactcagccaaggttgtgag	human	atto633
MYC_21	tggctaaatctttcagtctc	human	atto633
MYC_22	gtccaatttgaggcagttta	human	atto633
MYC_23	aaaaagttcttttatgccca	human	atto633
RPL5_1	cgctagggggtgggaaaagg	human	Quasar® 570
RPL5_2	catcctgcggaacagagacc	human	Quasar® 570
RPL5_3	gccttattcttaacaacttt	human	Quasar® 570
RPL5_4	cacttggtatctcttaaagt	human	Quasar® 570
RPL5_5	cctctcgtcgtcttctaaat	human	Quasar® 570
RPL5_6	tccgagcataataatcagtt	human	Quasar® 570
RPL5_7	ttatcttgtatcaccaagcg	human	Quasar® 570
RPL5_8	ctgtatttgggtgtgttgta	human	Quasar® 570
RPL5_9	ctctgtttgtcacacgaact	human	Quasar® 570
RPL5_10	acgggcataagcaatctgac	human	Quasar® 570
RPL5_11	gctgcgcagactatcatatc	human	Quasar® 570
RPL5_12	acaccatattttggcagttc	human	Quasar® 570
RPL5_13	agcataatttgtcaggccaa	human	Quasar® 570
RPL5_14	cagcaggccagtacaatatg	human	Quasar® 570
RPL5_15	ccaaacctattgagaagcct	human	Quasar® 570
RPL5_16	cttggccttcatagatcttg	human	Quasar® 570
RPL5_17	ttgtattcatcaccagtcac	human	Quasar® 570
RPL5_18	tggctgaccatcaatgcttt	human	Quasar® 570
RPL5_19	tccaaatagcaggtgaaggc	human	Quasar® 570
RPL5_20	cagtggtagttctggcaagg	human	Quasar® 570
RPL5_21	cttcagggcaccaaaaactt	human	Quasar® 570
RPL5_22	tgtgagggatagacaagcct	human	Quasar® 570
RPL5_23	taaccagggaatcgtttggt	human	Quasar® 570
RPL5_24	ctgcattaaattccttgctt	human	Quasar® 570

RPL5_25	atgatgtgcttccgatgtac	human	Quasar® 570
RPL5_26	gtaatctgcaacattctggc	human	Quasar® 570
RPL5_27	tcttcttccattaagtagcg	human	Quasar® 570
RPL5_28	actgtttcttgtaagcatct	human	Quasar® 570
RPL5_29	ggagttacgctgttctttat	human	Quasar® 570
RPL5_30	gagctttcttatacatctcc	human	Quasar® 570
RPL5_31	tggattctctcgtatagcag	human	Quasar® 570
RPL5_32	tcttgggcttcttttcatag	human	Quasar® 570
RPL5_33	ccacctcttcttttttaactt	human	Quasar® 570
RPL5_34	tgagcaagggacattttggg	human	Quasar® 570
RPL5_35	ttcttttgagctacccgatc	human	Quasar® 570
RPL5_36	ctgagctctgaggaagcttg	human	Quasar® 570
RPL5_37	aaattgctgggtttagctct	human	Quasar® 570
RPL5_38	agttgctgttcataagttta	human	Quasar® 570
RPL11_1	ccatgatggagagcaggaag	human	Quasar® 570
RPL11_2	ttctccttttcaccttgatc	human	Quasar® 570
RPL11_3	agtttgcggatgcgaagttc	human	Quasar® 570
RPL11_4	cccaacacagatgttgagac	human	Quasar® 570
RPL11_5	tggaaaacacaggggtctgc	human	Quasar® 570
RPL11_6	gatctgacagtgtatctagc	human	Quasar® 570
RPL11_7	atcttttcatttctccggat	human	Quasar® 570
RPL11_8	tcgaactgtgcagtggacag	human	Quasar® 570
RPL11_9	ttctccaagatttcttctgc	human	Quasar® 570
RPL11_10	tttcttaactcatactcccg	human	Quasar® 570
RPL11_11	tccagtatctgagaagttgt	human	Quasar® 570
RPL11_12	cctggatcccaaaaccaaag	human	Quasar® 570
RPL11_13	tttgatacccagatcgatgt	human	Quasar® 570
RPL11_14	tagataccaatgcttgggtc	human	Quasar® 570
RPL11_15	agcaccacatagaagtccag	human	Quasar® 570
RPL11_16	tcttgtctgcgatgctgaaa	human	Quasar® 570
RPL11_17	tctttgctgattctgtgttt	human	Quasar® 570
RPL11_18	atgatcccatcatacttctg	human	Quasar® 570
RPL11_19	acgggaatttatttgccagg	human	Quasar® 570
RPL11_20	ctttttattgctcttttgga	human	Quasar® 570
RPL32_1	gatgccgagaaggagatgg	human	Quasar® 570
RPL32_2	acgatcttgggcttcacaag	human	Quasar® 570
RPL32_3	gatgaacttcttggttctct	human	Quasar® 570
RPL32_4	catatcggtctgactggtgc	human	Quasar® 570
RPL32_5	cgccagttacgcttaatttt	human	Quasar® 570
RPL32_6	tacgaaccctgttgtcaatg	human	Quasar® 570
RPL32_7	aagatctggcccttgaatct	human	Quasar® 570
RPL32_8	tccataaccaatgttgggca	human	Quasar® 570
RPL32_9	ttgacgttgtggaccaggaa	human	Quasar® 570
RPL32_10	ttgcacatcagcagcacttc	human	Quasar® 570
RPL32_11	cgatctcggcacagtaagat	human	Quasar® 570
RPL32_12	gttcttggaggaaacattgt	human	Quasar® 570
RPL32_13	ctctttccacgatggctttg	human	Quasar® 570
RPL32_14	cctactcattttcttcactg	human	Quasar® 570
RPL32_15	tggccaagaagctgaagact	human	Quasar® 570
RPL32_16	acaatctctgtggcaaacta	human	Quasar® 570

RPL32_17	ttccaaaggggcttaagcaa	human	Quasar® 570
RPL32_18	tacaaatcccctccaaatgg	human	Quasar® 570
RPL32_19	ctgttcaaggactgagtgtc	human	Quasar® 570
RPL32_20	gatgactaaggctagtctgt	human	Quasar® 570
RPL32_21	caagtctgtacccctcatac	human	Quasar® 570
RPL32_22	cagaacctacctggtgtgag	human	Quasar® 570
RPL32_23	ccacaagcttcttcaagtgt	human	Quasar® 570
RPL32_24	aatgactacttgtggcttgg	human	Quasar® 570
RPL32_25	acttgtcacctaactttaca	human	Quasar® 570
RPL32_26	tctcacaagcatcacatgga	human	Quasar® 570
RPL32_27	tcatctggatatttccatgc	human	Quasar® 570
RPL32_28	caatttaggcatcccgtaag	human	Quasar® 570
RPL32_29	gtacatcatcctgttctttt	human	Quasar® 570
RPL32_30	ggattacctggaagagcaat	human	Quasar® 570
RPL32_31	tgcttttccagttaaccgtg	human	Quasar® 570
RPL32_32	ggagggttataggagactga	human	Quasar® 570
RPL32_33	tatacctgaagcagcagctg	human	Quasar® 570
RPL32_34	ccttggcaaactgctgtaac	human	Quasar® 570
RPL32_35	caattgtcaccagttaggtc	human	Quasar® 570
RPL32_36	tctgagtaccagtcaagagg	human	Quasar® 570
RPL32_37	ccctcatgacctatatacta	human	Quasar® 570
RPL32_38	tcataagtaccacatcccat	human	Quasar® 570
RPL32_39	acatcctgtaagcatttctg	human	Quasar® 570
RPL32_40	aagctttattatacccagcg	human	Quasar® 570
RPL32_41	agattcctgtctagactaga	human	Quasar® 570
RPL32_42	aggttttgaacaggagacaa	human	Quasar® 570

Table S3: smFISH probe sequences.

Appendix

The appendix includes the main text and figures of the publications resulting from my doctoral studies.

Towards a molecular understanding of the 5′TOP motif in regulating translation of ribosomal mRNAs
Hochstoeger, T., & Chao, J. A.
Seminars in Cell & Developmental Biology., 154:99-104. (2024)
https://doi.org/10.1016/j.semcdb.2023.06.001

Distinct roles of LARP1 and 4EBP1/2 in regulating translation and stability of 5′TOP mRNAs
Hochstoeger, T., Papasaikas, P., Piskadlo E., & Chao, J. A.
Science Advances., 10(7), eadi7830. (2024)
https://doi.org/10.1126/sciadv.adi7830

Seminars in Cell and Developmental Biology 154 (2024) 99–104

Contents lists available at ScienceDirect

Seminars in Cell and Developmental Biology

journal homepage: www.elsevier.com/locate/semcdb

Review

Towards a molecular understanding of the 5′TOP motif in regulating translation of ribosomal mRNAs

Tobias Hochstoeger [a,b], Jeffrey A. Chao [a,*]

[a] Friedrich Miescher Institute for Biomedical Research, 4058 Basel, Switzerland
[b] University of Basel, 4003 Basel, Switzerland

ARTICLE INFO

Keywords:
Ribosome
Translation
5′TOP
LARP1
MTOR

ABSTRACT

Vertebrate cells have evolved a simple, yet elegant, mechanism for coordinated regulation of ribosome biogenesis mediated by the 5′ terminal oligopyrimidine motif (5′TOP). This motif allows cells to rapidly adapt to changes in the environment by specifically modulating translation rate of mRNAs encoding the translation machinery. Here, we provide an overview of the origin of this motif, its characterization, and progress in identifying the key regulatory factors involved. We highlight challenges in the field of 5′TOP research, and discuss future approaches that we think will be able to resolve outstanding questions.

1. Regulation of ribosome biogenesis

In order for cells to grow and proliferate they must orchestrate the biogenesis of thousands of ribosomes, the cellular machines that carry out protein synthesis, every minute [1,2]. This endeavor is particularly challenging due to both the size of the macromolecular complex and the number of components that must be appropriately put together to generate functional ribosomes. In prokaryotes, this requires coordinating the production and assembly of three ribosomal RNAs (16 S, 23 S and 5 S rRNAs) and ~52 ribosomal proteins into two subunits (30 S small subunit, 50 S large subunit) that join to from the active 70 S ribosome [3]. This process becomes even more complex in eukaryotes, not only because of the partitioning of the cell into the nucleus and cytoplasm by the nuclear membrane, but the ribosome itself has increased in size and contains four ribosomal RNAs (18 S, 28 S, 5 S and 5.8 S rRNAs) as well as ~79 ribosomal proteins that must be assembled into the 40 S small subunit, 60 S large subunit and 80 S ribosome [4]. Importantly, synthesizing ribosomes at this scale utilizes considerable cellular resources necessitating that this process must be tightly regulated.

The production of stoichiometric levels of rRNAs and ribosomal proteins is controlled at multiple levels. In prokaryotes, regulation of the synthesis of rRNAs is achieved, in part, by the processing of a single pre-rRNA transcript into three distinct rRNAs [5]. While the prokaryotic ribosomal protein genes are located throughout the genome, many are arranged in operons which co-regulate their expression levels: one of the ribosomal proteins encoded in the operon can bind to a sequence within its own mRNA to repress the translation of all ribosomal proteins encoded in the operon [6,7]. In eukaryotes, three of the rRNAs (18 S, 28 S and 5.8 S rRNAs) are generated from the processing of a precursor transcript, however, the 5 S rRNA is encoded by a separate gene that is transcribed by RNA polymerase III instead of RNA polymerase I [8,9]. While co-regulation of eukaryotic ribosomal proteins does not occur through the arrangement of genes within operons, their coordinated expression has been shown to be regulated by specific transcriptional and post-transcriptional pathways that are controlled by the mTOR kinase in species ranging from plants, yeast and vertebrates [10–12].

The mTOR kinase is a central controller of cell growth, integrating nutrient cues and adjusting cell growth accordingly [13]. In both yeast and vertebrate cells, mTOR controls ribosome biogenesis through at least two main mechanisms: rRNA synthesis and ribosomal protein production [14]. While rRNA synthesis is transcriptionally regulated in both cases, control of ribosomal protein production is achieved in unique ways. In yeast, production of the ribosomal proteins is regulated mostly at the transcriptional level [15], with quick adaptation mediated by short mRNA half-lives (average half-life of ribosomal protein mRNAs: 16 min [16]). In vertebrates, production of ribosomal proteins is regulated mostly at the translational level by modulating translation of long-lived ribosomal protein mRNAs (average half-life of RP mRNAs in humans: >9 h [17]).

mTOR control of ribosomal protein translation becomes activated when vertebrate cells are exposed to unfavorable growth conditions (e.

* Corresponding author.
E-mail address: jeffrey.chao@fmi.ch (J.A. Chao).

https://doi.org/10.1016/j.semcdb.2023.06.001
Received 20 May 2022; Received in revised form 14 April 2023; Accepted 5 June 2023
Available online 12 June 2023

g., deprivation of amino acids, serum, oxygen or insulin) that leads to inhibition of the mTOR kinase, resulting in a rapid translational down-regulation of ribosomal protein mRNAs, thereby reducing the biogenesis of new ribosomes [12]. Conversely, providing nutrients to starved cells results in a rapid re-activation of ribosomal protein mRNA translation [12]. This has led to the hypothesis of a molecular switch that toggles vertebrate ribosomal protein mRNA translation by specific regulators that recognize unique features within these transcripts and are controlled by mTOR [18,19].

2. The 5′TOP motif

In the 1980 s, characterization of the sequences of ribosomal protein mRNAs from a variety of vertebrates led to the observation that this class of transcripts contained a conserved sequence motif at the 5′-end of the transcript that is directly adjacent to the 7-methylguanosine cap [20, 21–26]. Since this motif contained a conserved cytidine in the + 1 position followed by an uninterrupted stretch of 4–15 pyrimidine nucleotides it became known as the 5′ terminal oligopyrimidine (5′TOP) motif [27]. Initial studies of the 5′TOP motif determined that it was both essential and sufficient to mediate translational control because mutation of the first invariable nucleotide converts a 5′TOP mRNA into a non-5′TOP mRNA that is not rapidly repressed under stress [27], while mutating the 5′ end of a non-5′TOP mRNA enables it to be repressed like an endogenous 5′TOP mRNA during stress [28]. Additional sequence analysis of mRNAs that encode translation factors and other proteins involved in translation indicated that the 5′TOP motif is more broadly utilized to regulate additional aspects of translation beyond only ribosomal proteins [12,29].

This coordinated regulation of translation, however, requires a well-defined transcription start site. In vertebrates, ribosomal protein mRNAs have core promoters that contain a unique consensus motif found at the transcription start site of these genes termed the polypyrimidine initiator (TCT motif) [30,31]. The TCT motif comprises nucleotides in the − 2 to + 6 positions with respect to the transcription start site and is distinct from other core promoter motifs (e.g., TATA box). While the mechanism by which the TCT motif functions in transcription initiation is not fully understood, it ensures that the 5′UTR of ribosomal protein transcripts begins with an invariable cytosine followed by a short stretch of pyrimidine nucleotides [30]. Interestingly, the positioning of the 5′TOP motif at the 5′ end of mRNAs allows for the expression of both 5′TOP and non-5′TOP mRNAs for the same genes utilizing alternative transcription start sites (TSS), and recent evidence suggests that many genes indeed are expressed as both variants, with some cases of tissue-specific expression of the 5′TOP or non-5′TOP isoform of the transcript [32,33]. Nevertheless, the core set of 5′TOP mRNAs involved in translation were found to be constitutively expressed as 5′TOP mRNAs across 16 human tissues in a recent analysis of genome-wide transcription initiation events [33].

While the function of the 5′TOP motif in conferring mTOR-dependent translational regulation has been well established, the role of sequence elements located in the 5′UTR of these transcripts is unclear. Pyrimidine enriched translation elements (PRTE) are found downstream of the 5′ cap in the 5′UTR of many mTOR regulated mRNAs, with a large overlap of mRNAs that contain both a 5′TOP and PRTE [34]. Using ribosome profiling, 144 mRNAs were found to be sensitive to mTOR inhibition. Of those, 37 possessed only a 5′TOP element, 30 possessed only a PRTE within their 5′ UTR, and 61 mRNAs possessed both a 5′TOP and PRTE [34]. The PRTE consensus motif consists of an invariant uridine at position 6 of a 9 nt long pyrimidine stretch. As the core 5′TOP motif has been shown to be essential and sufficient for mTOR-dependent translational regulation, research has focused on studying the 5′TOP motif, and the function of the PRTE in contributing to this regulation remains to be determined.

3. Identification of *trans*-acting factors that regulate translation of 5′TOP mRNAs

While the conservation of the consensus sequence within the 5′TOP motif suggested that it could be specifically recognized by a *trans*-acting factor, it has proven difficult to identify its interaction partner. Since the 5′TOP motif is located at the 5′ end of mRNAs that are bound by the eIF4F complex (eIF4E, eIF4G and eIF4A) during translation initiation, the *trans*-acting factor could either be part of the canonical translation initiation machinery that also has partial specificity for the 5′TOP motif, or a specialized protein that selectively recognizes the 5′TOP motif. In both cases, the molecule mediating 5′TOP translational regulation needs to fulfill several criteria [18]. First, it is essential for selective 5′TOP translational regulation to occur and loss or mutation of the factor results in 5′TOP mRNAs and non-5′TOP mRNAs behaving similarly during stress. Second, it specifically interacts with the 5′TOP motif in order to provide a molecular link between the 5′TOP sequence and translational regulation. Third, its role in translational regulation can be altered in response to mTOR activity.

mTOR can globally regulate translation through phosphorylation of eIF4E binding proteins (4EBP1 and 4EBP2) and ribosomal protein S6 kinases (S6K1 and S6K2) [35]. Since both physiological and pharmacological inhibition of mTOR results in rapid translational repression of 5′TOP mRNAs and dephosphorylation of S6K and 4EBP1/2, they have both been proposed to be the 5′TOP motif specificity factor. S6K activity, however, could be uncoupled from 5′TOP regulation in S6K1/2 double knockout mice without abolishing rapamycin-sensitive 5′TOP regulation indicating that it was unlikely to be the main regulator [36,37]. Additionally, selective ribosome profiling also indicated that ribosomal protein S6, which is one of the substrates of S6K and could potentially mediate an interaction with 5′TOP transcripts during translation initiation, does not promote their translation [38]. When mTOR is inactivated under unfavorable growth conditions, 4EBP1/2 become dephosphorylated which enables their binding to eIF4E, blocking the eIF4E-eIF4G interaction and preventing the assembly of the eIF4F complex, thus inhibiting translation initiation. While eIF4E specifically recognizes the 5′ cap structure, its affinity for a capped oligo has also been shown to depend on the nucleotide in the + 1 position with a preference for adenine or guanine over cytosine [39]. While a more detailed analysis of eIF4E's sequence specificity has not been performed, this suggests that while eIF4E is a canonical translation factor, it may allow for selective reduction in 5′TOP mRNA translation when mTORC1 is inhibited and the pool of active eIF4E is reduced. Interestingly, while 5′TOP mRNAs are translated when mTOR is active, they have been found to be less efficiently translated than other housekeeping transcripts even in growing cells, as estimated by polysome analysis [12]. This suggests that their initiation is partially impaired which could result from reduced eIF4E affinity, however, it is also possible that mTOR is inactive in a subpopulation of cells even under nutrient rich conditions, which cannot be resolved by bulk methods such as polysome analysis. Consistent with a specific role of eIF4E, 4EBP1/2 double-knockout MEFs demonstrated an involvement of 4EBP1/2 in regulating 5′TOP mRNA translation, as loss of 4EBP1/2 resulted in a rescue of 5′TOP translational repression upon Torin1 treatment [29]. A follow-up study, however, demonstrated that under long-term oxygen deprivation or serum starvation, 4EBP1/2 double-knockout MEFs retain strong 5′TOP translational regulation indicating that an additional factor must be involved [40]. Miloslavski and colleagues were, however, able to replicate the initial finding by Thoreen et al. that loss of 4EBP1/2 is sufficient to rescue short-term pharmacological inhibition of 5′TOP translation indicating that different 5′TOP binding partners might function sequentially or with differing kinetics in order to repress translation.

Since the 5′TOP motif contains a stretch of sequential pyrimidines this sequence could be bound by a number of RNA-binding proteins that share this RNA-binding specificity. Among them, TIA1 and TIAR were reported to mediate translational repression of 5′TOP mRNAs under

amino acid starvation [41], but not hypoxia [40]. Knockdown of the TIA1 and TIAR also failed to rescue 5′TOP translational repression upon Torin1 treatment indicating that it may not be a general translational repressor of 5′TOP mRNA translation but could play a more specialized role [29].

More recently, LARP1 has emerged as the putative key specificity factor that regulates translation of 5′TOP mRNAs. LARP1 was first implicated in 5′TOP translational regulation in a proteomic screen for 5′ cap binding proteins whose binding is regulated by mTOR [42]. Early studies found that LARP1 also associates with PABP and has a stimulatory effect on mRNA translation [43,44]. More recently, it has become clear that LARP1 also plays a key role specifically in 5′TOP translational repression [45,46]. Importantly, a crystal structure revealed the specific binding of the LARP1 DM15 domain to the 5′ cap and the five nucleotides of the 5′TOP motif [47]. This structure suggested that the LARP1 DM15 domain directly binds the 5′ cap and 5′TOP motif and thereby competes with eIF4E and blocks translation initiation. The 5′TOP-binding activity of LARP1 is also regulated by mTORC1 via direct binding of LARP1 to Raptor (regulatory associated protein of mTORC1) and phosphorylation of LARP1 by the mTOR kinase on residues adjacent to the DM15 domain has been suggested to induce a conformational rearrangement of LARP1 and inhibit its binding to the 5′TOP motif [48]. A pull-down of endogenously tagged eIF4E cross-linked to mRNA 5′ ends (cap crosslinking and immunoprecipitation, capCLIP) also showed that 5′TOP mRNA reads are specifically depleted upon mTOR inhibition, consistent with a model in which LARP1 specifically competes with eIF4E for binding to these mRNAs [49].

Although LARP1 knockout leads to a reduction in the translational repression of 5′TOP mRNAs, experiments by several research groups have consistently found that there is only a partial rescue of 5′TOP mRNAs translation during mTORC1 inhibition [33,48]. LARP1 was deleted by CRISPR-Cas9 by two research groups in HEK293T cells independently, which made it possible to study 5′TOP translational repression in the absence of any LARP1 protein [33,48]. Both research groups found that loss of LARP1 is not sufficient for a full rescue of translational repression, suggesting the existence of one or more additional specificity mediating factors which are regulated downstream of mTORC1, but can function independent of LARP1 binding to the 5′TOP motif. It is possible that knockout of LARP1 leads to the upregulation of compensatory proteins that can mediate some 5′TOP translational repression in its stead. In order to identify a potential compensatory role of the LARP1 homologue LARP1B (also called LARP2), LARP1/LARP1B double knockout HEK cells were generated [33]. LARP1B, however, was not found to contribute to 5′TOP translational repression and therefore cannot explain the persistent sensitivity of 5′TOP mRNAs to mTORC1 inhibition. While there are other LARP family members, they do not contain the DM15 domain that recognizes the 5′TOP motif [50]. Consequently, the possible role of an additional factor that contributes to 5′TOP-specific regulation during mTORC1 inhibition has not been fully resolved.

4. Mechanism of LARP1′s interaction with 5′TOP transcripts

LARP1 is a large multidomain protein (1096 amino acids) that contains a La-module and the DM15 domain, however, most of the protein is predicted to be disordered [51]. While the DM15 domain's interaction with the 5′TOP motif has been extensively biochemically and structurally characterized, how the rest of the protein may contribute to regulation of 5′TOP transcripts is less well understood [47,52].

In vitro RNA-binding studies of the LARP1 La-motif have identified a sequence preference for both poly(A) RNAs as well as pyrimidine-rich sequences that are similar to the 5′TOP motif, but lack the 5′ cap [53]. Interestingly, it was found that the La-motif may interact with poly(A) RNA and the pyrimidine sequence simultaneously suggesting that this domain has at least two distinct RNA-binding surfaces. The La-module, consisting of a La-motif followed by an RNA recognition motif (RRM), is the common characteristic of the family of La and related proteins (LARPs), and combines two distinct RNA-binding activities. While it was assumed that LARP1 shares this domain architecture, recent experiments demonstrate that LARP1 only contains the La-motif, and the downstream region thought to be an RRM is unfolded [54].

The in vivo RNA-binding specificity of full-length LARP1 has also been determined using photoactivatable ribonucleoside-enhanced crosslinking and immunoprecipitation (PAR-CLIP), which determined that LARP1 binds to pyrimidine-rich sequences in the 5′UTR of transcripts and this interaction is enhanced upon mTOR inhibition [55]. The exact 5′TOP sequence, however, was not specifically identified by PAR-CLIP and the pyrimidine nucleotides were located distally from the cap in the 5′UTR though this discrepancy might arise for technical reasons associated with library preparation or biases caused by T1 RNase digestion. Interestingly, LARP1 was also found to bind to the 3′UTR of transcripts, albeit with limited sequence specificity. Additionally, LARP1 also contains a PABP-interacting motif-2 (PAM2) downstream of the La-motif that enables it to interact with the mademoiselle domain of PABPC1 [56]. This interaction with PABPC1 and, potentially, the polyA tail has been found to protect poly(A) tail length and stabilize the mRNA [44,56,57].

It remains unclear if the La-module and DM15 domain are able to simultaneously interact with the 5′TOP motif, PRTE, 3′UTR, poly(A) tail and PABC1 of the same transcripts or if any of these interactions are mutually exclusive and how the combination of the interactions affects 5′TOP regulation. While the La-motif and DM15 domain are separated by ~400 amino acids that do not contain any known globular domains, AlphaFold predicts that this region may not be entirely disordered and could bring the La-motif and DM15 domain in close physical proximity (Fig. 1) [58]. Though this conformation requires experimental validation, nonetheless, it suggests that the function of the individual domains may be more tightly coupled than previously appreciated and provides a framework for further characterization. It should be noted, however, that the individual isolated La-motif and DM15 domains have been shown to retain functionality indicating that they can function autonomously to some extent [46,48].

Though the regulation of 5′TOP translation and LARP1 has been well described, loss of LARP1 has also been found to result in a specific decrease in the mRNA stability of 5′TOP mRNAs [44,59]. As 5′TOP mRNAs are some of the most stable mRNAs in mammalian cells, it is tempting to speculate that LARP1 functions to protect this class of mRNAs from degradation and directly contributes to their high stability. This raises the question of how LARP1 is specifically recruited to these mRNAs to mediate stability under nutrient-rich conditions, when the DM15 domain is phosphorylated and unable to bind the 5′TOP motif [48]. Consequently, it has been suggested that LARP1 binds to 5′TOP mRNAs via its La-motif to either the 5′TOP or PRTE (in a cap-independent manner that does not block eIF4E) and the poly(A) tail and PABP, potentially circularizing mRNAs to allow translation while protecting them from decay (see Fig. 2). While evidence exists for the close-loop model in promoting translation and stability in yeast, current single-molecule RNA imaging in human cells has indicated that translating mRNAs are less compact than translationally-inhibited ones [60,61]. Therefore, LARP1 may specifically promote a closed-loop confirmation for only 5′TOP mRNAs to selectively promote their stability.

While the closed-loop model of 5′TOP mRNPs provides an explanation for their enhanced stability, it is not entirely clear where the specificity for 5′TOP transcripts comes from when mTORC1 is active and eIF4E is presumably bound to the 5′ cap. Additionally, it is not known if eIF4E and LARP1 can simultaneously interact on the same 5′UTR since there are conflicting reports of an indirect RNA-mediated interaction between these proteins [42,45,55]. Recent structural studies of the human 48 S preinitiation complex have suggested that initiation occurs via a cap-tethered mechanism that results in a "blind spot" of ~30 nucleotides adjacent to the 5′-cap, which could enable translation initiation to be compatible with LARP1 binding [62]. A recent study showed

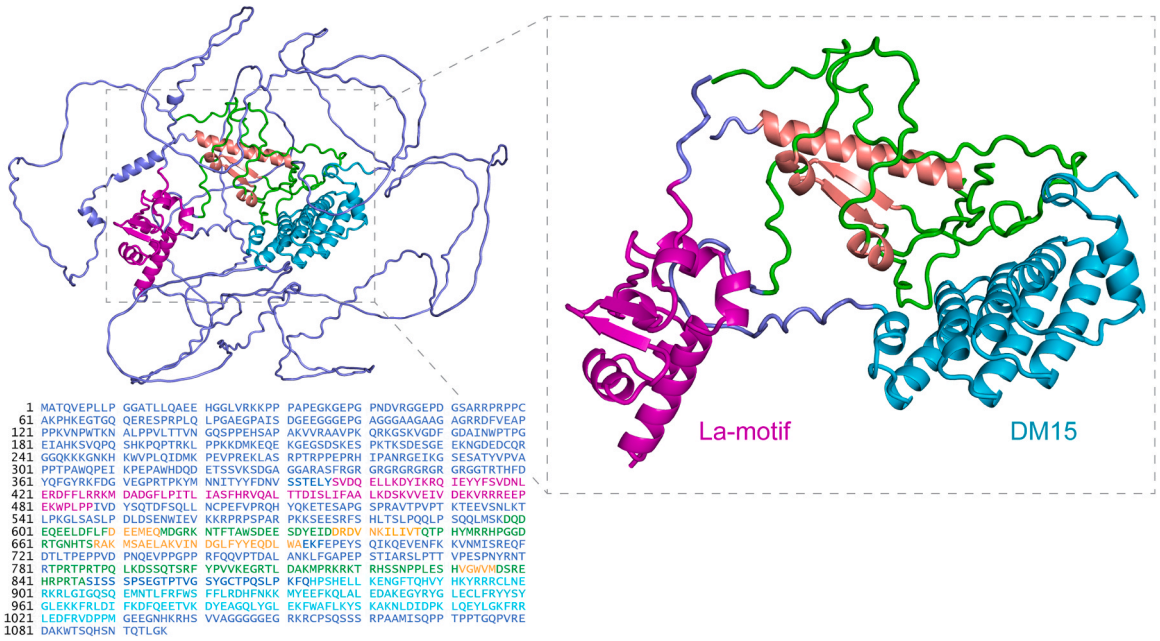

Fig. 1. : AlphaFold prediction of full-length human LARP1 structure. The known structured domains of the La-motif and DM15 are shown in magenta and cyan, respectively. Note the extensive disordered regions shown in blue. Additional predicted structural elements are marked in orange (with connecting loops in green) and could bring the La-motif and DM15 domain in close proximity. Shown here is the 1096 aa isoform, which is the main isoform expressed in human cells (see [51]).

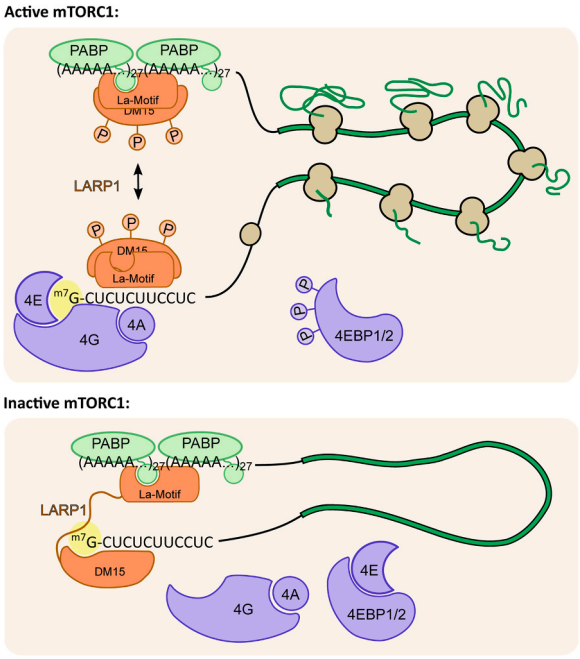

Fig. 2. : Interaction of LARP1 with a 5′TOP mRNA. Under nutrient-rich conditions (top), mTORC1 is active and phosphorylates both 4EBP1/2 and LARP1. The EIF4F complex (composed of 4E, 4 G, and 4 A) can bind the ^{m7}G cap and recruit the 43 S preinitiation complex. Under these conditions, LARP1′s La-motif can bind to either the 5′TOP motif or the poly(A)-tail and LARP1′s PAM2 motif can bind the mademoiselle domain of PABP. Under nutrient starvation (bottom), mTORC1 is inactive and 4EBP1/2 and LARP1 are dephosphorylated. 4EBP1/2 sequesters 4E, thereby blocking translation initiation, while LARP1 can bind the ^{m7}G cap with its DM15 domain and its La-motif and PAM2 could bind to the poly(A)-tail and PABP, respectively. Simultaneous binding of a single LARP1 molecule to both mRNA ends is possible under both active and inactive mTORC1 and could serve to protect the mRNAs from degradation. Further research will be needed to verify the existence of such LARP1-mediated 5′TOP mRNA closed loops and their functional implication.

that LARP1 has a protective effect on 5′TOP mRNA levels under prolonged mTOR inhibition, which is thought to preserve these mRNAs for reactivation of translation in a closed-loop conformation via DM15 binding to the 5′TOP and La-motif binding to the poly(A)tail/PABP [63]. It is possible that the closed-loop conformation only becomes relevant under mTOR inhibition, when LARP1 can circularize 5′TOP mRNAs without interference from translation initiation, thereby protecting them from the decay machinery.

5. Outlook

While the biological importance of the regulation of translation and stability of 5′TOP mRNAs during normal cell growth and disease has long been appreciated, the molecular mechanisms that enable this specific control have been challenging to elucidate. Any inhibition of a core cellular process that impacts ribosome biogenesis can be expected to have global pleiotropic effects making it difficult to isolate specific pathways, particularly when studying prolonged deprivation of amino acids or growth factors. While acute pharmacological inhibition of mTOR mitigates some of these experimental complications, the inhibition of translation or changes in mRNA stability are usually determined using ensemble techniques that measure the average change of all the 5′TOP mRNAs in thousands or even millions of cells. Consequently, cellular heterogeneity can mask differences between models for 5′TOP regulation and has prevented a detailed kinetic analysis of the effect of mTOR inhibition.

The recent development of single-molecule methods for directly imaging mRNAs and their translation and degradation provides an opportunity to further characterize the regulation of 5′TOP mRNAs [64, 65]. Using these approaches, it will be possible to directly measure both the fraction of individual mRNAs undergoing active translation as well as their ribosome occupancy in living cells [64]. Previously, we have characterized the localization and translation of 5′TOP reporter mRNAs in cells treated with sodium arsenite, which activates the integrated stress response, but does not inhibit mTOR, [66]. These experiments showed that stable association of a 5′TOP reporter mRNA to stress granules and processing bodies required both LARP1 and the 5′TOP motif indicating the potential of this system to characterize LARP1- and

5′TOP-dependent regulation. We anticipate that single-molecule imaging will enable quantification of the magnitude and timing of 5′TOP regulation during mTOR inhibition and how the *trans*-acting factors LARP1 and 4EBP1/2 exert their effects. Using these tools, it will be possible to precisely compare and contrast the efficiency of translational repression of a 5′TOP reporter in cells depleted of either LARP1 or 4EBP1/2 and long-term imaging of mRNA reporters will also enable researchers to precisely quantify translation parameters of 5′TOP mRNAs (e.g., initiation rates and bursting kinetics) [67]. Finally, further advances in imaging technologies may soon make it possible to directly observe binding of individual trans-acting factors to the 5′TOP motif in order to measure their impact on the translation status of individual mRNAs.

In parallel, advances in pull-down assays such as capCLIP will shed further light onto the regulators involved in displacing eIF4E from 5′TOP mRNAs upon mTOR inhibition. It will be interesting to see whether the specific displacement of eIF4E can still occur in absence of either LARP1 or 4EBP1/2, which will allow functional separation of the role of the cap-binding regulators of 5′TOP translation, and clarify whether their action is coupled or independent from each other.

Declaration of Competing Interest

The authors declare no conflicts of interest.

Acknowledgements

This work was supported by the Novartis Research Foundation, the Swiss National Science Foundation grant 31003A_182314 (J.A.C.), the SNF-NCCR RNA & Disease network and a Boehringer Ingelheim Fonds PhD Fellowship (T.H.). We would like to thank V. Bhaskar for help with structural modeling of Larp1.

References

[1] J.D. Lewis, D. Tollervey, Like attracts like: getting RNA processing together in the nucleus, Science 288 (5470) (2000) 1385–1389.
[2] J.R. Warner, The economics of ribosome biosynthesis in yeast, Trends Biochem Sci. 24 (11) (1999) 437–440.
[3] M. Kaczanowska, M. Rydén-Aulin, Ribosome biogenesis and the translation process in Escherichia coli, Microbiol. Mol. Biol. Rev. 71 (3) (2007) 477–494.
[4] E. Thomson, S. Ferreira-Cerca, E. Hurt, Eukaryotic ribosome biogenesis at a glance, J. Cell Sci. 126 (21) (2013) 4815–4821.
[5] R.T. Espejo, N. Plaza, Multiple ribosomal RNA operons in bacteria; their concerted evolution and potential consequences on the rate of evolution of their 16S rRNA, Front. Microbiol. (2018) 9.
[6] D.E. Draper, Mechanisms of ribosomal protein translational autoregulation. Post-transcriptional Control of Gene Expression, Springer, 1990, pp. 299–308.
[7] A. Mikhaylina, E. Nikonova, O. Kostareva, S. Tishchenko, Regulation of ribosomal protein synthesis in prokaryotes, Mol. Biol. 55 (1) (2021) 16–36.
[8] M. Ciganda, N. Williams, Eukaryotic 5S rRNA biogenesis, Wiley Inter. Rev. RNA 2 (4) (2011) 523–533.
[9] A.K. Henras, C. Plisson-Chastang, M.F. O'Donohue, A. Chakraborty, P.E. Gleizes, An overview of pre-ribosomal RNA processing in eukaryotes, Wiley Interdiscip. Rev.: RNA 6 (2) (2015) 225–242.
[10] M.R. Scarpin, S. Leiboff, J.O. Brunkard, Parallel global profiling of plant TOR dynamics reveals a conserved role for LARP1 in translation, eLife 9 (2020), e58795.
[11] T. Powers, P. Walter, Regulation of ribosome biogenesis by the rapamycin-sensitive TOR-signaling pathway in saccharomyces cerevisiae, Mol. Biol. Cell 10 (4) (1999) 987–1000.
[12] O. Meyuhas, Synthesis of the translational apparatus is regulated at the translational level, Eur. J. Biochem 267 (21) (2000) 6321–6330.
[13] T. Schmelzle, M.N. Hall, TOR, a central controller of cell growth, Cell 103 (2) (2000) 253–262.
[14] C. Mayer, I. Grummt, Ribosome biogenesis and cell growth: mTOR coordinates transcription by all three classes of nuclear RNA polymerases, Oncogene 25 (48) (2006) 6384–6391.
[15] D. Shore, S. Zencir, B. Albert, Transcriptional control of ribosome biogenesis in yeast: links to growth and stress signals, Biochem. Soc. Trans. 49 (4) (2021) 1589–1599.
[16] L.Y. Chan, C.F. Mugler, S. Heinrich, P. Vallotton, K. Weis, Non-invasive measurement of mRNA decay reveals translation initiation as the major determinant of mRNA stability, eLife 7 (2018), e32536.
[17] J.A. Schofield, E.E. Duffy, L. Kiefer, M.C. Sullivan, M.D. Simon, TimeLapse-seq: adding a temporal dimension to RNA sequencing through nucleoside recoding, Nat. Methods 15 (3) (2018) 221–225.
[18] O. Meyuhas, T. Kahan, The race to decipher the top secrets of TOP mRNAs, Biochim. Et Biophys. Acta (BBA) - Gene Regul. Mech. 1849 (7) (2015) 801–811.
[19] C. Schneider, F. Erhard, B. Binotti, A. Buchberger, J. Vogel, U. Fischer, An unusual mode of baseline translation adjusts cellular protein synthesis capacity to metabolic needs, Cell Rep. 41 (2) (2022), 111467.
[20] C. Huxley, M. Fried, The mouse rpL7a gene is typical of other ribosomal protein genes in it's 5′ region but differs in being located in a tight cluster of CpG-rich islands, Nucleic Acids Res. 18 (18) (1990) 5353–5357.
[21] P. Mariottini, C. Bagni, F. Annesi, F. Amaldi, Isolation and nucleotide sequences of cDNAs for Xenopus laevis ribosomal protein S8: similarities in the 5′ and 3′ untranslated regions of mRNAs for various r-proteins, Gene 67 (1) (1988) 69–74.
[22] I.T. Chen, D.J. Roufa, The transcriptionally active human ribosomal protein S17 gene, Gene 70 (1) (1988), 107-16.
[23] D.D. Rhoads, A. Dixit, D.J. Roufa, Primary structure of human ribosomal protein S14 and the gene that encodes it, Mol. Cell. Biol. 6 (8) (1986) 2774–2783.
[24] M. Wagner, R.P. Perry, Characterization of the multigene family encoding the mouse S16 ribosomal protein: strategy for distinguishing an expressed gene from its processed pseudogene counterparts by an analysis of total genomic DNA, Mol. Cell. Biol. 5 (12) (1985) 3560–3576.
[25] L.M. Wiedemann, R.P. Perry, Characterization of the expressed gene and several processed pseudogenes for the mouse ribosomal protein L30 gene family, Mol. Cell. Biol. 4 (11) (1984) 2518–2528.
[26] K.P. Dudov, R.P. Perry, The gene family encoding the mouse ribosomal protein L32 contains a uniquely expressed intron-containing gene and an unmutated processed gene, Cell 37 (2) (1984) 457–468.
[27] D. Avni, S. Shama, F. Loreni, O. Meyuhas, Vertebrate mRNAs with a 5'-terminal pyrimidine tract are candidates for translational repression in quiescent cells: characterization of the translational cis-regulatory element, Mol. Cell. Biol. 14 (6) (1994) 3822–3833.
[28] Y. Biberman, O. Meyuhas, Substitution of just five nucleotides at and around the transcription start site of rat β-actin promoter is sufficient to render the resulting transcript a subject for translational control, FEBS Lett. 405 (3) (1997) 333–336.
[29] C.C. Thoreen, L. Chantranupong, H.R. Keys, T. Wang, N.S. Gray, D.M. Sabatini, A unifying model for mTORC1-mediated regulation of mRNA translation, Nature 485 (7396) (2012) 109–113.
[30] T.J. Parry, J.W.M. Theisen, J.-Y. Hsu, Y.-L. Wang, D.L. Corcoran, M. Eustice, et al., The TCT motif, a key component of an RNA polymerase II transcription system for the translational machinery, Genes Dev. 24 (18) (2010) 2013–2018.
[31] A.M.G. van den Elzen, M.J. Watson, C.C. Thoreen, mRNA 5' terminal sequences drive 200-fold differences in expression through effects on synthesis, translation and decay, PLoS Genet. 18 (11) (2022), e1010532.
[32] C. Nepal, Y. Hadzhiev, P. Balwierz, E. Tarifeño-Saldivia, R. Cardenas, J.W. Wragg, et al., Dual-initiation promoters with intertwined canonical and TCT/TOP transcription start sites diversify transcript processing, Nat. Commun. 11 (1) (2020) 168.
[33] L. Philippe, A.M.G. van den Elzen, M.J. Watson, C.C. Thoreen, Global analysis of LARP1 translation targets reveals tunable and dynamic features of 5′ TOP motifs, Proc. Natl. Acad. Sci. USA 117 (10) (2020) 5319–5328.
[34] A.C. Hsieh, Y. Liu, M.P. Edlind, N.T. Ingolia, M.R. Janes, A. Sher, et al., The translational landscape of mTOR signalling steers cancer initiation and metastasis, Nature 485 (7396) (2012) 55–61.
[35] B.D. Fonseca, E.M. Smith, N. Yelle, T. Alain, M. Bushell, A. Pause, The ever-evolving role of mTOR in translation, Semin Cell Dev. Biol. 36 (2014) 102–112.
[36] M. Pende, S.H. Um, V. Mieulet, M. Sticker, V.L. Goss, J. Mestan, et al., S6K1 (-/-)/S6K2(-/-) mice exhibit perinatal lethality and rapamycin-sensitive 5'-terminal oligopyrimidine mRNA translation and reveal a mitogen-activated protein kinase-dependent S6 kinase pathway, Mol. Cell Biol. 24 (8) (2004) 3112–3124.
[37] I. Ruvinsky, N. Sharon, T. Lerer, H. Cohen, M. Stolovich-Rain, T. Nir, et al., Ribosomal protein S6 phosphorylation is a determinant of cell size and glucose homeostasis, Genes Dev. 19 (18) (2005) 2199–2211.
[38] J. Bohlen, M. Roiuk, A.A. Teleman, Phosphorylation of ribosomal protein S6 differentially affects mRNA translation based on ORF length, Nucleic Acids Res. 49 (22) (2021) 13062–13074.
[39] A. Tamarkin-Ben-Harush, J.J. Vasseur, F. Debart, I. Ulitsky, R. Dikstein, Cap-proximal nucleotides via differential eIF4E binding and alternative promoter usage mediate translational response to energy stress, Elife (2017) 6.
[40] R. Miloslavski, E. Cohen, A. Avraham, Y. Iluz, Z. Hayouka, J. Kasir, et al., Oxygen sufficiency controls TOP mRNA translation via the TSC-Rheb-mTOR pathway in a 4E-BP-independent manner, J. Mol. Cell Biol. 6 (3) (2014) 255–266.
[41] C.K. Damgaard, J. Lykke-Andersen, Translational coregulation of 5′TOP mRNAs by TIA-1 and TIAR, Genes Dev. 25 (19) (2011) 2057–2068.
[42] J. Tcherkezian, M. Cargnello, Y. Romeo, E.L. Huttlin, G. Lavoie, S.P. Gygi, et al., Proteomic analysis of cap-dependent translation identifies LARP1 as a key regulator of 5′TOP mRNA translation, Genes Dev. 28 (4) (2014) 357–371.
[43] C. Burrows, N. Abd Latip, S.J. Lam, L. Carpenter, K. Sawicka, G. Tzolovsky, et al., The RNA binding protein Larp1 regulates cell division, apoptosis and cell migration, Nucleic Acids Res. 38 (16) (2010) 5542–5553.
[44] K. Aoki, S. Adachi, M. Homoto, H. Kusano, K. Koike, T. Natsume, LARP1 specifically recognizes the 3′ terminus of poly(A) mRNA, FEBS Lett. 587 (14) (2013) 2173–2178.
[45] B.D. Fonseca, C. Zakaria, J.J. Jia, T.E. Graber, Y. Svitkin, S. Tahmasebi, et al., La-related protein 1 (LARP1) represses terminal oligopyrimidine (TOP) mRNA

translation downstream of mTOR complex 1 (mTORC1), J. Biol. Chem. 290 (26) (2015) 15996–16020.
[46] L. Philippe, J.J. Vasseur, F. Debart, C.C. Thoreen, La-related protein 1 (LARP1) repression of TOP mRNA translation is mediated through its cap-binding domain and controlled by an adjacent regulatory region, Nucleic Acids Res. 46 (3) (2018) 1457–1469.
[47] R.M. Lahr, B.D. Fonseca, G.E. Ciotti, H.A. Al-Ashtal, J.J. Jia, M.R. Niklaus, et al., La-related protein 1 (LARP1) binds the mRNA cap, blocking eIF4F assembly on TOP mRNAs, Elife (2017) 6.
[48] J.-J. Jia, R.M. Lahr, M.T. Solgaard, B.J. Moraes, R. Pointet, A.-D. Yang, et al., mTORC1 promotes TOP mRNA translation through site-specific phosphorylation of LARP1, Nucleic Acids Res. (2021).
[49] K.B. Jensen, B.K. Dredge, J. Toubia, X. Jin, V. Iadevaia, G.J. Goodall, et al., capCLIP: a new tool to probe translational control in human cells through capture and identification of the eIF4E–mRNA interactome, Nucleic Acids Res. 49 (18) (2021) e105-e..
[50] R.J. Maraia, S. Mattijssen, I. Cruz-Gallardo, M.R. Conte, The La and related RNA-binding proteins (LARPs): structures, functions, and evolving perspectives, WIREs RNA 8 (6) (2017), e1430.
[51] H. Schwenzer, M. Abdel Mouti, P. Neubert, J. Morris, J. Stockton, S. Bonham, et al., LARP1 isoform expression in human cancer cell lines, RNA Biol. 18 (2) (2021) 237–247.
[52] K.C. Cassidy, R.M. Lahr, J.C. Kaminsky, S. Mack, B.D. Fonseca, S.R. Das, et al., Capturing the mechanism underlying TOP mRNA binding to LARP1, Structure (2019).
[53] H.A. Al-Ashtal, C.M. Rubottom, T.C. Leeper, A.J. Berman, The LARP1 La-module recognizes both ends of TOP mRNAs, RNA Biol. (2019) 1–11.
[54] G. Kozlov, S. Mattijssen, J. Jiang, S. Nyandwi, T. Sprules, R. Iben James, et al., Structural basis of 3′-end poly(A) RNA recognition by LARP1, Nucleic Acids Res. 50 (16) (2022) 9534–9547.
[55] S. Hong, M.A. Freeberg, T. Han, A. Kamath, Y. Yao, T. Fukuda, et al., LARP1 functions as a molecular switch for mTORC1-mediated translation of an essential class of mRNAs, Elife (2017) 6.
[56] S. Mattijssen, G. Kozlov, S. Gaidamakov, A. Ranjan, B.D. Fonseca, K. Gehring, et al., The isolated La-module of LARP1 mediates 3′ poly(A) protection and mRNA stabilization, dependent on its intrinsic PAM2 binding to PABPC1, RNA Biol. 18 (2) (2021) 275–289.
[57] K. Ogami, Y. Oishi, K. Sakamoto, M. Okumura, R. Yamagishi, T. Inoue, et al., mTOR- and LARP1-dependent regulation of TOP mRNA poly(A) tail and ribosome loading, Cell Rep. 41 (4) (2022), 111548.
[58] J. Jumper, R. Evans, A. Pritzel, T. Green, M. Figurnov, O. Ronneberger, et al., Highly accurate protein structure prediction with AlphaFold, Nature 596 (7873) (2021) 583–589.
[59] A. Gentilella, F.D. Moron-Duran, P. Fuentes, G. Zweig-Rocha, F. Riano-Canalias, J. Pelletier, et al., Autogenous control of 5′TOP mRNA stability by 40S ribosomes, Mol. Cell 67 (1) (2017), 55-70 e4.
[60] N. Amrani, S. Ghosh, D.A. Mangus, A. Jacobson, Translation factors promote the formation of two states of the closed-loop mRNP, Nature 453 (7199) (2008) 1276–1280.
[61] S. Adivarahan, N. Livingston, B. Nicholson, S. Rahman, B. Wu, O.S. Rissland, et al., Spatial organization of single mRNPs at different stages of the gene expression pathway, Mol. Cell 72 (4) (2018), 727-738.e5.
[62] J. Brito Querido, M. Sokabe, S. Kraatz, Y. Gordiyenko, J.M. Skehel, C.S. Fraser, et al., Structure of a human 48S translational initiation complex, Science 369 (6508) (2020) 1220–1227.
[63] P. Fuentes, J. Pelletier, C. Martinez-Herráez, V. Diez-Obrero, F. Iannizzotto, T. Rubio, et al., The 40S-LARP1 complex reprograms the cellular translatome upon mTOR inhibition to preserve the protein synthetic capacity, Sci. Adv. 7 (48) (2021), eabg9275.
[64] M.E. Tanenbaum, L.A. Gilbert, L.S. Qi, J.S. Weissman, R.D. Vale, A protein-tagging system for signal amplification in gene expression and fluorescence imaging, Cell 159 (3) (2014) 635–646.
[65] I. Horvathova, F. Voigt, A.V. Kotrys, Y. Zhan, C.G. Artus-Revel, J. Eglinger, et al., The dynamics of mRNA turnover revealed by single-molecule imaging in single cells, Mol. Cell 68 (3) (2017), 615-625.e9.
[66] D. Mateju, B. Eichenberger, F. Voigt, J. Eglinger, G. Roth, J.A. Chao, Single-molecule imaging reveals translation of mRNAs localized to stress granules, Cell 183 (7) (2020), 1801-1812.e13.
[67] Livingston N.M., Kwon J., Valera O., Saba J.A., Sinha N.K., Reddy P., et al. Bursting Translation on Single mRNAs in Live Cells. bioRxiv. 2022:2022.11.07.515520.

MOLECULAR BIOLOGY

Distinct roles of LARP1 and 4EBP1/2 in regulating translation and stability of 5′TOP mRNAs

Tobias Hochstoeger[1,2], Panagiotis Papasaikas[1], Ewa Piskadlo[1], Jeffrey A. Chao[1]*

A central mechanism of mTOR complex 1 (mTORC1) signaling is the coordinated translation of ribosomal protein and translation factor mRNAs mediated by the 5′-terminal oligopyrimidine motif (5′TOP). Recently, La-related protein 1 (LARP1) was proposed to be the specific regulator of 5′TOP mRNA translation downstream of mTORC1, while eIF4E-binding proteins (4EBP1/2) were suggested to have a general role in translational repression of all transcripts. Here, we use single-molecule translation site imaging of 5′TOP and canonical mRNAs to study the translation of single mRNAs in living cells. Our data reveal that 4EBP1/2 has a dominant role in repression of translation of both 5′TOP and canonical mRNAs during pharmacological inhibition of mTOR. In contrast, we find that LARP1 selectively protects 5′TOP mRNAs from degradation in a transcriptome-wide analysis of mRNA half-lives. Our results clarify the roles of 4EBP1/2 and LARP1 in regulating 5′TOP mRNAs and provide a framework to further study how these factors control cell growth during development and disease.

INTRODUCTION

For cellular homeostasis, ribosome biogenesis needs to be tightly coupled to nutrient availability. In eukaryotic cells, mechanistic target of rapamycin complex 1 (mTORC1) is the central signaling hub that integrates nutrient cues to match cell growth by stimulating or inhibiting ribosome biogenesis (*1*, *2*). When nutrients are available, active mTORC1 promotes translation by the phosphorylation of key substrates such as ribosomal S6 kinases (S6K1/2) and eukaryotic translation initiation factor 4E-binding proteins (4EBP1/2) that stimulate eukaryotic initiation factor 4F (eIF4F) assembly and translation. When nutrients are limited, mTORC1 substrates are dephosphorylated, allowing 4EBP1/2 to bind and sequester the cap-binding eukaryotic translation initiation factor 4E (eIF4E), thereby inhibiting mRNA translation initiation. In addition, the La-related protein 1 (LARP1) has recently been described as a direct mTORC1 substrate and translational regulator (*3*–*7*). While mTORC1-dependent translation regulation acts on all mRNAs via multiple routes, it exerts a much more rapid and pronounced effect on ribosomal protein and translation factor mRNAs (~100 mRNAs) that carry a 5′-terminal oligopyrimidine motif (5′TOP, 4 to 15 pyrimidines) directly adjacent to the 5′ cap (*8*).

While it has been well established that the 5′TOP motif is both essential and sufficient for rapid mTORC1-mediated translational regulation (*9*, *10*), the underlying molecular mechanism has been challenging to resolve (*11*). Both 4EBP1/2 and LARP1 have been found to contribute to 5′TOP translational inhibition, as loss of either factor partially relieved 5′TOP translational repression in cells acutely treated with the mTOR inhibitor Torin1 (*4*, *5*, *12*–*14*). Although binding of 4EBP1/2 to eIF4E reduces cap-dependent translation of all transcripts, eIF4E may have lower affinity for 5′TOP mRNAs, which could make them more sensitive to mTORC1 inhibition (*15*, *16*). Recently, cocrystal structures of LARP1 bound to both the 5′ cap and the first five nucleotides of a 5′TOP oligo suggested that LARP1 could specifically repress 5′TOP mRNAs upon mTORC1 inhibition, leading to a model in which dephosphorylated LARP1 specifically binds the 5′ end of 5′TOP mRNAs to prevent assembly of the eIF4F complex (*17*).

An additional layer of ribosome biogenesis control is the pool of 5′TOP mRNAs available for translation, which are among the most highly expressed and stable transcripts in eukaryotic cells (*18*, *19*). LARP1 has been found to associate with poly(A)-binding protein cytoplasmic 1 (PABPC1) and inhibit deadenylation of mRNA transcripts (*20*–*23*). It is, however, unclear how LARP1 is recruited to the mRNAs it stabilizes, the importance of the 5′TOP motif for target selection, and the relevance of mTORC1 activity in this process. Crosslinking studies have found LARP1 associates with thousands of mRNAs including 5′TOP mRNAs, and a subset of these transcripts have increased binding upon mTORC1 inhibition (*7*, *24*, *25*). In contrast, polyA tail sequencing in mTOR active cells has found LARP1 to inhibit mRNA deadenylation globally but that 5′TOP transcripts were among the most strongly affected transcripts upon LARP1 depletion (*26*).

In this study, we sought to clarify the roles of LARP1 and 4EBP1/2 in regulating the translation and stability of 5′TOP mRNAs. Direct measurements of translation of 5′TOP and non-5′TOP (canonical) mRNAs using single-molecule SunTag imaging revealed a dominant role of 4EBP1/2 in mediating 5′TOP translational repression. In contrast, we find a highly selective role of LARP1 in protecting 5′TOP mRNAs from degradation by measuring transcriptome-wide changes in mRNA half-lives using metabolic mRNA labeling (SLAM-seq). Our study provides insights into the distinct roles of LARP1 and 4EBP1/2 in mediating 5′TOP regulation and a framework for further investigations into the mechanisms by which these factors regulate cell growth under normal physiological conditions and disease.

RESULTS

Single-molecule imaging of translation during mTOR inhibition

To study the regulation of translation during mTOR inhibition, we engineered a HeLa cell line that expresses fluorescent proteins for single-molecule imaging of mRNA [nuclear localized MS2 coat protein (MCP)-Halo] and translation [single-chain-variable fragment

[1]Friedrich Miescher Institute for Biomedical Research, 4058 Basel, Switzerland. [2]University of Basel, 4003 Basel, Switzerland.
*Corresponding author. Email: jeffrey.chao@fmi.ch

(scFv)-GFP], together with the reverse tetracycline-controlled transactivator to enable induction of reporter mRNAs (*27*). Into this cell line, we integrated two different constructs into a single genomic locus under the control of a doxycycline-inducible promoter. The reporter mRNAs were identical except for their 5′ untranslated region (5′UTR), where one contains the full-length 60*S* ribosomal protein L32 (RPL32) 5′UTR that begins with a 5′TOP motif, and the other has a canonical 5′UTR that does not contain a 5′TOP sequence. The coding sequence encodes 24 GCN4 epitope tags for translation site imaging [SunTag; (*28*)] followed by Renilla luciferase for bulk measurements of translation and the FK506 binding protein 1A (FKBP1A)–derived destabilization domain to reduce the accumulation of mature proteins (*29*). In addition, the 3′UTR contains 24 MS2 stem loops for mRNA imaging (Fig. 1A). The 5′-end of both reporter mRNAs

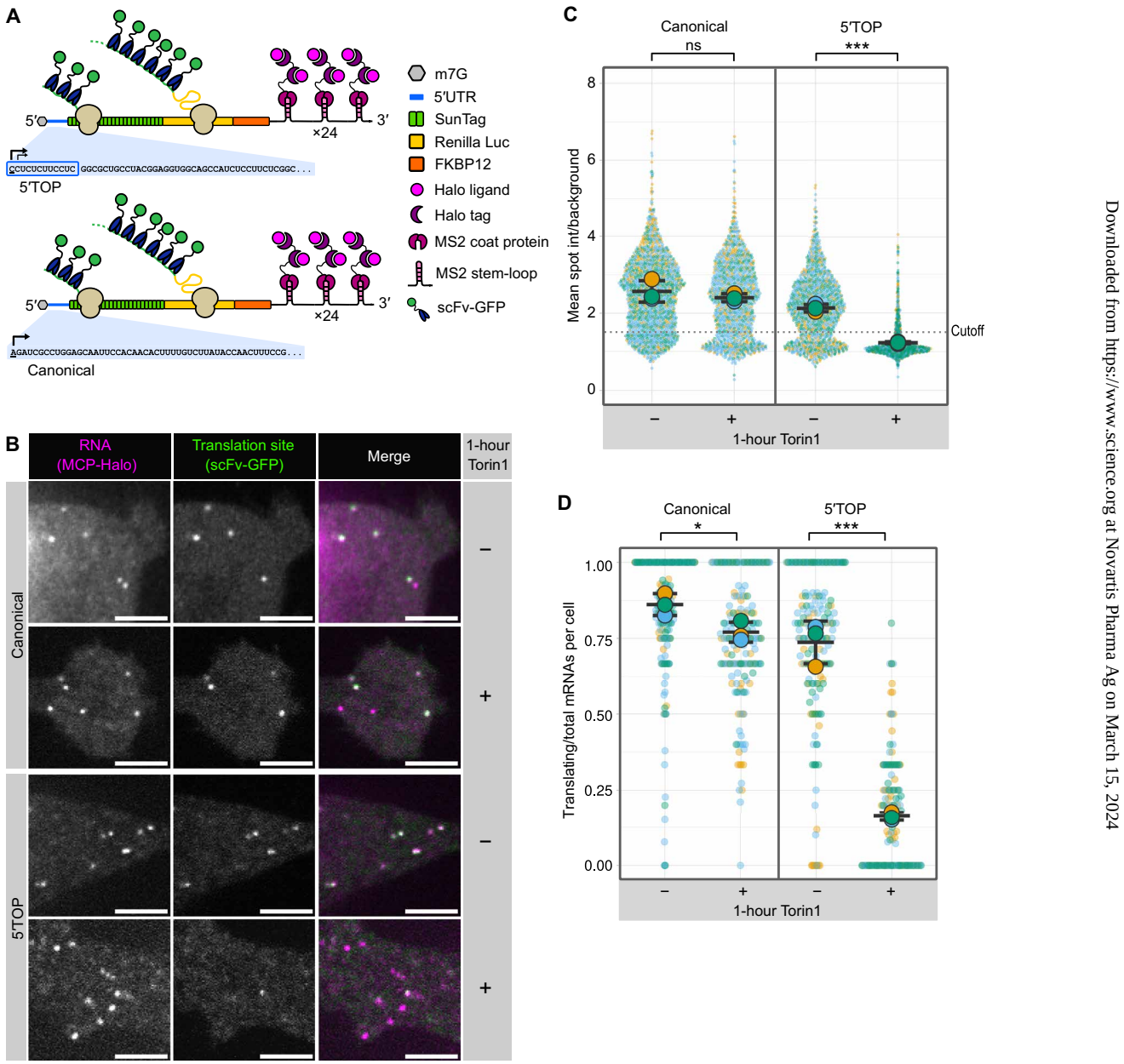

Fig. 1. Single-molecule imaging recapitulates 5′TOP translational repression. (**A**) Schematic representation of reporter mRNAs for single-molecule imaging of translation. The 5′TOP reporter contains the full-length RPL32 5′UTR, whereas the canonical reporter has a control 5′UTR of similar length. Black arrows indicate transcription start sites. (**B**) Representative images of canonical and 5′TOP reporter mRNAs (MCP-Halo foci, magenta) undergoing translation (scFv-GFP foci, green) in the absence or presence of mTOR inhibitor Torin 1 (250 nM, 1 hour). Scale bars, 5 μm. (**C**) Translation site intensities of canonical and 5′TOP reporter mRNAs quantified in absence or presence of Torin 1 (250 nM, 1 hour). SunTag intensities are plotted for all mRNAs (colored circles) overlaid with the mean ± SD (≥1089 mRNAs per condition, $n = 3$). (**D**) Fraction of mRNAs undergoing translation quantified per cell for canonical and 5′TOP reporter in the absence or presence of Torin 1 (250 nM, 1 hour). Values are plotted for each cell (colored circles) overlaid with the mean ± SD (≥162 cells per condition, $n = 3$). For statistics, unpaired *t* tests were performed, with statistical significance claimed when $P < 0.05$ (ns, not significant; *$P < 0.05$; ***$P < 0.001$).

was sequenced to determine the transcription start sites. All 5′TOP transcripts contained a 5′TOP motif and the canonical transcripts initiated with AGA, which is similar to the most common transcription start site (fig. S1) (*30*). To inhibit mTOR, we used the adenosine triphosphate (ATP)–competitive inhibitor Torin1, which has been widely used to study the translation of 5′TOP mRNAs. For both the 5′TOP and canonical mRNA reporter cell lines, Torin1 treatment for 1 hour resulted in inhibition of mTORC1 as seen by 4EBP1 dephosphorylation, consistent with previous results (fig. S2) (*24*, *31*).

To observe the effect of mTORC1 inhibition on translation, we induced expression of the reporter mRNAs in both cell lines and imaged them in either the presence or absence of Torin1. Treatment with Torin1 was found to strongly repress translation of most 5′TOP transcripts as seen by the disappearance of scFv-GFP spots that colocalized with mRNA spots, whereas the canonical mRNAs were largely unaffected (Fig. 1B). For quantification of single mRNAs and their translation, we used a high-throughput image analysis pipeline that tracks individual mRNAs and measures the corresponding SunTag intensities. mRNA trajectories were determined using single-particle tracking of MCP-Halo spots, and scFv-GFP intensities at those same coordinates were quantified for each mRNA as background-corrected mean spot intensity (SunTag intensity). Using this analysis pipeline, we quantified the translation of >1000 mRNAs for both the 5′TOP and canonical mRNA cell lines (Fig. 1C), which revealed a broad distribution of SunTag intensities for both types of transcripts indicating a heterogeneity of ribosomes engaged in translation of individual transcripts (*27*, *28*). The average SunTag intensity for the 5′TOP mRNAs was slightly lower compared to the canonical mRNAs indicating fewer ribosomes engaged in translation when mTOR is active (Fig. 1C). The mean SunTag intensity for the 5′TOP mRNAs decreased markedly upon Torin1 treatment, whereas the mean SunTag intensity of the canonical mRNAs decreased only slightly.

While changes in SunTag intensity indicate differences in ribosome number, translation site imaging can also be used to quantify the fraction of transcripts actively translating within a cell. Puromycin treatment, which inhibits translation due to premature termination, was used to measure SunTag spot intensities in the absence of translation to calibrate a threshold for identifying translating mRNAs (>1.5-fold over background; fig. S3). Quantifying translation as the fraction of translating mRNAs per cell revealed slightly fewer translating 5′TOP mRNAs (mean: 74%) compared to the canonical mRNAs (mean: 86%) when mTOR is active (Fig. 1D). Upon 1-hour Torin1 treatment, the fraction of translating 5′TOP mRNAs per cell decreased drastically (mean: 16%), although many cells retained a minor fraction of translating 5′TOP mRNAs. In contrast, the fraction of translating canonical mRNAs decreased only slightly upon Torin1 treatment (mean: 77%). To determine whether the remaining fraction of translating 5′TOP mRNAs after 1-hour Torin1 treatment represented stalled ribosomes, Torin1-treated cells were cotreated with harringtonine, which stalls ribosome at the start codon and allows elongating ribosomes to run-off. Addition of harringtonine abolished the remaining translation sites in the Torin1-treated 5′TOP cell line within 10 min (fig. S4), demonstrating that the low number of 5′TOP mRNAs that colocalize with SunTag signal are still actively translating.

To verify our findings with other mTOR inhibitors, we repeated the imaging of canonical and 5′TOP mRNAs with the allosteric mTOR inhibitor Rapamycin (*32*) and the ATP-competitive mTOR inhibitors PP242 and TAK228 (*33*, *34*). While PP242 and TAK228 treatment closely mirror the response seen for Torin1 treatment, Rapamycin treatment did not significantly alter the translation of either canonical or 5′TOP mRNAs (fig. S5). Rapamycin insensitivity has been described for a number of cell lines including HeLa (*35*), and, in agreement with previous studies (*31*, *36*), we find that Rapamycin selectively inhibits S6K1 phosphorylation, while levels of phosphorylated 4EBP1 remain high (fig. S6). Together, our data capture both inter- and intracellular variability in the translation of canonical and 5′TOP mRNAs in the presence and absence of mTOR inhibitors, providing direct translation measurements independent of effects arising from transcriptional regulation or mRNA stability.

LARP1 KO partially rescues translation of 5′TOP mRNAs during Torin1 treatment

Recently, LARP1 has been found to specifically bind the 5′TOP motif in an mTOR-dependent manner to regulate translation (*3*, *17*, *24*). To further investigate the role of LARP1 in translational repression of 5′TOP mRNAs during mTOR inhibition, we generated LARP1 CRISPR-Cas9 knockouts (KOs) in the 5′TOP and canonical mRNA cell lines. Genomic DNA sequencing confirmed frameshift mutations in all alleles of *LARP1* exon 4 that are upstream of any domain of known function (amino acids 205 to 240) (fig. S7, A and B). Loss of LARP1 protein in the KO cell lines was confirmed by Western blot analysis using two LARP1 antibodies targeting either the N- or C-terminal regions, which did not detect alternative LARP1 isoforms (fig. S7C). Loss of LARP1 did not disrupt the regulation of other mTORC1 targets, as seen by dephosphorylation of 4EBP1, S6K1, and RPS6 upon 1-hour Torin1 treatment (fig. S7D). Consistent with earlier reports in human embryonic kidney (HEK) cells, deletion of LARP1 in HeLa cells resulted in decreased cell proliferation (*4*, *5*).

Following the validation of the LARP1 KO cell lines, we quantified the translation of 5′TOP and canonical mRNAs (>600 mRNAs per condition) in the absence of LARP1 (fig. S8A). Analysis of SunTag intensities of the canonical and 5′TOP mRNAs revealed similar translation levels in the LARP1 KO compared to wild type (WT), indicating that LARP1 does not regulate 5′TOP mRNA translation in cells when mTOR is active. Upon 1-hour Torin1 treatment, canonical mRNAs decreased slightly in mean SunTag intensity, whereas the 5′TOP mRNAs decreased more strongly (Fig. 2A). Calculating the fraction of translating mRNAs per cell revealed that the canonical mRNAs show a mild response to Torin1 in the absence of LARP1 (mean untreated: 87%, mean 1-hour Torin1: 75%; Fig. 2B), mirroring the response observed for the canonical mRNAs in LARP1 WT cells. The 5′TOP mRNAs in LARP1 KO cells displayed a partial rescue of translation upon Torin1 treatment (mean untreated: 79%, mean 1-hour Torin1: 41%) compared to LARP1 WT cells (mean 1-hour Torin1: 16%). The incomplete rescue of 5′TOP mRNA translation in the absence of LARP1 suggested the existence of additional trans-acting factors in mediating 5′TOP translational repression.

One possible trans-acting factor that could repress 5′TOP mRNAs in the absence of LARP1 is the homolog LARP1B (also called LARP2), which shares the DM15 domain that binds the 5′TOP motif, although it is lowly expressed in HeLa cells. To test this possibility, we used CRISPR-Cas9 to generate KOs of LARP1B in the LARP1 KO background (fig. S9A). Genomic DNA sequencing of the edited alleles identified frameshift mutations in all alleles of *LARP1B* exon 4, and polymerase chain reaction (PCR) confirmed loss of WT *LARP1B* mRNA (fig. S9, B and C). Western blot analysis confirmed unperturbed mTORC1 signaling in the LARP1/1B KO cells, as seen by

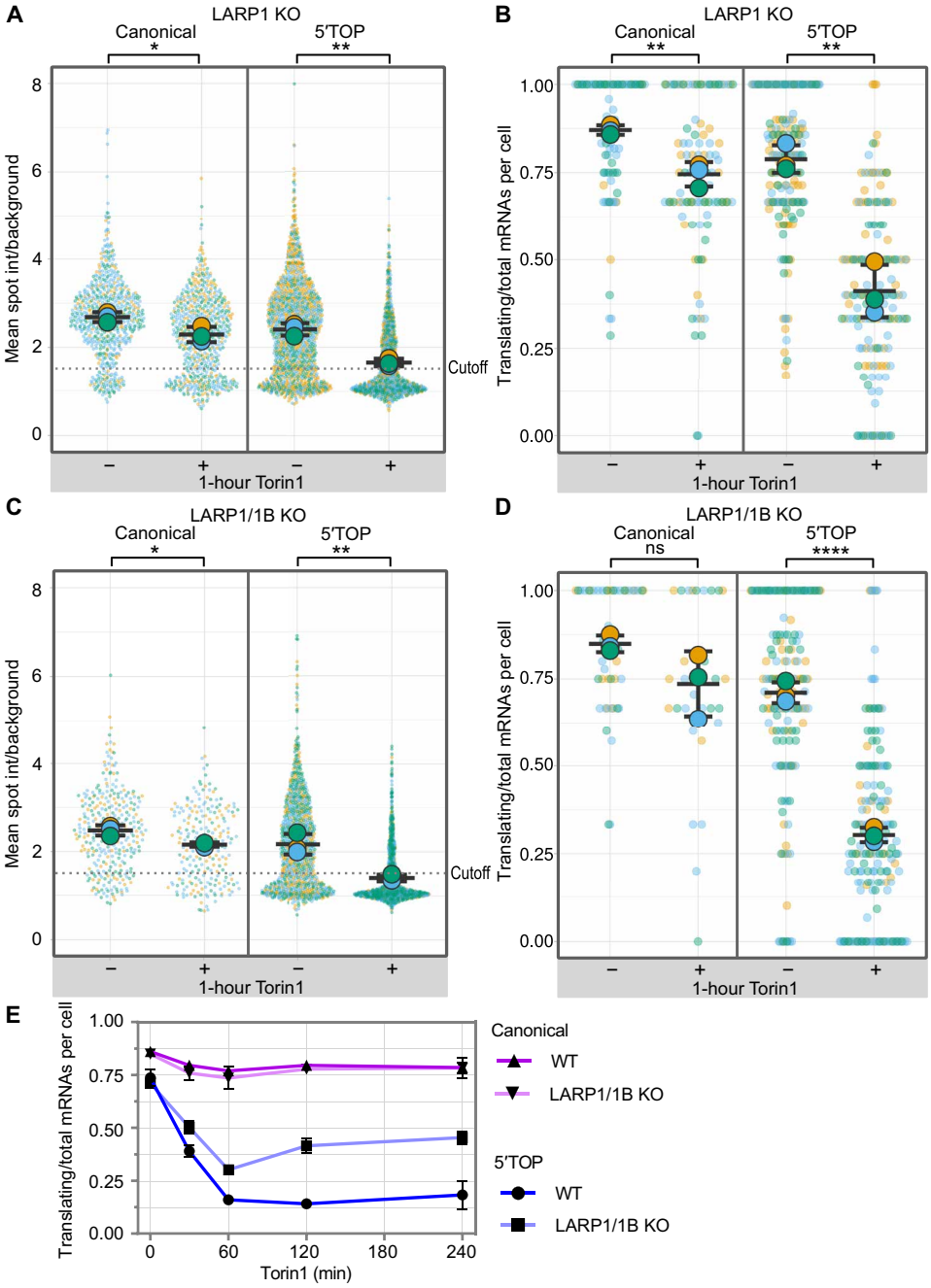

Fig. 2. Loss of LARP1 partially alleviates 5′TOP translational repression during Torin1 treatment. (**A**) Quantification of translation site intensities in LARP1 KO cells ± Torin1 (250 nM, 1 hour). SunTag intensities are plotted for all mRNAs overlaid with the mean ± SD (≥652 mRNAs per condition, $n = 3$). (**B**) Fraction of mRNAs undergoing translation quantified per cell in LARP1 KO cells ± Torin1 (250 nM, 1 hour). Values are plotted for each cell (colored circles) overlaid with the mean ± SD (≥91 cells per condition, $n = 3$). (**C**) Quantification of translation site intensities in LARP1/1B KO cells ± Torin1 (250 nM, 1 hour). SunTag intensities are plotted for all mRNAs (colored circles) overlaid with the mean ± SD (≥218 mRNAs per condition, $n = 3$). (**D**) Fraction of mRNAs undergoing translation quantified per cell in LARP1/1B KO cells ± Torin1 (250 nM, 1 hour). Values are plotted for each cell (colored circles) overlaid with the mean ± SD (≥30 cells per condition, $n = 3$). For statistics, unpaired *t* tests were performed, with statistical significance claimed when $P < 0.05$ (*$P < 0.05$, **$P < 0.01$, ****$P < 0.0001$). (**E**) Time course of fraction of translating mRNAs per cell for canonical and 5′TOP reporter cell lines in the presence (WT) or absence of LARP1/1B (KO). Cells were treated with 0-, 30-, 60-, 120-, and 240-min Torin1. Values are plotted as the mean ± SEM (≥30 cells per condition, $n = 3$).

dephosphorylation of 4EBP1, S6K1, and RPS6 upon 1-hour Torin1 treatment (fig. S9D).

Following the validation of the LARP1/1B KO cell lines, we quantified the translation of 5′TOP and canonical mRNAs (>200 mRNAs per condition) in the absence of LARP1/1B (fig. S8B). Both the distribution of SunTag intensities (Fig. 2C) and the fraction of translating canonical and 5′TOP mRNAs per cell (Fig. 2D) responded similarly to Torin1 treatment (1 hour) as obtained for LARP1 KO cells, suggesting that LARP1B does not affect 5′TOP translational regulation. These results are consistent with an earlier study in HEK cells, which also found that translational repression of endogenous 5′TOP transcripts could not be rescued further by combinatory deletion of LARP1/1B (*37*), arguing against functional redundancy of LARP1 and LARP1B.

While we did not observe a rescue of 5′TOP translation when cells were treated with Torin1 for 1 hour, we could not exclude the possibility that the effect of loss of LARP1/1B might be more pronounced at other time points. To characterize the kinetics of Torin1-mediated translational inhibition, we performed SunTag imaging of the canonical and 5′TOP cell lines at additional time points (30 min, 2 hours, and 4 hours; Fig. 2E). For both WT and LARP1/1B KO cells, the canonical mRNAs showed a gradual decrease in translation during the first hour of Torin1 treatment that remained low at later time points. To test whether prolonged mTOR inhibition is required to repress canonical mRNA translation, we quantified translation of canonical mRNAs in WT cells treated with Torin1 for 24 hours. The majority of canonical mRNAs remained translating at this longer time point (fig. S10). 5′TOP mRNAs in WT cells decreased in translation within 1 hour of Torin1 to a minor fraction of translating mRNAs (30-min Torin1: 39%, 1-hour Torin1: 16%) and remained at this level at the 2-hour (14%) and 4-hour (19%) time points (Fig. 2E). In LARP1/1B KO cells, translation of 5′TOP mRNAs also decreased with no change in the timing of repression but a decrease in its extent (30-min Torin1: 50%, 1-hour Torin1: 30%); however, at the 2-hour (42%) and 4-hour (46%) time points, we observed a slight increase in translation. These results suggested that while LARP1 may contribute to translational repression of 5′TOP mRNAs, it is not the dominant regulatory factor during mTOR inhibition.

4EBP1/2 knockdown rescues translation of 5′TOP mRNAs during Torin1 treatment

4EBP1/2 are thought to generally repress translation during mTORC1 inhibition but have also been previously implicated in specifically affecting 5′TOP mRNAs (*12*). Using lentiviral infection, stable short hairpin RNA (shRNA)–mediated knockdown (KD) cell lines were generated in the WT and LARP1/1B KD background for both 5′TOP and canonical mRNA cell lines. Western blot analysis confirmed the depletion of 4EBP1/2 levels in all four cell lines (fig. S11, A and B). Furthermore, the dephosphorylation of RPS6 and residual 4EBP1 upon 1-hour Torin1 indicated that mTORC1 signaling was unperturbed in the 4EBP1/2 KD cell lines (fig. S11, C and D).

Having validated the 4EBP1/2 KD cell lines, we measured the translation of canonical and 5′TOP mRNAs in the absence of 4EBP1/2 (fig. S12). In untreated cells, the reduction of 4EBP1/2 resulted in increased SunTag intensities for both canonical and 5′TOP mRNAs in cell lines with WT LARP1 (Fig. 3A, >1000 mRNAs per condition) and LARP1/1B KO (Fig. 3C, >700 mRNAs per condition) compared to cells with WT levels of 4EBP1/2 (Fig. 1C). This suggested that when mTOR is active, 4EBP1/2 can still weakly repress translation initiation presumably through fluctuations in mTOR signaling during cell growth. Unexpectedly, the SunTag intensities of both canonical and 5′TOP mRNAs were not reduced upon 1-hour Torin1 treatment in 4EBP1/2 KD cell lines with WT LARP1 (Fig. 3A) or LARP1/1B KO (Fig. 3C). Analyzing the fraction of translating canonical mRNAs revealed no change in translation upon Torin1 treatment for cells with WT LARP1 (Fig. 3B) and LARP1/1B KO (Fig. 3D), in contrast to the previously observed mild decrease in translation of canonical mRNAs upon 1-hour Torin1 (Fig. 1D). The fraction of translating 5′TOP mRNAs was not significantly reduced by Torin1 treatment in 4EBP1/2 KD cell lines with WT LARP1 (Fig. 3B; untreated: 77%, treated: 70%) or LARP1/1B KO (Fig. 3D; untreated: 79%, treated: 77%), indicating a full rescue of translation compared to the previous partial rescue observed in LARP1 KO cells. To exclude the possibility that translational repression is delayed in the absence of 4EBP1/2, we investigated the kinetics of mTOR inhibition in the 4EBP1/2 KD cell lines (Fig. 3E), which revealed that canonical and 5′TOP mRNAs remain similarly insensitive to Torin1 treatment at prolonged Torin1 treatment (2 and 4 hours). These experiments indicate that despite the difference in magnitude of translational repression during Torin1 treatment, 4EBP1/2 is responsible for the weak inhibition of canonical mRNAs and the stronger inhibition of 5′TOP mRNAs. Our data support a model where 5′TOP mRNAs are intrinsically more sensitive to 4EBP1/2-mediated translational regulation, which results in a minor difference in translation when mTOR is active and a pronounced difference in translation when mTOR is inhibited.

Alternatively, our data could potentially be explained by the presence of additional cis-acting sequence elements within the RPL32 5′UTR of our 5′TOP mRNA reporter that were absent in the 5′UTR of the canonical mRNAs. The RPL32 5′UTR is 50 nucleotides in length and contains the 5′TOP motif (positions +1 to +11) as well as a pyrimidine-rich translational element (PRTE) at positions +38 to +47 (fig. S13A). A PRTE is found in the 5′UTRs of the majority of 5′TOP mRNAs and has been proposed to also be an alternative binding site for LARP1, although its contribution to translational regulation during mTOR inhibition remains largely unknown (*7*). To further dissect the contribution of the 5′TOP and PRTE motifs, we generated two additional live-cell imaging cell lines carrying a single-copy genomic integration of modified RPL32 5′UTR reporters, one where only the 5′TOP motif was mutated (Δ5′TOP) and one where the 5′TOP and the PRTE motifs were mutated (Δ5′TOP/PRTE; fig. S13A). We confirmed the sequence of the 5′UTRs in the Δ5′TOP and Δ5′TOP/PRTE mRNAs by 5′-end sequencing and imaged their translation in the absence or presence of Torin1. We found that both the Δ5′TOP and Δ5′TOP/PRTE mRNAs responded only weakly to Torin1 treatment, with a similar decrease in the fraction of translating mRNAs per cell as observed for the canonical mRNAs (fig. S13, B, C, and H), which is consistent with previous reports that the 5′TOP motif is both necessary and sufficient for the selective translational repression upon mTOR inhibition (*9*, *10*).

Next, we generated both CRISPR-Cas9 LARP1 KO and shRNA-mediated 4EBP1/2 KD cell lines carrying the Δ5′TOP mRNAs and validated the loss of the respective protein and unperturbed mTORC1 signaling by Western blot (fig. S14, A and B). Similar to our previous experiments with canonical mRNAs (Figs. 2B and 3B), we found that loss of LARP1 did not alleviate the mild translational repression of Δ5′TOP mRNAs upon Torin1 treatment (fig. S13, D and E) and

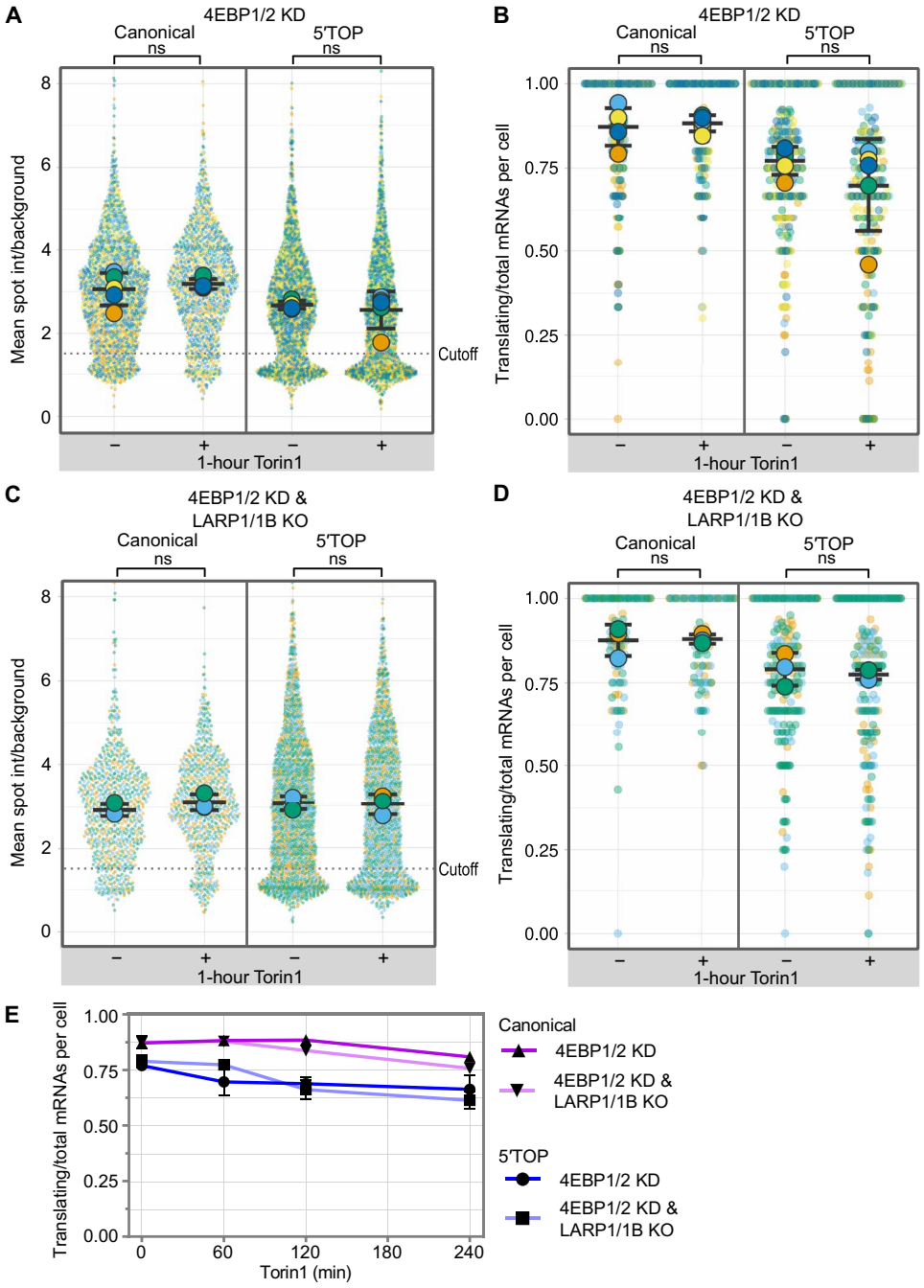

Fig. 3. Loss of 4EBP1/2 is sufficient to alleviate 5′TOP translational repression during Torin1 treatment. (**A**) Quantification of translation site intensities of reporter mRNAs in 4EBP1/2 KD cells ± Torin1 (250 nM, 1 hour). SunTag intensites are plotted for all mRNAs (colored circles) overlaid with the mean ± SD (≥1344 mRNAs per condition, $n = 5$). (**B**) Fraction of mRNAs undergoing translation quantified per cell for reporter mRNAs in 4EBP1/2 KD cells ± Torin1 (250 nM, 1 hour). Values are plotted for each cell (colored circles) overlaid with the mean ± SD (≥204 cells per condition, $n = 5$). (**C**) Quantification of translation site intensities of reporter mRNAs in 4EBP1/2 KD_LARP1/1B KO cells ±1 hour Torin1 (250 nM). SunTag intensities are plotted for all mRNAs overlaid with the mean ± SD (≥783 mRNAs per condition, $n = 3$). (**D**) Fraction of mRNAs undergoing translation quantified per cell of reporter mRNAs in 4EBP1/2 KD_LARP1/1B KO cells ± Torin1 (250 nM, 1 hour). Values are plotted for each cell (colored circles) overlaid with the mean ± SD (≥97 cells per condition, $n = 3$). For statistics, unpaired *t* tests were performed, with statistical significance claimed when $P < 0.05$. (**E**) Time course of fraction of translating mRNAs per cell for canonical and 5′TOP reporters in 4EBP1/2 KD cells with WT LARP1 or with LARP1/1B KO. Cells were treated with 0-, 30-, 60-, 120-, and 240-min Torin1. Values are plotted as the mean ± SEM (≥97 cells per condition, $n = 3$ to 5).

that depletion of 4EBP1/2 fully alleviated Torin1-mediated translational repression (fig. S13, F to H).

LARP1 KO results in global decreased mRNA stability of 5′TOP mRNAs

In addition to its role in 5′TOP translational repression, LARP1 has been reported to protect mRNAs from degradation (*20*, *21*, *26*, *38*, *39*). It is now unclear whether this protective role of LARP1 is restricted to 5′TOP mRNAs, TOP-like mRNAs, or affects all mRNAs (*37*). To study the effect of LARP1 and 4EBP1/2 loss on global gene expression in growing cells when mTOR is active, we extracted total RNA from our cell lines and performed RNA sequencing (RNA-seq). The canonical and 5′TOP mRNA cell lines of the same genotype were sequenced together as biological replicates since expression of different reporter mRNAs should not have a global effect on gene expression and combining the independently generated cell lines reduces potential off-target effects caused by either CRISPR KO or shRNA KD.

To determine the effect of LARP1 loss on gene expression, we compared the transcriptome of LARP1 KO and WT cells (12,403 transcripts, counts per million (CPM) > 1, pseudogenes excluded). As expected, *LARP1* transcript levels were down-regulated in the KO cell lines to 30% of WT levels (table S1). Volcano plot analysis of the transcriptome changes of KO versus WT cell lines (biological replicates: $n = 2$ for LARP1 WT, $n = 8$ for LARP1 KO) revealed that the most significantly affected mRNAs are endogenous 5′TOP mRNAs, which are almost all down-regulated in the LARP1 KO cells (Fig. 4A, blue circles). Analyzing all known 5′TOP mRNAs (table S2), 70 of 94 5′TOPs are found to be significantly down-regulated [$\log_2$ fold change (FC) ≤ -0.5, $-\log_{10} P$ value ≥ 5], as well as 85 significantly down-regulated non-5′TOP RNAs and 40 significantly up-regulated non-5′TOP RNAs (orange circles). In contrast, previously identified TOP-like mRNAs, which were predicted to be translationally regulated by LARP1 based on sequence similarity (*37*), were mostly unaffected in their expression.

To determine whether depletion of 4EBP1/2 also affected the levels of 5′TOP transcripts, we compared the transcriptome of 4EBP1/2 KD cells to WT cells (13,832 transcripts, CPM > 1, pseudogenes excluded). Consistent with shRNA KD of 4EBP1/2, we found the levels of these two transcripts to be reduced by 91% (*4EBP1*) and 71% (*4EBP2*) and that *LARP1* expression was unaltered in both cell lines. A small number of transcripts showed significantly altered expression; however, these do not include known 5′TOP mRNAs (65 transcripts; Fig. 4B, orange circles, absolute $\log_2$ FC ≥ 0.5, $-\log 10$ *P* value ≥ 5, table S3). In addition, the altered mRNAs did not match mRNAs described to be sensitive to eIF4E levels in mice (*40*). In contrast to the dominant role of 4EBP1/2 in regulating translation during mTOR inhibition, these results indicate that LARP1 regulates levels of 5′TOP transcripts when mTOR is active (Fig. 4C). To validate our RNA-seq results with an orthogonal approach, we performed single-molecule fluorescence in situ hybridization (smFISH) on three endogenous 5′TOP transcripts (*RPL5*, *RPL11*, and *RPL32*) and a non-5′TOP control (*MYC*), which confirmed the selective decrease of 5′TOP mRNAs in the LARP1 KO cell lines, with no change of 5′TOP mRNAs in the 4EBP1/2 KD cell lines (fig. S15).

The selective down-regulation of endogenous 5′TOP mRNAs we observed in the absence of LARP1 suggested that LARP1 specifically stabilizes 5′TOP mRNAs. To confirm that the changes in steady-state expression were caused by mRNA destabilization and were not due to changes in transcription, we performed global mRNA half-life measurements using metabolic 4-thiouridine labeling [SLAM-seq (*19*)]. WT and LARP1 KO cells of both canonical and 5′TOP cell lines were incubated with 4-thiouridine for 24 hours, followed by washout and harvesting of cells over a 12-hour time course. Half-lives of mRNAs were calculated using a single-exponential decay fit for 9837 transcripts ($R^2 \geq 0.75$, pseudogenes excluded, table S4). In agreement with previous measurements of mammalian mRNA half-lives, the global median half-life for both WT and LARP1 KO HeLa cell lines was ~4 hours (fig. S16A), indicating that loss of LARP1 does not globally destabilize all mRNAs. Correlation analyses showed a high correlation in mRNA half-lives among the four cell lines ($r = 0.90$ to 0.94), allowing us to compare the mRNA half-lives in WT versus LARP1 KO cell lines (Fig. 4D, $n = 2$). In agreement with our RNA-seq results, nearly all 94 5′TOP mRNAs detected in the SLAM-seq experiment have decreased mRNA stability, with 66 5′TOP mRNAs changing by >2-fold (Fig. 4D). A few 5′TOP mRNAs seem largely unaffected by LARP1 loss (including *PABPC1*), suggesting the potential involvement of additional stabilizing factors for these transcripts. Furthermore, the length of the 5′TOP motif or presence of a PRTE motif within the 5′UTR does not correlate with the change in mRNA half-lives (fig. S16B). Only six non-5′TOP mRNAs were found to be destabilized >2-fold, and three of these transcripts (*NOP53*, *LGALS1*, and *SLC25A6*) have annotated transcription start sites that contain 5′ TOP motifs, suggesting that they could be similarly regulated in HeLa cells. Taken as a whole, our results support a model of LARP1-mediated stabilization that is highly selective for 5′TOP mRNAs.

DISCUSSION

In this study, we used single-molecule imaging to study the regulation of translation of 5′TOP mRNAs upon mTOR inhibition that allowed us to directly quantify the effect of LARP1 and 4EBP1/2. By imaging and quantifying the translation status of individual mRNAs, we find that 4EBP1/2 plays a dominant role compared to LARP1 in mediating 5′TOP translational repression during short-term (30 min to 4 hours) pharmacological inhibition of mTOR in HeLa cells. Previously, studies that used genome-wide ribosome or polysome profiling determined that LARP1 and 4EBP1/2 regulate 5′TOP translation during mTOR inhibition (*3*, *4*, *12*, *13*, *37*, *41*, *42*); however, the magnitude of their respective contributions was difficult to measure due to the inherent limitations of these approaches. We believe that this highlights the power of single-molecule imaging methods for quantifying translation in living cells to determine the specific effects of translation factors.

While our results indicate that 4EBP1/2 is the critical factor in mediating 5′TOP translational repression, the underlying molecular mechanism is not entirely clear. Although we cannot exclude the possibility of a still unknown factor acting downstream of 4EBP1/2, we favor a model where the translation of 5′TOP mRNAs is more sensitive to active eIF4E levels. In vitro experiments have determined that eIF4E binds with ~3-fold weaker affinity to m^7GTP-capped oligonucleotides with a +1 cytosine than either purine, which is consistent with translation of 5′TOP mRNAs being slightly lower than a non-5′TOP mRNA when mTOR is active and then preferentially repressed when available eIF4E levels become extremely limited during mTOR inhibition (*16*, *43*, *44*). This model is also in line with previous work that found inducible overexpression of eIF4E to specifically up-regulate the translation of 5′TOP mRNAs (*45*), as

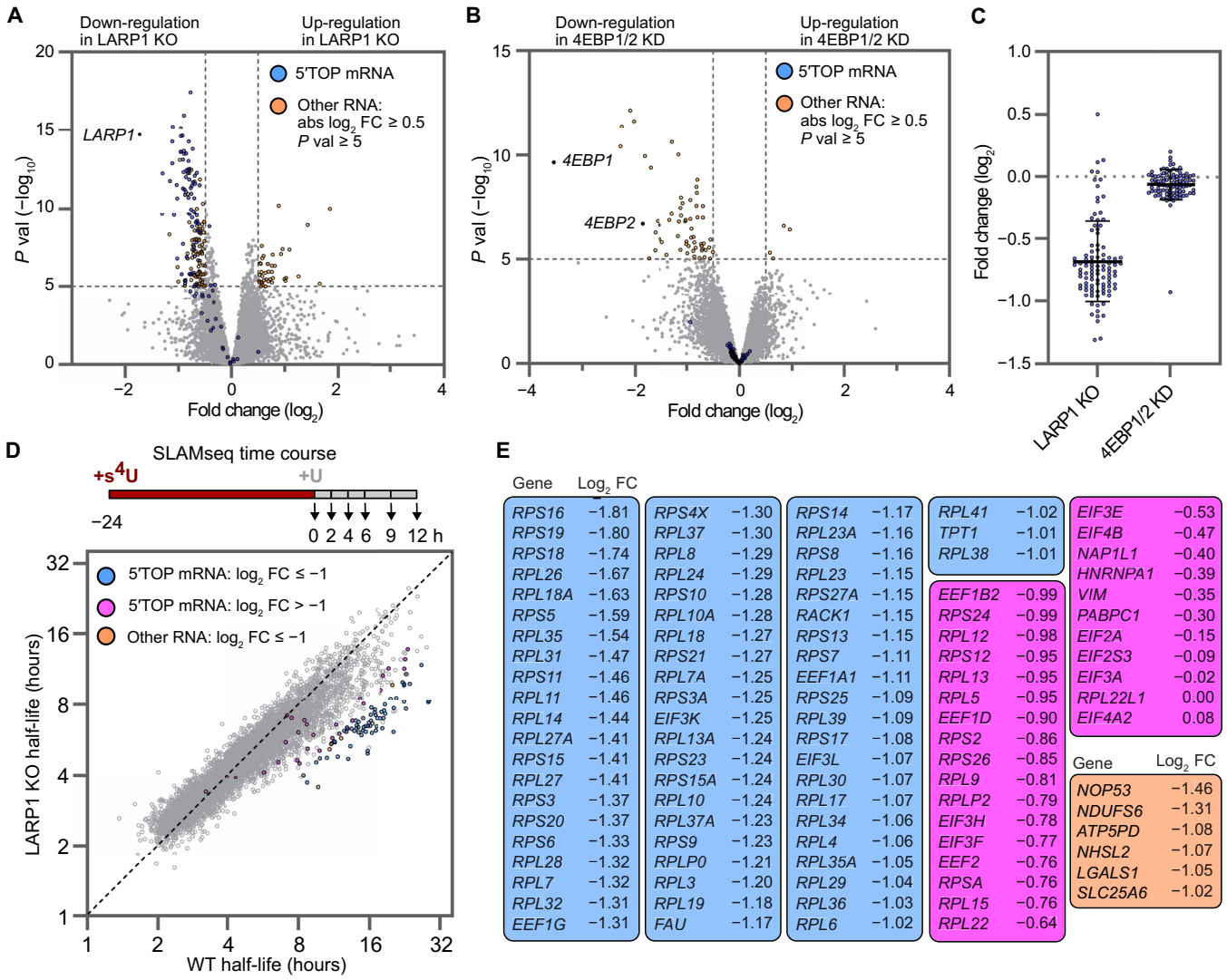

Fig. 4. Loss of LARP1 results in selective destabilization of 5′TOP mRNAs. (**A**) Differential gene expression analysis of LARP1 KO cells compared to WT cell lines. Significantly down- and up-regulated mRNAs are highlighted ($-\log_{10}$ *P* value ≥5 and absolute $\log_2$ FC ≥ 0.5) indicating all classical 5′TOP mRNAs (blue circles) as well as all significant non-5′TOP mRNAs (orange circles). For WT, data are the average of $n = 2$ biological replicates (canonical and 5′TOP reporter cell lines, averaged). For LARP1 KO, data are the average of $n = 8$ biological replicates (four KO clones of each reporter cell line). (**B**) Differential gene expression analysis of 4EBP1/2 KD reporter cell lines compared to WT reporter cell lines. Significantly down- and up-regulated mRNAs are highlighted (orange circles, $-\log_{10}$ *P* value ≥5 and absolute $\log_2$ FC ≥ 0.5). 5′TOP mRNAs (blue) are unaffected by 4EBP1/2 KD. Data shown for $n = 2$ biological replicates (canonical and 5′TOP reporter cell lines, averaged). (**C**) FC of 5′TOP mRNAs shown in (A) and (B). Mean FC ($\log_2$) in LARP1 KO cells = −0.68, in 4EBP1/2 KD cells = −0.06. (**D**) Correlation plot of mRNA half-lives in LARP1 KO compared to WT reporter cells. Experimental setup of global mRNA stability analysis using s^4U labeling (SLAM-seq) shown on top, with 24 hours s^4U labeling, washout, and time point collection. RNAs with significantly decreased stability ($\log_2$ FC ≤ −1) are highlighted for 5′TOP mRNAs (blue circles) and non-5′TOP mRNAs (orange circles), as well as nonsignificantly down-regulated 5′TOP mRNAs (magenta circles). (**E**) List of all RNAs highlighted in (D), ranked by $\log_2$ FC for 5′TOP mRNAs and non-5′TOP mRNAs separately.

well as recent work that showed that 5′TOP mRNAs are less sensitive to mTOR inhibition in acutely PABPC1-depleted cells where global mRNA levels are reduced (*46*).

In the x-ray structure of human eIF4E in complex with m^7pppA, the C-terminal tail of eIF4E adopts a conformation that enables Thr^{205} to form a hydrogen bond with the exocyclic amine of the adenine base (*47*). While the position of the eIF4E C-terminal tail has not been determined when bound to longer RNA sequences, phosphorylation of Ser^{209} is known to enhance translation, indicating that additional residues in this region may have functional roles (*48*). Alternatively, other canonical translation factors (e.g., eIF4G or 4EBP1/2) may also contribute to 5′TOP specificity through additional interactions (*49*, *50*).

While LARP1 may not be the key repressor in 5′TOP translational regulation, our data support a major role of LARP1 in mediating 5′TOP mRNA stability when mTOR is active. Previous work established a link between LARP1 and mRNA stability, with LARP1 binding both PABP and the polyA tail and inhibiting deadenylation (*20*–*22*, *24*, *38*, *39*, *51*, *52*). It has been unclear whether this protective role is restricted to 5′TOP mRNAs as binding to PABP/polyA is anticipated to not be selective, and crosslinking studies have found LARP1 complexed with thousands of mRNAs (*7*, *24*, *25*). Our results

show a highly selective destabilization of nearly all 5′TOP mRNAs upon loss of LARP1, with virtually all other mRNAs being largely unaffected. Similarly, a recent study found that loss of LARP1 resulted in rapid deadenylation of short polyA tails of all mRNAs, with 5′TOP mRNAs being more affected than other types of mRNAs (*26*). It is possible that differences in LARP1 depletion or measurement of mRNA stability or polyA-tail length may account for the differences in specificity for 5′TOP mRNAs between the studies.

Previous studies have focused on the role of LARP1 in protecting 5′TOP mRNAs in mTOR inhibited cells, as LARP1 has been shown to be recruited to 5′TOP mRNAs upon mTOR inhibition (*24*, *51*). Our findings raise the intriguing question of how LARP1 can be specifically recruited to 5′TOP mRNAs when mTOR is active. While it has been proposed that LARP1 can interact with its La motif with both the 5′TOP motif and PABP (*39*), it is not clear that this interaction is compatible with eIF4F binding and translation initiation. Recent structural work of the human 48*S* preinitiation complex suggests that there could be a "blind spot" of ~30 nucleotides adjacent to the cap that might allow LARP1 to bind the 5′TOP sequence without blocking initiation, although this model requires biochemical and structural characterization (*53*). We do not observe any correlation between change in mRNA half-lives with either length of 5′TOP motif or the presence of a PRTE in the 5′UTR, suggesting that the position of the pyrimidines directly adjacent to the cap is necessary for this effect on mRNA stability. LARP1 was shown to promote the localization of ribosomal mRNAs in a PRTE-dependent manner but did not require the stricter 5′ TOP motif, suggesting that LARP1's interaction with ribosomal mRNAs and its functional consequence could be context dependent (*54*).

While our translation site imaging experiments are limited to the characterization of four reporter mRNAs (canonical, 5′TOP, Δ5′TOP, and Δ5′TOP/PRTE), we have shown that the results are consistent with previous studies that characterized endogenous ribosomal protein mRNAs; however, single-molecule experiments in living cells allow more accurate quantification of the effect of loss of LARP1 and 4EBP1/2. We anticipate that similar results would be obtained with 5′TOP sequences derived from ribosomal protein mRNAs other than RPL32, although the magnitude of the difference in translational repression could be different if compared to another non-5′TOP transcript. In addition, the continued development of methodologies for imaging translation of single mRNAs for extended time periods and the interplay of translation with mRNA decay will enable the dynamics of mTOR regulation to be quantified in greater detail (*55*, *56*).

MATERIALS AND METHODS

Materials

All antibodies used in this study are listed in Table 1. All chemicals, plasmids, viruses, cell lines, single guide RNA (sgRNA), and shRNA used in this study are listed in table S5.

Cell culture

The HeLa-11ht cell lines expressing either RPL32 5′TOP SunTag or non-5′TOP canonical SunTag mRNAs used in this study were previously generated in the Chao lab (*27*), and the corresponding plasmids are available from Addgene (#119946 and #119945). The reporter cell lines were grown in 10% fetal calf serum–Dulbecco's modified Eagle's medium (FCS-DMEM) medium containing glucose (4.5 g/liter), penicillin and streptomycin (100 μg/ml), 4 mM L-glutamine, and 10% fetal bovine serum (FBS) at 37°C and 5% CO_2. To maintain the reverse tetracycline-controlled transactivator (rtTA2-M2) for inducible expression, the medium was supplemented with G418 (0.2 mg/ml). HEK293T cells used for lentivirus production were grown in 10% FCS-DMEM medium containing glucose (4.5 g/liter), penicillin and streptomycin (100 μg/ml), 4 mM L-glutamine, and 10% FBS at 37°C and 5% CO_2.

Validation of transcription start sites for 5′TOP and canonical SunTag transcripts

For mapping of transcription start sites, total RNA was converted into full-length adapter-ligated double-stranded cDNA using the TeloPrime Full-Length cDNA Amplification Kit V2 (Lexogen), which uses a cap-specific adapter selective for intact mRNAs. cDNA 5′-terminal sequences were amplified by PCR using a gene-specific primer and TeloPrime forward primer, cloned into the pCR-Blunt vector (Thermo Fisher Scientific), and sequenced.

Table 1. Antibodies. IgG, immunoglobulin G.

Primary antibodies	Provider	Catalog no.
LARP1	Bethyl Labs	A302-087A
LARP1	Cell Signaling Technology	70180
TUBA1B	Cell Signaling Technology	3873
MTOR	Cell Signaling Technology	2983
Pho-RPS6 (Ser$^{235/236}$)	Cell Signaling Technology	2211
Pho-RPS6 (Ser$^{235/236}$)	Cell Signaling Technology	4856
Pho-4EBP1 (Ser^{65})	Cell Signaling Technology	9451
4EBP1	Cell Signaling Technology	9452
4EBP2	Sigma-Aldrich	MABS1865
Pho-S6K1 (Thr^{389})	Cell Signaling Technology	9234
Secondary antibodies		
IRDye 680RD Goat anti-Mouse IgG	LI-COR	926-68070
IRDye 800CW Goat anti-Rabbit IgG	LI-COR	926-32211

CRISPR KO cell line generation

To generate LARP1 CRISPR KO clones, parental HeLa-11ht cell lines expressing the reporter mRNAs were transiently cotransfected with two Cas9 plasmids, each containing Cas9 and a sgRNA targeting a sequence within exon 4 of *LARP1*, enhancing efficiency of KO cell line generation (*57*, *58*). Transient transfections were performed following the manufacturer's instructions using Lipofectamine 2000 (Invitrogen) and Opti-MEM (Thermo Fisher Scientific). Two days after transient transfections, highly transfected cells were single-cell–sorted into 96-well plates for monoclonal selection (10% highest mCherry-positive cells, using Cas9-T2A-mCherry). Single clonal cell populations were screened for loss of LARP1 by immunostaining (Bethyl Labs, #A302-087A) in 96-well plates. For both 5′TOP and canonical SunTag cell lines, four KO clones each were verified by Western blot for loss of LARP1 protein expression.

To generate LARP1B CRISPR KO clones, the LARP1 KO reporter cell lines were similarly cotransfected with two Cas9 plasmids carrying two different sgRNAs targeting sequences within exon 4 of *LARP1B*. Following the same steps as described for generating LARP1 KO cell lines, clonal cell populations were screened by PCR for the presence of truncated *LARP1B* alleles and subsequently verified by genomic DNA sequencing and cDNA amplification.

shRNA stable KD cell lines

To generate 4EBP1/2 KD cells, two lentiviruses expressing different resistance genes were used that contained shRNA sequences from the RNAi Consortium public library that were previously described (*12*). The 4EBP1 shRNA lentivirus carrying puromycin resistance was purchased as lentiviral particles (Sigma-Aldrich). The 4EBP2 shRNA was cloned into the pLKO.1_BlastR lentiviral backbone (*59*). To produce 4EBP2 shRNA lentivirus, HEK293T cells were co-transfected with the 4EBP2 shRNA, the psPax2 envelope, and the vsv-G packaging plasmids using Fugene6 (Promega) according to the manufacturer's instructions. The supernatant containing viral particles was harvested daily for the next 4 days, centrifuged at 500*g* for 10 min, and filtered through a 0.45-μm filter to remove cell debris. The viral particles were concentrated by precipitation using the Lenti-X concentrator (Clontech) and resuspended in cell culture medium.

For infection of HeLa cells expressing the reporter mRNAs, 10,000 cells were seeded in 12-well dishes and co-infected the next day with 4EBP1 and 4EBP2 shRNA viruses in medium supplemented with polybrene (4 μg/ml; Merck). Cells were grown until confluency and reseeded into six-well dishes before addition of puromycin (1 μg/ml; InvivoGen) and blasticidin (5 μg/ml; InvivoGen). Uninfected HeLa-11ht cells were used to determine the minimal antibiotic concentrations that resulted in lethality within 2 to 5 days. Double-resistant cell lines with dual integration of 4EBP1/2 shRNAs were validated by Western blot for efficient stable KD of the targeted proteins.

Genomic DNA extraction

For genotyping of CRISPR-edited cell lines, cells were harvested by trypsinization, and the genomic DNA was extracted using the DNeasy kit (Qiagen) according to the manufacturer's instructions. Primers specific to the target genes were designed using the Primer-Blast tool (https://ncbi.nlm.nih.gov/tools/primer-blast/). Genomic DNA was amplified using Phusion High-Fidelity polymerase (New England Biolabs), PCR products were cleaned using a PCR purification kit (Qiagen), and purified PCR products were cloned into the pCR-Blunt vector (Thermo Fisher Scientific). For each cell line, a minimum of 10 clones were isolated and analyzed by Sanger sequencing to identify all edited alleles.

SDS-PAGE and Western blotting

For protein extraction, cells were harvested by trypsinization and lysed in radioimmunoprecipitation assay buffer (150 mM NaCl, 50 mM tris, 0.1% SDS, 0.5% sodium deoxycholate, and 1% Triton X-100) supplemented with 1× protease inhibitor (Bimake.com) and Super-Nuclease (Sino Biological). Cell lysate was centrifuged at 12,000 rpm for 10 min to remove cell debris, and the supernatant was loaded on a 4 to 15% gradient gel using loading buffer supplemented with 100 mM dithiothreitol. Following SDS–polyacrylamide gel electrophoresis (SDS-PAGE), proteins were transferred onto nitrocellulose or polyvinylidene difluoride (PVDF) membranes by semi-dry transfer (Trans-Blot Turbo) and blocked in 5% bovine serum albumin–TBST buffer (tris-buffered saline supplemented with 0.1% Tween 20) for 1 hour at room temperature (RT). Primary antibodies were incubated overnight at 4°C in TBST or Intercept blocking buffer (LI-COR) supplemented with 0.1% Tween 20. The next day, the membrane was washed three to five times in TBST and incubated for 1 hour at RT with the fluorescent secondary antibodies diluted 1:10,000 in Intercept blocking buffer with 0.1% Tween 20 (supplemented with 0.01% SDS for PVDF membranes). Following three to five washes in TBST, membranes were transferred to phosphate-buffered saline (PBS), and antibody fluorescence was detected at 700 and 800 nm using an Odyssey infrared imaging system (LI-COR).

Total RNA extraction and cDNA synthesis

For total RNA extraction, cells were harvested by trypsinization and lysed in RNA lysis buffer following the RNA Miniprep kit (Agilent). Genomic DNA contamination was reduced by on-column deoxyribonuclease (DNase) digestion as described in the manual, and purified RNA was stored at −80°C. For validation of LARP1B CRISPR KO, total RNA was reverse-transcribed to cDNA, which was used as the template for cDNA amplification of edited *LARP1B* transcripts. *LARP1B* transcripts were amplified as described above for genomic DNA validation.

Live-cell imaging

For live-cell imaging, cells were seeded at low density (20 to 30,000) in 35-mm glass-bottom μ-dishes (Ibidi) and grown for 2 to 3 days. On the day of imaging, the cells were incubated with JF549 or JF646 dyes [HHMI Janelia Research Campus; (*60*)] to label the MCP-Halo coat protein for 30 min, unbound dye was removed (three washes, PBS), and cells were kept in culture medium until imaging. For induction of reporter mRNAs, doxycycline (1 μg/ml; Sigma-Aldrich) was added to each dish at appropriate time points before each imaging session (30 min) to ensure the same duration of doxycycline induction at the start of imaging for all dishes of an experiment.

At the start of imaging of each dish, culture medium was replaced with FluoroBrite imaging DMEM (Thermo Fisher Scientific) supplemented with 10% FCS, 2 mM glutamine, and doxycycline (1 μg/ml). To inhibit mTOR, cells were treated with 250 nM Torin1, 100 nM Rapamycin, 2.5 μM PP242, or 250 nM TAK228 (INK128) for the specified duration, and the inhibitor was maintained throughout the imaging session. To inhibit translation, cells were treated with puromycin (100 μg/ml) 5 min before the start of imaging, which was

maintained throughout imaging. To allow elongating ribosomes to run-off, cells were treated with harringtonine (3 μg/ml) 10 min before the start of imaging, which was maintained throughout imaging. For all experiments, the start of the 30-min imaging window was recorded as the time point shown in the figures (e.g., imaging 60 to 90 min after Torin1 addition = 60-min time point).

Cells were kept at 37°C and 5% CO_2 throughout image acquisition. All dual-color live-cell imaging was performed on an inverted Ti2-E Eclipse (Nikon) microscope equipped with a CSU-W1 scan head (Yokogawa), two back-illuminated EMCCD cameras iXon-Ultra-888 (Andor) with chroma ET525/50 m and ET575lp emission filters and an MS-2000 motorized stage (Applied Scientific Instrumentation). Cells were illuminated with 561 Cobolt Jive (Cobolt), 488 iBeam Smart, 639 iBeam Smart (Toptica Photonics) lasers, and a VS-Homogenizer (Visitron Systems GmbH). Using a CFI Plan Apochromat Lambda 100× oil/numerical aperture (NA) 1.45 objective (Nikon), images were obtained with a pixel size of 0.134 μm. To allow for simultaneous tracking of mRNA and translation sites, both channels were simultaneously acquired by both cameras at 20 Hz for 100 frames in a single *Z* plane (5-s movies).

Live-cell data analysis

For image analysis, the first 5 to 14 frames of each movie (500 ms) were selected for single-particle tracking. First, images were corrected for any offset between the two cameras using TetraSpeck fluorescent beads acquired on each imaging day. Using the FIJI (*61*, *62*) descriptor-based registration plugin (*63*) in affine transformation mode, a transformation model was obtained to correct the bead offset and applied to all images of an imaging day using a custom macro (*64*). Subsequently, fine correction of remaining offsets between images were corrected for each dish individually using the FIJI translate function run in a custom macro, correcting for offsets occurring progressively throughout an imaging session.

Single-particle tracking and translation site quantification were performed as described previously (*64*). In short, using the KNIME analytics platform and a custom-build data processing workflow, regions of interest (ROIs) were manually annotated in the mRNA channel, selecting cytosolic regions with multiple bright spots. Annotation solely in the mRNA channel excludes any bias in selection attributable to the translational state of the cell. Next, spots in the ROIs corresponding to single mRNAs were tracked using TrackMate (*65*) integrated in KNIME, using the "Laplacian of Gaussian" detector with an estimated spot radius of 200-nm and subpixel localization. Detection thresholds were adjusted on the basis of the signal-to-noise ratio of images and varied between 1.25 and 2. For particle linking, the parameters linking max distance (600 nm), gap closing max distance (1200 nm), and gap closing max frame gap (2) were optimized for single-particle tracking of mRNAs. To assay whether an mRNA is translating, the mean intensity of the SunTag channel was measured at the coordinates of each mRNA spot and quantified as FC/ROI background intensity. A cutoff of <1.5 fold/background was determined to classify an mRNA as nontranslating based on calibration data using the translation inhibitor harringtonine. Excluding cells with <3 mRNAs, the fraction of translating mRNAs per cell was calculated (translating/all mRNAs per ROI). For data visualization, the fraction of translating mRNAs per cell and translation site intensities were plotted using SuperPlots (https://huygens.science.uva.nl/SuperPlotsOfData/), showing all data points together with the mean (±SD) of each biological replicate (*66*).

RNA sequencing

For RNA-seq, total RNA samples extracted using the RNA Miniprep kit (Agilent) were assessed for RNA integrity using the Agilent Tapestation, and library preparation was performed using the Illumina TruSeq Stranded mRNA reagents according to the manufacturer's protocol. Libraries were sequenced on the Illumina HiSeq2500 (GEO submission GSE233183: single reads, 50 cycles) or NovaSeq6000 platforms (GEO submission GSE233182: paired-end reads, 100 cycles).

For our analysis, we used a reference list of experimentally validated 5′TOP mRNAs (*37*), expanded with additional experimentally verified 5′TOP mRNAs (*RACK1* and *EIF3K*) as well as computationally predicted 5′TOP mRNAs with known roles in translation (*EIF2A*, *EIF2S3*, *EIF3L*, *EIF4A2*, and *RPL22L1*) (*37*). The presence or absence of a PRTE in the 5′UTR was taken from Hsieh *et al.* (*14*) and expanded by manual annotation for the subset of 5′TOP mRNAs not listed (table S2).

Sequenced reads were aligned against the human genome (GENCODE GRCh38 primary assembly, https://gencodegenes.org/human/release_38.html) using R version 4.1.1 with Bioconductor version 3.13 to execute the qAlign tool [QuasR package, version 1.32.0, (*67*)], with default parameters except for aligner = "Rhisat2," splicedAlignment = "TRUE," allowing only uniquely mapping reads. Raw gene counts were obtained using the qCount tool (QuasR) with a TxDb generated from gencode.v38.primary_assembly.annotation.gtf as query, with default parameters counting only alignments on the opposite strand as the query region. The count table was filtered to only keep genes which had at least 1 cpm in at least three samples.

Single-molecule fluorescence in situ hybridization

For smFISH, HeLa-11ht cell lines were seeded on high-precision glass coverslips placed in 12-well tissue culture plates, grown for 2 days to reach ~50% confluency, and fixed using 4% paraformaldehyde (10 min, RT). To detect endogenous mRNAs, atto633-conjugated smFISH probes targeting human *MYC* mRNA were generated by enzymatic oligonucleotide labeling (*68*), using Amino-11-ddUTP and Atto633-NHS. Quasar570-conjugated smFISH probes targeting *RPL5*, *RPL11*, and *RPL32* were purchased ready-to-use (Biosearch Technologies). smFISH was performed as described previously (*64*). Briefly, fixed cells were washed twice in PBS (5 min), permeabilized overnight in 70% ethanol, washed thrice in smFISH wash buffer (2× SSC, 10% formamide, 5 min), and hybridized with smFISH probes (2× SSC, 10% formamide, 10% dextran sulfate, 125 nM Quasar570/atto633 smFISH probe) at 37°C for 4 hours. Coverslips were washed twice with smFISH wash buffer (30 min) and mounted on glass slides using Prolong Gold mounting medium containing 4′,6-diamidino-2-phenylindole. Cells were imaged using an upright spinning-disk confocal microscope equipped with a CSU-W1 scan head (Yokogawa) and sCMOS detectors. Using a Plan Apochromat 63× oil/NA 1.4 objective, Z-stacks were obtained with a pixel size of 103 nm and Z-stack spacing of 200 nm using single-camera sequential acquisition.

Analysis of smFISH data was performed using custom-build Python scripts. Nuclei were segmented in three-dimensional (3D) using the triangle threshold method, merged nuclei were split by applying a seeded watershed on the Euclidian distance transformed segmentation mask, and segmentation nuclei with an area < 200 or a solidity < 0.5 were removed. The cytoplasm was segmented on a maximum intensity projection by using the median as a threshold to obtain a semantic segmentation and then splitting this segmentation into cell

instance with a seeded watershed applied to the Euclidian distance transform of the semantic segmentation. The maximum projection of the 3D nuclei labeling was taken as seeds for cell segmentation. mRNA spots were detected using a Laplacian of Gaussian filter to detect diffraction limited spots and refined by applying a h-maxima detector to remove detections below a transcript-specific threshold.

SLAM-seq

For metabolic labeling (SLAMseq), HeLa-11ht cell lines were incubated with a dilution series of 4-thiouridine (S4U) for 24 hours, exchanging S4U-containing media every 3 hours according to the manufacturer's instructions. S4U cytotoxicity was assessed using a luminescent cell viability assay, and the half-maximal inhibitory concentration (IC_{50}) was calculated at 209 μM ($n = 2$). On the basis of the IC_{50}, a trial RNA-seq was conducted with 24-hour S4U labeling using a dilution series (0, 3, 6, 12, 24, and 48 μM) of S4U and exchanging media every 3 hours. The 12 μM S4U concentration was selected as the optimal experimental S4U concentration with minimal effects on gene expression for all cell lines.

For assessing global RNA half-lives, HeLa-11ht cell lines were labeled with 12 μM S4U for 24 hours (exchanging media every 3 hours), labeling was stopped using 100× excess uridine (1.2 mM), and cells were harvested at time points 0, 2, 4, 6, 9, and 12 hours after the uridine quench. For isolation of total RNA, RNA was extracted using an RNA miniprep kit (Agilent) with on-column DNase digestion, followed by iodoacetamide treatment and ethanol precipitation of modified total RNA. For RNA-seq, total RNA was assessed for RNA integrity using the Agilent Tapestation, and library preparation was performed using the Illumina TruSeq Stranded Total RNA Library Prep Gold kit according to the manufacturer's protocol. Libraries were sequenced on the Illumina NextSeq500 (GEO submission GSE233186: single reads, 75 cycles). Samples were submitted as three independent technical replicates (cells harvested on separate days), with the exception of one sample with only two replicates (E6_0h).

In total, ~3.7 billion SLAMseq reads were produced corresponding to ~52 M reads per replicate. 4-Thiouridine incorporation events were analyzed using the SlamDunk software (v0.3.4) for SLAMseq analysis (*69*). SLAMseq reads were first reverse complemented to match the hard-coded assumed SlamDunk orientation using fastx_reverse_complement from the FASTX-toolkit (http://hannonlab.cshl.edu/fastx_toolkit) with default settings. The resulting fastq files were mapped to the reference genome (GENCODE GRCh38 primary assembly) with slamdunk map and parameters -5 0 -ss q. The mapped reads were subsequently filtered to only retain intragenic mappings according to the reference transcriptome (GRCh38, GENCODE v33) with a high identity using slamdunk filter and parameters -mi 0.9. Single-nucleotide polymorphism (SNP) variants in the samples were called with slamdunk snp with parameters -c 1 -f 0.2. The SNP variants from all samples were combined in a single master vcf file by indexing the individual vcf file using tabix of the htslib package (https://github.com/samtools/htslib, v1.9, 07/2018) and merging using vcf-merge from the VCFtools package (*70*). 4-Thiouridine incorporation and conversion rates were calculated separately for exonic gene segments of the reference transcriptome using slamdunk count with default parameters and the master SNP vcf file for SNP filtering. The exonic segments counts were then aggregated to obtain gene-level total mapping reads, multimapping reads, and converted reads counts. During aggregation, total and converted counts from exonic segment with multimappers were downweighted by the fraction of multimappers over the total mapped reads of the exonic segment (fm). Last, gene conversion rates were calculated as the number of gene-level aggregated converted reads over the gene-level aggregated total read counts.

Gene conversion rates in each context were fitted to an exponential time decay model to obtain gene half-life estimates. Fitting was performed by nonlinear least squares using the R stats::nls function. Example fit command: *fit < - nls[rates ~ exp(a + k*time points) ,control = list(minFactor = 1e-7, tol = 1e-05,maxiter = 256)]* where rates are the conversion rates for the gene (including all replicates) and time points are the corresponding times in hours. The half-life (in minutes) was obtained from the fitted coefficient [$t_{1/2} = -1/k*\ln(2)*60$]. Half-life estimates and the fitting R^2 values are listed in table S4 for all transcripts with $R^2 \geq 0.75$ in all conditions.

Statistical analysis

For live-cell imaging, biological replicates (n) were defined as independent days of imaging. Statistical analyses were performed using GraphPad Prism, with n numbers and statistical tests described in the figure legends. Technical replicates within biological replicates were pooled before statistical tests.

For RNA-seq analysis of LARP1 WT cells, biological replicates (n) were defined as independent clonal cell lines (canonical and 5′TOP mRNA cell lines, $n = 2$). For RNA-seq of LARP1 KO clones, four single-cell derived clones were sequenced for both canonical and 5′TOP cell lines and treated as independent biological replicates ($n = 8$ total). For each n, three independent replicates (cells harvested on separate days) were submitted for RNA-seq and averaged before statistical tests. Differential gene expression was calculated with the Bioconductor package edgeR [version 3.34.0, (*71*)] using the quasi-likelihood F test after applying the calcNormFactors function, obtaining the dispersion estimates and fitting the negative binomial generalized linear models.

For SLAM-seq analysis, biological replicates (n) were defined as independent clonal cell lines for both LARP1 WT and LARP1 KO cells (canonical and 5′TOP mRNA cell lines, $n = 2$). For analysis of changes in mRNA stability, the estimated half-lives were averaged for n1 and n2, and changes in mRNA stability were calculated between genotypes ($\log_2$ FC). Significant differences in mRNA stability were classified with abs $\log_2$ FC ≥ 1, excluding spurious transcripts overlapping in sequence with known 5′TOP mRNAs (read-through transcripts *AC135178.3*, *AP002990.1*, *AC245033.1*, lncRNA *AL022311.1*, *MIR4426*, and *MIR3654*).

Supplementary Materials

This PDF file includes:

Figs. S1 to S16
Table S2
Legends for tables S1, S3 to S6
Legends for movies S1 to S20

Other Supplementary Material for this manuscript includes the following:

Tables S1, S3 to S6
Movies S1 to S20

REFERENCES AND NOTES

1. G. Y. Liu, D. M. Sabatini, mTOR at the nexus of nutrition, growth, ageing and disease. *Nat. Rev. Mol. Cell Biol.* **21**, 183–203 (2020).
2. S. Battaglioni, D. Benjamin, M. Wälchli, T. Maier, M. N. Hall, mTOR substrate phosphorylation in growth control. *Cell* **185**, 1814–1836 (2022).

3. J.-J. Jia, R. M. Lahr, M. T. Solgaard, B. J. Moraes, R. Pointet, A. D. Yang, G. Celucci, T. E. Graber, H. D. Hoang, M. R. Niklaus, I. A. Pena, A. K. Hollensen, E. M. Smith, M. Chaker-Margot, L. Anton, C. Dajadian, M. Livingstone, J. Hearnden, X. D. Wang, Y. Yu, T. Maier, C. K. Damgaard, A. J. Berman, T. Alain, B. D. Fonseca, mTORC1 promotes TOP mRNA translation through site-specific phosphorylation of LARP1. *Nucleic Acids Res.* **49**, 3461–3489 (2021).
4. B. D. Fonseca, C. Zakaria, J. J. Jia, T. E. Graber, Y. Svitkin, S. Tahmasebi, D. Healy, H. D. Hoang, J. M. Jensen, I. T. Diao, A. Lussier, C. Dajadian, N. Padmanabhan, W. Wang, E. Matta-Camacho, J. Hearnden, E. M. Smith, Y. Tsukumo, A. Yanagiya, M. Morita, E. Petroulakis, J. L. González, G. Hernández, T. Alain, C. K. Damgaard, La-related protein 1 (LARP1) represses terminal oligopyrimidine (TOP) mRNA translation downstream of mTOR complex 1 (mTORC1). *J. Biol. Chem.* **290**, 15996–16020 (2015).
5. L. Philippe, J. J. Vasseur, F. Debart, C. C. Thoreen, La-related protein 1 (LARP1) repression of TOP mRNA translation is mediated through its cap-binding domain and controlled by an adjacent regulatory region. *Nucleic Acids Res.* **46**, 1457–1469 (2018).
6. J. Tcherkezian, M. Cargnello, Y. Romeo, E. L. Huttlin, G. Lavoie, S. P. Gygi, P. P. Roux, Proteomic analysis of cap-dependent translation identifies LARP1 as a key regulator of 5'TOP mRNA translation. *Genes Dev.* **28**, 357–371 (2014).
7. S. Hong, M. A. Freeberg, T. Han, A. Kamath, Y. Yao, T. Fukuda, T. Suzuki, J. K. Kim, K. Inoki, LARP1 functions as a molecular switch for mTORC1-mediated translation of an essential class of mRNAs. *eLife* **6**, e25237 (2017).
8. O. Meyuhas, T. Kahan, The race to decipher the top secrets of TOP mRNAs. *Biochim. Biophys. Acta* **1849**, 801–811 (2015).
9. Y. Biberman, O. Meyuhas, Substitution of just five nucleotides at and around the transcription start site of rat β-actin promoter is sufficient to render the resulting transcript a subject for translational control. *FEBS Lett.* **405**, 333–336 (1997).
10. D. Avni, S. Shama, F. Loreni, O. Meyuhas, Vertebrate mRNAs with a 5'-terminal pyrimidine tract are candidates for translational repression in quiescent cells: Characterization of the translational cis-regulatory element. *Mol. Cell. Biol.* **14**, 3822–3833 (1994).
11. A. J. Berman, C. C. Thoreen, Z. Dedeic, J. Chettle, P. P. Roux, S. P. Blagden, Controversies around the function of LARP1. *RNA Biol.* **18**, 207–217 (2021).
12. C. C. Thoreen, L. Chantranupong, H. R. Keys, T. Wang, N. S. Gray, D. M. Sabatini, A unifying model for mTORC1-mediated regulation of mRNA translation. *Nature* **485**, 109–113 (2012).
13. R. Miloslavski, E. Cohen, A. Avraham, Y. Iluz, Z. Hayouka, J. Kasir, R. Mudhasani, S. N. Jones, N. Cybulski, M. A. Rüegg, O. Larsson, V. Gandin, A. Rajakumar, I. Topisirovic, O. Meyuhas, Oxygen sufficiency controls TOP mRNA translation via the TSC-Rheb-mTOR pathway in a 4E-BP-independent manner. *J. Mol. Cell Biol.* **6**, 255–266 (2014).
14. A. C. Hsieh, Y. Liu, M. P. Edlind, N. T. Ingolia, M. R. Janes, A. Sher, E. Y. Shi, C. R. Stumpf, C. Christensen, M. J. Bonham, S. Wang, P. Ren, M. Martin, K. Jessen, M. E. Feldman, J. S. Weissman, K. M. Shokat, C. Rommel, D. Ruggero, The translational landscape of mTOR signalling steers cancer initiation and metastasis. *Nature* **485**, 55–61 (2012).
15. L. Lindqvist, H. Imataka, J. Pelletier, Cap-dependent eukaryotic initiation factor-mRNA interactions probed by cross-linking. *RNA* **14**, 960–969 (2008).
16. A. Tamarkin-Ben-Harush, J. J. Vasseur, F. Debart, I. Ulitsky, R. Dikstein, Cap-proximal nucleotides via differential eIF4E binding and alternative promoter usage mediate translational response to energy stress. *eLife* **6**, e21907 (2017).
17. R. M. Lahr, B. D. Fonseca, G. E. Ciotti, H. A. al-Ashtal, J. J. Jia, M. R. Niklaus, S. P. Blagden, T. Alain, A. J. Berman, La-related protein 1 (LARP1) binds the mRNA cap, blocking eIF4F assembly on TOP mRNAs. *eLife* **6**, e24146 (2017).
18. J. A. Schofield, E. E. Duffy, L. Kiefer, M. C. Sullivan, M. D. Simon, TimeLapse-seq: Adding a temporal dimension to RNA sequencing through nucleoside recoding. *Nat. Methods* **15**, 221–225 (2018).
19. V. A. Herzog, B. Reichholf, T. Neumann, P. Rescheneder, P. Bhat, T. R. Burkard, W. Wlotzka, A. von Haeseler, J. Zuber, S. L. Ameres, Thiol-linked alkylation of RNA to assess expression dynamics. *Nat. Methods* **14**, 1198–1204 (2017).
20. G. Kozlov, S. Mattijssen, J. Jiang, S. Nyandwi, T. Sprules, J. R. Iben, S. L. Coon, S. Gaidamakov, A. M. Noronha, C. J. Wilds, R. J. Maraia, K. Gehring, Structural basis of 3′-end poly(A) RNA recognition by LARP1. *Nucleic Acids Res.* **50**, 9534–9547 (2022).
21. S. Mattijssen, G. Kozlov, S. Gaidamakov, A. Ranjan, B. D. Fonseca, K. Gehring, R. J. Maraia, The isolated La-module of LARP1 mediates 3′ poly(A) protection and mRNA stabilization, dependent on its intrinsic PAM2 binding to PABPC1. *RNA Biol.* **18**, 275–289 (2021).
22. K. Ogami, Y. Oishi, K. Sakamoto, M. Okumura, R. Yamagishi, T. Inoue, M. Hibino, T. Nogimori, N. Yamaguchi, K. Furutachi, N. Hosoda, H. Inagaki, S. I. Hoshino, mTOR- and LARP1-dependent regulation of TOP mRNA poly(A) tail and ribosome loading. *Cell Rep.* **41**, 111548 (2022).
23. K. Ogami, Y. Oishi, T. Nogimori, K. Sakamoto, S.-i. Hoshino, LARP1 facilitates translational recovery after amino acid refeeding by preserving long poly(A)-tailed TOP mRNAs. *bioRxiv*, 716217 (2019). https://doi.org/10.1101/716217.
24. E. M. Smith, N. E. H. Benbahouche, K. Morris, A. Wilczynska, S. Gillen, T. Schmidt, H. A. Meijer, R. Jukes-Jones, K. Cain, C. Jones, M. Stoneley, J. A. Waldron, C. Bell, B. D. Fonseca, S. Blagden, A. E. Willis, M. Bushell, The mTOR regulated RNA-binding protein LARP1 requires PABPC1 for guided mRNA interaction. *Nucleic Acids Res.* **49**, 458–478 (2020).
25. M. Mura, T. G. Hopkins, T. Michael, N. Abd-Latip, J. Weir, E. Aboagye, F. Mauri, C. Jameson, J. Sturge, H. Gabra, M. Bushell, A. E. Willis, E. Curry, S. P. Blagden, LARP1 post-transcriptionally regulates mTOR and contributes to cancer progression. *Oncogene* **34**, 5025–5036 (2015).
26. J. Park, M. Kim, H. Yi, K. Baeg, Y. Choi, Y. S. Lee, J. Lim, V. N. Kim, Short poly(A) tails are protected from deadenylation by the LARP1–PABP complex. *Nat. Struct. Mol. Biol.* **30**, 330–338 (2023).
27. J. H. Wilbertz, F. Voigt, I. Horvathova, G. Roth, Y. Zhan, J. A. Chao, Single-molecule imaging of mRNA localization and regulation during the integrated stress response. *Mol. Cell* **73**, 946–958.e7 (2019).
28. M. E. Tanenbaum, L. A. Gilbert, L. S. Qi, J. S. Weissman, R. D. Vale, A protein-tagging system for signal amplification in gene expression and fluorescence imaging. *Cell* **159**, 635–646 (2014).
29. L. A. Banaszynski, L.-C. Chen, L. A. Maynard-Smith, A. G. L. Ooi, T. J. Wandless, A rapid, reversible, and tunable method to regulate protein function in living cells using synthetic small molecules. *Cell* **126**, 995–1004 (2006).
30. P. Carninci, A. Sandelin, B. Lenhard, S. Katayama, K. Shimokawa, J. Ponjavic, C. A. Semple, M. S. Taylor, P. G. Engström, M. C. Frith, A. R. Forrest, W. B. Alkema, S. L. Tan, C. Plessy, R. Kodzius, T. Ravasi, T. Kasukawa, S. Fukuda, M. Kanamori-Katayama, Y. Kitazume, H. Kawaji, C. Kai, M. Nakamura, H. Konno, K. Nakano, S. Mottagui-Tabar, P. Arner, A. Chesi, S. Gustincich, F. Persichetti, H. Suzuki, S. M. Grimmond, C. A. Wells, V. Orlando, C. Wahlestedt, E. T. Liu, M. Harbers, J. Kawai, V. B. Bajic, D. A. Hume, Y. Hayashizaki, Genome-wide analysis of mammalian promoter architecture and evolution. *Nat. Genet.* **38**, 626–635 (2006).
31. C. C. Thoreen, S. A. Kang, J. W. Chang, Q. Liu, J. Zhang, Y. Gao, L. J. Reichling, T. Sim, D. M. Sabatini, N. S. Gray, An ATP-competitive mammalian target of rapamycin inhibitor reveals rapamycin-resistant functions of mTORC1. *J. Biol. Chem.* **284**, 8023–8032 (2009).
32. S. Wullschleger, R. Loewith, M. N. Hall, TOR signaling in growth and metabolism. *Cell* **124**, 471–484 (2006).
33. B. Apsel, J. A. Blair, B. Gonzalez, T. M. Nazif, M. E. Feldman, B. Aizenstein, R. Hoffman, R. L. Williams, K. M. Shokat, Z. A. Knight, Targeted polypharmacology: Discovery of dual inhibitors of tyrosine and phosphoinositide kinases. *Nat. Chem. Biol.* **4**, 691–699 (2008).
34. K. Jessen, S. Wang, L. Kessler, X. Guo, J. Kucharski, J. Staunton, L. Lan, M. Elia, J. Stewart, J. Brown, L. Li, K. Chan, M. Martin, P. Ren, C. Rommel, Y. Liu, Abstract B148: INK128 is a potent and selective TORC1/2 inhibitor with broad oral antitumor activity. *Mol. Cancer Ther.* **8** (Suppl. 1), B148-8 (2009).
35. B. Hassan, A. Akcakanat, T. Sangai, K. W. Evans, F. Adkins, A. K. Eterovic, H. Zhao, K. Chen, H. Chen, K. A. do, S. M. Xie, A. M. Holder, A. Naing, G. B. Mills, F. Meric-Bernstam, Catalytic mTOR inhibitors can overcome intrinsic and acquired resistance to allosteric mTOR inhibitors. *Oncotarget* **5**, 8544–8557 (2014).
36. Y. Huo, V. Iadevaia, Z. Yao, I. Kelly, S. Cosulich, S. Guichard, L. J. Foster, C. G. Proud, Stable isotope-labelling analysis of the impact of inhibition of the mammalian target of rapamycin on protein synthesis. *Biochem. J.* **444**, 141–151 (2012).
37. L. Philippe, A. M. G. van den Elzen, M. J. Watson, C. C. Thoreen, Global analysis of LARP1 translation targets reveals tunable and dynamic features of 5′ TOP motifs. *Proc. Natl. Acad. Sci.* **117**, 5319–5328 (2020).
38. K. Aoki, S. Adachi, M. Homoto, H. Kusano, K. Koike, T. Natsume, LARP1 specifically recognizes the 3′ terminus of poly(A) mRNA. *FEBS Lett.* **587**, 2173–2178 (2013).
39. H. A. Al-Ashtal, C. M. Rubottom, T. C. Leeper, A. J. Berman, The LARP1 La-Module recognizes both ends of TOP mRNAs. *RNA Biol.* **18**, 248–258 (2021).
40. M. L. Truitt, C. S. Conn, Z. Shi, X. Pang, T. Tokuyasu, A. M. Coady, Y. Seo, M. Barna, D. Ruggero, Differential requirements for eIF4E dose in normal development and cancer. *Cell* **162**, 59–71 (2015).
41. C. C. Thoreen, The molecular basis of mTORC1-regulated translation. *Biochem. Soc. Trans.* **45**, 213–221 (2017).
42. V. Gandin, L. Masvidal, L. Hulea, S. P. Gravel, M. Cargnello, S. McLaughlan, Y. Cai, P. Balanathan, M. Morita, A. Rajakumar, L. Furic, M. Pollak, Porco JA Jr, J. St-Pierre, J. Pelletier, O. Larsson, I. Topisirovic, nanoCAGE reveals 5' UTR features that define specific modes of translation of functionally related MTOR-sensitive mRNAs. *Genome Res.* **26**, 636–648 (2016).
43. A. M. G. van den Elzen, M. J. Watson, C. C. Thoreen, mRNA 5′ terminal sequences drive 200-fold differences in expression through effects on synthesis, translation and decay. *PLOS Genet.* **18**, e1010532 (2022).
44. O. Meyuhas, Synthesis of the translational apparatus is regulated at the translational level. *Eur. J. Biochem.* **267**, 6321–6330 (2000).
45. Y. Mamane, E. Petroulakis, Y. Martineau, T. A. Sato, O. Larsson, V. K. Rajasekhar, N. Sonenberg, Epigenetic activation of a subset of mRNAs by eIF4E explains its effects on cell proliferation. *PLOS ONE* **2**, e242 (2007).
46. S. Kajjo, S. Sharma, R. W. Brothers, V. Delisle, R. M. Fabian, PABPC plays a critical role in establishing mTORC-mediated translational control. *Under Preparation.*, (2023).

47. K. Tomoo, X. Shen, K. Okabe, Y. Nozoe, S. Fukuhara, S. Morino, T. Ishida, T. Taniguchi, H. Hasegawa, A. Terashima, M. Sasaki, Y. Katsuya, K. Kitamura, H. Miyoshi, M. Ishikawa, K. Miura, Crystal structures of 7-methylguanosine 5'-triphosphate (m(7)GTP)- and P(1)-7-methylguanosine-P(3)-adenosine-5',5'-triphosphate (m(7)GpppA)-bound human full-length eukaryotic initiation factor 4E: Biological importance of the C-terminal flexible region. *Biochem. J.* **362** (Pt. 3), 539–544 (2002).
48. L. Furic, L. Rong, O. Larsson, I. H. Koumakpayi, K. Yoshida, A. Brueschke, E. Petroulakis, N. Robichaud, M. Pollak, L. A. Gaboury, P. P. Pandolfi, F. Saad, N. Sonenberg, eIF4E phosphorylation promotes tumorigenesis and is associated with prostate cancer progression. *Proc. Natl. Acad. Sci. U.S.A.* **107**, 14134–14139 (2010).
49. B. Zinshteyn, M. F. Rojas-Duran, W. V. Gilbert, Translation initiation factor eIF4G1 preferentially binds yeast transcript leaders containing conserved oligo-uridine motifs. *RNA* **23**, 1365–1375 (2017).
50. H. Jin, W. Xu, R. Rahman, D. Na, A. Fieldsend, W. Song, S. Liu, C. Li, M. Rosbash, TRIBE editing reveals specific mRNA targets of eIF4E-BP in *Drosophila* and in mammals. *Sci. Adv.* **6**, eabb8771 (2020).
51. P. Fuentes, J. Pelletier, C. Martinez-Herráez, V. Diez-Obrero, F. Iannizzotto, T. Rubio, M. Garcia-Cajide, S. Menoyo, V. Moreno, R. Salazar, A. Tauler, A. Gentilella, The 40*S*-LARP1 complex reprograms the cellular translatome upon mTOR inhibition to preserve the protein synthetic capacity. *Sci. Adv.* **7**, eabg9275 (2021).
52. A. Gentilella, F. D. Morón-Duran, P. Fuentes, G. Zweig-Rocha, F. Riaño-Canalias, J. Pelletier, M. Ruiz, G. Turón, J. Castaño, A. Tauler, C. Bueno, P. Menéndez, S. C. Kozma, G. Thomas, Autogenous control of 5′TOP mRNA stability by 40S ribosomes. *Mol. Cell* **67**, 55–70.e4 (2017).
53. J. Brito Querido, M. Sokabe, S. Kraatz, Y. Gordiyenko, J. M. Skehel, C. S. Fraser, V. Ramakrishnan, Structure of a human 48S translational initiation complex. *Science* **369**, 1220–1227 (2020).
54. R. Goering, A. Arora, M. C. Pockalny, J. M. Taliaferro, RNA localization mechanisms transcend cell morphology. *eLife* **12**, e80040 (2023).
55. N. M. Livingston, J. Kwon, O. Valera, J. A. Saba, N. K. Sinha, P. Reddy, B. Nelson, C. Wolfe, T. Ha, R. Green, J. Liu, B. Wu, Bursting translation on single mRNAs in live cells. *Mol. Cell* **83**, 2276–2289.e11 (2022).
56. P. Dave, G. Roth, E. Griesbach, D. Mateju, T. Hochstoeger, J. A. Chao, Single-molecule imaging reveals translation-dependent destabilization of mRNAs. *Mol. Cell* **83**, 589–606.e6 (2023).
57. L. Cong, F. A. Ran, D. Cox, S. Lin, R. Barretto, N. Habib, P. D. Hsu, X. Wu, W. Jiang, L. A. Marraffini, F. Zhang, Multiplex genome engineering using CRISPR/Cas systems. *Science* **339**, 819–823 (2013).
58. V. T. Chu, T. Weber, B. Wefers, W. Wurst, S. Sander, K. Rajewsky, R. Kühn, Increasing the efficiency of homology-directed repair for CRISPR-Cas9-induced precise gene editing in mammalian cells. *Nat. Biotechnol.* **33**, 543–548 (2015).
59. D. M. Bryant, A. Datta, A. E. Rodríguez-Fraticelli, J. Peränen, F. Martín-Belmonte, K. E. Mostov, A molecular network for de novo generation of the apical surface and lumen. *Nat. Cell Biol.* **12**, 1035–1045 (2010).
60. J. B. Grimm, B. P. English, J. Chen, J. P. Slaughter, Z. Zhang, A. Revyakin, R. Patel, J. J. Macklin, D. Normanno, R. H. Singer, T. Lionnet, L. D. Lavis, A general method to improve fluorophores for live-cell and single-molecule microscopy. *Nat. Methods* **12**, 244–250 (2015).
61. J. Schindelin, I. Arganda-Carreras, E. Frise, V. Kaynig, M. Longair, T. Pietzsch, S. Preibisch, C. Rueden, S. Saalfeld, B. Schmid, J. Y. Tinevez, D. J. White, V. Hartenstein, K. Eliceiri, P. Tomancak, A. Cardona, Fiji: An open-source platform for biological-image analysis. *Nat. Methods* **9**, 676–682 (2012).
62. C. T. Rueden, J. Schindelin, M. C. Hiner, B. E. DeZonia, A. E. Walter, E. T. Arena, K. W. Eliceiri, ImageJ2: ImageJ for the next generation of scientific image data. *BMC Bioinformatics* **18**, 529 (2017).
63. S. Preibisch, S. Saalfeld, J. Schindelin, P. Tomancak, Software for bead-based registration of selective plane illumination microscopy data. *Nat. Methods* **7**, 418–419 (2010).
64. D. Mateju, B. Eichenberger, F. Voigt, J. Eglinger, G. Roth, J. A. Chao, Single-molecule imaging reveals translation of mRNAs localized to stress granules. *Cell* **183**, 1801–1812.e13 (2020).
65. J.-Y. Tinevez, N. Perry, J. Schindelin, G. M. Hoopes, G. D. Reynolds, E. Laplantine, S. Y. Bednarek, S. L. Shorte, K. W. Eliceiri, TrackMate: An open and extensible platform for single-particle tracking. *Methods* **115**, 80–90 (2017).
66. S. J. Lord, K. B. Velle, R. D. Mullins, L. K. Fritz-Laylin, SuperPlots: Communicating reproducibility and variability in cell biology. *J. Cell Biol.* **219**, e202001064 (2020).
67. D. Gaidatzis, A. Lerch, F. Hahne, M. B. Stadler, QuasR: Quantification and annotation of short reads in R. *Bioinformatics* **31**, 1130–1132 (2015).
68. I. Gaspar, F. Wippich, A. Ephrussi, Terminal deoxynucleotidyl transferase mediated production of labeled probes for single-molecule FISH or RNA capture. *Bio Protoc.* **8**, e2750 (2018).
69. T. Neumann, V. A. Herzog, M. Muhar, A. von Haeseler, J. Zuber, S. L. Ameres, P. Rescheneder, Quantification of experimentally induced nucleotide conversions in high-throughput sequencing datasets. *BMC Bioinformatics* **20**, 258 (2019).
70. P. Danecek, A. Auton, G. Abecasis, C. A. Albers, E. Banks, M. A. DePristo, R. E. Handsaker, G. Lunter, G. T. Marth, S. T. Sherry, G. McVean, R. Durbin, 1000 Genomes Project Analysis Group, The variant call format and VCFtools. *Bioinformatics* **27**, 2156–2158 (2011).
71. A. T. Lun, Y. Chen, G. K. Smyth, It's DE-licious: A recipe for differential expression analyses of RNA-seq experiments using quasi-likelihood methods in edgeR. *Methods Mol. Biol.* **1418**, 391–416 (2016).

Acknowledgments: We thank V. Herzog for advice on SLAMseq methodology, S. Smallwood and H.-R. Hotz for support with transcriptomics, T.-O. Buchholz, F. Voigt, L. Gelman, L. Plantard, and S. Reither for microscopy and image analysis support, H. Kohler for cell sorting, and all members of the Chao lab for input and helpful discussions. We thank E. Griesbach for MYC smFISH probe generation. A donation was made to the Henrietta Lacks Foundation to acknowledge the use of HeLa cells in our research. **Funding:** This work was supported by the Novartis Research Foundation (J.A.C), a Swiss National Science Foundation Sinergia grant (CRSII5-205884), the SNF-NCCR RNA & Disease network (51NF40-205601), and a Boehringer Ingelheim Fonds PhD fellowship (T.H.). **Author contributions:** Conceptualization: J.A.C. and T.H. Methodology: T.H., P.P., and E.P. Investigation: T.H. Visualization: T.H. and P.P. Supervision: J.A.C. Writing—original draft: T.H. and J.A.C. Writing—review and editing: T.H. and J.A.C. **Competing interests:** The authors declare they have no competing interests. **Data and materials availability:** All data needed to evaluate the conclusions in the paper are present in the paper and/or the Supplementary Materials. Sequencing data for this study has been deposited in the GEO repository (GSE233187). All reagents generated in this study are available from the lead contact, J.A.C. (jeffrey.chao@fmi.ch), with a completed material transfer agreement. All original code (KNIME workflows and ImageJ macros) and image analysis output files have been deposited at Zenodo and are publicly available (10.5281/zenodo.10057405).

Submitted 17 May 2023
Accepted 16 January 2024
Published 16 February 2024
10.1126/sciadv.adi7830